UC Berkeley
UC Berkeley Electronic Theses and Dissertations

Title

Algebraic curves, Grassmannians, and integrable systems

Permalink

https://escholarship.org/uc/item/3q02f3n9

Author

Mandelshtam, Yelena

Publication Date

2024

Peer reviewed|Thesis/dissertation

Algebraic curves, Grassmannians, and integrable systems

by

Yelena Mandelshtam

A dissertation submitted in partial satisfaction of the

requirements for the degree of

Doctor of Philosophy

in

Mathematics

in the

Graduate Division

of the

University of California, Berkeley

Committee in charge:

Professor Bernd Sturmfels, Chair
Professor Sylvie Corteel
Professor Hannah Larson

Spring 2024

Algebraic curves, Grassmannians, and integrable systems

Abstract

Algebraic curves, Grassmannians, and integrable systems

by

Yelena Mandelshtam

Doctor of Philosophy in Mathematics

University of California, Berkeley

Professor Bernd Sturmfels, Chair

Problems in physics often inspire mathematical solutions, occasionally leading to the development of new mathematical objects. Mathematicians may then explore these constructs independently, sometimes uncovering new compelling physical interpretations in the process. This thesis contributes to this dynamic interplay between mathematical abstraction and physical reality, with a focus on algebraic curves. It aims to present findings that resonate with and are useful to both the mathematics and physics communities

We first explore the connections between algebraic curves and integrable systems, focusing on the KP equation, a nonlinear partial differential equation describing the motion of water waves. Our approach is based on the connection established by Krichever and Shiota, which showed that one can construct KP solutions starting from algebraic curves using their theta functions. This lead also to a new perspective on the classical Schottky Problem which has interested algebraic geometers for several decades. In this thesis, we explore KP solutions arising from curves which are not smooth, having at worst nodal singularities. We introduce the Hirota variety, which parameterizes KP solutions arising from such curves. Examining the geometry of the Hirota variety provides a new approach to the Schottky problem, which we study for irreducible rational nodal curves. We conjecture and prove up to genus nine a solution to the Schottky problem for rational nodal curves.

When applying algebraic geometry or combinatorics to areas of physics such as integrable systems or particle physics, positivity, in particular the positive Grassmannian, plays a major role. In the last decade it has garnered much attention from physicists through its connection with scattering amplitudes, which can be computed as volumes of amplituhedra. An amplituhedron is the image of the nonnegative Grassmannian $\mathrm{Gr}_{\geq 0}(k, n)$ under a totally positive linear map $\tilde{Z} : \mathrm{Gr}(k, n) \to \mathrm{Gr}(k, k + m)$. In this dissertation we study Grasstopes: generalizations of amplituhedra in which we allow arbitrary linear maps. As a result, we give a full description of $m = 1$ Grasstopes, recovering some results about $m = 1$ amplituhedra, and introduce some new directions of study. Though so far the study of Grasstopes has been

motivated by pure mathematical interest, one hope is that physicists may come up with a use for them as well.

We continue to draw inspiration from particle physicists in our study of the positive orthogonal Grassmannian. We initiate the study of the positive orthogonal Grassmannian geometrically, for not necessarily maximal dimensions, and with varying signature coming from the quadratic form. In particular we prove that, for arbitrary signature, the positive orthogonal Grassmannian for $\mathrm{OGr}_{\geq 0}(1, n)$ is a positive geometry, confirming physicists' intuition.

Finally, we highlight the value of computation in algebraic geometry by revisiting classical problems. The centuries-old uniformization theorem states that an algebraic curve is equivalent to a compact Riemann surface. However, connecting a Riemann surface to an algebraic curve utilizes Riemann theta functions, which are infinite sums of exponentials, so this classical equivalence is transcendental, leaving a divide between analytic and algebraic approaches. In this thesis we make a step in bridging this divide. We present an algorithm which uses discrete Riemann surfaces to approximate the Riemann matrix of any square-tileable translation surface. We apply our algorithm to specific examples of Jenkins-Strebel representatives, a dense family of translation surfaces, leading to several conjectures about their underlying algebraic curves. We also study two-dimenstional linear spaces of symmetric matrices, addressing questions motivated by algebraic statistics and optimization. These spaces have many properties determined by their Segre symbols, which also provide a stratification of the ambient Grassmannian.

MAME

(for mom)

Contents

List of Figures

List of Tables

Acknowledgments

First and foremost, I would like to express my deepest gratitude to my advisor Bernd Sturmfels, whose guidance and support have been invaluable in the last five years. Bernd, I am continually impressed and inspired by your visionary approach to research, your boundless energy, generosity with your time, and unwavering enthusiasm for our field. It is a privilege to have been mentored by someone of your caliber, and I consider myself incredibly lucky to be part of the wonderful community you have created. Your dedication to both your students and the advancement of mathematics is truly special and sets a standard that I aspire to emulate in my own career.

Thank you also to my other collaborators: Simonetta Abenda, Daniele Agostini, Türkü Özlüm Çelik, Yassine El Maazouz, Sam Fairchild, Claudia Fevola, Dmitrii Pavlov, and Lizzie Pratt. I am lucky to have enjoyed every single one of my collaborations very much. I have learned so much from working with each of you, and have had a lot of fun discovering new math together. I hope I get many opportunities to work with you again.

I am grateful to Lauren Williams, Sam Fairchild, Daniele Agostini and other professors that have supported my career, especially by inviting me to speak at seminars or writing me letters of recommendation for my various applications. Your belief in my work has been instrumental in shaping my academic trajectory. The experiences have not only enhanced my confidence but have also fostered a sense of belonging within the broader mathematical community. Thank you especially to Daniele for adopting me as an almost student of yours and supporting me as if I were one. Many thanks to my dissertation committee for taking the time to read this thesis and give me feedback.

I spent a large fraction of my PhD at MPI MiS in Leipzig - thank you to my colleagues and friends in Germany who truly made it a second home for me. I am extremely grateful for the time I got to spend forming relationships with you. A special thank you to Mirke, Saskia, and Heike for making everything so smooth and helping me navigate German bureaucracy.

Thank you to my US friends - whether in the Bay Area, Seattle, Boston, or NYC - I am grateful for the ways that your friendship has enriched my life, whether through hiking, climbing, foraging escapades, making hot pot, sharing book recommendations, or strolling around some city. I appreciate your company in this special time of my life.

Finally, thank you to my family for your support and unconditional love. To my grandpa Yasha for being my very first math teacher. To my mom for being my second one, and for inspiring and supporting me in ways that only someone like you could. Thanks dad for teaching me Gaussian elimination - you were the first to predict the importance of linear algebra to my life. Thank you Olya for being my role model. I am honored and proud to be mixed up with you so often. You inspire me to try new things and make me believe that anything is possible. Thank you Andrei for being my first math student and a source of joy since you were born. I am so lucky I got to grow up with you all as my family. Last but not least, thank you Alex for your support and love while I worked on my PhD, surpassing anything I could have imagined. I cannot express how much your enthusiasm and willingness to embark on adventures together means to me.

Chapter 1

Background and introduction

1.1 Overview and contributions

This thesis is divided into three main parts. Part I, consisting of Chapters 2 and 3, focuses on the connections between algebraic curves and integrable systems. Part II, consisting of Chapters 4 and 5, explores Grassmannians and positive geometry through the lens of computation and algebraic geometry. Finally, Part III, consisting of Chapters 6 and 7, highlights computation in algebraic geometry while revisiting classical results.

In Chapter 1 (the current chapter), I present some of the preliminary material that is necessary for the research presented in the rest of the thesis. Though future chapters may refer to definitions or ideas presented anywhere in this chapter, Section 1.2 is particularly relevant for Chapters 2, 3, and 6, while Section 1.3 is more relevant for Chapters 4 and 5.

Part I of this thesis regards the interplay between algebraic geometry and integrable systems, central to which is the Kadomtsev-Petviashvili (KP) equation. This is a nonlinear partial differential equation whose solution function represents the amplitude of a shallow water wave. Krichever provided an algebro-geometric procedure to construct a KP solution from a point on a complex algebraic curve [78]. We study KP solutions whose underlying algebraic curves undergo tropical degenerations. The curve in the limit becomes singular with possibly many irreducible components. Through a tropical degeneration, the limiting object can be described entirely combinatorially, and we use such combinatorial data to perform a degeneration also at the level of the KP solution. We show that this procedure gives rise to solitons, a subset of KP solutions that have been proven to have a fascinating connection with the theory of total positivity for the Grassmannian [74].

Chapter 2 is based on the paper [7], joint with Daniele Agostini, Claudia Fevola, and Bernd Sturmfels. In it we describe and introduce the degenerations at the level of curves, Riemann theta functions, and KP solutions. We introduce the Hirota variety, which is a space parameterizing soliton solutions to the KP equation associated with a nodal curve. We find its defining equations and characterize the Hirota variety for some examples. We also present some computational results. Certain Riemann-Roch spaces on a curve X are

encoded as points on the Sato Grassmannian. Following [91], we present an algorithm and its `Maple` implementation for computing these points and the resulting tau functions, for X hyperelliptic. We also present an algorithm for obtaining KP solitons explicitly from nodal rational curves.

In Chapter 3, we continue the thread of KP solutions from nodal curves, but we narrow our focus to irreducible rational nodal curves, and we study their Hirota varieties in detail. In this case, the Riemann theta function, in the limit $\epsilon \to 0$, is supported on the g-dimensional cube $\mathcal{C} = \{0,1\}^g$. Of particular interest is the irreducible subvariety of the Hirota variety defined as the image of a parameterization map, which we call the main component. Proving that this is an irreducible component of the Hirota variety corresponds to solving a classical problem in algebraic geometry, namely the weak Schottky problem for rational nodal curves. We conjecture a solution that we prove up to genus nine using computational tools. Finally, we study the equations of the main component of the Hirota variety and how they relate to the combinatorics of the cube. We conclude the chapter with a more explicit discussion on the Schottky problem for irreducible rational nodal curves. This chapter is based on the publication [45] which is joint work with Claudia Fevola.

In Part II, we shift our focus to Grassmannians and positive geometry. We open with Chapter 4, which presents some preliminary results from ongoing work with Yassine El Maazouz. In it we study the positive part of the orthogonal Grassmannian $\mathrm{OGr}_{\geq 0}(k, n)$. The definition of the orthogonal Grassmannian depends on a choice of a symmetric quadratic form. Previous work on the positive orthogonal Grassmannian ([53, 66, 67]) has focused on only one such choice, and only on the positive orthogonal Grassmannian $\mathrm{OGr}_{\geq 0}(n, 2n)$. In this chapter, we study the positive orthogonal Grassmannian for quadratic forms with arbitrary signature given by (p, q). We present some results for $\mathrm{OGr}_{\geq 0}^{(p,q)}(n, 2n)$ for arbitrary (p, q), and we completely characterize the positive orthogonal Grassmannian $\mathrm{OGr}_{\geq 0}^{p,q}(1, n)$, in particular showing that it is a positive geometry, as predicted by physicists in [66].

In Chapter 5, based on [85], joint with Dmitrii Pavlov and Elizabeth Pratt, we study Grasstopes. A Grasstope is the image of the totally nonnegative Grassmannian $\mathrm{Gr}_{\geq 0}(k, n)$ under a linear map $\mathrm{Gr}(k, n) \dashrightarrow \mathrm{Gr}(k, k + m)$. This is a generalization of the amplituhedron, a geometric object of great importance to calculating scattering amplitudes in physics. The amplituhedron is a Grasstope arising from a totally positive linear map, that is, one whose representative matrix is totally positive. While amplituhedra are relatively well-studied and a point of major focus in the emerging field of positive geometry, much less is known about general Grasstopes. We study Grasstopes in the $m = 1$ case and show that they can be characterized as unions of cells of a hyperplane arrangement satisfying a certain sign variation condition, extending work in [72]. Inspired by this characterization, we also suggest a notion of a Grasstope arising from an arbitrary oriented matroid.

Finally, in Part III we revisit classical problems using modern techniques with an emphasis on computation. Chapter 6 is based on the classical equivalence of Riemann surfaces and algebraic curves. This equivalence, due to Riemann, leaves a divide between the analytic and the algebraic in the sense that it does not give a recipe for explicitly translating one to the other. This becomes transcendental as connecting a Riemann surface to an algebraic

curve utilizes Riemann theta functions. In this chapter, we use the theory of discrete Riemann surfaces to give an algorithm for approximating the Jacobian variety of a translation surface whose polygon can be decomposed into squares. We first implement the algorithm in the case of L-shaped polygons where the algebraic curve is already known. We also ,implement the algorithm in any genus for specific examples of Jenkins-Strebel representatives, a dense family of translation surfaces that, until now, lived squarely on the analytic side of the transcendental divide between Riemann surfaces and algebraic curves. Using Riemann theta functions, we give numerical experiments and resulting conjectures up to genus 5. This chapter is based on [26], which is joint work with Türkü Özlüm Çelik and Sam Fairchild.

Chapter 7 begins by revisiting the history of the study of pencils of quadrics, or two-dimensional linear subspaces in the space $\mathbb{S}^n$ of (real or complex) symmetric $n \times n$ matrices, according to the classification by Segre symbols [65], addressing questions motivated by algebraic statistics and optimization. We begin with a linear algebra perspective on Theorem 7.1.1 of Weierstrass and Segre. We denote by $\mathcal{L}^{-1}$ the set of the inverses of all invertible matrices in a pencil $\mathcal{L}$. Its closure in $\mathbb{P}(\mathbb{S}^n)$ is a projective curve, called the reciprocal curve and denoted $\mathbb{P}\mathcal{L}^{-1}$. We prove that, when $\mathcal{L}$ is nonsingular, $\mathbb{P}\mathcal{L}^{-1}$ is a rational normal curve. We express its degree in terms of the Segre symbol of the pencil and determine its prime ideal. This chapter is based on [46], which is joint with Claudia Fevola and Bernd Sturmfels.

Although there is a natural division in topics among the chapters in this thesis, there are many themes that are shared among the different chapters and parts. In particular, the work done in Part II with Grassmannians has a clear connection with Part I in that the Grassmannian, and especially the positive Grassmannian, plays a role in finding solutions to the KP equation ([74]). In [1], the authors associate to a given positroid cell (i.e. family of KP soliton solutions) a degenerate M-*curve*, that is a curve with the maximum possible number of disjoint real components. There is considerable overlap between the soliton solutions resulting from our approach in Part I and approaches directly from the positive Grassmannian, and a direct link is undoubtedly waiting to be discovered. Tools coming from the computational study of curves in Chapter 6 promise to help us understand curves, in particular M-curves, as well as the Schottky problem, more deeply. We hope that as the reader studies the material in the ostensibly unrelated chapters, she will find that tools and ideas learned from one area of mathematics can play unexpectedly important roles in the other areas pursued. In this dissertation, we collect a wealth of knowledge about subjects including curves, theta functions, Grassmannians, positivity, and computation with the expectation that these will continue to come together in beautiful ways yet to be discovered.

1.2 Algebraic curves, theta functions, and the Schottky problem

An algebraic curve is an algebraic variety of dimension one. Any such variety, if contained in a projective space, is birationally equivalent via projection to a projective plane curve,

that is a variety given as the zero set of a homogeneous polynomial in three variables. The uniformization theorem, dating back to the time of Riemann, states that an algebraic curve is equivalent to a compact Riemann surface, or a compact one-dimensional complex manifold. See Figure 1.1 for an example. On the left, it is drawn as the real part of the zero set of the homogeneous polynomial $y^2 z - x^3 - 7z^3$. Dehomogenized with respect to z it can be drawn in the affine plane as the zero set of $y^2 - x^3 - 7$. On the right is a complex (analytic) picture.
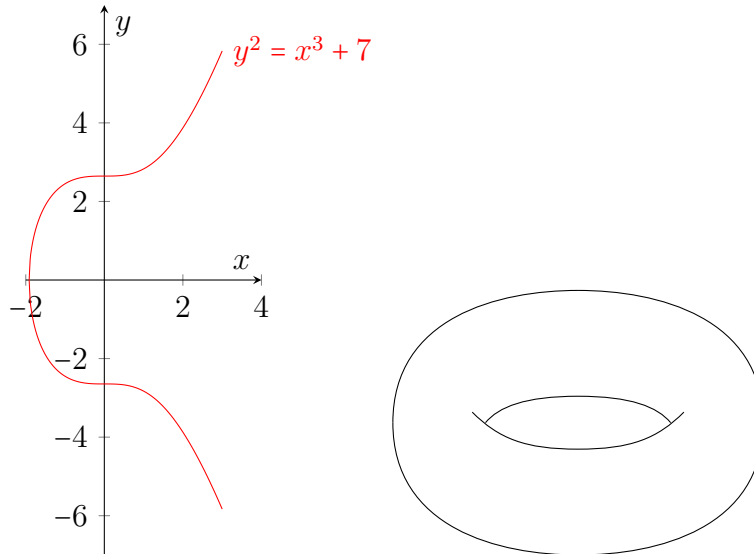
Figure 1.1: A genus one (elliptic) curve, algebraic (left) and analytic (right).

Among central objects underlying the connection between the analytic and algebraic side of this object are *theta functions*. These are complex-valued functions

$$\theta(\mathbf{z} \mid \tau) \;=\; \sum_{\mathbf{n} \in \mathbb{Z}^g} \exp\left(\pi i \mathbf{n}^T \tau \mathbf{n} + \mathbf{n}^T \mathbf{z}\right) \tag{1.1}$$

where τ is a *Riemann matrix*, a square matrix that encodes the topological and geometric properties of the curve.

The Riemann matrix is obtained as follows. Let $\mathcal{C}$ be a complex smooth algebraic curve of genus g. The space $\mathrm{H}^0(\mathcal{C}, \Omega_{\mathcal{C}}^1)$, of holomorphic differential one-forms on $\mathcal{C}$ has dimension g, and $\mathrm{H}_1(\mathcal{C}, \mathbb{Z})$ is a free abelian group with $2g$ generators. Let $\alpha_1, \ldots, \alpha_g, \beta_1, \ldots, \beta_g$ be a symplectic basis of $\mathrm{H}_1(\mathcal{C}, \mathbb{Z})$ and let $\omega_1, \ldots, \omega_g$ be a basis of $\mathrm{H}^0(\mathcal{C}, \Omega_{\mathcal{C}}^1)$.

The *period matrix* is the $g \times 2g$ matrix:

$$(\tau_1 \mid \tau_2) := \left(\left(\int_{\alpha_i} \omega_j\right) \middle| \left(\int_{\beta_i} \omega_j\right)\right) \tag{1.2}$$

and $\tau := \tau_1^{-1} \tau_2$ is called a *Riemann matrix* of the algebraic curve $\mathcal{C}$. Riemann showed that, for any choice of symplectic basis of $\mathrm{H}_1(\mathcal{C}, \mathbb{Z})$, there exists a choice of basis of holomorphic

differentials $\omega_1, \ldots, \omega_g$ such that the resulting Riemann matrix lies in the set of $g \times g$ symmetric matrices with positive definite imaginary part with complex entries. This set is known as the *Siegel upper half space* $\mathbb{H}_g$.

Not every matrix in $\mathbb{H}_g$ is a Riemann matrix: the *Schottky problem* (Problem 1.2.1) asks to determine the locus of Riemann matrices as a subset of $\mathbb{H}_g$. Below we will develop the language to define the Schottky problem more precisely.

The $2g$ columns of the period matrix $(\tau_1 | \tau_2)$ generate a lattice $\Lambda = \tau \cdot \mathbb{Z} \subset \mathbb{C}^g$. The Jacobian of the curve $\mathcal{C}$ is the abelian group defined as the quotient

$$\operatorname{Jac}(\mathcal{C}) := \mathbb{C}^g / \Lambda.$$

The Jacobian can also be defined independently of the choice of basis. Consider the map

$$\varphi : H_1(\mathcal{C}, \mathbb{Z}) \longrightarrow H^0(\mathcal{C}, \omega_{\mathcal{C}})^{\vee}$$
$$\gamma \longmapsto \left(\omega \mapsto \int_{\gamma} \omega \right),$$

which integrates holomorphic one-forms along one-cycles. The image of φ is a discrete lattice of maximal rank inside $H^0(\mathcal{C}, \omega_{\mathcal{C}})^{\vee}$. Therefore, the Jacobian can also be defined as the quotient by this lattice:

$$\operatorname{Jac}(\mathcal{C}) := H^0(\mathcal{C}, \omega_{\mathcal{C}})^{\vee} / H_1(\mathcal{C}, \mathbb{Z}).$$

The map which takes an algebraic curve to its Jacobian can be explicitly represented by a map which takes an algebraic curve to a Riemann matrix. It can also be written as a map on moduli spaces. Let $\mathcal{M}_g$ denote the moduli space of smooth algebraic curves of genus g and let $\mathcal{A}_g$ be the moduli space of principally polarized abelian varieties of dimension g. Formally, we have an isomorphism

$$\mathcal{A}_g \cong \mathcal{H}_g / \operatorname{Sp}(2g, \mathbb{Z}),$$

between $\mathcal{A}_g$ and the quotient of the Siegel upper half-space by the symplectic group with action defined by

$$\begin{pmatrix} E & F \\ G & H \end{pmatrix} \cdot B = (GB + H)^{-1}(EB + F).$$

Then, the *Torelli map*

$$J : \mathcal{M}_g \longrightarrow \mathcal{A}_g$$
$$\mathcal{C} \mapsto \operatorname{Jac}(\mathcal{C})$$

is a map of moduli spaces, mapping curves to Jacobians. Torelli's Theorem, states that the map J is injective, meaning that curves are identified up to isomorphism by their Jacobians. The map is, however, not surjective for $g > 3$, and one seeks to describe its image. The Schottky problem is a classical problem in algebraic geometry asking to characterize Jacobian varieties amongst all abelian varieties.

Problem 1.2.1 (Schottky Problem)**.** Find the defining equations for the locus of Jacobians, defined as the closure of $J(\mathcal{M}_g)$ in $\mathcal{A}_g$.

Problem 1.2.2 (Weak Schottky Problem)**.** Find defining equations for the locus of Jacobians, defined as the closure of $J(\mathcal{M}_g)$ in $\mathcal{A}_g$, up to extra irreducible components.

It is known that $\dim(\mathcal{M}_g) = 3g - 3$ and $\dim(\mathcal{A}_g) = \binom{g+1}{2}$. For $g \leq 3$ these dimensions coincide, so in these cases the Schottky problem is trivial, in the sense that essentially every polarized abelian variety is the Jacobian of a curve. For genus $g \geq 4$, one has a proper inclusion $J(\mathcal{M}_g) \subset \mathcal{A}_g$.

In the literature of the Schottky problem and the Torelli theorem, theta functions play a central role [61]. The *theta function with characteristic* $\varepsilon, \delta \in \{0,1\}^g$ is a complex-valued function defined on $\mathbb{C}^g \times \mathbb{H}_g$:

$$\theta\begin{bmatrix}\varepsilon\\\delta\end{bmatrix}(\mathbf{z}\,|\,\tau) \;=\; \sum_{\mathbf{n}\in\mathbb{Z}^g} \exp\left(\pi i \left(\mathbf{n}+\frac{\varepsilon}{2}\right)^T \tau\left(\mathbf{n}+\frac{\varepsilon}{2}\right) + \left(\mathbf{n}+\frac{\varepsilon}{2}\right)^T\left(\mathbf{z}+\frac{\delta}{2}\right)\right). \tag{1.3}$$

When $\varepsilon = \delta = 0$, this is exactly the *Riemann theta function* (1.1), and differs by an exponential factor from the latter. The characteristic is called even, and odd if $\varepsilon \cdot \delta \equiv 0, 1 \pmod 2$ respectively. So there are $2^{g-1}(2^g + 1)$ odd and $2^{g-1}(2^g + 1)$ even characteristics. For fixed τ, the values $\theta\begin{bmatrix}\varepsilon\\\delta\end{bmatrix}(\mathbf{0}\,|\,\tau)$ at $\mathbf{z} = \mathbf{0}$ are known as *theta constants*. We will also use the term theta constant for the evaluation of the derivatives of the theta function at $\mathbf{0}$, which we denote as follows:

$$\theta_{ij\ldots}^{\varepsilon,\delta} := \frac{\partial}{\partial z_i}\frac{\partial}{\partial z_j}\ldots\theta\begin{bmatrix}\varepsilon\\\delta\end{bmatrix}(\mathbf{z}\,|\,\tau)\Big|_{\mathbf{z=0}}. \tag{1.4}$$

When $g = 4$, the so-called Schotkky-Igusa modular form defines an analytic hypersurface [68, Theorem 1] in terms of theta functions, which describes the Schottky locus. For higher genera, the Schottky problem has proven to be hard, with only partial solutions so far (see [9, 68, 43, 6]). The only known solution to the Schottky problem was given by Shiota [100] through a connection with the KP equation (discussed in the next chapter), where fundamental objects are again the theta functions (1.3). A complete algebro-geometric solution is still missing.

Theta functions also play an important role in encoding geometric properties of the curve. For instance, the theta constants can determine (non)hyperellipticity of a curve. A curve is *hyperelliptic* if it admits a degree two cover of $\mathbb{P}^1$. This cover is often called the *hyperelliptic map*. As a plane curve, any hyperelliptic curve is the vanishing locus of a polynomial of the form

$$y^2 - h(x)y - f(x),$$

where h is a polynomial of degree $< g + 2$ and f has degree $2g + 1$ or $2g + 1$, for g the genus of the curve. In its simplest form, we may consider equations of the form $y^2 = f(x)$, and the

corresponding double cover of $\mathbb{P}^1$ is ramified at $\deg(f)$ points (i.e. the zeroes of f.) These are called the branch points of the hyperelliptic map.

For a hyperelliptic curve, the values of (1.4) give the branch points. In the case of non-hyperelliptic curves, (1.4) gives the so-called *multitangent hyperplanes* of the canonical model in $\mathbb{P}^{g-1}$. For instance, these are bitangent lines of smooth plane quartics in genus 3 or tritangent planes of smooth space sextics in genus 4. It has been proven that the odd theta characteristics recover its algebraic curve [23]. For explicit reconstructions the algebraic curve from their multitangent hyperplanes for small genera see [28, 27, 82, 83]. Mathematical software packages are available to compute with theta functions, such as [6, 32, 50, 54], which enable us to carry out experiments.

1.3 Grassmannians and positive geometry

The *real Grassmannian* $\mathrm{Gr}(k,n)$ is the variety parameterizing k-dimensional subspaces of an n-dimensional vector space $\mathbb{R}^n$. This can be identified with the variety of $(k-1)$-dimensional subspaces of an $(n-1)$-dimensional real projective space $\mathbb{P}^{n-1}$. A linear space, considered as an element of $\mathrm{Gr}(k,n)$, can be represented by a $k \times n$ matrix A whose rows span the space. However, as a choice of basis is not unique, one must view the Grassmannian as the space of $k \times n$ matrices modulo left multiplication by GL_k, to account for possible changes of basis. The Grassmannian $\mathrm{Gr}(k,n)$ can be realized as a subvariety of the projective space $\mathbb{P}^{\binom{n}{k}-1}$ via the *Plücker embedding*, which sends a matrix A representing an element in $\mathrm{Gr}(k,n)$ to the vector of its maximal minors, or determinants of its $k \times k$ submatrices. The maximal minors of A are called *Plücker coordinates*. We express the Plücker coordinate corresponding to a minor indexed by the set of columns $I \in \binom{[n]}{k}$ as p_I. This embedding does not depend on the choice of matrix representative for the vector space. As an algebraic variety, the Grassmannian is cut out by the *Plücker relations*, which are homogeneous equations describing the relationships between maximal minors of a $k \times n$ matrix. See Example 1.3.1 for a derivation in low dimensions.

Example 1.3.1. The Grassmannian $\mathrm{Gr}(2,4)$ parameterizes two-dimensional subspaces of $\mathbb{R}^4$. Each subspace can be represented by a 2×4 matrix A. In the generic case, we can row reduce it to look like

$$A = \begin{pmatrix} 1 & 0 & a & b \\ 0 & 1 & c & d \end{pmatrix}.$$

The Plücker embedding sends the matrix A to the point $(1 : c : -a : d : -b : ad - bc) \in \mathbb{P}^5$, where we order the points in reverse lexicographic order by minor indices. One can check that applying row operations to A will yield the same point in projective space under the Plücker embedding. Furthermore, it is clear that not every point in $\mathbb{P}^5$ can be obtained as the image of the Plücker map. The image consists exactly of the points $p = (p_{12} : p_{13} : p_{23} : p_{14} : p_{24} : p_{34})$ which satisfy $p_{12}p_{34} - p_{13}p_{24} + p_{14}p_{23} = 0$. In this way we have realized $\mathrm{Gr}(2,4)$ as a subvariety of $\mathbb{P}^5$.

The Plücker relations for general k, n can be derived analogously. They have the form

$$\sum_{l=1}^{k+1} (-1)^l p_{I \cup j_l} p_{J \setminus j_l} = 0,$$

with one relation for each pair of sets $I, J = \{j_1, \ldots j_{k+1}\}$ with $|I| = k - 1$ and $j_1 \le j_2 \le \cdots \le j_{k+1}$. The relations are not, in general, algebraically independent. For more details on the Grassmannian and the Plücker embedding see [88, Chapter 5].

The *totally nonnegative Grassmannian* $\mathrm{Gr}_{\ge 0}(k, n)$ is the subset of $\mathrm{Gr}(k, n)$ consisting of the elements whose non-zero Plücker coordinates all have the same sign [93, 114]. Each element in $\mathrm{Gr}_{\ge 0}(k, n)$ can be represented by a *totally nonnegative* $k \times n$ matrix, that is, by a matrix with nonnegative maximal minors. The *totally positive Grassmannian* $\mathrm{Gr}_{> 0}(k, n)$ is a subset of $\mathrm{Gr}(k, n)$ consisting of the elements whose Plücker coordinates are all non-zero and have the same sign. Elements of $\mathrm{Gr}_{> 0}(k, n)$ can be represented by $k \times n$ matrices with strictly positive maximal minors (such matrices are called *totally positive*).

Example 1.3.2 ($\mathrm{Gr}_{\ge 0}(2, 4)$)**.** The nonnegative Grassmannian $\mathrm{Gr}_{\ge 0}(2, 4)$ is a semialgebraic set in $\mathbb{P}^5$. In addition to the one Plücker relation, it is defined by the inequalities p_{12}, p_{13}, p_{14}, $p_{23}, p_{24}, p_{34} \ge 0$. In terms of the entries of a representative matrix A, as in Example 1.3.1, it is given by the inequalities $c, d \ge 0$, $a, b \le 0$, and $ad \ge bc$. If these equalities are changed to be strict, the resulting matrix will be totally positive.

Although the positive Grassmannian is not an algebraic variety, it possesses a remarkable amount of structure. Since its introduction by Postnikov in [93], it has been studied extensively and associated with numerous combinatorial objects. The role that positivity plays has yet to be completely understood, though the extent of beautiful mathematics that emerges from it suggests that there is something deep behind it. Since the introduction of the *amplituhedron* in [11], it has also become clear that positivity plays a very important role in some areas of physics. In recent years, physicists and mathematicians have begun to attempt to formalize this phenomenon, with the introduction of *positive geometry* [10].

Formally, a positive geometry is defined as a pair $(X, X_{\ge 0})$, where X is an irreducible complex projective variety of dimension d and $X_{\ge 0} \subset X$ is a full-dimensional semialgebraic set satisfying, in addition to some technical assumptions (listed in [10]), the following recursive conditions regarding the boundaries of $X_{\ge 0}$ and existence of a *canonical form*.

1. If $d = 0$ then $X = X_{\ge 0}$ consists of a single point with a 0-form $\Omega = \pm 1$, with sign dependent on the orientation of $X_{\ge 0}$

2. For $d > 0$, every boundary component $(C, C_{\ge 0})$ of $(X, X_{\ge 0})$ is a $(d - 1)$-dimensional positive geometry.

3. There exists a unique nonzero rational form Ω on X with singularities only on the boundary components, and with residue on C equal to the canonical form of $(C, C_{\ge 0})$ on each boundary component C.

The rather technical definition of a positive geometry attempts to capture important properties which make a space amenable to computations in physics. In a sense, the definition generalizes polytopes having faces of all dimensions, which are polytopes themselves. Indeed, polytopes are all positive geometries and it is fairly simple to write down their canonical forms. A less simple but still very important example of a positive geometry is the totally nonnegative Grassmannian as a subset of the Grassmannian [81]. Finding new examples of positive geometries is an interesting topic in its own right, since the existence of a canonical form satisfying the positive geometry axioms is a highly nontrivial property that is usually quite difficult to verify.

The currently accepted definition of a positive geometry unfortunately excludes some objects that one might believe intuitively "should" be included. Notably, a disk is not a positive geometry for the reason that it has no zero-dimensional boundary. This is may be unexpected since it can be approximated with arbitrary precision by polytopes, which are positive geometries. Furthermore, the interior of a disk can be thought of as the "positive part" of a space since it is defined by an inequality. General spectrahedra, which for similar reasons may be expected to be positive geometries, are also excluded. This suggests that the definition may need to be extended in order to include more objects that one might like to consider "positive."

Part I

Algebraic curves and integrable systems

Overview

This part of the dissertation is based on the papers "KP Solitons from Tropical Limits" [7] and a follow-up paper called "Hirota Varieties and Rational Nodal Curves" [45]. The former is joint work with Daniele Agostini, Claudia Fevola, and Bernd Sturmfels, and the latter is joint with Claudia Fevola.

In the interplay between integrable systems and algebraic geometry [1, 5, 38, 76, 78, 90, 91], the study of complex algebraic curves is connected to the *Kadomtsev-Petviashvili (KP) equation*

$$\frac{\partial}{\partial x}\left(4p_t - 6pp_x - p_{xxx}\right) = 3p_{yy}. \tag{1.5}$$

This is a heavily studied nonlinear partial differential equation for an unknown function p that describes the evolution of certain water waves. The value of the function $p(x, y, t)$ gives the height of a shallow water wave at space coordinates (x, y) and time t.

In the next two chapters, given a smooth complex algebraic curve, we write B for its Riemann matrix, which is normalized to have negative definite real part. Note that this is a slightly different normalization from the one used in Section 1.2. Their relationship is that $B = -i\tau$, where τ is the Riemann matrix from Section 1.2. The purpose of this is to emphasize real numbers and real solutions. One considers the associated Riemann theta function

$$\theta = \theta(\mathbf{z}\,|\,B) = \sum_{\mathbf{c}\in\mathbb{Z}^g} \exp\left[\frac{1}{2}\mathbf{c}^T B\mathbf{c} + \mathbf{c}^T\mathbf{z}\right]. \tag{1.6}$$

In a breakthrough result which combined previously disparate areas of mathematics [78], Krichever constructed g-phase solutions to the KP equation as follows. Let $\tau(x, y, t)$ be obtained from (1.6) by setting $\mathbf{z} = \mathbf{u}x + \mathbf{v}y + \mathbf{w}t$. Here, $\mathbf{u} = (u_1, \ldots, u_g)$, $\mathbf{v} = (v_1, \ldots, v_g)$, $\mathbf{w} = (w_1, \ldots, w_g)$ are coordinates on the weighted projective space $\mathbb{WP}^{3g-1}$ that is defined by

$$\deg(u_i) = 1, \ \deg(v_i) = 2, \ \deg(w_i) = 3 \quad \text{for } i = 1, 2, \ldots, g. \tag{1.7}$$

We require that the trivariate tau function $\tau(x, y, t)$ satisfies Hirota's differential equation

$$\tau\tau_{xxxx} - 4\tau_{xxx}\tau_x + 3\tau_{xx}^2 + 4\tau_x\tau_t - 4\tau\tau_{xt} + 3\tau\tau_{yy} - 3\tau_y^2 = 0. \tag{1.8}$$

Under this hypothesis, the following function satisfies (1.5), and we call it the *KP solution*:

$$p(x, y, t) = 2\frac{\partial^2}{\partial x^2}\log\tau(x, y, t). \tag{1.9}$$

The *Dubrovin threefold* associated to a curve studied in [5] comprises all points $(\mathbf{u}, \mathbf{v}, \mathbf{w})$ in $\mathbb{WP}^{3g-1}$ for which (1.8) holds. This space parameterizes solutions to the KP equation associated to a smooth curve, and is a variety of dimension 3. It has many interesting properties, and we refer the reader to [5] for a complete description as well as for a detailed explanation of Krichevers parameterization of KP solutions.

Our aim in this part of the thesis is to associate solutions of the KP equation to curves that are not smooth. To this end, we work with curves which have nodal singularities, and work to come up with analogs of objects such as theta functions and the Dubrovin threefold. In Chapter 2 we develop the tools required to do this, and introduce the *Hirota variety* associated to a family of nodal curves. In Chapter 3 we focus our attention on rational nodal curves and study their Hirota varieties in detail.

Chapter 2

KP solitons from nodal curves

2.1 Introduction

In order to study analogs of objects defined for smooth curves, we may think of a nodal curve as a smooth curve which is defined over a non-archimedean field $\mathbb{K}$ such as $\mathbb{Q}(\epsilon)$ or the Puiseux series $\mathbb{C}\{\{\epsilon\}\}$. This can be regarded as a family of smooth curves which degenerates as $\epsilon \to 0$. The Riemann matrix B_ϵ depends analytically on the parameter ϵ, and hence so do the tau function and the KP solution. For $\epsilon \to 0$, the function $p(x,y,t)$ becomes a soliton solution of the KP equation (1.5). One of our aims is to compute these degenerations and resulting KP solitons [1, 74] explicitly using computer algebra.

In the tropical limit, the infinite sum over $\mathbb{Z}^g$ in the theta function becomes a finite sum

$$\theta_{\mathcal{C}}(\mathbf{z}) \;=\; a_1 \exp[\,\mathbf{c}_1^T \mathbf{z}\,] \;+\; a_2 \exp[\,\mathbf{c}_2^T \mathbf{z}\,] \;+\; \cdots \;+\; a_m \exp[\,\mathbf{c}_m^T \mathbf{z}\,], \tag{2.1}$$

where $\mathcal{C} = \{\mathbf{c}_1, \mathbf{c}_2, \ldots, \mathbf{c}_m\}$ is a certain subset of the integer lattice $\mathbb{Z}^g$. Each lattice point $\mathbf{c}_i = (c_{i1}, \ldots, c_{ig})$ specifies a linear form $\mathbf{c}_i^T \mathbf{z} = \sum_{j=1}^g c_{ij} z_j$, just like in (1.6). The coefficients $\mathbf{a} = (a_1, a_2, \ldots, a_m)$ are unknowns that serve as coordinates on the algebraic torus $(\mathbb{K}^*)^m$.

Example 2.1.1 ($g = 2$). Consider a genus two curve $y^2 = f_i(x)$ where $f_i(x)$ is a polynomial of degree six with coefficients in $\mathbb{Q}(\epsilon)$. Here are two instances corresponding to Figures 2.1 and 2.2:

$$\begin{array}{rcl} f_1(x) & = & (x-1)(x-2\epsilon)(x-3\epsilon^2)(x-4\epsilon^3)(x-5\epsilon^4)(x-6\epsilon^5), \\ f_2(x) & = & (x-1)(x-1-\epsilon)(x-2)(x-2-\epsilon)(x-3)(x-3-\epsilon). \end{array} \tag{2.2}$$

Note that f_2 is an example of a degeneration as in [91, §7]. For any fixed $\epsilon \in \mathbb{C}^*$, we can compute the Dubrovin threefold in $\mathbb{WP}^5$, using [5, Theorem 3.7], and derive KP solutions from its points. The difficulty is to maintain ϵ as a parameter and to understand what happens for $\epsilon \to 0$.

As will be explained in detail in Example 2.3.3, one configuration in $\mathbb{Z}^2$ that arises here is the square $\mathcal{C} = \{(0,0), (1,0), (0,1), (1,1)\}$. In order for the associated theta function $\theta_{\mathcal{C}} = a_{00} + a_{10}\exp[z_1] + a_{01}\exp[z_2] + a_{11}\exp[z_1 + z_2]$ to yield a KP solution, the following three

polynomial identities are necessary and sufficient:

$$u_1^4 - 4u_1w_1 + 3v_1^2 = 0, \qquad ((u_1{+}u_2)^4 - 4(u_1{+}u_2)(w_1{+}w_2) + 3(v_1{+}v_2)^2)\, a_{00}a_{11}$$
$$u_2^4 - 4u_2w_2 + 3v_2^2 = 0, \qquad + ((u_1{-}u_2)^4 - 4(u_1{-}u_2)(w_1{-}w_2) + 3(v_1{-}v_2)^2)\, a_{01}a_{10} = 0.$$

If these conditions hold then $p(x, y, t)$ can be written as a $(2, 4)$-soliton by [74, §2.5]. The arguments and importance of this example will be made more precise in future sections.

This chapter is organized as follows. In Section 2.2 we review the derivation of tropical Riemann matrices. Theorem 2.2.3 characterizes degenerations of theta functions from algebraic curves over $\mathbb{K}$. Proposition 2.2.4 shows that $\mathcal{C}$ is the vertex set of a Delaunay polytope in $\mathbb{Z}^g$. In Section 2.3 we study the Hirota variety $\mathcal{H}_\mathcal{C}$, which lives in $(\mathbb{K}^*)^m \times \mathbb{WP}^{3g-1}$. A point $(\mathbf{a}, (\mathbf{u}, \mathbf{v}, \mathbf{w}))$ lies on the Hirota variety if and only if (1.8) holds for (2.1). We saw $\mathcal{H}_\mathcal{C}$ for $g = 2$ and $\mathcal{C} = \{0, 1\}^2$ in Example 2.1.1. Theorem 2.3.6 characterizes the Hirota variety of the g-simplex.

A key idea in this chapter is to never compute a Riemann matrix or the theta function (1.6). Instead we follow the approach in [76, 90, 91] that rests on the Sato Grassmannian (Theorem 2.4.2). This setting is entirely algebraic and hence amenable to symbolic computation over $\mathbb{K}$. Section 2.4 explains the computation of tau functions from points on the Sato Grassmannian.

In Section 2.5 we start from an algebraic curve X over $\mathbb{K}$. Certain Riemann-Roch spaces on X are encoded as points on the Sato Grassmannian. Following [91], we present an algorithm and its `Maple` implementation for computing these points and the resulting tau functions, for X hyperelliptic. Proposition 2.5.5 addresses the case when X is reducible. This is followed up in Section 2.6, where we present Algorithm 2.6.2 for KP solitons from nodal rational curves.

There is a substantial body of literature on the connection between the KP equation and algebraic geometry: see for example [1, 38, 74, 76, 78, 91, 90]. Some of what follows below has appeared elsewhere in a different language. We conclude the introduction with what we see as the three main new results presented in this chapter: the degeneration of the theta functions via Delaunay polytopes in Theorem 2.2.3 and the equations for the corresponding Hirota varieties in Corollary 2.3.2, the Gröbner basis for the Hirota variety of the simplex in Theorem 2.3.6, and the explicit method for computing soliton solutions from nodal rational curves in Algorithm 2.6.2.

2.2 Tropical curves and Delaunay polytopes

We work over a field $\mathbb{K}$ of characteristic zero with a non-archimedean valuation. Let X be a *Mumford curve* of genus g, that is, X is a smooth curve over $\mathbb{K}$ whose Berkovich analytification is a graph with g cycles. This metric graph is the tropicalization $\mathrm{Trop}(X)$ of a faithful embedding of X. In spite of the recent advances in [69], computing $\mathrm{Trop}(X)$ from X remains a nontrivial task. All our examples were derived with methods described in [21].

If the curve X is hyperelliptic, given by an equation $y^2 = f(x)$, then $\text{Trop}(X)$ is a metric graph with a harmonic two-to-one map onto the phylogenetic tree encoding the roots of $f(x)$. The combinatorics of harmonic maps is subtle. We refer to [19, Definition 2.2] for an explanation.

Example 2.2.1 ($g = 2$). Let $f(x)$ be of degree six. The six roots determine a subtree with six leaves in the Berkovich line. The edge lengths are invariants of the semistable model [21] over the valuation ring of $\mathbb{K}$. There are two combinatorial types of trivalent trees with six leaves: the *caterpillar* and the *snowflake*. These are realized by the two polynomials in Example 2.1.1.
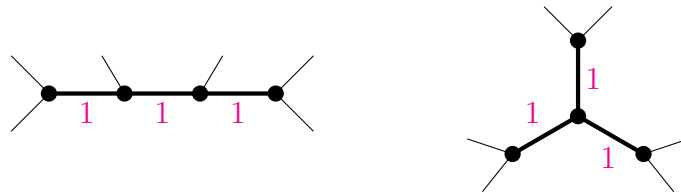
Figure 2.1: The metric trees defined by the polynomials f_1 (left) and f_2 (right) in (2.2)

Each trivalent metric tree with $2g + 2$ leaves has a unique hyperelliptic covering by a metric graph of genus g. It is found as follows. Every edge e of the tree will either have one edge or two edges lying above it in the graph. The two cases are distinguished by cutting the tree at e. If the two components remaining have an even number of leaves each, then the edge e has two edges above it in the graph. If the two components have an odd number of leaves each, then the edge does not split. A vertex in the tree can either have one or two vertices lying above it as well. If a vertex has either a leaf or an edge that does not split, then the vertex does not split. If the vertex is only adjacent to edges that do split, then the vertex splits. Then there is a unique way to build a metric graph satisfying the above. This is the content of [19, Lemma 2.4]. The edge lengths of the resulting genus g graph are obtained from those of the tree by stretching or shrinking with a factor of 2, depending on whether the edge split. See Example 2.2.2. Figure 2.2 shows the graphs that give a two-to-one map to the trees in Figure 2.1.
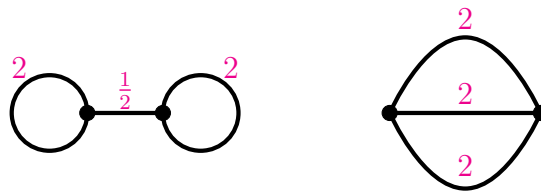
Figure 2.2: The metric graphs $\text{Trop}(X)$ for the curves X in Example 2.1.1 and Figure 2.1

Example 2.2.2. We show how to obtain the metric graph $\mathrm{Trop}(X)$ for the snowflake in Figure 2.2. Following the procedure described above, we find that for each edge of the snowflake, the two components obtained by cutting at the edge both have an even number of leaves, so each edge splits. The three outside vertices have leaves, so they do not split, while the middle vertex splits. Figure 2.3 shows the resulting metric graph, lying above the snowflake. The edges above the edges which split each have the same length. When every pair of edges connected to a degree two vertex is replaced with a single edge whose edge length is the sum of the original two edges, the result is exactly the metric graph in Figure 2.2.
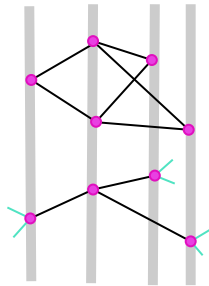
Figure 2.3: The metric graph on the right of Figure 2.2 covers the snowflake of Figure 2.1 by bending at the "elbows" as shown.

From the tropical curve $\mathrm{Trop}(X)$ we can read off the tropical Riemann matrix Q. This is a positive definite real symmetric $g \times g$ matrix. Fix a basis of cycles in $\mathrm{Trop}(X)$ and write them as the g rows of a matrix Λ whose columns are labeled by the edges. Let Δ be the diagonal matrix whose entries are the edge lengths of $\mathrm{Trop}(X)$. Then we have $Q = \Lambda \Delta \Lambda^T$.

The genus two graphs in Figure 2.2 have three edges. Their Riemann matrices are

$$Q_1 = \begin{bmatrix} 1 & 0 & 0 \\ 0 & 0 & 1 \end{bmatrix} \begin{bmatrix} 2 & 0 & 0 \\ 0 & \frac{1}{2} & 0 \\ 0 & 0 & 2 \end{bmatrix} \begin{bmatrix} 1 & 0 \\ 0 & 0 \\ 0 & 1 \end{bmatrix} = \begin{bmatrix} 2 & 0 \\ 0 & 2 \end{bmatrix} \quad \text{and} \quad Q_2 = \begin{bmatrix} 1 & -1 & 0 \\ 0 & 1 & -1 \end{bmatrix} \begin{bmatrix} 2 & 0 & 0 \\ 0 & 2 & 0 \\ 0 & 0 & 2 \end{bmatrix} \begin{bmatrix} 1 & 0 \\ -1 & 1 \\ 0 & -1 \end{bmatrix} = \begin{bmatrix} 4 & -2 \\ -2 & 4 \end{bmatrix}.$$

We now consider the degeneration of our curve X over $\mathbb{K} = \mathbb{C}\{\{\epsilon\}\}$ to its tropical limit. The Riemann matrix can be written in the form $B_\epsilon = -\frac{1}{\epsilon}Q + R(\epsilon)$, where $R(\epsilon)$ is a symmetric $g \times g$ matrix whose entries are complex analytic functions in ϵ that converge as $\epsilon \to 0$.

Fix a point $\mathbf{a} \in \mathbb{R}^g$. Replacing $\mathbf{z}$ by $\mathbf{z} + \frac{1}{\epsilon}Q\mathbf{a}$ in the Riemann theta function (1.6), we obtain

$$\theta\left(\mathbf{z} + \frac{1}{\epsilon}Q\mathbf{a} \,\middle|\, B_\epsilon\right) = \sum_{\mathbf{c} \in \mathbb{Z}^g} \exp\left[-\frac{1}{2\epsilon}\mathbf{c}^T Q\mathbf{c} + \frac{1}{\epsilon}\mathbf{c}^T Q\mathbf{a}\right] \cdot \exp\left[\frac{1}{2}\mathbf{c}^T R(\epsilon)\mathbf{c} + \mathbf{c}^T \mathbf{z}\right]. \tag{2.3}$$

This expression converges for $\epsilon \to 0$ provided $\mathbf{c}^T Q\mathbf{c} - 2\mathbf{c}^T Q\mathbf{a} \geq 0$ for all $\mathbf{c} \in \mathbb{Z}^g$. Equivalently,

$$\mathbf{a}^T Q\mathbf{a} \leq (\mathbf{a} - \mathbf{c})^T Q(\mathbf{a} - \mathbf{c}) \quad \text{for all } \mathbf{c} \in \mathbb{Z}^g. \tag{2.4}$$
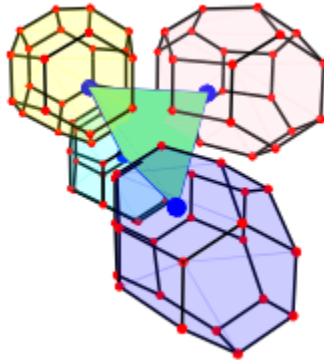
Figure 2.4: A Delaunay polytope and Voronoi cells associated to its vertices.

This means that the distance from $\mathbf{a}$ to the origin, in the metric given by Q, is at most the distance to any other lattice point $\mathbf{c} \in \mathbb{Z}^g$. In other words, (2.4) means that $\mathbf{a}$ belongs to the *Voronoi cell* for Q. Under this hypothesis, we now consider the associated *Delaunay set*

$$\mathcal{D}_{\mathbf{a},Q} = \left\{ \mathbf{c} \in \mathbb{Z}^g : \mathbf{a}^T Q \mathbf{a} = (\mathbf{a} - \mathbf{c})^T Q (\mathbf{a} - \mathbf{c}) \right\}. \tag{2.5}$$

This is the set of vertices of a polytope in the Delaunay subdivision of $\mathbb{Z}^g$ induced by Q. If $\mathbf{a}$ is a vertex of the Voronoi cell then the Delaunay polytope $\mathrm{conv}(\mathcal{D}_{\mathbf{a},Q})$ is g-dimensional. See Figure 2.4 for an example of a Delaunay polytope and its surrounding Voronoi cells. The Delaunay polytope in the figure is given by the green tetrahedron. The four colored permutohedra should be thought of as being glued together, they are Voronoi cells with tetrahedra as corresponding Delaunay cells.

As in [4, §4], we observe that $\exp\left[-\frac{1}{2\epsilon}\mathbf{c}^T Q \mathbf{c} + \frac{1}{\epsilon}\mathbf{c}^T Q \mathbf{a}\right]$ converges to 1 for $\mathbf{c} \in \mathcal{D}_{\mathbf{a},Q}$ and to 0 for $\mathbf{c} \in \mathbb{Z}^g \backslash \mathcal{D}_{\mathbf{a},Q}$. We have thus derived the following generalization of [4, Theorem 4]:

Theorem 2.2.3. *Fix a point $\mathbf{a}$ in the Voronoi cell of the tropical Riemann matrix Q. For $\epsilon \to 0$, the series (2.3) converges to a theta function (2.1) supported on the Delaunay set $\mathcal{C} = \mathcal{D}_{\mathbf{a},Q}$, namely*

$$\theta_{\mathcal{C}}(\mathbf{x}) = \sum_{\mathbf{c} \in \mathcal{C}} a_{\mathbf{c}} \exp\left[\mathbf{c}^T \mathbf{z}\right], \quad \text{where} \quad a_{\mathbf{c}} = \exp\left[\frac{1}{2}\mathbf{c}^T R(0)\mathbf{c}\right]. \tag{2.6}$$

The Delaunay polytope $\mathrm{conv}(\mathcal{C})$ can have any dimension between 0 and g, depending on the location of $\mathbf{a}$ in the Voronoi cell (2.4). If $\mathbf{a}$ lies in the interior then $\mathcal{C} = \{\mathbf{0}\}$ is just the origin. We are most interested in the case when $\mathbf{a}$ is a vertex of the Voronoi cell, and we now assume this to be the case. This ensures that $\mathcal{C}$ is the vertex set of a g-dimensional Delaunay polytope. For fixed g, there is only a finite list of Delaunay polytopes, up to lattice isomorphism. Thanks to [40] and its references, that list is known for $g \le 6$. However, not every Delaunay polytope arises from a curve X and its tropical Riemann matrix $Q = \Lambda \Delta \Lambda^T$. To illustrate these points, we present the list of all relevant Delaunay polytopes for $g \le 4$.

Proposition 2.2.4. *The complete list of Delaunay polytopes $\mathcal{C}$ arising from metric graphs for $g \leq 4$ is as follows. For $g = 2$ there are two types: triangle and square. For $g = 3$ there are five types: tetrahedron, square-based pyramid, octahedron, triangular prism and cube. For $g = 4$ there are 17 types. These $\mathcal{C}$ have between 5 and 16 vertices. They are listed in Table 2.1.*

Proof. For any edge e of the graph, let $\lambda_e \in \mathbb{Z}^g$ be the associated column of Λ. The Voronoi cell is a zonotope, obtained by summing line segments parallel to λ_e for all e. It has **a** as a vertex. After reorienting edges, in the corresponding expression of **a** as a linear combination of the vectors λ_e, all coefficients are positive. This means that the Delaunay polytope equals

$$\mathrm{conv}(\mathcal{C}) \quad = \quad \left\{ \mathbf{c} \in \mathbb{R}^g : 0 \leq \lambda_e^T \mathbf{c} \leq 1 \text{ for all edges } e \right\}. \tag{2.7}$$

Our task is to classify the polytopes (2.7) for all graphs of genus g and all their orientations. For $g = 2$ this is easy, and for $g = 3$ it was done in [4, Theorem 4]. We see from [4, Figure 2] that every Delaunay polytope can be realized by a curve over $\mathbb{K}$. For $g = 4$ we started from the classification of 19 Delaunay polytopes in [41, Theorem 6.2], labeled $1, 2, \ldots, 16$ in [41, Table V] and labeled A,B,C in [41, Table VI]. Two types do not arise from graphs, namely the pyramid over the octahedron (#B) and the cross polytope (#C). The other 17 Delaunay polytopes all arise from graphs. They are listed in Table 2.1. The second row gives the number of vertices. The third row gives the number of facets. These two numbers uniquely identify the isomorphism type of $\mathcal{C}$. The last row indicates which graphs give rise to that Delaunay polytope. We refer to the 16 graphs of genus 4 by the labeling used in [30, Table 1]. Table 2.1 was constructed by a direct computation. It establishes the $g = 4$ case in Proposition 2.2.4. $\square$

polytopes	1	2	3	4	5	6	7	8	9	10	11	12	13	14	15	16	A
vertices	5	6	7	7	8	8	8	9	9	9	10	10	10	12	12	16	6
facets	5	6	6	8	7	9	6	7	9	6	7	12	10	7	10	8	9
graphs	1,2,3,4 5,7,10,13	1,3,4 5,6,9	3,7,10	4	7	5	8,11,15	6	10	12	11	9	13	12	15	16	2

Table 2.1: The 17 Delaunay polytopes that arise from the 16 graphs of genus 4. Polytopes are labeled as in [41, Tables V and VI] and graphs are labeled as in [30, Table 1]. For instance, the complete bipartite graph $K_{3,3}$ is #2, and it has two Delaunay polytopes, namely the simplex (#1) and the cyclic 4-polytope with 6 vertices (#A). The polytope #3 has 7 vertices and 6 facets. It is the pyramid over the triangular prism, and it arises from three graphs (#3,7,10).

2.3 Hirota varieties

Starting from the theta function of the configuration $\mathcal{C}$ in (2.1), we consider the tau function

$$\tau(x,y,t) \;=\; \theta_{\mathcal{C}}(\mathbf{u}x + \mathbf{v}y + \mathbf{w}t) \;=\; \sum_{i=1}^{m} a_i \exp\left[\Big(\sum_{j=1}^{g} c_{ij}u_j\Big) x + \Big(\sum_{j=1}^{g} c_{ij}v_j\Big) y + \Big(\sum_{j=1}^{g} c_{ij}w_j\Big) t\right].$$

The *Hirota variety* $\mathcal{H}_{\mathcal{C}}$ consists of all points $\big(\mathbf{a},(\mathbf{u},\mathbf{v},\mathbf{w})\big)$ in the parameter space $(\mathbb{K}^*)^m \times \mathbb{WP}^{3g-1}$ for which $\tau(x,y,t)$ satisfies Hirota's differential equation (1.8). Thus $\mathcal{H}_{\mathcal{C}}$ is an analogue to the Dubrovin threefold [5] for the classical Riemann theta function of a smooth curve.

We recall from [74, equation (2.25)] that (1.8) can be written via the Hirota differential operators as $P(D_x, D_y, D_t)\tau \bullet \tau = 0$, for the special polynomial $P(x,y,t) = x^4 - 4xt + 3y^2$. For any fixed index j, the equation $P(u_j, v_j, w_j) = 0$ defines a curve in the weighted projective plane $\mathbb{WP}^2$. More generally, for any two indices k, ℓ in $\{1,\ldots,m\}$, we consider the hypersurface in $\mathbb{WP}^{3g-1}$ defined by

$$P_{k\ell}(\mathbf{u},\mathbf{v},\mathbf{w}) \;:=\; P\big((\mathbf{c}_k - \mathbf{c}_\ell)\cdot\mathbf{u},\; (\mathbf{c}_k - \mathbf{c}_\ell)\cdot\mathbf{v},\; (\mathbf{c}_k - \mathbf{c}_\ell)\cdot\mathbf{w}\big).$$

This expression is unchanged if we switch k and ℓ. The defining equations of the Hirota variety $\mathcal{H}_{\mathcal{C}}$ can be obtained from the following lemma, which is proved by direct computation.

Lemma 2.3.1. *The result of applying the differential operator (1.8) to the function $\tau(x,y,t)$ equals*

$$\sum_{1\leq k < \ell \leq m} a_k a_\ell\, P_{k\ell}(\mathbf{u},\mathbf{v},\mathbf{w}) \exp\left[\big((\mathbf{c}_k + \mathbf{c}_\ell)\cdot\mathbf{u}\big) x + \big((\mathbf{c}_k + \mathbf{c}_\ell)\cdot\mathbf{v}\big) y + \big((\mathbf{c}_k + \mathbf{c}_\ell)\cdot\mathbf{w}\big) t \right]. \qquad (2.8)$$

The polynomials defining the Hirota variety of $\mathcal{C}$ are the coefficients we obtain by writing (2.8) as a linear combination of distinct exponentials. These correspond to points in the set

$$\mathcal{C}^{[2]} \;=\; \big\{\, \mathbf{c}_k + \mathbf{c}_\ell \;:\; 1 \leq k < \ell \leq m \,\big\} \quad \subset \; \mathbb{Z}^g.$$

A point $\mathbf{d}$ in $\mathcal{C}^{[2]}$ is *uniquely attained* if there exists precisely one index pair (k,ℓ) such that $\mathbf{c}_k + \mathbf{c}_\ell = \mathbf{d}$. In that case, (k,ℓ) is a *unique pair*, and this contributes the quartic $P_{k\ell}(\mathbf{u},\mathbf{v},\mathbf{w})$ to our defining equations. If $\mathbf{d} \in \mathcal{C}^{[2]}$ is not uniquely attained, then the coefficient we seek is

$$\sum_{\substack{1\leq k < \ell \leq m \\ \mathbf{c}_k + \mathbf{c}_\ell = \mathbf{d}}} P_{k\ell}(\mathbf{u},\mathbf{v},\mathbf{w})\, a_k a_\ell. \qquad (2.9)$$

Corollary 2.3.2. *The Hirota variety $\mathcal{H}_{\mathcal{C}}$ is defined by the quartics $P_{k\ell}$ for all unique pairs (k,ℓ) and by the polynomials (2.9) for all non-uniquely attained points $\mathbf{d} \in \mathcal{C}^{[2]}$. If all points in $\mathcal{C}^{[2]}$ are uniquely attained then $\mathcal{H}_{\mathcal{C}}$ is defined by the $\binom{m}{2}$ quartics $P_{k\ell}(\mathbf{u},\mathbf{v},\mathbf{w})$, so its equations do not involve the coefficients $a_1,\ldots,a_m$. This is the case when $\mathcal{C}$ is the vertex set of a simplex.*

Example 2.3.3 (The Square)**.** Let $g = 2$ and $\mathcal{C} = \{0,1\}^2$ as in Example 2.1.1. Here,

$$\mathcal{C}^{[2]} = \{(0,1),(1,0),(1,1),(1,2),(2,1)\}.$$

The Hirota variety $\mathcal{H}_\mathcal{C}$ is a complete intersection of codimension three in $(\mathbb{K}^*)^4 \times \mathbb{WP}^5$. There are four unique pairs (k, ℓ) and these contribute the two quartics $P_{13} = P_{24} = u_1^4 - 4u_1 w_1 + 3v_1^2$ and $P_{12} = P_{34} = u_2^4 - 4u_2 w_2 + 3v_2^2$. The point $\mathbf{d} = (1,1)$ is not uniquely attained in $\mathcal{C}^{[2]}$. The polynomial (2.9) contributed by this $\mathbf{d}$ equals

$$P(u_1 + u_2, v_1 + v_2, w_1 + w_2)\, a_{00}a_{11} \;+\; P(u_1 - u_2, v_1 - v_2, w_1 - w_2)\, a_{01}a_{10}. \tag{2.10}$$

For any point in $\mathcal{H}_\mathcal{C}$, we can write $\tau(x,y,t)$ as a $(2,4)$-soliton, as shown in [74, § 2.5].

Example 2.3.4 (The Cube)**.** Let $g = 3$ and consider the tropical degeneration of a smooth plane quartic to a rational quartic. By [4, Example 6], the associated theta function equals

$$\theta_\mathcal{C} \;=\; a_{000} + a_{100}\exp[z_1] + a_{010}\exp[z_2] + a_{001}\exp[z_3] + a_{110}\exp[z_1 + z_2] \\ + a_{101}\exp[z_1 + z_3] + a_{011}\exp[z_2 + z_3] + a_{111}\exp[z_1 + z_2 + z_3]. \tag{2.11}$$

We compute the Hirota variety in $(\mathbb{K}^*)^8 \times \mathbb{WP}^8$. The set $\mathcal{C}^{[2]}$ consists of 19 points. Twelve are uniquely attained, one for each edge of the cube. These give rise to the three familiar quartics $u_j^4 - 4u_j w_j + 3v_j^2$, one for each edge direction $\mathbf{c}_k - \mathbf{c}_\ell$. Six points in $\mathcal{C}^{[2]}$ are attained twice. They contribute equations like (2.10), one for each of the six facets of the cube. Finally, the point $\mathbf{d} = (1,1,1)$ is attained four times. The polynomial (2.9) contributed by $\mathbf{d}$ equals

$$\begin{aligned} & P(\, u_1 + u_2 + u_3,\ v_1 + v_2 + v_3,\ w_1 + w_2 + w_3\,)\, a_{000}a_{111} \\ +\ & P(\, u_1 + u_2 - u_3,\ v_1 + v_2 - v_3,\ w_1 + w_2 - w_3\,)\, a_{001}a_{110} \\ +\ & P(\, u_1 - u_2 + u_3,\ v_1 - v_2 + v_3,\ w_1 - w_2 + w_3\,)\, a_{010}a_{101} \\ +\ & P(\, -u_1 + u_2 + u_3,\ -v_1 + v_2 + v_3,\ -w_1 + w_2 + w_3\,)\, a_{100}a_{011}. \end{aligned} \tag{2.12}$$

We restrict to the 9-dimensional component of $\mathcal{H}_\mathcal{C}$ that lies in $\{a_{000}a_{110}a_{101}a_{011} = a_{001}a_{010}a_{100}a_{111}\}$. Its image in $\mathbb{WP}^8$ has dimension 5, with fibers that are cones over $\mathbb{P}^1 \times \mathbb{P}^1 \times \mathbb{P}^1$. They are defined by seven equations arising from non-unique (k, ℓ). Six of these are binomials (2.10). Extending [74, §2.5], we identify $\tau(x,y,t)$ with $(3,6)$-solitons for

$$A \;=\; \begin{pmatrix} 1 & 1 & 0 & 0 & 0 & 0 \\ 0 & 0 & 1 & 1 & 0 & 0 \\ 0 & 0 & 0 & 0 & 1 & 1 \end{pmatrix}. \tag{2.13}$$

By definition, a $(3,6)$-soliton for the matrix A has the form

$$\tilde{\tau}(x,y,t) \;=\; \sum_I \prod_{\substack{i,j \in I \\ i<j}} (\kappa_j - \kappa_i) \cdot \exp\left[x \cdot \sum_{i \in I} \kappa_i + y \cdot \sum_{i \in I} \kappa_i^2 + t \cdot \sum_{i \in I} \kappa_i^3 \right], \tag{2.14}$$

where I runs over the eight bases $135, 136, 145, 146, 235, 236, 245, 246$. To get from (2.11) to this form, we use the following parametric representation of the main component in $\mathcal{H}_C$:

$$
\begin{aligned}
u_1 &= \kappa_1 - \kappa_2, & v_1 &= \kappa_1^2 - \kappa_2^2, & w_1 &= \kappa_1^3 - \kappa_2^3, \\
u_2 &= \kappa_3 - \kappa_4, & v_2 &= \kappa_3^2 - \kappa_4^2, & w_2 &= \kappa_3^3 - \kappa_4^3, \\
u_3 &= \kappa_5 - \kappa_6, & v_3 &= \kappa_5^2 - \kappa_6^2, & w_3 &= \kappa_5^3 - \kappa_6^3, \\
a_{111} = (\kappa_3 - \kappa_5)(\kappa_1 - \kappa_5)(\kappa_1 - \kappa_3)\lambda_0\lambda_1\lambda_2\lambda_3, && a_{011} = (\kappa_3 - \kappa_5)(\kappa_2 - \kappa_5)(\kappa_2 - \kappa_3)\lambda_0\lambda_2\lambda_3, \\
a_{101} = (\kappa_4 - \kappa_5)(\kappa_1 - \kappa_5)(\kappa_1 - \kappa_4)\lambda_0\lambda_1\lambda_3, && a_{001} = (\kappa_4 - \kappa_5)(\kappa_2 - \kappa_5)(\kappa_2 - \kappa_4)\lambda_0\lambda_3, \\
a_{110} = (\kappa_3 - \kappa_6)(\kappa_1 - \kappa_6)(\kappa_1 - \kappa_3)\lambda_0\lambda_1\lambda_2, && a_{010} = (\kappa_3 - \kappa_6)(\kappa_2 - \kappa_6)(\kappa_2 - \kappa_3)\lambda_0\lambda_2, \\
a_{100} = (\kappa_4 - \kappa_6)(\kappa_1 - \kappa_6)(\kappa_1 - \kappa_4)\lambda_0\lambda_1, && a_{000} = (\kappa_4 - \kappa_6)(\kappa_2 - \kappa_6)(\kappa_2 - \kappa_4)\lambda_0.
\end{aligned}
$$

If we multiply (2.14) by $\exp\big[-(\kappa_2+\kappa_4+\kappa_6)\,x-(\kappa_2^2+\kappa_4^2+\kappa_6^2)\,y-(\kappa_2^3+\kappa_4^3+\kappa_6^3)\,t\,\big]$ then we obtain the desired function $\theta_C(\mathbf{u}x+\mathbf{v}y+\mathbf{w}t)$ for the above generic point on the Hirota variety. The extraneous exponential factor disappears after we pass from $\tilde{\tau}(x,y,t)$ to $\partial_x^2 \log(\tilde{\tau}(x,y,t))$. Both versions of the $(3,6)$-soliton satisfy (1.8) and they represent the same solution to the KP equation (1.5). An analogous construction for the cube $\mathcal{C} = \{0,1\}^g$ in any dimension g is studied in the next chapter.

We now consider the simplex $\mathcal{C} = \{\mathbf{0}, \mathbf{e}_1, \ldots, \mathbf{e}_g\}$. This arises from plane quartics ($g = 3$) that degenerate to four lines or to a conic plus two lines [4, Example 5]. The tau function is

$$
\tau(x,y,t) \;=\; a_0 + a_1 \exp[u_1 x + v_1 y + w_1 t] + a_2 \exp[u_2 x + v_2 y + w_2 t] + \cdots + a_g \exp[u_g x + v_g y + w_g t].
$$

We know from Corollary 2.3.2 that the conditions imposed by Hirota's differential equation (1.8) do not depend on $\mathbf{a}$ but only on $\mathbf{u}, \mathbf{v}, \mathbf{w}$. We thus consider the Hirota variety $\mathcal{H}_C$ in $\mathbb{WP}^{3g-1}$.

Lemma 2.3.5. *The Hirota variety $\mathcal{H}_C$ of the simplex $\mathcal{C}$ is the union of two irreducible components of dimension g in $\mathbb{WP}^{3g-1}$. One of the two components has the following parametric representation:*

$$
u_j \mapsto \kappa_j - \kappa_0, \quad v_j \mapsto \kappa_j^2 - \kappa_0^2, \quad w_j \mapsto \kappa_j^3 - \kappa_0^3 \quad \text{for } j = 1, 2, \ldots, g. \tag{2.15}
$$

The other component is obtained from (2.15) by the sign change $v_j \mapsto -v_j$ for $j = 1, \ldots, g$.

Proof. By Corollary 2.3.2, the variety $\mathcal{H}_C$ is defined by the quartics $P(u_i, v_i, w_i)$ and $P(u_i - u_j, v_i - v_j, w_i - w_j)$. The first g quartics imply $u_j = \kappa_j - \kappa_{j+g}$, $v_j = \kappa_j^2 - \kappa_{j+g}^2$, $w_j = \kappa_j^3 - \kappa_{j+g}^3$ for $j = 1, \ldots, g$. Under these substitutions, the remaining $\binom{g}{2}$ quartics factor into products of expressions $\kappa_i - \kappa_j$. Analyzing all cases up to symmetry reveals the two components. $\square$

Setting $t = \kappa_0$ and $\kappa_j = u_j + t$, the parameterization (2.15) of $\mathcal{H}_C$ can be written as follows:

$$
u_j \mapsto u_j, \quad v_j \mapsto 2u_j t + u_j^2, \quad w_j \mapsto 3u_j t^2 + 3u_j^2 t + u_j^3 \quad \text{for } j = 1, 2, \ldots, g. \tag{2.16}
$$

Theorem 2.3.6. *The prime ideal of the Hirota variety in (2.15) is minimally generated by*

(a) *the* $\binom{g}{2}$ *cubics* $\underline{v_i u_j} - v_j u_i - u_i u_j (u_i - u_j)$ *for* $1 \leq i < j \leq g$,

(b) *the* g *quartics* $\underline{4w_i u_i} - 3v_i^2 - u_i^4$ *for* $i = 1, \ldots, g$,

(c) *the* $g(g-1)$ *quartics* $\underline{4w_j u_i} - 3v_i v_j + 3u_i(u_i - u_j)v_j - u_i u_j^3$ *for* $i \neq j$, *and*

(d) *the* $\binom{g}{2}$ *quintics* $\underline{4w_i v_j} - 4w_j v_i + 3u_i v_j(v_j - v_i) + u_i v_j(u_j - u_i)(u_i - 2u_j) + u_i u_j^3(u_i - u_j)$.

These $2g^2 - g$ *ideal generators are a minimal Gröbner basis with the underlined leading terms.*

Proof. We consider the subalgebra of $\mathbb{K}[t, u_1, \ldots, u_g]$ that is generated by the $3g$ polynomials in the parametrization (2.16). We sort terms by t-degree. We claim that this is a *Khovanskii basis*, or *canonical basis*, as defined in [73] or [104, Chapter 11]. The parametrization given by the leading monomials $u_j \mapsto u_j$, $v_j \mapsto 2u_j t$, $w_j \mapsto 3u_j t^2$ defines a toric variety, namely the embedding of $\mathbb{P}^1 \times \mathbb{P}^{g-1}$ into $\mathbb{P}^{3g-1}$ by the very ample line bundle $\mathcal{O}(2,1)$. Its toric ideal is generated by the leading binomials $v_i u_j - v_j u_i$, $4w_i u_i - 3v_i^2$, $4w_j u_i - 3v_i v_j$, $w_i v_j - w_j v_i$ seen in (a)-(d). In fact, by [104, §14.A], these $2g^2 - g$ quadrics form a square-free Gröbner basis with underlined leading monomials. Under the correspondence in [104, Theorem 8.3], this initial ideal corresponds to a unimodular triangulation of the associated polytope $(2\Delta_1) \times \Delta_{g-1}$.

One checks directly that the polynomials (a), (b), (c), (d) vanish for (2.16). Since only two indices i and j appear, by symmetry, it suffices to do this check for $g = 2$. Hence the generators of the toric ideal are the leading binomials of certain polynomials that vanish on the Hirota variety. By [73, Theorem 2.17] or [104, Corollary 11.5], this proves the Khovanskii basis property. Geometrically speaking, we have constructed a toric degeneration from the Hirota variety to a toric variety in $\mathbb{WP}^{3g-1}$. Furthermore, using [73, Proposition 5.2] or [104, Corollary 11.6 (1)] we conclude that the polynomials in (a)-(d) are a Gröbner basis for the prime ideal of (2.16), where the term order is chosen to select the underlined leading terms. $\qquad\square$

Using the methods described above, we can compute the Hirota variety $\mathcal{H}_C$ for each of the known Delaunay polytopes $\mathcal{C}$, starting with those in Proposition 2.2.4. We did this above for the triangle, the square, the tetrahedron and the cube. Here is one more example.

Example 2.3.7 (Triangular prism)**.** Let $g = 3$ and take θ_C to be the six-term theta function

$$a_{000} + a_{100} \exp[z_1] + a_{001} \exp[z_3] + a_{101} \exp[z_1 + z_3] + a_{011} \exp[z_2 + z_3] + a_{111} \exp[z_1 + z_2 + z_3].$$

The prism $\mathcal{C}$ arises in the degeneration as in Theorem 2.2.3 from a smooth quartic to a cubic plus a line. This is the second diagram in Figures 1 and 2 in [5, page 11]. The Hirota variety is cut out by four quartics in u_i, v_i, w_i, one for each edge direction, plus three relations involving the a_{ijk}, one for each of the three quadrangle facets. The edges from the two triangle facets define a reducible variety of codimension 3. One irreducible component is given by

$$\langle\, u_1^4 + 3v_1^2 - 4u_1 w_1, \ u_2^4 + 3v_2^2 - 4u_2 w_2, \ u_1^2 u_2 + u_1 u_2^2 - u_2 v_1 + u_1 v_2 \,\rangle.$$

Together with the four other relations, this defines an irreducible variety of codimension 4 inside $(\mathbb{K}^*)^6 \times \mathbb{WP}^8$. That irreducible Hirota variety has the parametric representation

$$
\begin{aligned}
u_1 &= \kappa_1 - \kappa_2, & v_1 &= \kappa_1^2 - \kappa_2^2, & w_1 &= \kappa_1^3 - \kappa_2^3, \\
u_2 &= \kappa_2 - \kappa_3, & v_2 &= \kappa_2^2 - \kappa_3^2, & w_2 &= \kappa_2^3 - \kappa_3^3, \\
u_3 &= \kappa_4 - \kappa_5, & v_3 &= \kappa_4^2 - \kappa_5^2, & w_3 &= \kappa_4^3 - \kappa_5^3,
\end{aligned}
$$
$$
a_{000} = (\kappa_1 - \kappa_4)\lambda_0, \quad a_{100} = (\kappa_2 - \kappa_4)\lambda_0\lambda_1, \quad a_{110} = (\kappa_3 - \kappa_4)\lambda_0\lambda_1\lambda_2,
$$
$$
a_{001} = (\kappa_1 - \kappa_5)\lambda_0\lambda_3, \ a_{101} = (\kappa_2 - \kappa_5)\lambda_0\lambda_1\lambda_3, \ a_{111} = (\kappa_3 - \kappa_5)\lambda_0\lambda_1\lambda_2\lambda_3.
$$

This allows us to write the τ-function as a $(2,5)$-soliton, with $A = \begin{pmatrix} 1 & 1 & 1 & 0 & 0 \\ 0 & 0 & 0 & 1 & 1 \end{pmatrix}$. The six bases of the matrix A correspond to the six terms in $\theta_{\mathcal{C}}$, in analogy to the cube (2.11).

2.4   The Sato Grassmannian

The Sato Grassmannian is a device for encoding all solutions to the KP equation. Recall that the classical Grassmannian $\mathrm{Gr}(k,n)$ parametrizes k-dimensional subspaces of $\mathbb{K}^n$. It is a projective variety in $\mathbb{P}^{\binom{n}{k}-1}$, cut out by quadratic relations known as *Plücker relations*. Following [88, Chapter 5], the Plücker coordinates p_I are indexed by k-element subsets I of $\{1, 2, \ldots, n\}$. As is customary in Schubert calculus [88, §5.3], we identify these $\binom{n}{k}$ subsets with partitions λ that fit into a $k \times (n-k)$ rectangle. Such a partition λ is a sequence $(\lambda_1, \lambda_2, \ldots, \lambda_k)$ of integers that satisfy $n - k \geq \lambda_1 \geq \lambda_2 \geq \cdots \geq \lambda_k \geq 0$. The corresponding Plücker coordinate $c_\lambda = p_I$ is the maximal minor of a $k \times n$ matrix M of unknowns, as in [88, §5.1], where the columns are indexed by $I = \{\lambda_k + 1, \lambda_{k-1} + 2, \ldots, \lambda_2 + k - 1, \lambda_1 + k\}$. With this notation, the Plücker relations for $\mathrm{Gr}(k,n)$ are quadrics in the unknowns c_λ.

Example 2.4.1. We revisit [88, Example 5.9] with Plücker coordinates indexed by partitions. The Grassmannian $\mathrm{Gr}(3,6)$ is a 9-dimensional subvariety in $\mathbb{P}^{19}$. Its prime ideal is generated by 35 Plücker quadrics. These are found easily by the following two lines in Macaulay2 [59]:

```
R = QQ[c,c1,c11,c111,c2,c21,c211,c22,c221,c222,c3,c31,c311,
c32,c321,c322,c33,c331,c332,c333];   I = Grassmannian(2,5,R)
```

The output consists of 30 three-term relations, like $\underline{c_{211}c_{22}} - c_{21}c_{221} + c_2c_{222}$ and five four-term relations, like $\underline{c_{221}c_{31}} - c_{21}c_{321} + c_{11}c_{331} + c c_{333}$. These quadrics form a minimal Gröbner basis.

The *Sato Grassmannian* SGM is the zero set of the Plücker relations in the unknowns c_λ, where we now drop the constraint that λ fits into a $k \times (n-k)$-rectangle. Instead, we allow arbitrary partitions λ. What follows is the description of a minimal Gröbner basis for SGM.

Partitions are order ideals in the poset $\mathbb{N}^2$. The set of all order ideals, ordered by inclusion, is a distributive lattice, known as *Young's lattice*. Consider any two partitions λ and μ that are incomparable in Young's lattice. They fit into a common $k \times (n-k)$-rectangle, for some k and n. There is a canonical Plücker relation for $\mathrm{Gr}(k,n)$ that has leading monomial $c_\lambda c_\mu$.

It is known that these *straightening relations* form a minimal Gröbner basis for fixed k and n. This property persists as k and $n-k$ increase, hence yielding a Gröbner basis for SGM.

The previous paragraph paraphrases the definition in [37, 99] of the Sato Grassmannian as an inverse limit of projective varieties. This comes from the diagram of maps $\mathrm{Gr}(k,n+1) \dashrightarrow \mathrm{Gr}(k,n)$ and $\mathrm{Gr}(k+1,n+1) \dashrightarrow \mathrm{Gr}(k,n)$, where these rational maps are given by dropping the last index. This corresponds to *deletion* and *contraction* in matroid theory [88, Chapter 13]. One checks that the simultaneous inverse limit for $k \to \infty$ and $n-k \to \infty$ is well-defined. The straightening relations in our equational description above are those in [37, Example 4.1]. That they form a Gröbner basis is best seen using Khovanskii bases [73, Example 7.3].

We next present the parametric representation of SGM that is commonly used in KP theory. Let $V = \mathbb{K}((z))$ be the field of formal Laurent series with coefficients in our ground field $\mathbb{K}$. Consider the natural projection map $\pi: V \to \mathbb{K}[z^{-1}]$ onto the polynomial ring in z^{-1}. We regard V and $\mathbb{K}[z^{-1}]$ as $\mathbb{K}$-vector spaces, with Laurent monomials z^i serving as bases. Points in the Sato Grassmannian SGM correspond to $\mathbb{K}$-subspaces $U \subset V$ such that

$$\dim \mathrm{Ker}\, \pi_{|U} \;=\; \dim \mathrm{Coker}\, \pi_{|U}, \tag{2.17}$$

and this common dimension is finite. We can represent $U \in \mathrm{SGM}$ via a doubly infinite matrix as follows. For any basis $(f_1, f_2, f_3, \dots)$ of U, the jth basis vector is a Laurent series,

$$f_j(z) \;=\; \sum_{i=-\infty}^{+\infty} \xi_{i,j} z^{i+1}.$$

Then U is the column span of the infinite matrix $\xi = (\xi_{i,j})$ whose rows are indexed from top to bottom by $\mathbb{Z}$ and whose columns are indexed from right to left by $\mathbb{N}$. The i-th row of ξ corresponds to the coefficients of z^{i+1}. Sato proved that a subspace U of V satisfies (2.17) if and only if there is a basis, called a *frame* of U, whose corresponding matrix has the shape

$$\xi \;=\; \begin{pmatrix}
\ddots & \vdots & \vdots & \vdots & & \vdots & \cdots & \vdots \\
\cdots & 1 & 0 & 0 & & 0 & \cdots & 0 \\
\cdots & * & 1 & 0 & & 0 & \cdots & 0 \\
\cdots & * & * & \xi_{-\ell,\ell} & & \xi_{-\ell,\ell-1} & \cdots & \xi_{-\ell,1} \\
\cdots & * & * & \xi_{-\ell+1,\ell} & & \xi_{-\ell+1,\ell-1} & \cdots & \xi_{-\ell+1,1} \\
& \vdots & \vdots & \vdots & & \vdots & \cdots & \vdots \\
\cdots & * & * & \xi_{-1,\ell} & & \xi_{-1,\ell-1} & \cdots & \xi_{-1,1} \\
\cdots & * & * & \xi_{0,\ell} & & \xi_{0,\ell-1} & \cdots & \xi_{0,1} \\
\cdots & * & * & \xi_{1,\ell} & & \xi_{1,\ell-1} & \cdots & \xi_{1,1} \\
& \vdots & \vdots & \vdots & & \vdots & \cdots & \vdots
\end{pmatrix}. \tag{2.18}$$

This matrix is infinite vertically, infinite on the left and, most importantly, it is eventually lower triangular with 1 on the diagonal, at the $(-n, n)$ positions. The space U is described by the positive integer ℓ and the submatrix with ℓ linearly independent columns whose upper left entry is $\xi_{-\ell,\ell}$. This description implies that a subspace U of V satisfies (2.17) if and only if

$$\text{there exists } \ell \in \mathbb{N} \text{ such that } \quad \dim U \cap V_n \;=\; n+1 \quad \text{ for all } n \geq \ell, \tag{2.19}$$

where $V_n = z^{-n}\mathbb{K}[[z]]$ denotes the space of Laurent series with a pole of order at most n.

The Plücker coordinates on SGM are computed as minors ξ_λ of the matrix ξ. Think of a partition λ as a weakly decreasing sequence of nonnegative integers that are eventually zero. Setting $m_i = \lambda_i - i$ for $i \in \mathbb{N}$, we obtain the associated *Maya diagram* $(m_1, m_2, m_3, \dots)$. This is a vector of strictly decreasing integers $m_1 > m_2 > \dots$ such that $m_i = -i$ for large enough i. Partitions and Maya diagrams are in natural bijection. Given any partition λ, we consider the matrix $(\xi_{m_i,j})_{i,j \geq 1}$ whose row indices $m_1, m_2, m_3, \dots$ are the entries in the Maya diagram of λ. Thanks to the shape of the matrix ξ, it makes sense to take the determinant

$$\xi_\lambda := \det(\xi_{m_i,j}). \tag{2.20}$$

This Plücker coordinate is a scalar in $\mathbb{K}$ that can be computed as a maximal minor of the finite matrix to the lower right of $\xi_{-\ell,\ell}$ in (2.18). We summarize our discussion as a theorem.

Theorem 2.4.2. *The Sato Grassmannian SGM is the inverse limit of the classical Grassmannians $\mathrm{Gr}(k, n) \subset \mathbb{P}^{\binom{n}{k}-1}$ as both k and $n-k$ tend to infinity. A parametrization of SGM is given by the matrix minors $c_\lambda = \xi_\lambda$ in (2.20), where λ runs over all partitions. The equations of SGM are the quadratic Plücker relations, shown in [37, Example 4.1] and in Example 2.4.1.*

We now connect the Grassmannians above to our study of solutions to the KP equation. Fix positive integers $k < n$ and a vector of parameters $\kappa = (\kappa_1, \kappa_2, \dots, \kappa_n)$. For each k-element index set $I \in \binom{[n]}{k}$ we introduce an unknown p_I that serves as a Plücker coordinate. Our ansatz for solving (1.8) is now the following linear combination of exponential functions:

$$\tau(x, y, t) = \sum_{I \in \binom{[n]}{k}} p_I \cdot \prod_{\substack{i,j \in I \\ i < j}} (\kappa_j - \kappa_i) \cdot \exp\left[x \cdot \sum_{i \in I} \kappa_i + y \cdot \sum_{i \in I} \kappa_i^2 + t \cdot \sum_{i \in I} \kappa_i^3 \right]. \tag{2.21}$$

Proposition 2.4.3. *The function τ is a solution to Hirota's equation (1.8) if and only if the point $p = (p_I)_{I \in \binom{[n]}{k}}$ lies in the Grassmannian $\mathrm{Gr}(k, n)$, i.e. there is a $k \times n$ matrix $A = (a_{ij})$ such that, for all $I \in \binom{[n]}{k}$, the coefficient p_I is the $k \times k$-minor of A with column indices I.*

Proof. This follows from [74, Theorem 1.3]. $\square$

We define a (k, n)-*soliton* to be any function $\tau(x, y, t)$ where $\kappa \in \mathbb{R}^n$ and $p \in \mathrm{Gr}(k, n)$. Even the case $k = 1$ is interesting. Writing $A = \begin{pmatrix} a_1 & a_2 & \cdots & a_n \end{pmatrix}$, the $(1, n)$-soliton equals

$$\tau(x, y, t) = \sum_{i=1}^{n} a_i \exp\left[x \cdot \kappa_i + y \cdot \kappa_i^2 + t \cdot \kappa_i^3 \right].$$

If we now set $n = g + 1$ and we divide the sum above by its first exponential term then we obtain the tau function that was associated with the g-simplex in Lemma 2.3.5. Hence the KP solutions that arise when the Delaunay polytope is a simplex are precisely the $(1, n)$-solitons.

We next derive the Sato representation in [74, Definition 1.3], that is, we express $\tau(x, y, t)$ as a linear combination of Schur polynomials. Let λ be a partition with at most three parts, written $\lambda_1 \geq \lambda_2 \geq \lambda_3 \geq 0$. Following [74, §1.2.2], the associated Schur polynomial $\sigma_\lambda(x, y, t)$ can be defined as follows. We first introduce the *elementary Schur polynomial* $\varphi_j(x, y, t)$ by the series $\exp[\, x\lambda + y\lambda^2 + t\lambda^3 \,] = \sum_{j=0}^\infty \varphi_j(x, y, t)\lambda^j$. The *Schur polynomial* σ_λ for the partition $\lambda = (\lambda_1, \lambda_2, \lambda_3)$ is the determinant of the Jacobi-Trudi matrix of size 3×3:

$$\sigma_\lambda(x, y, t) \;=\; \det\big(\varphi_{\lambda_i - i + j}(x, y, t)\big)_{1 \leq i, j \leq 3}.$$

To be completely explicit, we list Schur polynomials for partitions λ with $\lambda_1 + \lambda_2 + \lambda_3 \leq 4$:

$$\sigma_\varnothing = 1, \quad \sigma_1 = x, \quad \sigma_{11} = \tfrac{1}{2}x^2 - y, \quad \sigma_2 = \tfrac{1}{2}x^2 + y, \; \sigma_{111} = \tfrac{1}{6}x^3 - xy + t, \quad \sigma_3 = \tfrac{1}{6}x^3 + xy + t,$$

$$\sigma_{21} = \tfrac{1}{3}x^3 - t, \; \sigma_{211} = \tfrac{1}{8}x^4 - \tfrac{1}{2}x^2 y - \tfrac{1}{2}y^2, \; \sigma_{22} = \tfrac{1}{12}x^4 - tx + y^2, \; \sigma_{31} = \tfrac{1}{8}x^4 + \tfrac{1}{2}x^2 y - \tfrac{1}{2}y^2, \; \ldots$$

For a partition λ as above, we set $\lambda_4 = \cdots = \lambda_k = 0$. For $I = \{i_1 < i_2 < \cdots < i_k\}$ we set

$$\Delta_\lambda(\kappa_i, i \in I) \quad := \quad \det \begin{pmatrix} \kappa_{i_1}^{\lambda_1 + k - 1} & \kappa_{i_2}^{\lambda_1 + k - 1} & \cdots & \kappa_{i_k}^{\lambda_1 + k - 1} \\ \kappa_{i_1}^{\lambda_2 + k - 2} & \kappa_{i_2}^{\lambda_2 + k - 2} & \cdots & \kappa_{i_k}^{\lambda_2 + k - 2} \\ \vdots & \vdots & \ddots & \vdots \\ \kappa_{i_1}^{\lambda_k} & \kappa_{i_2}^{\lambda_k} & \cdots & \kappa_{i_k}^{\lambda_k} \end{pmatrix}.$$

The empty partition gives the Vandermonde determinant $\Delta_\varnothing(\kappa_i, i \in I) = \prod_{\substack{i,j \in I \\ i < j}} (\kappa_j - \kappa_i)$.

Lemma 2.4.4. *The exponential function indexed by I in the formula (2.21) has the expansion*

$$\exp\left[x \cdot \sum_{i \in I} \kappa_i \;+\; y \cdot \sum_{i \in I} \kappa_i^2 \;+\; t \cdot \sum_{i \in I} \kappa_i^3 \right] \;=\; \Delta_\varnothing(\kappa_i, i \in I)^{-1} \cdot \sum_{\lambda_1 \geq \lambda_2 \geq \lambda_3 \geq 0} \Delta_\lambda(\kappa_i, i \in I) \cdot \sigma_\lambda(x, y, t).$$

Proof. The unknowns x, y, t play the role of power sum symmetric functions in $r_1, r_2, \ldots$:

$$x \;=\; r_1 + r_2 + r_3 = p_1(r), \;\; y \;=\; \frac{1}{2}(r_1^2 + r_2^2 + r_3^2) = \frac{1}{2}p_2(r), \;\; t \;=\; \frac{1}{3}(r_1^3 + r_2^3 + r_3^3) \;=\; \frac{1}{3}p_3(r).$$

It suffices to prove the statement after this substitution. By [74, Remark 1.5], we have $\sigma_\lambda(x, y, t) = s_\lambda(r_1, r_2, r_3)$, where s_λ is the usual Schur function as a symmetric polynomial, which satisfies $\Delta_\lambda(\kappa_i, i \in I) = s_\lambda(\kappa_i, i \in I) \cdot \Delta_\varnothing(\kappa_i, i \in I)$. Our identity can be rewritten as

$$\exp\left[p_1(w) \cdot p_1(\kappa) + \frac{1}{2}p_2(w) \cdot p_2(\kappa) + \frac{1}{3}p_3(w) \cdot p_3(\kappa) \right] = \sum_{\lambda_1 \geq \lambda_2 \geq \lambda_3 \geq 0} s_\lambda(\kappa_i, i \in I) \cdot s_\lambda(r_1, r_2, r_3).$$

This is precisely the classical Cauchy identity, as stated in [103, page 386]. $\qquad\square$

By substituting the formula in Lemma 2.4.4 into the right hand side of (2.21), we obtain :

Proposition 2.4.5. *The (k, n)-soliton has the following expansion into Schur polynomials*

$$\tau(x, y, t) \;=\; \sum_{\lambda_1 \geq \lambda_2 \geq \lambda_3 \geq 0} c_\lambda \cdot \sigma_\lambda(x, y, t), \qquad \text{where} \quad c_\lambda = \sum_{I \in \binom{[n]}{k}} p_I \cdot \Delta_\lambda(\kappa_i, i \in I). \qquad (2.22)$$

For any point ξ in the Sato Grassmannian SGM we now define a tau function as follows:

$$\tau_\xi(x, y, t) \;=\; \sum_\lambda \xi_\lambda \, \sigma_\lambda(x, y, t). \tag{2.23}$$

The sum is over all possible partitions. We can now state the main result of Sato's theory.

Theorem 2.4.6 (Sato). *For any $\xi \in$ SGM, the tau function τ_ξ satisfies Hirota's equation* (1.8).

Actually, Sato's theorem is much more general. From a frame ξ as in (2.18), we define

$$\tau(t_1, t_2, t_3, t_4, \dots) \;=\; \sum_\lambda \xi_\lambda \, \sigma_\lambda(t_1, t_2, t_3, t_4, \dots)$$

The sum is over all partitions. This function in infinitely many variables is a solution to the *KP hierarchy*, which is an infinite set of differential equations which generalize the KP equation. Moreover, every solution to the KP hierarchy arises from the Sato Grassmannian in this way. The tau functions that we consider here arise from the general case by setting

$$t_1 = x, \quad t_2 = y, \quad t_3 = t, \quad t_4 = t_5 = \dots = 0.$$

We refer to [74, Theorem 1.3] for a first introduction and numerous references. We may also start with an ansatz $\tau(x, y, t) = \sum_\lambda c_\lambda \sigma_\lambda(x, y, t)$, and examine the quadratic equations in the unknowns c_λ that are imposed by (1.8). This leads to polynomials that vanish on SGM.

Remark 2.4.7. We can view Proposition 2.4.3 as a special case of Theorem 2.4.6, given that the Sato Grassmannian contains all classical Grassmannians $\mathrm{Gr}(k, n)$. Here is an explicit description. We fix distinct scalars $\kappa_1, \dots, \kappa_n$ in $\mathbb{K}^*$. Points in $\mathrm{Gr}(k, n)$ are represented by matrices A in $\mathbb{K}^{k \times n}$. Following [76, §3.1] and [91, §2.2], we turn A into an infinite matrix ξ as in (2.18). Let $\Lambda(\kappa)$ denote the $\infty \times n$ matrix whose rows are $(\kappa_1^\ell, \kappa_2^\ell, \dots, \kappa_n^\ell)$ for $\ell = 0, 1, 2, \dots$. We define $A(\kappa) := \Lambda(\kappa) \cdot A^T$. This is the $\infty \times k$ matrix whose jth column is given by the coefficients of

$$\sum_{i=1}^{n} \frac{a_{ji}}{1 - \kappa_i z} \;=\; \sum_{\ell=0}^{\infty} \sum_{i=1}^{n} \kappa_i^\ell \, a_{ji} \cdot z^\ell.$$

This verifies [91, Theorem 3.2]. Indeed, the double infinite matrix representing τ equals

$$\xi \;=\; \begin{bmatrix} \mathbf{1} & \mathbf{0} \\ \mathbf{0} & A(\kappa) \end{bmatrix},$$

where $\mathbf{0}$ and $\mathbf{1}$ are infinite zero and identity matrices. In particular, the first nonzero row of $A(\kappa)$ is at the row $-k$ of ξ. The corresponding basis $(f_1, f_2, f_3, \dots)$ of the space U is given by

$$f_j = \frac{1}{z^{k-1}} \sum_{i=1}^n \frac{a_{ji}}{1 - \kappa_i z}, \quad \text{for } j = 1, \dots, k, \qquad f_j = \frac{1}{z^{j-1}}, \quad \text{for } j \geq k+1. \qquad (2.24)$$

The Plücker coordinates c_λ indexed by partitions with at most three parts are certain minors of $A(\kappa)$, and these are expressed in terms of maximal minors of A by the formula in (2.22).

2.5   Tau functions from algebraic curves

Let X be a smooth projective curve of genus g defined over a field $\mathbb{K}$ of characteristic zero. In this section we show how certain Riemann-Roch spaces on X define points in the Sato Grassmannian SGM. Using Theorem 2.4.6, we obtain KP solutions by choosing appropriate bases of these spaces. The relevant theory is known since the 1980s; see [74, 76, 99]. We begin with the exposition in [91, §4]. Our aim is to develop tools to carry this out in practice.

Fix a divisor D of degree $g - 1$ on X and a distinguished point $p \in X$, both defined over $\mathbb{K}$. For any integer $n \in \mathbb{N}$, we consider the Riemann-Roch space $H^0(X, D + np)$. For $m < n$ there is an inclusion $H^0(X, D + mp) \subseteq H^0(X, D + np)$. As n increases, we obtain a space $H^0(X, D + \infty p)$ of rational functions on the curve X whose pole order at p is unconstrained.

Let z denote a local coordinate on X at p. Each element in $H^0(X, D + \infty p)$ has a unique Laurent series expansion in z and hence determines an element in $V = \mathbb{K}((z))$. Let $m = \mathrm{ord}_p(D)$ be the multiplicity of p in D. Multiplication by z^{m+1} defines the $\mathbb{K}$-linear map:

$$\iota \colon H^0(X, D + \infty p) \to V, \qquad s = \sum_{n \in \mathbb{Z}} s_n z^n \mapsto \sum_{n \in \mathbb{Z}} s_n z^{n+m+1}.$$

Proposition 2.5.1 ([91, Theorem 4.1])**.** *The space* $U = \iota(H^0(X, D + \infty p)) \subset V$ *lies in SGM.*

Proof. The map ι is injective because a rational function on an irreducible curve X is uniquely determined by its Laurent series. Setting $V_n = z^{-n}\mathbb{K}[[z]] \subset V$ as in Section 2.4, we have

$$\dim U \cap V_n = h^0(X, D + (n+1)p) = n + 1 + h^1(X, D + (n+1)p). \qquad (2.25)$$

The second equality is the Riemann-Roch Theorem, with $\deg(D) = g - 1$. Hence (2.19) holds provided $h^1(X, D + (n+1)p) = 0$. This happens for $n \geq g - 1$, by degree considerations. $\square$

Following [91], we examine the case $g = 2$. A smooth curve of genus two is hyperelliptic:

$$X = \left\{ y^2 = (x - \lambda_1)(x - \lambda_2) \cdots (x - \lambda_6) \right\}.$$

Here $\lambda_1, \lambda_2, \dots, \lambda_6 \in \mathbb{K}$ are pairwise distinct. Let p be one of the two preimages of the point at infinity under the double cover $X \to \mathbb{P}^1$. Using the local coordinate $z = \frac{1}{x}$ at p, we write

$$y = \pm\sqrt{(x - \lambda_1) \cdots (x - \lambda_6)} = \pm\frac{1}{z^3} \cdot \sum_{n=0}^{+\infty} \alpha_n z^n,$$

where $\alpha_0 = 1$ and the α_i are polynomials in $\lambda_1, \ldots, \lambda_6$. We consider three kinds of divisors:

$$D_0 = p, \ D_1 = p_1 \ \text{and} \ D_2 = p_1 + p_2 - p,$$

where $p_1 = (c_1, y_1)$, $p_2 = (c_2, y_2)$ are general points on X. For $m \geq 3$, consider the functions

$$\begin{array}{rcl}
g_m(x) & = & \sum_{j=0}^{m} \alpha_j x^{m-j}, \\
f_m(x,y) & = & \frac{1}{2}\left(x^{m-3}y + g_m(x)\right), \\
h_j(x,y) & = & \frac{f_3(x,y)-f_3(c_j,-y_j)}{x-c_j} \quad = \quad \frac{y+g_3(x)-(-y_j+g_3(c_j))}{2(x-c_j)} \qquad \text{for } j = 1,2.
\end{array}$$

These rational functions are series in z with coefficients that are polynomials in $\lambda_1, \ldots, \lambda_6$. We write U_i for the image of the Riemann-Roch space $H^0(X, D_i + \infty p)$ under the inclusion ι.

Lemma 2.5.2 ([91, Lemma 5.2]). *The set* $\{1, f_3, f_4, f_5, \ldots\}$ *is a basis of* U_0, *the set* $\{1, f_3, f_4, f_5, \ldots\} \cup \{h_1\}$ *is a basis of* U_1, *and* $\{1, f_3, f_4, f_5, \ldots\} \cup \{h_1, h_2\}$ *is a basis of* U_2.

This lemma furnishes us with an explicit basis for the $\mathbb{K}$-vector space U in Proposition 2.5.1. This basis is a frame in the sense of Sato theory. It gives us the matrix ξ in (2.18), from which we compute the Plücker coordinates (2.20) and the tau function (2.23). This process is a symbolic computation over the ground field $\mathbb{K}$. No numerics are needed. For general curves of genus $g \geq 3$, the same is possible, but it requires computing a basis for U, e.g. using [64].

Our approach differs greatly from the computation of KP solutions from the curve X via theta functions as in [5, 38, 78]. That would require the computation of the Riemann matrix of X, which cannot be done over $\mathbb{K}$. This is why we adopted the SGM approach in [76, 91].

We implemented the method described above in `Maple` for $D_0 = p$ on hyperelliptic curves over $\mathbb{K} = \mathbb{Q}(\epsilon)$. If λ is a partition with n parts, then the Plücker coordinate ξ_λ is the minor given by the n right-most columns of ξ and the rows given by the first n parts in the Maya diagram of λ. Since the tau function (2.23) is an infinite sum over all partitions, our code does not provide an exact solution to the Hirota equation (1.8). Instead, it computes the truncated tau function

$$\tau[n] := \sum_{i=1}^{n} \sum_{\lambda \vdash i} \xi_\lambda \, \sigma_\lambda(x, y, t), \tag{2.26}$$

where n is the order of precision. In our experiments we evaluated (2.26) up to $n = 12$ on a range of hyperelliptic curves of genus $g = 2, 3, 4$. The first non-zero $\tau[n]$ is $\tau[g] = \sigma_{(g)}(x, y, t)$ [91, Proposition 6.3]. When plugging (2.26) into the left hand side of (1.8), we get an expression in x, y, t whose terms of low order vanish. The following facts were observed for this expression. For $n > g+2$, the term of lowest degree has degree $n+g-3$, and the monomial that appears in that lowest degree $n+g-3 = 1, 2, 3, \ldots$ is $x, y, t, xt, yt, t^2, xt^2, yt^2, t^3, xt^3, yt^3, t^4, \ldots$.

We use our `Maple` code to study (k, n)-solitons arising from the degenerations in [91]. Namely, we explore the limit for $\epsilon \to 0$ for hyperelliptic curves of genus $g = n - 1$ given by

$$y^2 = (x - \kappa_1)(x - \kappa_1 - \epsilon) \cdots (x - \kappa_n)(x - \kappa_n - \epsilon). \tag{2.27}$$

Set $h(z) = (1 - \kappa_1 z)\cdots(1 - \kappa_n z)$. For $\epsilon \to 0$ the frame found in Lemma 2.5.2 degenerates to

$$U = \left\{1, z^{-n}h(z), z^{-(n+1)}h(z), z^{-(n+2)}h(z), z^{-(n+3)}h(z), \dots\right\}. \tag{2.28}$$

Observe that $z^{-n}h(z)$ gets expanded to

$$z^{-n} + z^{-(n-1)}\left(-\sum_{i=1}^{n}\kappa_i\right) + z^{-(n-2)}\left(\sum_{1 \le i \le j \le n}\kappa_i\kappa_j\right) + z^{-(n-3)}\left(\sum_{1 \le i \le j \le l \le n}\kappa_i\kappa_j\kappa_l\right) + O(z^{-(n-4)}).$$

Following [91, §7], one multiplies all elements in U by $h(z)^{-1}$ in order to obtain a soliton solution. By [91, Theorem 3.2], we obtain a $(1,n)$-soliton solution given by the matrix

$$A = \left(\left(\prod_{i \ne 1}(\kappa_1 - \kappa_i)\right)^{-1} \quad \left(\prod_{i \ne 2}(\kappa_2 - \kappa_i)\right)^{-1} \quad \cdots \quad \left(\prod_{i \ne n}(\kappa_n - \kappa_i)\right)^{-1}\right).$$

Example 2.5.3. The soliton that arises from the genus 2 curve defined by the polynomial $f_2(x)$ in (2.2) is a $(1,3)$-soliton given by the matrix $A = \left(\frac{1}{2} \quad -1 \quad \frac{1}{2}\right)$ and parameters $\kappa = (1, 2, 3)$.

We computed the tau function for a range of curves over $\mathbb{K} = \mathbb{Q}(\epsilon)$. Their limit as $\epsilon \to 0$ is not the same as the tau functions obtained from the combinatorial methods in Section 2.2:

Example 2.5.4. Let X be the hyperelliptic curve of genus 3 given by $y^2 = f(x)$ where $f(x)$ is

$$(x+1+\epsilon)(x+1+2\epsilon)(x+1+\epsilon+\epsilon^2)(x+1+2\epsilon+\epsilon^2)(x+2+\epsilon)(x+2+2\epsilon)(x+2+\epsilon+\epsilon^2)(x+2+2\epsilon+\epsilon^2).$$

In Figure 2.5 we exhibit the subtree with 8 leaves that arises from the 8 roots of $f(x)$ and the corresponding metric graph of genus 3 which maps to it under the hyperelliptic covering.
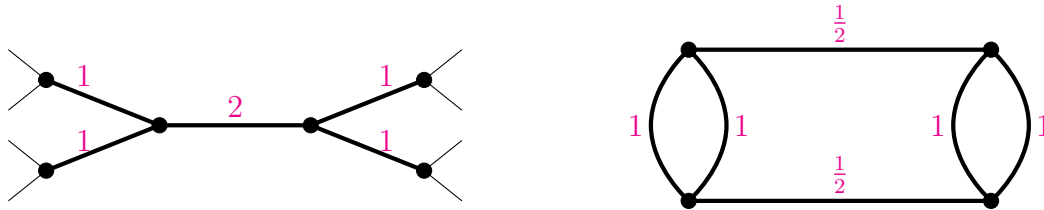
Figure 2.5: The metric tree (left) and the metric graph (right) for the curve X

For a suitable cycle basis, the tropical Riemann matrix equals $Q = \begin{bmatrix} 2 & -1 & 0 \\ -1 & 3 & -1 \\ 0 & -1 & 2 \end{bmatrix}$. This appears in the second row in [4, Table 4]: the Voronoi polytope is the hexarhombic dodecahedron. This corresponds to the tropical degeneration from a smooth quartic to a conic and

two lines in $\mathbb{P}^2$. According to [4, Theorem 4] there are two types of Delaunay polytopes in this case, namely the tetrahedron (4 vertices) and the pyramid (5 vertices). The theta function (2.1) for the tetrahedron equals $\theta_{\mathcal{C}}(z) = a_{000} + a_{100} \exp[z_1] + a_{010} \exp[z_2] + a_{001} \exp[z_3]$. The Hirota variety lives in $(\mathbb{K}^*)^4 \times \mathbb{WP}^8$, and it is characterized by Theorem 2.3.6. Each point on the Hirota variety gives a KP solution. The theta function for the pyramid equals

$$\theta_{\mathcal{C}'}(z) = a_{000} + a_{100} \exp[z_1] + a_{001} \exp[z_3] + a_{101} \exp[z_1 + z_3] + a_{111} \exp[z_1 + z_2 + z_3].$$

The Hirota variety $\mathcal{H}_{\mathcal{C}'} \subset (\mathbb{K}^*)^5 \times \mathbb{WP}^8$ is cut out by eight quadrics P_{ij} as in Section 2.3, plus

$$P(u_1 + u_3, v_1 + v_3, w_1 + w_3) \, a_{000} a_{101} \;+\; P(u_1, v_1, w_1) \, a_{001} a_{101}.$$

The resulting tau functions differ from those obtained by setting $\epsilon = 0$ in our `Maple` output. This happens because $y^2 = f(x)$ is not a semistable model. The special fiber of that curve at $\epsilon = 0$ does not have ordinary singularities: it has two singular points of the form $y^2 = x^4$. On the other hand, if the curve at $\epsilon = 0$ is rational and has nodal singularities, as in (2.27), then we get soliton solutions at the limit. We shall see this more precisely in the next section.

After this combinatorial interlude, we now return to Proposition 2.5.1, and explore this for a singular curve X. Suppose X is connected, has arithmetic genus g, and all singularities are nodal. We recall briefly how to compute $H^0(X, E)$ when E is a divisor supported in the smooth locus of X. If X is irreducible, then we consider the normalization $\widetilde{X} \to X$, that separates the nodes of X. The divisor E lifts to $\widetilde{X}$, and $H^0(X, E)$ is a subspace of $H^0(\widetilde{X}, E)$. It consists of rational functions which coincide on the points of $\widetilde{X}$ that map to the nodes of X. If $X = X_0 \cup \cdots \cup X_r$ is reducible, then $H^0(X, E)$ is a subspace of $\bigoplus_{i=0}^r H^0(X_i, E_{|X_i})$. Its elements are tuples $(f_0, f_1, \ldots, f_r)$ where f_i and f_j coincide on $X_i \cap X_j$.

Fix a divisor D of degree $g-1$ and a point p, where all points are smooth on X and defined over $\mathbb{K}$. We wish to compute $H^0(X, D + \infty p)$. Riemann-Roch holds for X and hence so does (2.25). In order for the proof of Proposition 2.5.1 to go through, we need two conditions:

(∗) A rational function in $H^0(X, D+np)$ is uniquely determined by its Laurent series at p.

(∗∗) We have $h^1(X, D + np) = 0$ for $n \gg 0$.

Our next result characterizes when these two conditions hold. Let X_0 be the irreducible component of X that contains p, and let $X_0' = \overline{X \backslash X_0}$ be the curve obtained by removing X_0. Set $Z = X_0 \cap X_0'$ and denote the restrictions of the divisor D to X_0, X_0' by D_0, D_0' respectively.

Proposition 2.5.5. *Condition* (∗) *holds if and only if* $H^0(X_0', D_0' - Z) = 0$. *Condition* (∗∗) *holds if and only if* $H^1(X_0', D_0') = 0$. *These are vanishing conditions on the curve* X_0'.

Proof. If X is irreducible then (∗) holds since rational functions are determined by their series on the normalization $\widetilde{X}$. If X is reducible then X_0' is nonempty. We need that the restriction

$$H^0(X, D + np) \longrightarrow H^0(X_0, D_0 + np)$$

is injective. The kernel of this map consists exactly of those rational functions in $H^0(X_0', D_0')$ which vanish on Z. In other words, the kernel is the space $H^0(X_0', D_0' - Z)$, as desired.

Also for the second statement, we can take X to be reducible. Consider the exact sequence

$$0 \longrightarrow \mathcal{O}_X(D + np) \longrightarrow \mathcal{O}_{X_0}(D_0 + np) \oplus \mathcal{O}_{X_0'}(D_0') \longrightarrow \mathcal{O}_Z(D_0 + np) \longrightarrow 0.$$

Taking global sections we see that $H^1(X, D+np)$ surjects onto $H^1(X_0', D_0')$, since $\dim(Z) = 0$. Hence $H^1(Z, D_0 + np) = 0$. In particular, if $H^1(X, D + np) = 0$ then $H^1(X_0', D_0') = 0$.

Conversely, suppose $H^1(X_0', D_0') = 0$. Since X_0 is irreducible, we have $H^1(X_0, D_0+np) = 0$ for $n \gg 0$. The long exact sequence tells us that $H^1(X, D + np) = 0$ as soon as the map

$$H^0(X_0, D_0 + np) \oplus H^0(X_0', D_0') \longrightarrow H^0(Z, D + np), \qquad (f_0, f_0') \mapsto f_{0|Z} - f_{0|Z}'$$

is surjective. Actually, the map $H^0(X_0, D + np) \to H^0(Z, D + np)$ is surjective for $n \gg 0$. Indeed, $H^1(X_0, D - Z + np) = 0$ for $n \gg 0$ since p is an ample divisor on the curve X_0. $\square$

Remark 2.5.6. Here we presented the case of nodal curves for simplicity, but the same discussion holds true, with essentially the same proofs, for an arbitrary singular curve.

Remark 2.5.7. The two conditions in Proposition 2.5.5 are automatically satisfied when the curve X is irreducible. In that case we always get a point U in the Sato Grassmannian.

2.6   Nodal rational curves

Our long-term goal is to fully understand the points $U(\epsilon)$ in the Sato Grassmannian that represent Riemann-Roch spaces of a smooth curve over a valued field, such as $\mathbb{K} = \mathbb{Q}(\epsilon)$. We explained how these points are computed, and we implemented this in `Maple` for the case of hyperelliptic curves. Our approach is similar to [76, 90, 91]. For a given Mumford curve, it remains a challenge to lift the computation to the valuation ring (such as $\mathbb{Q}[\epsilon]$) and correctly encode the limiting process as $\epsilon \to 0$. In this section we focus on what happens in the limit.

Consider a nodal reducible curve $X = X_0 \cup \cdots \cup X_r$, where each irreducible component X_i is rational. The arithmetic genus g is the genus of the dual graph. We present an algorithm whose input is a divisor D of degree $g - 1$ and a point p, supported in the smooth locus of X. The algorithm checks the conditions in Proposition 2.5.5, and, if these are satisfied, it outputs a soliton solution that corresponds to $U = \iota(H^0(X, D + \infty p))$.

We start with some remarks on interpolation of rational functions on $\mathbb{P}^1$. Consider distinct points $\kappa_1, \ldots, \kappa_a$ and $\kappa_{1,1}, \kappa_{1,2}, \ldots, \kappa_{b,1}, \kappa_{b,2}$ on $\mathbb{P}^1$. We also choose a divisor $D_0 = m_1 p_1 + \cdots + m_s p_s + mp$, which is supported away from the previous points. Choose also scalars $\lambda_1, \ldots, \lambda_a, \mu_1, \ldots, \mu_b \in \mathbb{K}$. We wish to compute all functions f in $H^0(\mathbb{P}^1, D_0 + \infty p)$ satisfying

$$f(\kappa_j) = \lambda_j \text{ for } j = 1, \ldots, a \qquad \text{and} \qquad f(\kappa_{j,1}) = f(\kappa_{j,2}) = \mu_j \text{ for } j = 1, \ldots, b. \qquad (2.29)$$

To do so, we choose an affine coordinate x on $\mathbb{P}^1$ such that $p = \infty$. Then we define

$$P(x) := \prod_{j=1}^{s} (x - p_j)^{m_j} \qquad \text{and} \qquad K(x) := \prod_{j=1}^{a} (x - \kappa_j) \cdot \prod_{j=1}^{b} (x - \kappa_{j,1})(x - \kappa_{j,2}).$$

Write $K'(x)$ for the derivative of the polynomial $K(x)$. An interpolation argument shows:

Lemma 2.6.1. *A rational function f in $H^0(\mathbb{P}^1, D_0 + \infty p)$ satisfies condition* (2.29) *if and only if*

$$f(x) = \frac{K(x)}{P(x)} \left[\sum_{j=1}^{a} \lambda_j \frac{P(\kappa_j)}{K'(\kappa_j)} \frac{1}{x - \kappa_j} + \sum_{j=1}^{b} \mu_j \left(\frac{P(\kappa_{j,1})}{K'(\kappa_{j,1})} \frac{1}{x - \kappa_{j,1}} + \frac{P(\kappa_{j,2})}{K'(\kappa_{j,2})} \frac{1}{x - \kappa_{j,2}} \right) + H(x) \right],$$

where $\mu_1, \ldots, \mu_b \in \mathbb{K}$ and $H(x)$ is a polynomial in $\mathbb{K}[x]$.

Lemma 2.6.1 gives a way to compute the Riemann-Roch space $H^0(X, E)$ when E is a divisor on a nodal rational curve X as above. The normalization of such a curve is an union of projective lines. On each line we need to compute rational functions with prescribed values at certain points (corresponding to the intersection of two components of X) and at certain pairs of points (corresponding to the nodes in the components of X).

Algorithm 2.6.2. The following steps compute the soliton (2.21) associated to the curve data.

Input: A reducible curve $X = X_0 \cup \cdots \cup X_r$ as above, with a smooth point p and a divisor D of degree $g - 1$ supported also on smooth points. Everything is defined over $\mathbb{K}$.

(1) Let X_0, X_0', D_0, D_0', Z be as in Section 2.5. Write $Z = \{q_1, \ldots, q_a\}$ and let $n_1, \ldots, n_b$ be the nodes in X_0. If $\nu \colon \mathbb{P}^1 \to X_0$ is the normalization of X_0 we set $\kappa_j := \nu^{-1}(q_j)$ and $\{\kappa_{j,1}, \kappa_{j,2}\} = \nu^{-1}(n_j)$. We also write $D_0 = m_1 p_1 + \cdots + m_s p_s + mp$, we fix an affine coordinate x on $\mathbb{P}^1$ such that $p = \infty$, and we compute $P(x)$ and $K(x)$ as in (2.29).

(2) Compute a basis $Q_1, Q_2, \ldots, Q_\ell$ of $H^0(X_0', D_0')$. If $\ell = \deg D_0' + 1 - p_a(X_0')$ then proceed. Otherwise return "Condition $(**)$ in Proposition 2.5.5 fails" and terminate.

(3) Compute the Riemann-Roch space $H^0(X_0', D_0' - Z)$. If this is zero then proceed. Otherwise return "Condition $(*)$ in Proposition 2.5.5 fails" and terminate.

(4) Define the $\ell \times a$ matrix A and the $b \times 2b$ matrix B by

$$A_{i,j} := \frac{Q_i(p_j) P(\kappa_j)}{K'(\kappa_j)}, \quad B_{j,2j-1} := \frac{P(\kappa_{j,1})}{K'(\kappa_{j,i})}, \quad B_{j,2j} := \frac{P(\kappa_{j,2})}{K'(\kappa_{j,2})}, \quad B_{i,j} := 0 \text{ otherwise.}$$

Output: The $(\ell + b) \times (a + 2b)$ matrix $\begin{pmatrix} A & 0 \\ 0 & B \end{pmatrix}$. This represents the soliton solution for the point $\iota(H^0(X, D + \infty p))$ in the Sato Grassmannian SGM, after a gauge transformation.

Proposition 2.6.3. *Algorithm 2.6.2 is correct.*

Proof. By Riemann-Roch, we have $h^0(X'_0, D'_0) = h^1(X'_0, D'_0) + \deg D'_0 + 1 - p_a(X'_0)$. Hence condition $(**)$ in Proposition 2.5.5 is satisfied if and only if the condition in step (2) of Algorithm 2.6.2 is satisfied. Moreover, condition $(*)$ in Proposition 2.5.5 is precisely the condition in step (3). Hence, we need to show that the output of the algorithm corresponds to $\iota(H^0(X, D + \infty p))$, after a gauge transformation. However, we know that any element of $H^0(X, D + \infty p)$ can be written as $(f, \sum_j \lambda_j Q_j)$ such that $f \in H^0(X_0, D_0 + \infty p)$ and

$$f(\kappa_j) = \sum_i \lambda_i Q_i(\kappa_j), \text{ for } j = 1, \dots, a \qquad \text{and} \qquad f(\kappa_{j,1}) = f(\kappa_{j,2}) \text{ for } j = 1, \dots, b.$$

At this point, Lemma 2.6.1 gives us a basis of $\iota(H^0(X, D + \infty p))$. Remark 2.4.7 shows that this corresponds exactly to the matrix given by the algorithm, after a gauge transformation. $\qquad \square$

We illustrate the algorithm in the following examples.

Example 2.6.4. Let X be an irreducible rational curve with g nodes. Algorithm 2.6.2 returns a matrix B for a $(g, 2g)$-soliton. This is consistent with (2.13). Note that X is a tropical limit where the graph is one node with g loops and the Delaunay polytope is the g-cube. This is discussed in much more detail in Chapter 3.

Example 2.6.5 ($g = 2$). Let X be the union of two smooth rational curves X_0, X_1 meeting at three points $Z = \{q_1, q_2, q_3\}$. This curve is the special fiber of the genus 2 curve $\{y^2 = f_2(x)\}$ in Example 2.1.1. It corresponds to the graph on the right in Figure 2.2. We choose a smooth point $p \in X_0 \backslash Z$, and we consider three different divisors of degree one: $p, -2q + 3p$ and $3q - 2p$, where q is a smooth point in X_1. We apply Algorithm 2.6.2 to these three instances.

- Take $D = p$. Then $H^0(X'_0, D'_0) = H^0(\mathbb{P}^1, \mathcal{O}) = \mathbb{K}$ has the constant function 1 as basis. The conditions in steps (2) and (3) are both satisfied, and the algorithm gives us the soliton solution corresponding to the matrix $A = \left(\frac{1}{K'(\kappa_1)} \quad \frac{1}{K'(\kappa_2)} \quad \frac{1}{K'(\kappa_3)} \right)$. Note that the Delaunay polytope $\mathcal{C}$ is the triangle, and the approach in Section 2.3 leads to the gauge-equivalent matrix $A = \begin{pmatrix} 1 & 1 & 1 \end{pmatrix}$. This also arises for $z_1 = 0$ in Example 2.3.7.

- Take $D_2 = -2q + 3p$. Then $H^0(X'_0, D'_0) \cong H^0(\mathbb{P}^1, -2q) = 0$ and the condition in step (2) is not satisfied. Hence we do not get a point in the Sato Grassmannian.

- Take $D_3 = 3q - 2p$. Then $H^0(X'_0, D'_0) \cong H^0(\mathbb{P}^1, 3q)$ has dimension 4 and the condition in step (2) is satisfied. However, $H^0(X'_0, D'_0 - Z) \cong H^0(\mathbb{P}^1, \mathcal{O}) \neq 0$ so the condition in step (3) is not satisfied, and we do not get a point in the Sato Grassmannian.

Example 2.6.6 ($g = 3$). Consider four general lines $X = X_0 \cup X_1 \cup X_2 \cup X_3$ in $\mathbb{P}^2$. Set $X_0 \cap X_i = \kappa_i$ and $X_i \cap X_j = q_{ij}$ for $i, j \in \{1, 2, 3\}$. We fix the divisor $D = p_1 + p_2 + p_3 - p$, for general points $p \in X_0$ and $p_i \in X_i$ for $i = 1, 2, 3$. After the preparatory set-up in step (1), we compute $H^0(X'_0, D'_0)$ in step (2). This is the space of functions (g_1, g_2, g_3) in $\bigoplus_{i=1}^3 H^0(X_i, p_i)$

such that $g_i(q_{ij}) = g_j(q_{ij})$ for $i, j \in \{1, 2, 3\}$. Choose affine coordinates x_i on X_i for $i = 1, 2, 3$ such that $p_i = \infty$. We compute the following basis for $H^0(X'_0, D'_0)$:

$$Q_1 = \left(0, \frac{x_2 - q_{12}}{q_{23} - q_{12}}, \frac{x_3 - q_{13}}{q_{23} - q_{12}}\right), \quad Q_2 = \left(\frac{x_1 - q_{12}}{q_{13} - q_{12}}, 0, \frac{x_3 - q_{23}}{q_{13} - q_{23}}\right), \quad Q_3 = \left(\frac{x_1 - q_{13}}{q_{12} - q_{13}}, \frac{x_2 - q_{23}}{q_{12} - q_{13}}, 0\right).$$

Hence $\ell = 3$ and the condition in step (2) holds. We also find that $H^0(X'_0, D'_0 - Z) = 0$, so that the condition in step (3) is satisfied as well. Algorithm 2.6.2 outputs the soliton matrix

$$A \; = \; \begin{pmatrix} 0 & \frac{\kappa_1 - q_{12}}{q_{13} - q_{12}} \frac{1}{K'(\kappa_1)} & \frac{\kappa_1 - q_{13}}{q_{12} - q_{13}} \frac{1}{K'(\kappa_1)} \\ \frac{\kappa_2 - q_{12}}{q_{23} - q_{12}} \frac{1}{K'(\kappa_2)} & 0 & \frac{\kappa_2 - q_{23}}{q_{12} - q_{13}} \frac{1}{K'(\kappa_2)} \\ \frac{\kappa_3 - q_{13}}{q_{23} - q_{12}} \frac{1}{K'(\kappa_3)} & \frac{\kappa_3 - q_{23}}{q_{13} - q_{23}} \frac{1}{K'(\kappa_3)} & 0 \end{pmatrix}. \tag{2.30}$$

The curve X is the last one in [4, Figure 2]. The Delaunay polytope $\mathcal{C}$ is a tetrahedron as in Figure 2.4, so Theorem 2.3.6 applies. It would be desirable to better understand the relationship between the soliton solution (2.30), the Hirota variety $\mathcal{H}_{\mathcal{C}}$, and the Dubrovin variety in [5, Example 6.2].

We end with a few words of conclusion. There are two ways to obtain a tau function from a smooth curve: via the theta function and the Dubrovin threefold as in [5], or via the Sato Grassmannian as in Section 2.5. In this chapter we presented a parallel for tropical limits of smooth curves: namely, the Delaunay polytopes and Hirota varieties of Sections 2.1–2.3, or the Sato Grassmannian as in Section 2.5. Our next goal is to better understand this process in families. An essential step is to clarify the relation between the degeneration of theta functions via $\mathbf{a} \in \mathcal{C}$ as in (2.3) and the choice of the divisor D and point p in Algorithm 2.6.2.

Chapter 3

Restricting to rational nodal curves

3.1 Introduction

In this chapter, we restrict our attention to irreducible rational nodal curves. For the case of an irreducible rational nodal curve X of genus g, the dual graph consists of one unique node with precisely g cycles, one for each node, and the associated tropical Riemann matrix is the identity matrix of size g (see Figure 3.1). The induced metric is the Euclidean metric, so the Voronoi and Delaunay subdivisions are both tiled by g-dimensional unit cubes centered at lattice points and lattice points shifted by $(1/2)^g$, respectively.
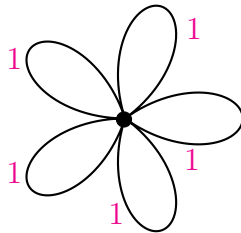
Figure 3.1: The metric graph for an irreducible rational nodal curve of genus 5

The *degenerate Riemann theta function* associated to X is a finite sum of exponentials

$$\theta_{\mathcal{C}}(\mathbf{z}) \;=\; a_1 \exp[\mathbf{c}_1^T \mathbf{z}] \;+\; a_2 \exp[\mathbf{c}_2^T \mathbf{z}] \;+\; \ldots \;+\; a_{2^g} \exp[\mathbf{c}_{2^g}^T \mathbf{z}] \tag{3.1}$$

supported on the configuration of points $\mathcal{C} = \{0,1\}^g$ in the integer lattice $\mathbb{Z}^g$. Each of these points $\mathbf{c}_i = (\mathbf{c}_{i1}, \mathbf{c}_{i2}, \ldots, \mathbf{c}_{ig})$ determines a linear form $\mathbf{c}_i^T \mathbf{z} = \sum_{j=i}^g c_{ij} z_j$ and the coefficients $\mathbf{a} = (a_1, a_2, \ldots, a_{2^g})$ are unknowns that play the role of coordinates on the algebraic torus $(\mathbb{C}^*)^{2^g}$.

The *Hirota variety* $\mathcal{H}_{\mathcal{C}}$ associated to X, introduced in the previous chapter, lives in the parameter space given by the product of the algebraic torus $(\mathbb{C}^*)^{2^g}$ with coordinates $\mathbf{a} = (a_1, \ldots, a_{2^g})$, and the weighted projective space $\mathbb{WP}^{3g-1}$ whose coordinates are the vectors

$\mathbf{u} = (u_1, \ldots, u_g)$, $\mathbf{v} = (v_1, \ldots, v_g)$, and $\mathbf{w} = (w_1, \ldots, w_g)$ with weights 1,2, and 3, for u_i, v_i, and w_i respectively. It parameterizes the points $(\mathbf{a}, (\mathbf{u}, \mathbf{v}, \mathbf{w})) \in (\mathbb{C}^*)^{2g} \times \mathbb{WP}^{3g-1}$ such that the τ-function $\tau(x, y, t) = \theta_{\mathcal{C}}(\mathbf{u}x + \mathbf{v}w + \mathbf{w}t)$ satisfies Hirota's bilinear equation (1.8), providing a sufficient condition for the function

$$p(x, y, t) = 2\frac{\partial^2}{\partial x^2} \log \tau(x, y, t) \tag{3.2}$$

to be a solution for the KP equation.

Finding solutions to the KP equation is related to the *Schottky problem*, in that a theta function satisfies the KP equation when the corresponding abelian variety is a Jacobian of a curve [79, 100]. As discussed in Section 1.2, the Schottky problem is unsolved and difficult for genus $g \geq 5$. Many approaches to the Schottky problem have been developed (e.g., [9, 68]) and an explicit solution to the weak Schottky problem was provided in [43] and investigated numerically for genus 5 in [6]. The proof of Theorem 3.2.3 in our paper relies on a solution to the weak Schottky problem for nodal curves, which we provide for $g \leq 9$.

This chapter is organized as follows. In Section 3.2, we introduce the Hirota variety of a rational nodal curve and discuss its main component. We prove for genus $g \leq 9$ that this is an irreducible component of dimension $3g$ and we explain how this relates to the Schottky problem. Section 3.3 studies the equations of the main component of the variety $\mathcal{H}_{\mathcal{C}}$ and how this relates to the combinatorics of the cube.

3.2 The main component of the Hirota variety

Let X be a rational nodal curve of genus g. The degenerate theta function (3.1) associated to X is supported on the vertices of the g-dimensional cube $\mathcal{C}$ whose vertices are all possible binary g-dimensional vectors. The Hirota variety $\mathcal{H}_{\mathcal{C}}$ lives in the space $(\mathbb{C}^*)^{2g} \times \mathbb{WP}^{3g-1}$ with coordinate ring $\mathbb{C}[\mathbf{a}^{\pm 1}, \mathbf{u}, \mathbf{v}, \mathbf{w}]$, where $\deg(u_i) = 1, \deg(v_i) = 2$, and $\deg(w_i) = 3$, for $i = 1, 2, \ldots, g$.

We now want to investigate the subvariety of the Hirota variety $\mathcal{H}_{\mathcal{C}}$, denoted by $\mathcal{H}_{\mathcal{C}}^I$, where the superscript I stands for 'invertible'. We define this to be the Zariski closure of the set

$$\left\{ (\mathbf{a}, (\mathbf{u}, \mathbf{v}, \mathbf{w})) \in \mathcal{H}_{\mathcal{C}} \ : \ \mathbf{u} \neq \mathbf{0} \right\}. \tag{3.3}$$

This subvariety contains an irreducible subvariety of $\mathcal{H}_{\mathcal{C}}$ which we call the *main component*, denoted by $\mathcal{H}_{\mathcal{C}}^M$. In order to rigorously define $\mathcal{H}_{\mathcal{C}}^M$, consider the map from the affine space $\mathbb{C}^{3g}$ with coordinates $(\lambda_1, \ldots, \lambda_g, \kappa_1, \kappa_2, \ldots, \kappa_{2g})$ into the ambient space of the Hirota variety $\mathcal{H}_{\mathcal{C}}$ given by

$$\phi : \mathbb{C}^{3g} \ \dashrightarrow \ (\mathbb{C}^*)^{2g} \times \mathbb{WP}^{3g-1} \tag{3.4}$$

$$(\lambda_1, \ldots, \lambda_g, \kappa_1, \kappa_2, \ldots, \kappa_{2g}) \longrightarrow (a_{\mathbf{c}_1}, a_{\mathbf{c}_2}, \ldots, a_{\mathbf{c}_{2g}}, \mathbf{u}, \mathbf{v}, \mathbf{w})$$

where the coordinates $\mathbf{a} = (a_{\mathbf{c}_1}, a_{\mathbf{c}_2}, \ldots, a_{\mathbf{c}_{2g}})$ are indexed by the points in $\mathcal{C} = \{0, 1\}^g$. The image of ϕ is defined as follows:

$$u_i = \kappa_{2i-1} - \kappa_{2i}, \quad v_i = \kappa_{2i-1}^2 - \kappa_{2i}^2, \quad w_i = \kappa_{2i-1}^3 - \kappa_{2i}^3 \qquad \text{for all } i = 1, 2, \ldots, g,$$

$$a_{\mathbf{c}} = \prod_{\substack{i,j \in I \\ i<j}} (\kappa_i - \kappa_j) \prod_{i:c_i=1} \lambda_i, \quad \text{where } I = \{2i : c_i = 0\} \cup \{2i - 1 : c_i = 1\} \quad \text{for all } \mathbf{c} \in \mathcal{C}. \tag{3.5}$$

We call the closure of the image of ϕ the *main component of* $\mathcal{H}_{\mathcal{C}}$ and denote it by $\mathcal{H}_{\mathcal{C}}^M$.

In the first part of this section we explain the geometric intuition that leads us to the definition of the main component $\mathcal{H}_{\mathcal{C}}^M$ by way of the *Abel map* for curves and the *theta divisor*, see [8]. In the second part we focus on the study of the main component and on its connection with the weak and the classical Schottky problem.

The Theta Divisor of a Rational Nodal Curve

Let X be a curve as above and denote by $n_1, n_2, \ldots, n_g$ its nodes. The normalization $\nu : \tilde{X} \to X$ that separates the g nodes of X is given by a projective line. We can consider $\kappa_1, \kappa_2, \ldots, \kappa_{2g}$ to be points on $\mathbb{P}^1$ and set $\nu^{-1}(n_i) := \{\kappa_{2i-1}, \kappa_{2i}\}$. Hence, each rational curve with only nodal singularities corresponds to a copy of $\mathbb{P}^1$ and $2g$ points on it. This fact motivates that the moduli space of rational nodal curves has dimension $2g - 3$, where one subtracts 3 to account for the dimension of the automorphism group of $\mathbb{P}^1$. We can find a basis of canonical differentials for such curves as

$$\omega_i = \frac{1}{y} \left(\frac{1}{1 - \kappa_{2i}y} - \frac{1}{1 - \kappa_{2i-1}y} \right) dy \qquad \text{for } i = 1, 2, \ldots, g,$$

when fixing $y = 1/x$ as local coordinate. These define a map $\alpha' : (\mathbb{P}^1)^{g-1} \dashrightarrow \mathbb{C}^g$ such that

$$(y_1, \ldots, y_{g-1}) \longmapsto \left(\sum_{i=1}^{g-1} \int_0^{y_i} \omega_j \right)_{j=1,2,\ldots,g} \qquad \text{where} \qquad \int_0^{y_i} \omega_j = \log \left(\frac{1 - \kappa_{2j-1}y_i}{1 - \kappa_{2j}y_i} \right).$$

The (generalized) Jacobian of the curve X is an algebraic torus $(\mathbb{C}^*)^g$. Exponentiation allows us to map into the Jacobian through the map $\mathbb{C}^g \to (\mathbb{C}^*)^g$ given by $((z_1, \ldots, z_g) \mapsto (\exp[z_1], \ldots, \exp[z_g]))$. The composition gives the Abel map $\alpha : (\mathbb{P}^1)^{g-1} \dashrightarrow (\mathbb{C}^*)^g$ defined by

$$(y_1, \ldots, y_{g-1}) \longmapsto \left(\prod_{i=1}^{g-1} \frac{1 - \kappa_1 y_i}{1 - \kappa_2 y_i}, \prod_{i=1}^{g-1} \frac{1 - \kappa_3 y_i}{1 - \kappa_4 y_i}, \ldots, \prod_{i=1}^{g-1} \frac{1 - \kappa_{2g-1}y_i}{1 - \kappa_{2g}y_i} \right). \tag{3.6}$$

The theta divisor of X is the image of the Abel map α up to translation. We will motivate later that we expect each point in the main component of the Hirota variety $\mathcal{H}_{\mathcal{C}}^M$ to correspond (non-injectively) to the choice of a curve in this moduli space and a theta divisor. Following this reasoning, the projection of $\mathcal{H}_{\mathcal{C}}^M$ into the space $(\mathbb{C}^*)^{2g}$ has dimension $3g - 3$, accounting for the choice of a rational nodal curve and its theta divisor. For each point in

this projection, the fiber is a threefold (analogous to the Dubrovin threefold studied in [5]) given by

$$\{\,(\mathbf{u}, \mathbf{v}, \mathbf{w}) \in \mathbb{WP}^{3g-1} \;:\; \tau(x, y, t) = \theta_{\mathcal{C}}(\mathbf{u}x + \mathbf{v}y + \mathbf{w}t) \text{ solves } (1.8)\,\}.$$

Thus, the expected dimension of the main component is $2g - 3 + g + 3 = 3g$. This discussion provides also a way to parameterize the main component of the Hirota variety. The idea is that the choice of the curve X yields $2g$ parameters $\kappa_1, \kappa_2, \ldots, \kappa_{2g}$, and the family of theta divisors corresponding to shifts of the unknown vector $\mathbf{z} \in \mathbb{C}^g$ yields g parameters $\lambda_1, \ldots, \lambda_g$. In particular, we are able to compute, using `Macaulay2`, the theta divisor as a shift (through a change of variables) of the image of the map (3.6) up to genus 6. This is done following the method described in [88, Corollary 4.8]. The equation of the theta divisor returned by the code coincides precisely with (3.15) with coefficients $\mathbf{a} = (a_1, a_2, \ldots, a_{2g})$ parameterized in a way which can be shown, through a change of coordinates and some calculations, to be geometrically equivalent to (3.5), up to the λ parameters. More precisely, this justifies that the parameterization in (3.4) is not unique. The torus action on the theta divisor provides new suitable parameterizations. The approach for computing the theta divisor was inspired by [3].

To understand how the λ parameters arise, we consider the Riemann theta function (3.1) evaluated at a point $\mathbf{z} \in \mathbb{C}^g$ and at a shift of it, namely

$$\theta_{\mathcal{C}}(\mathbf{z} + \mathbf{h}) = \sum_{\mathbf{c} \in \mathcal{C}} a_{\mathbf{c}} \exp[\mathbf{c}^T \mathbf{h}] \exp[\mathbf{c}^T \mathbf{z}],$$

where $\mathbf{h} = (h_1, h_2, \ldots, h_g) \in \mathbb{C}^g$ represents the shift. These both provide solutions to the KP equation (with nonzero u_i), hence they correspond to points in $\mathcal{H}_{\mathcal{C}}^M$. More explicitly, letting $\lambda_i := \exp[h_i]$, we see that for a point $(\mathbf{a}, (\mathbf{u}, \mathbf{v}, \mathbf{w})) \in \mathcal{H}_{\mathcal{C}}^M$, the point $(\tilde{\mathbf{a}}, (\mathbf{u}, \mathbf{v}, \mathbf{w})) \in \mathcal{H}_{\mathcal{C}}^M$, where $\tilde{\mathbf{a}} = (a_{\mathbf{c}} \exp[\mathbf{c}^T \mathbf{h}]) = (a_{\mathbf{c}} \prod_{i : c_i = 1} \lambda_i)$. Thus, we conclude that the choice of theta divisor is exactly represented by the parameterizing variables $\lambda_1, \ldots, \lambda_g$.

Example 3.2.1. ($g = 3$) This example is intended to clarify the role of the parameters in the case of the 3-cube. For the κ parameters, as in the proof above we fix $\kappa_1, \ldots, \kappa_6 \in \mathbb{P}^1$. The differentials $\omega_1, \omega_2, \omega_3$, after the coordinate change $y = 1/x$, are given by

$$\omega_1 \;=\; \frac{1}{y} \left(\frac{1}{1 - \kappa_2 y} - \frac{1}{1 - \kappa_1 y} \right) dy, \qquad \omega_2 \;=\; \frac{1}{y} \left(\frac{1}{1 - \kappa_4 y} - \frac{1}{1 - \kappa_3 y} \right) dy,$$

$$\omega_3 \;=\; \frac{1}{y} \left(\frac{1}{1 - \kappa_6 y} - \frac{1}{1 - \kappa_5 y} \right) dy.$$

Then the Abel map $\alpha : (\mathbb{P}^1)^2 \dashrightarrow (\mathbb{C}^*)^3$ is defined by

$$(y_1, y_2) \mapsto \left(\left(\frac{1 - \kappa_1 y_1}{1 - \kappa_2 y_1} \right) \cdot \left(\frac{1 - \kappa_1 y_2}{1 - \kappa_2 y_2} \right), \left(\frac{1 - \kappa_3 y_1}{1 - \kappa_4 y_1} \right) \cdot \left(\frac{1 - \kappa_3 y_2}{1 - \kappa_4 y_2} \right), \left(\frac{1 - \kappa_5 y_1}{1 - \kappa_6 y_1} \right) \cdot \left(\frac{1 - \kappa_5 y_2}{1 - \kappa_6 y_2} \right) \right).$$

We find the implicit equation cutting out the image of this map in `Macaulay2` with the code

```
I = ideal(q1*(1-k2*y1)*(1-k2*y2)-(1-k1*y1)*(1-k1*y2),
          q2*(1-k4*y1)*(1-k4*y2)-(1-k3*y1)*(1-k3*y2),
          q3*(1-k6*y1)*(1-k6*y2)-(1-k5*y1)*(1-k5*y2));
J = eliminate(I,{y1,y2})
```

The resulting equation gives exactly the familiar theta function for $g = 3$, with the $a_\mathbf{c}$ parameterized by the κ_i's. For the λ parameters, we consider the theta functions

$$\theta(\mathbf{z}) = a_{000} + a_{100}\exp[z_1] + a_{010}\exp[z_2] + a_{001}\exp[z_3] + a_{110}\exp[z_1 + z_2] \qquad (3.7)$$
$$+ a_{101}\exp[z_1 + z_3] + a_{011}\exp[z_2 + z_3] + a_{111}\exp[z_1 + z_2 + z_3]$$

and

$$\theta(\mathbf{z} + \mathbf{h}) = a_{000} + a_{100}\exp[h_1]\exp[z_1] + a_{010}\exp[h_2]\exp[z_2] + a_{001}\exp[h_3]\exp[z_3]$$
$$+ a_{110}\exp[h_1 + h_2]\exp[z_1 + z_2] + a_{101}\exp[h_1 + h_3]\exp[z_1 + z_3]$$
$$+ a_{011}\exp[h_2 + h_3]\exp[z_2 + z_3] + a_{111}\exp[h_1 + h_2 + h_3]\exp[z_1 + z_2 + z_3].$$

Letting $\lambda_i := \exp[h_i]$, we have

$$\theta(\mathbf{z} + \mathbf{h}) = a_{000} + \lambda_1 a_{100}\exp[z_1] + \lambda_2 a_{010}\exp[z_2] + \lambda_3 a_{001}\exp[z_3] + \lambda_1\lambda_2 a_{110}\exp[z_1 + z_2]$$
$$+ \lambda_1\lambda_3 a_{101}\exp[z_1 + z_3] + \lambda_2\lambda_3 a_{011}\exp[z_2 + z_3] + \lambda_1\lambda_2\lambda_3 a_{111}\exp[z_1 + z_2 + z_3].$$

This gives us g parameterizing factors λ_i with $i = 1, 2, \ldots, g$ for the variables $a_\mathbf{c}$.

The code used in Example 3.2.1 is available at the repository website `MathRepo` [44] of MPI-MiS via the link

$$\text{https://mathrepo.mis.mpg.de/HirotaVarietyRationalNodalCurve.} \qquad (3.8)$$

Geometry of the main component

The following result justifies the definition of the main component $\mathcal{H}_\mathcal{C}^M$ and provides a connection with soliton solutions to the KP equation.

Theorem 3.2.2. *Consider the map ϕ given in (3.4). This is a birational map onto its image, which is an irreducible subvariety of $\mathcal{H}_\mathcal{C}^M$ and has dimension $3g$.*

Proof. Let I be as in (3.5). Let $K \subseteq \mathbb{C}^{3g}$ be the closed set where at least two of the κ_i coincide. The expression of $\tau(x, y, t) = \theta_\mathcal{C}(\mathbf{u}x + \mathbf{v}y + \mathbf{w}t)$ where $(\mathbf{a}, (\mathbf{u}, \mathbf{v}, \mathbf{w}))$ is attained as the image of a point in $\mathbb{C}^{3g} \setminus K$ through the map ϕ, described in (3.4), is a point in the Hirota variety $\mathcal{H}_\mathcal{C}$. This is because it can be expressed as a $(g, 2g)$-soliton [75] for the matrix

$$A = \begin{pmatrix} \lambda_1 & 1 & 0 & 0 & 0 & 0 & \ldots & 0 & 0 \\ 0 & 0 & \lambda_2 & 1 & 0 & 0 & \ldots & 0 & 0 \\ 0 & 0 & 0 & 0 & \lambda_3 & 1 & \ldots & 0 & 0 \\ \vdots & \vdots & \vdots & \vdots & \vdots & \vdots & \ddots & \vdots & \vdots \\ 0 & 0 & 0 & 0 & 0 & 0 & \ldots & \lambda_g & 1 \end{pmatrix} \qquad (3.9)$$

Indeed, if we denote $E_i := \exp(\kappa_i x + \kappa_i^2 y + \kappa_i^3 t)$, then plugging the parameterization in $\theta_{\mathcal{C}}(\mathbf{u}x + \mathbf{v}y + \mathbf{w}t)$, we obtain:

$$\tilde{\tau}_{\mathcal{C}}(x,y,t) = \frac{1}{E_2 E_4 \cdots E_{2g}} \left(\sum_I \prod_{i<j\in I} (\kappa_i - \kappa_j) \prod_{i:c_i=1} \lambda_i \prod_{i\in I} E_i \right). \tag{3.10}$$

Here the sets I that define the sum are the same ones defined in (3.5). The extraneous exponential factor $(E_2 E_4 \cdots E_{2g})^{-1}$ disappears after we pass from $\tilde{\tau}(x,y,t)$ to $\partial_x^2 \log(\tilde{\tau}(x,y,t))$. Both versions of the $(g,2g)$-soliton satisfy Hirota's bilinear form and they represent the same solution to the KP equation. Hence, it follows that the image of $\mathbb{C}^{3g}$ through the map ϕ is contained in $\mathcal{H}_{\mathcal{C}}$.

Furthermore, the map ϕ is invertible outside the closed set where the u_i's vanish: given a point $(\mathbf{a}, (\mathbf{u}, \mathbf{v}, \mathbf{w}))$ in the image one can write

$$\kappa_{2i-1} = \frac{u_i^2 + v_i}{2u_i} \qquad \text{and} \qquad \kappa_{2i} = \frac{v_i - u_i^2}{2u_i}, \tag{3.11}$$

and the λ_i's can be obtained sequentially, starting from λ_1, by plugging in the values for the κ variables into the a_i's. Hence we can conclude that the map ϕ is birational. This implies that the closure of the image is irreducible and of dimension $3g$. $\qquad\square$

Notice that the method above gives a way to parameterize solutions arising from a genus g rational nodal curve as $(g,2g)$-solitons. This is also consistent with [7, Example 29].

In what follows we show that $\mathcal{H}_{\mathcal{C}}^M$ is an irreducible component of $\mathcal{H}_{\mathcal{C}}$ whose points correspond to genus g rational nodal curves. This is equivalent to solving a version of the *weak Schottky problem*. In fact, $\mathcal{H}_{\mathcal{C}}^M$ parameterizes some solutions to the KP equation arising from irreducible rational nodal curves of genus g, and hence corresponds to a variety containing the locus of Jacobians of such curves as an irreducible component.

Theorem 3.2.3. *For genus $g \leq 9$, the subvariety $\mathcal{H}_{\mathcal{C}}^M$ is an irreducible component of the Hirota variety.*

Proof. The proof is mainly computational. A direct computation performed in `Macaulay2` shows that the Jacobian matrix of the Hirota variety $\mathcal{H}_{\mathcal{C}}$ evaluated at the image of a general point in $\mathbb{C}^{3g}$ through ϕ has rank $r-3g$, where r is the dimension of the space $(\mathbb{C}^*)^{2g} \times \mathbb{WP}^{3g-1}$. Hence the map ϕ is dominant into the main component $\mathcal{H}_{\mathcal{C}}^M$. $\qquad\square$

The code used for the proof above can be found at (3.8). What makes the computation challenging for higher genus is mainly the fast growth of the number of variables $\mathbf{a} = (a_{\mathbf{c}_1}, a_{\mathbf{c}_2}, \ldots, a_{\mathbf{c}_{2g}})$. One possible way to compute the ideal defining the variety $\mathcal{H}_{\mathcal{C}}$ is to use the condition provided by the Hirota's bilinear form (1.8), which becomes difficult when the genus is larger than 7. To avoid this computation, we implement the equations cutting out $\mathcal{H}_{\mathcal{C}}$ via the combinatorial description provided in [7, Section 3].

The parameterization for the main component of the Hirota variety associated to the 3-dimensional cube was already developed in [7, Example 8] even though the definition of

the main component was not clearly stated yet. We revisit this example, working out the details providing the intuition behind Theorem 3.2.2.

Example 3.2.4 ($g = 3$). The 3-cube associated to the dual graph of a rational nodal quartic is the support of the degenerate theta function (3.7). The Hirota variety $\mathcal{H}_\mathcal{C}$ in $(\mathbb{C}^*)^8 \times \mathbb{WP}^8$ is cut out by 19 polynomial equations. These are displayed in Example 2.3.4. A direct computation shows that the ideal defining $\mathcal{H}_\mathcal{C}$ has five minimal associated primes, hence the Hirota variety has five irreducible components in $(\mathbb{C}^*)^8 \times \mathbb{WP}^8$. If we restrict to the main component, then we can observe that the additional quartic relation

$$a_{000}a_{110}a_{101}a_{011} \;=\; a_{100}a_{010}a_{001}a_{111} \tag{3.12}$$

holds. The main component has dimension 9, while its image in $\mathbb{WP}^8$ has dimension 5 and it is defined by the equations $u_1^4 + 3v_1^2 - 4u_1w_1$, $u_2^4 + 3v_2^2 - 4u_2w_2$, $u_3^4 + 3v_3^2 - 4u_3w_3$, with fibers given by cones over $\mathbb{P}^1 \times \mathbb{P}^1 \times \mathbb{P}^1$. The following is a parametric representation of the main component in $\mathcal{H}_C$:

$$u_1 = \kappa_1 - \kappa_2, \quad v_1 = \kappa_1^2 - \kappa_2^2, \quad w_1 = \kappa_1^3 - \kappa_2^3,$$
$$u_2 = \kappa_3 - \kappa_4, \quad v_2 = \kappa_3^2 - \kappa_4^2, \quad w_2 = \kappa_3^3 - \kappa_4^3,$$
$$u_3 = \kappa_5 - \kappa_6, \quad v_3 = \kappa_5^2 - \kappa_6^2, \quad w_3 = \kappa_5^3 - \kappa_6^3,$$
$$a_{111} = (\kappa_3 - \kappa_5)(\kappa_1 - \kappa_5)(\kappa_1 - \kappa_3)\lambda_1\lambda_2\lambda_3, \quad a_{011} = (\kappa_3 - \kappa_5)(\kappa_2 - \kappa_5)(\kappa_2 - \kappa_3)\lambda_2\lambda_3,$$
$$a_{101} = (\kappa_4 - \kappa_5)(\kappa_1 - \kappa_5)(\kappa_1 - \kappa_4)\lambda_1\lambda_3, \quad a_{001} = (\kappa_4 - \kappa_5)(\kappa_2 - \kappa_5)(\kappa_2 - \kappa_4)\lambda_3,$$
$$a_{110} = (\kappa_3 - \kappa_6)(\kappa_1 - \kappa_6)(\kappa_1 - \kappa_3)\lambda_1\lambda_2, \quad a_{010} = (\kappa_3 - \kappa_6)(\kappa_2 - \kappa_6)(\kappa_2 - \kappa_3)\lambda_2,$$
$$a_{100} = (\kappa_4 - \kappa_6)(\kappa_1 - \kappa_6)(\kappa_1 - \kappa_4)\lambda_1, \quad a_{000} = (\kappa_4 - \kappa_6)(\kappa_2 - \kappa_6)(\kappa_2 - \kappa_4).$$

It provides a way of identifying the τ-function arising from (3.7) with a $(3,6)$-soliton for the matrix

$$A \;=\; \begin{pmatrix} \lambda_1 & 1 & 0 & 0 & 0 & 0 \\ 0 & 0 & \lambda_2 & 1 & 0 & 0 \\ 0 & 0 & 0 & 0 & \lambda_3 & 1 \end{pmatrix}. \tag{3.13}$$

The description given in this example of the projection of the main component $\mathcal{H}_\mathcal{C}^M$ into the space $\mathbb{WP}^{3g-1}$ reveals itself to be true for any genus:

Proposition 3.2.5. *The projection of $\mathcal{H}_\mathcal{C}^M$ into $\mathbb{WP}^{3g-1}$ is a $(2g-1)$-dimensional variety defined by the vanishing of $u_i^4 + 3v_i^2 - 4u_iw_i$ for $i = 1, 2, \ldots, g$.*

Proof. One direction (i.e., that the relations $u_i^4 + 3v_i^2 - 4u_iw_i$ hold in the projection) is immediate, as these are polynomials defining the Hirota variety (see Lemma 3.3.2) that do not include any a_i. For the other direction, it suffices to exhibit a point in $\mathcal{H}_\mathcal{C}^M$ for any $(\mathbf{u}, \mathbf{v}, \mathbf{w})$ which satisfy $u_i^4 + 3v_i^2 - 4u_iw_i$ for all $i \in [g]$. Using the inverse map in (3.11), given any u_i, v_i, w_i satisfying $u_i^4 + 3v_i^2 - 4u_iw_i = 0$, we uniquely determine (up to a scaling factor) $\kappa_{2i-1}, \kappa_{2i}$. We can then choose arbitrary $\lambda_1, \ldots, \lambda_g$ to get a point $(\mathbf{a}, (\mathbf{u}, \mathbf{v}, \mathbf{w}))$, so we are done. $\qquad\square$

We conclude this section by stating two conjectures which consolidate and generalize the results above to any genus. Indeed a generalization of Theorem 3.2.3 would provide a solution to the weak Schottky problem for rational nodal curves of genus g.

Weak Schottky Problem. For any genus g, the main component of the Hirota variety $\mathcal{H}_{\mathcal{C}}^{M}$ is a $3g$-dimensional irreducible component of $\mathcal{H}_{\mathcal{C}}$ with a parametric representation given by (3.5).

Strong Schottky Problem. $\mathcal{H}_{\mathcal{C}}^{M} = \mathcal{H}_{\mathcal{C}}^{I}$.

Notice that one direction of the Schottky problem is immediate from the proof of Theorem 3.2.2: a sufficiently generic choice of κ_i ensures that, in the image, the u_i are nonzero, thus $\mathcal{H}_{\mathcal{C}}^{M} \subseteq \mathcal{H}_{\mathcal{C}}^{I}$. The other direction is more difficult. To prove it, one would need to show that any point in $\mathcal{H}_{\mathcal{C}}^{I}$ can be parameterized as in (3.5).

3.3 Combinatorics of the Hirota variety

The results in this section describe in detail facts which we use in many of the proofs in section 3.2. We begin by explaining how the nodal singularities on the curve X induce the degenerate theta function in (3.1). To each curve of genus g we associate a metric graph Γ of genus g. This graph has a vertex for each irreducible component, one edge for each intersection point between two components, and a node on an irreducible component gives a loop on the corresponding vertex. Hence, if X is a rational nodal curve of genus g, the corresponding metric graph Γ is given by one unique node and g cycles. Figure 3.1 illustrates an example when $g = 5$.

The way we read off the tropical Riemann matrix Q from a tropical curve is described in [19, 29]. More explicitly, to determine such positive definite real symmetric $g \times g$ matrix one needs to fix a basis of cycles in Γ and write these as the g rows of a matrix Λ whose columns are labeled by the edges of the graph. Let Δ be the diagonal matrix whose entries are the edge lengths of Γ, then we define $Q := \Lambda \Delta \Lambda^{T}$. Hence, for X being a rational nodal curve the matrices Λ and Δ both equal the identity matrix I_g, returning $Q = I_g$ as the tropical Riemann matrix. Theorem 3 in [7] describes the Riemann theta function (1.1) when the curve degenerates. In our case, the distance induced on $\mathbb{R}^g$ is the Euclidean distance and we can fix the point $\mathbf{a} = \left(\frac{1}{2}, \frac{1}{2}, \ldots, \frac{1}{2}\right) \in \mathbb{R}^g$ as a vertex of the *Voronoi cell* for I_g given by the cube with vertices $\left(\pm\frac{1}{2}, \pm\frac{1}{2}, \ldots, \pm\frac{1}{2}\right)$. Under these hypotheses, the support of the degenerate theta function is the Delaunay set

$$\mathcal{C} = \mathcal{D}_{\mathbf{a}, I_g} = \left\{ \mathbf{c} \in \mathbb{Z}^g : \|\mathbf{a}\|^2 = \|\mathbf{a} - \mathbf{c}\|^2 \right\} = \{0, 1\}^g, \tag{3.14}$$

where $\|\cdot\|$ denotes the Euclidean norm. The degenerate theta function is then a finite sum of 2^g exponentials

$$\theta_{\mathcal{C}}(\mathbf{z}) = \sum_{\mathbf{c} \in \{0,1\}^g} a_{\mathbf{c}} \exp\left[\mathbf{c}^T \mathbf{z}\right], \quad \text{where} \quad a_{\mathbf{c}} = \exp\left[\frac{1}{2} \mathbf{c}^T R_0 \mathbf{c}\right]. \tag{3.15}$$

Here the matrix R_0 is the limit of a matrix R_ϵ which is a symmetric $g \times g$ matrix with entries given by complex analytic functions in ϵ converging for $\epsilon \to 0$. This comes from degenerating the family of Riemann matrices given by $B_\epsilon = -\frac{1}{\epsilon}Q + R_\epsilon$. The matrices B_ϵ lie in the Schottky locus. Corollary 2.3.2 describes the polynomials defining the Hirota variety associated to $\mathcal{C}$. These correspond to points in the set

$$\mathcal{C}^{[2]} \;=\; \big\{\, \mathbf{c}_k + \mathbf{c}_\ell \;:\; 1 \le k < \ell \le m \,\big\} \quad \subset \; \mathbb{Z}^g,$$

where one says that a point $\mathbf{d}$ in $\mathcal{C}^{[2]}$ is *uniquely attained* if there exists precisely one index pair (k, ℓ) such that $\mathbf{c}_k + \mathbf{c}_\ell = \mathbf{d}$. Let $P(x, y, t) = x^4 + 3y^2 - 4xt$. The polynomials defining $\mathcal{H}_\mathcal{C}$ are explicitly given by the quartics

$$P_{k\ell}(\mathbf{u}, \mathbf{v}, \mathbf{w}) \;:=\; P\big((\mathbf{c}_k - \mathbf{c}_\ell) \cdot \mathbf{u},\, (\mathbf{c}_k - \mathbf{c}_\ell) \cdot \mathbf{v},\, (\mathbf{c}_k - \mathbf{c}_\ell) \cdot \mathbf{w} \big), \qquad (3.16)$$

when $\mathbf{d} = \mathbf{c}_k + \mathbf{c}_\ell$ is uniquely attained, and by

$$\sum_{\substack{1 \le k < \ell \le m \\ \mathbf{c}_k + \mathbf{c}_\ell = \mathbf{d}}} P_{k\ell}(\mathbf{u}, \mathbf{v}, \mathbf{w}) a_k a_\ell,$$

when $\mathbf{d} \in \mathcal{C}^{[2]}$ is not uniquely attained. Hence, to better understand the variety $\mathcal{H}_\mathcal{C}$ we investigate the elements in the set $\mathcal{C}^{[2]}$. We say that a point $\mathbf{c} \in \mathcal{C}^{[2]}$ is attained n times if there exist n distinct pairs (k, ℓ) such that $\mathbf{c}_k + \mathbf{c}_\ell = \mathbf{d}$.

Proposition 3.3.1. *A point $\mathbf{c} = (c_1, \ldots, c_g)$ in $\mathcal{C}^{[2]}$ is attained 2^{d-1} times, where $d = |\{i : c_i = 1\}|$.*

Proof. For a point $\mathbf{c} \in \mathcal{C}^{[2]}$, consider the set of indices $I = \{i : c_i \ne 1\}$. Suppose now $\mathbf{c} = \mathbf{c}_1 + \mathbf{c}_2$ for some points $\mathbf{c}_1, \mathbf{c}_2 \in \mathcal{C}$. Then, for any $i \in I$, if $c_i = 0$ then $c_{1i} = c_{2i} = 0$, while if $c_i = 2$ then $c_{1i} = c_{2i} = 1$. In the first case, this means that both $\mathbf{c}_1$ and $\mathbf{c}_2$ lie on the face of the g-cube defined by the i-th coordinate hyperplane $x_i = 0$. In the latter case, $\mathbf{c}_1, \mathbf{c}_2$ lie on the face defined by $x_i = 1$. The full set I of indices corresponding to elements $\ne 1$ defines a set of restrictions on x_i for $i \in I$. In fact, it defines a face of codimension $|I|$ (and thus dimension d) that $\mathbf{c}_1$ and $\mathbf{c}_2$ lie on. For the indices $i \in [g] \setminus I$, we have exactly one of c_{1i}, c_{2i} equal to 1. This gives exactly 2^{d-1} such pairs. These pairs can be viewed as diagonals of the faces defined by the restrictions given by I: they are the points which are distinct from one another in each coordinate except for the ones fixed by the face. $\qquad\square$

As discussed in the proof, the points in $\mathcal{C}^{[2]}$ correspond to d-dimensional faces of the g-cube, where d is the number of coordinates equal to 1. Hence $|\mathcal{C}^{[2]}| = \sum_{d=1}^{g} 2^{g-d}\binom{g}{d}$ and the pairs that sum to points in $\mathcal{C}^{[2]}$ correspond to diagonals of the associated face. See Figure 3.2 which illustrates this. In the picture, the blue edge of the three-cube corresponds to the point $(1, 2, 2) \in \mathcal{C}^{[2]}$, which is attained once. The pink two-dimensional face of the cube corresponds to the point $(2, 1, 1)$, which is attained twice, by the two diagonals of the face. Another way to count $|\mathcal{C}^{[2]}|$ is to observe that it consists exactly of the points in $\{0, 1, 2\}^g$ which have at least one 1, so there are $3^g - 2^g$ of them.
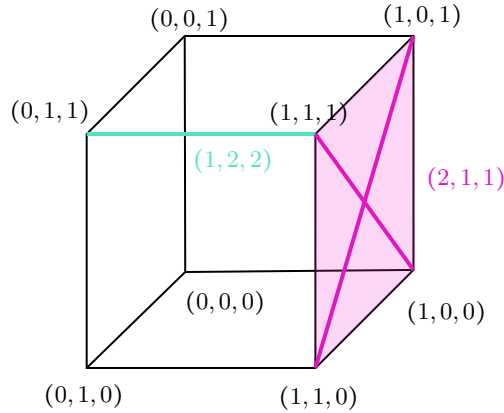
Figure 3.2: The three-cube and a visual representation of points represented once (the blue edge) and twice(the pink facet).

We now investigate the polynomials arising from the points in $\mathcal{C}^{[2]}$. The points which are attained once correspond to the edges (one-dimensional faces) of the cube and the unique pair that adds up to such a point are the two vertices $\mathbf{c}_k, \mathbf{c}_\ell$ comprising the edge. Hence these points contribute the quartic (3.16), one can notice that this quartic depends only on the difference $\mathbf{c}_k - \mathbf{c}_\ell$, which is the same for all edges going in the same direction (that is, all edges whose corresponding point in $\mathcal{C}^{[2]}$ has the unique 1 at the same index). This reasoning yields the immediate result

Lemma 3.3.2. *The set $\mathcal{C}^{[2]}$ contains $g2^{g-1}$ points which are uniquely attained. These contribute as generators of the ideal defining the Hirota variety $\mathcal{H}_\mathcal{C}$ with g quartics of the form $u_i^4 - 4u_iw_i + 3v_i^2$, for $i = 1, 2, \ldots, g$.*

Recall that the Hirota variety lies in the ambient space $(\mathbb{C}^\star)^{2g} \times \mathbb{WP}^{3g-1}$. The coordinate ring is $\mathbb{C}[\mathbf{a}^{\pm 1}, \mathbf{u}, \mathbf{v}, \mathbf{w}]$ and the ideal defining $\mathcal{H}_\mathcal{C}$ has $g + \sum_{d=2}^g 2^{g-d}\binom{g}{d}$ generators with respect to inclusion, one for each edge direction, and one for each face of every dimension from 2 up to g.

The combinatorics of the cube has already been shown to be important when studying the generators of the Hirota variety. In what follows we discuss more the combinatorics of the cube as it relates to the main component, presenting a more general version of Lemma 3.3.2. We begin with some definitions.

A face of the g-cube is defined by fixing $g - d$ indices of the corresponding points. Let the non-fixed indices be given by the set I. We call this set the *direction* of the face. For two faces with the same direction, their *difference* is the set J of fixed indices in the two faces which are different.

Example 3.3.3. The direction of an edge is given by a set with one element, namely the index of the standard basis vector to which the edge is parallel. The difference of two edges

on the same two dimensional face is also a one-element set, consisting of the index of the second standard basis vector defining the face (in addition to the standard basis vector given by the direction). Also see Figure 3.3 for an example in the three-cube. The four blue edges in the picture have the same direction $\{1\}$. The two pink facets have the same direction $\{2,3\}$. The difference of edges 1 and 2 is $\{3\}$, while the difference between 1 and 3 is $\{2,3\}$.
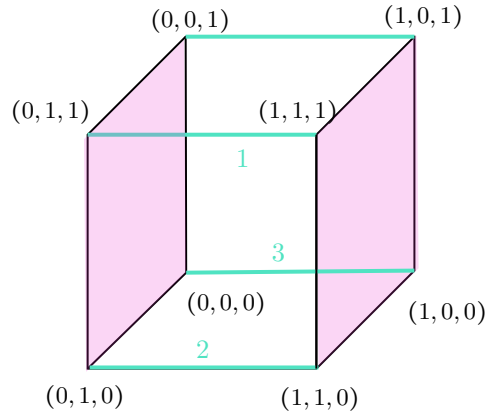
Figure 3.3: A visualization of face directions in the three-cube.

In the following result, we restrict to the main component $\mathcal{H}_\mathcal{C}^M$ of the Hirota variety. We are interested in the points in $\mathcal{H}_\mathcal{C}^M$ that also verify the quartic relations

$$a_{\mathbf{c}_1} a_{\mathbf{c}_2} a_{\mathbf{c}_3} a_{\mathbf{c}_4} = a_{\mathbf{d}_1} a_{\mathbf{d}_2} a_{\mathbf{d}_3} a_{\mathbf{d}_4}, \quad \text{with} \quad \sum_{i=1}^4 \mathbf{c}_i = \sum_{i=1}^4 \mathbf{d}_i, \quad \sum_{i=1}^4 \mathbf{c}_i^2 = \sum_{i=1}^4 \mathbf{d}_i^2, \qquad (3.17)$$

where $\mathbf{c}_i, \mathbf{d}_i$ are points in $\{0,1\}^g$. For $g = 3$ there exists a unique relation of this type, namely the one in (3.12). In particular, when the a_i are exponentials of the form $a_{\mathbf{c}} = \exp[\frac{1}{2}\mathbf{c}R_0\mathbf{c}^T]$, as in (3.15), then they verify these quartic relations. More generally, one has

Lemma 3.3.4. *The closure of the image of the map* $\psi : Sym^2(\mathbb{C}^g) \to \mathbb{P}^{2^g-1}$ *defined by*

$$R \mapsto \left(a_{\mathbf{c}} = \exp\left[\frac{1}{2}\mathbf{c}^T R\mathbf{c}\right] \right)_{\mathbf{c} \in \{0,1\}^g} \qquad (3.18)$$

is cut out by the equations in (3.17) *and the additional equation* $a_{\mathbf{0}} = 1$.

Proof. An immediate computation shows that the points in the image of ψ verify the relations in (3.17) and $a_{\mathbf{0}} = 1$. To show the other inclusion, we consider a point $\mathbf{a} \in \mathbb{P}^{2^g-1}$ with entries indexed by points in $\mathcal{C}^{[2]}$ such that it verifies the desired equations. Then we can define the matrix $R \in \mathrm{Sym}^2(\mathbb{C}^g)$ with entries given by $R_{ii} = 2\log a_{\mathbf{e}_i}$ and $R_{ij} = \log \frac{a_{\mathbf{e}_i + \mathbf{e}_j}}{a_{\mathbf{e}_i} a_{\mathbf{e}_j}}$, where the $\mathbf{e}_i$'s denote the standard basis of $\mathbb{Z}^g$.

Moreover, if we take a point point $a_{\mathbf{c}_1}$ verifying a quartic (3.17) and assume that the $a_{\mathbf{c}_i}, a_{\mathbf{d}_i}$ involved in the relation are exponentials as in the image of ψ, then expanding the relation we obtain that $a_{\mathbf{c}_1}$ is also of the form $\exp\left[\frac{1}{2}\mathbf{c}_1^T R \mathbf{c}_1\right]$. Hence, we can proceed inductively on n for elements of type $\tilde{\mathbf{a}}_n = a_{\mathbf{e}_1 + \cdots + \mathbf{e}_n}$. We write $a_{\mathbf{e}_i} = a_{\mathbf{i}}$ and $a_{\mathbf{e}_i + \mathbf{e}_j} = a_{\mathbf{i+j}}$. Then $\tilde{\mathbf{a}}_n$ verifies a relation of type

$$\tilde{\mathbf{a}}_n = \frac{a_{\mathbf{1}+\cdots+(\mathbf{n-1})} \cdot a_{\mathbf{1}+\cdots+(\mathbf{n-2})+\mathbf{n}} \cdot a_{(\mathbf{n-1})+\mathbf{n}} \cdot a_{\mathbf{0}}}{a_{\mathbf{1}+\cdots+(\mathbf{n-2})} \cdot a_{\mathbf{n-1}} \cdot a_{\mathbf{n}}}$$

This concludes the proof. $\qquad\square$

Theorem 3.3.5. *There are $\binom{g}{d}$ face directions for each dimension d, and all faces with the same direction contribute the same quartic, up to a multiple, to the ideal defining $\mathcal{H}_{\mathcal{C}}^M$.*

Proof. Consider two d-dimensional faces of the g-cube with the same direction. This means that their corresponding points $\mathbf{c}_1, \mathbf{c}_2 \in \mathcal{C}^{[2]}$ have 1s in exactly the same positions. Both points have 2^{d-1} pairs which sum to them, and these pairs can be put in a correspondence. Namely, for a pair $\mathbf{c}_k, \mathbf{c}_\ell$ that sums to $\mathbf{c}_1$, the pair $\tilde{\mathbf{c}}_k, \tilde{\mathbf{c}}_\ell$ is a pair that sums to $\mathbf{c}_2$, where $\tilde{\mathbf{a}}$ is obtained from $\mathbf{a}$ by changing the entry from 0 to 1 (or vice-versa) for every index in the difference of the two faces. For the two pairs, $(\mathbf{c}_k, \mathbf{c}_\ell)$ and $(\tilde{\mathbf{c}}_k, \tilde{\mathbf{c}}_\ell)$, their corresponding quartic P_{kl} is the same, since it is easy to see that $\mathbf{c}_k - \mathbf{c}_\ell = \tilde{\mathbf{c}}_k - \tilde{\mathbf{c}}_\ell$. The generators of the ideal $\mathcal{I}(\mathcal{H}_{\mathcal{C}})$ corresponding to the faces are of the form $\sum_{k,\ell:\mathbf{c}_k+\mathbf{c}_\ell=\mathbf{c}} P_{k\ell} a_{\mathbf{c}_k} a_{\mathbf{c}_\ell}$. We will now show that, when we restrict to the component above, the d-dimensional face with direction D contributes the same quartic, up to a multiple, as the face corresponding to the point $\mathbf{c} = \sum_{i \in D} \mathbf{e}_i$, where the $\mathbf{e}_i$ are standard basis vectors. We have already shown that the $P_{k\ell}$ are the same for faces with the same direction. Thus it is sufficient to show that the polynomial

$$a_{\mathbf{c}_k} a_{\mathbf{c}_\ell} - d \cdot a_{\tilde{\mathbf{c}}_k} a_{\tilde{\mathbf{c}}_\ell}$$

is in the ideal defining $\mathcal{H}_{\mathcal{C}}^M$, where d is some factor (in fact, a product of some $a_{\mathbf{c}}$'s) which does not depend on k, ℓ. Instead it depends only on the difference and direction of the two faces.

For ease of computations, we fix a direction D and we will take one of the faces (F_1) to be the face corresponding to the point $\mathbf{c}_1 = \sum_{i \in D} \mathbf{e}_i$. The other face (F_2) is a face with direction D and difference E from F_1. This means that the point corresponding to F_2 is $\mathbf{c}_2 = \sum_{i \in D} \mathbf{e}_i + \sum_{i \in E} 2\mathbf{e}_i$. Since we will show that the quartic contributed by F_2 is the same as the one contributed by F_1 up to a multiple, this will show that all faces with the same direction contribute essentially the same polynomial to the ideal of $\mathcal{H}_{\mathcal{C}}^M$.

Recall that the $a_{\mathbf{c}}$ are given by $\exp\left[\frac{1}{2}\mathbf{c} R \mathbf{c}^T\right]$, where we write R for R_0. Consider a pair $\mathbf{c}_k, \mathbf{c}_\ell$ that sum to $\mathbf{c}_1$. Then $D = D_1 \cup D_2$, where $D_1 \cap D_2 = \varnothing$ and $\mathbf{c}_k = \sum_{i \in D_1} \mathbf{e}_i$ and $\mathbf{c}_\ell = \sum_{i \in D_2} \mathbf{e}_i$. It follows that $\tilde{\mathbf{c}}_k = \sum_{i \in D_1 \cup E} \mathbf{e}_i$ and $\tilde{\mathbf{c}}_\ell = \sum_{i \in D_2 \cup E} \mathbf{e}_i$.

We will now use the linear algebra fact that for a symmetric $g \times g$ symmetric matrix, the following hold

$$\left(\sum_{i \in I} \mathbf{e}_i\right) R \left(\sum_{j \in J} \mathbf{e}_j^T\right) = \sum_{i \in I, j \in J} R_{ij}$$

Then, we have

$$a_{\tilde{\mathbf{c}}_k} a_{\tilde{\mathbf{c}}_\ell} \;=\; \exp\left[\sum_{i,j\in D_1\cup E} R_{ij}\right]\exp\left[\sum_{i,j\in D_2\cup E} R_{ij}\right] \;=\; \exp\left[\sum_{i,j\in D\cup E} R_{ij}\right]\exp\left[\sum_{i,j\in E} R_{ij}\right] \qquad (3.19)$$

which one can easily see is a multiple of $\exp\left[\sum_{i,j\in D} R_{ij}\right] = a_{\tilde{\mathbf{c}}_k} a_{\tilde{\mathbf{c}}_\ell}$ which only depends on the sets D and E, as desired.

$\square$

One can observe that Theorem 3.3.5 is a generalization of Lemma 3.3.2 to equations arising from points in $\mathcal{C}^{[2]}$ which correspond to higher dimensional faces. This holds for points in the main component $\mathcal{H}_{\mathcal{C}}^M$. Moreover, Theorem 3.3.5 reduces the number of potentially non-redundant relations holding in the ideal defining the variety $\mathcal{H}_{\mathcal{C}}^M$ to $2^g - 1$. This is also the codimension of $\mathcal{H}_{\mathcal{C}}^M$ inside its ambient space $(\mathbb{C}^*)^{2g} \times \mathbb{WP}^{3g-1}$. Our code in (3.8) verifies that this set of generators defines a variety which is a complete intersection, of which $\mathcal{H}_{\mathcal{C}}^M$ is a component for $g \leq 9$.

Quartic relations and the Schottky locus

We conclude with a discussion relating the quartic relations among the a_i parameters and the Schottky problem. The *classical Schottky problem*, studied by Riemann and Schottky, requires one to write down the defining equations for the *Schottky locus* $\mathfrak{I}_g$, namely the subset of abelian varieties corresponding to Jacobians of curves. In fact, the *second order theta constants* [57] define an embedding of $\mathcal{A}_g$ into a projective space $\mu : \mathcal{A}_g \hookrightarrow \mathbb{P}^{2^g-1}$ and to solve the Schottky problem one aims to determine the defining ideal of $\mu(\mathfrak{I}_g) \subset \mu(\mathcal{A}_g)$. Hence, the Schottky problem concerns the maps

$$\mathcal{M}_g \xrightarrow{J} \mathcal{A}_g \hookrightarrow \mathbb{P}^{2^g-1}. \qquad (3.20)$$

Moreover, the space $\mathcal{A}_g$ is parameterized by the *Siegel upper-half space* $\mathfrak{H}_g$, namely the set of complex symmetric $g \times g$ matrices with positive definite imaginary part. As explained in the introduction, in genus 3, a dimension count shows that in this case the Schottky problem is trivial. In genus 4, the ideal $\mathfrak{I}_4$ is an analytic hypersurface in $\mathfrak{H}_4$. Furthermore, in genus 3 the second order theta constants verify an equation of degree 16 which leads to the equation characterizing Jacobians of curves in genus 4, i.e., Igusa's equation, see [56, Example 6.2], [68]. An analogous situation can be described when looking at the degenerate theta functions arising from irreducible rational nodal curves. The map ψ in (3.18) provides an embedding of the space $Sym^2(\mathbb{C}^g)$ in the projective space $\mathbb{P}^{2^g-1}$. The dimension count for these spaces is analogous to the one for the spaces involved in (3.20). In particular, for genus 3, we find that $\overline{im(\psi)} = \overline{Sym^2(\mathbb{C}^3)}$ inside $\mathbb{P}^7$. Note that the image of the map ψ is contained in the locus $V(a_{111}a_{100}a_{010}a_{001} - a_{110}a_{101}a_{011}a_{000})$, where the relation among the a_i's comes from (3.12). Equality then follows by a direct computation since these are both irreducible varieties of equal dimension. We believe a similar situation should hold for higher genus.

Part II

Grassmannians

Chapter 4

Positivity for the orthogonal Grassmannian

4.1 Introduction and background

This chapter is based on ongoing joint work with Yassine El Maazouz. The positive orthogonal Grassmannian was first considered and studied by particle physicists in [66, 67] in the context of scattering amplitudes in ABJM theory. They observed many combinatorial phenomena which were later proved and supplemented in [53], which also associated the positive Orthogonal Grassmannian $\mathrm{OGr}_{\geq 0}(n, 2n)$ to planar Ising models. It is expected that the positive orthogonal Grassmannian is a positive geometry [66, 10].

In all of the previous studies, the orthogonal Grassmannian was considered only with one choice of quadratic form which has alternating signature. This choice of form has so far proved sufficient for the purposes of applying it to ABJM theory and Ising models. Nevertheless, it is still mathematically interesting to consider alternate choices of signature for the quadratic forms. In addition, an explicit proof that the positive Grassmannian is a positive geometry is still missing. In this chapter we initiate the study of the positive orthogonal Grassmannian for forms other than the form with alternating signature, and make a step towards showing that the positive orthogonal Grassmannian is a positive geometry. We prove it for $\mathrm{OGr}_{\geq 0}(1, n)$ in any signature.

4.2 The orthogonal Grassmannian

Preliminaries

Let E be a vector space of dimension n over a field k and Q a non-degenerate symmetric bilinear form. We call a subspace $V \subset E$ *isotropic* with respect to Q if $Q(v, v') = 0$ for any $v, v' \in V$. We denote by $\mathrm{OGr}(k, E)$ the Grassmannian of k-dimensional isotropic subspaces of E. In this paper we work with $E = \mathbb{R}^n$, and denote the orthogonal Grassmannian by

$\mathrm{OGr}(k,n)$. We denote by $X_{k,n}$ the variety of k-dimensional linear subspaces $V \subset E$ such that

$$Q(v,v) = 0 \text{ for all } v \in V.$$

It is clear that $\mathrm{OGr}(k,n) \subset X_{k,n}$.

Proposition 4.2.1. *1. $X_{k,n}$ is empty when $k > n/2$.*

2. $\mathrm{OGr}(k,2k)$ has two irreducible connected components.

3. $\mathrm{OGr}(k,n)$ where $n \neq 2k$ has one irreducible component.

Proof. This is the Proposition on page 735 of [60]. □

Theorem 4.2.2. *The orthogonal Grassmannian $\mathrm{OGr}(2,n)$ is cut out by the following equations in $\mathbb{P}^{\binom{n}{2}-1}$ in addition to the Plücker relations:*

$$\sum_k p_{ik}p_{jk} = 0, \quad \text{for } 1 \leq i \leq j \leq n, \tag{4.1}$$

where the $p_{i,j}$ are the Plücker coordinates with the convention $p_{i,j} = -p_{j,i}$. It has dimension $2n - 7$.

Proof. Let $p = (p_{i,j})$ be a point in $\mathrm{OGr}(2,n)$. Then there exists an isotropic plane $V \subset \mathbb{C}^n$ corresponding to p. The plane V is spanned by two linearly independent row vectors:

$$\begin{pmatrix} a_{1,1} & a_{1,2} & \dots & a_{1,n} \\ a_{2,1} & a_{2,2} & \dots & a_{2,n} \end{pmatrix}.$$

The Plücker coordinates can then be written as follows:

$$p_{i,j} = a_{1,i}a_{2,j} - a_{1,j}a_{2,i}.$$

Hence for any $1 \leq i \leq j \leq n$ we get

$$\sum_{k=1}^{n} p_{i,k}p_{j,k} = \sum_{k=1}^{n}(a_{1,i}a_{2,k} - a_{1,k}a_{2,i})(a_{1,j}a_{2,k} - a_{1,k}a_{2,j})$$

$$= a_{1,i}a_{1,j}\left(\sum_{k=1}^{n} a_{2,k}^2\right) - (a_{1,i}a_{2,j} + a_{1,j}a_{2,i})\left(\sum_{k=1}^{n} a_{1,k}a_{2,k}\right) + a_{2,i}a_{2,j}\left(\sum_{k=1}^{n} a_{1,k}^2\right).$$

But since V is isotropic we deduce that the latter sum is 0 for every $1 \leq i \leq j \leq n$. On the other hand, let p be a point in the Grassmannian $\mathrm{Gr}(2,n)$ which satisfies the equations above. We need to show that this point represents an isotropic subplane of $\mathbb{C}^n$. Using the S_n action on $\mathrm{OGr}(2,n)$ (which permutes the columns of the $2 \times n$ matrix) we may assume that $p_{1,2} = 1$. Hence we can pick the span of the two row vectors

$$\begin{pmatrix} 1 & 0 & -p_{2,3} & -p_{2,4} \dots & -p_{2,n} \\ 0 & 1 & p_{1,3} & p_{1,4} \dots & p_{1,n} \end{pmatrix}$$

as the plane represented by the Plücker coordinates p in $\mathrm{Gr}(2, n)$. Since p satisfies the relations listed above, we deduce that this plane is isotropic and thus $p \in \mathrm{OGr}(2, n)$. $\qquad \square$

Based on computations, we have the following conjecture, which we hope to prove using Schubert calculus or Gröbner basis methods.

Conjecture 1. The orthogonal Grassmannian $\mathrm{OGr}(2, n)$ has degree under the embedding in Theorem 4.2.2 given by:

$$\deg(\mathrm{OGr}(2, n)) = \deg(\mathrm{Gr}(2, n)) + 6 \frac{(2(n-3))!}{(n-3)!(n-1)!}. \tag{4.2}$$

For general k, n we have the following result which gives defining equations cutting out $\mathrm{OGr}(k, n)$.

Theorem 4.2.3. *In addition to the Plücker relations, the orthogonal Grassmannians* $\mathrm{OGr}(k, n)$ *is cut out by the following equations in* $\mathbb{P}^{\binom{n}{k}-1}$:

$$\sum_{k=1}^{n} \varepsilon(Ik)\varepsilon(Jk)\, p_{Ik}p_{Jk} = 0, \quad \text{for ordered sets } I, J \in \binom{[n]}{k-1}. \tag{4.3}$$

where $\epsilon(Ik)$ denotes the sign of the permutation ordering the sequence Ik.

Proof. Let $p = (p_{i,j})$ be a point in $\mathrm{OGr}(2, n)$. Then there exists an isotropic plane $V \subset \mathbb{C}^n$ corresponding to p and V is spanned by two linearly independent row vectors:

$$A = \begin{pmatrix} a_{1,1} & a_{1,2} & \cdots & \cdots & a_{1,n} \\ a_{2,1} & a_{2,2} & \cdots & \cdots & a_{2,n} \\ \vdots & \vdots & \cdots & \cdots & \vdots \\ a_{k,1} & a_{k,2} & \cdots & \cdots & a_{k,n} \end{pmatrix}.$$

The Plücker coordinates can then be written as follows:

$$p_{j_1 < \cdots < j_k} = \sum_{\sigma \in S_k} \epsilon(\sigma) \prod_{\ell=1}^{k} a_{\ell j_{\sigma(\ell)}}.$$

Fix two ordered subsets $I = (i_1 < \cdots < i_{k-1})$ and $J = (j_1 < \cdots < j_{k-1})$ in $[n]$. We then have

$$\sum_{\ell=1}^{n} \varepsilon(I\ell)\varepsilon(J\ell)p_{I\ell}p_{J\ell} = \sum_{i=1}^{n} \sum_{\sigma,\tau \in S_k} \epsilon(\sigma\tau) \prod_{s=1}^{k-1} a_{\sigma(s),i_s} b_{\tau(s),j_s} a_{\sigma(k),i} b_{\tau(k),i}$$

$$= \sum_{\sigma,\tau \in S_k} \epsilon(\sigma\tau) \prod_{s=1}^{k-1} a_{\sigma(s),i_s} b_{\tau(s),j_s} \left(\sum_{i=1}^{n} a_{\sigma(k),i} b_{\tau(k),i} \right).$$

But, since V is isotropic, the last sum is 0 so we deduce that

$$\sum_{\ell=1}^{n} \epsilon(I\ell)\epsilon(J\ell)p_{I\ell}p_{J\ell} = 0.$$

Conversely, let p be a point in $\mathrm{Gr}(k,n)$ such that:

$$\sum_{\ell=1}^{n} \epsilon(I\ell)\epsilon(J\ell)p_{I\ell}p_{J\ell} = 0 \quad \text{for all } I, J \subset \binom{[n]}{k}.$$

Using the S_n-action on $\mathrm{Gr}(k,n)$, we may without loss of generality assume that $p_I = 1$ where $I = \{1 < 2 < \cdots < k\}$. So we can write the vector subspace of $\mathbb{C}^n$ represented by p as the row span of the matrix:

$$A = \begin{pmatrix} 1 & 0 & \cdots & 0 & (-1)^{k-1}p_{(I\smallsetminus 1)\cup\{k+1\}} & (-1)^{k-1}p_{(I\smallsetminus 1)\cup\{k+2\}} & \cdots & (-1)^{k-1}p_{(I\smallsetminus 1)\cup\{n\}} \\ 0 & \ddots & \cdots & \vdots & (-1)^{k-2}p_{(I\smallsetminus 2)\cup\{k+1\}} & (-1)^{k-2}p_{(I\smallsetminus 2)\cup\{k+2\}} & \cdots & (-1)^{k-2}p_{(I\smallsetminus 2)\cup\{n\}} \\ \vdots & \vdots & \ddots & \vdots & \vdots & \vdots & & \vdots \\ 0 & \cdots & 0 & 1 & p_{(I\smallsetminus k)\cup\{k+1\}} & p_{(I\smallsetminus k)\cup\{k+2\}} & \cdots & p_{(I\smallsetminus k)\cup\{n\}} \end{pmatrix}.$$

From the equations, we can see that the rows of this matrix are orthogonal to themselves and to one another. So we deduce that $p \in \mathrm{OGr}(k,n)$. $\qquad\square$

Proposition 4.2.4. *The ratio of two complementary Plücker coordinates in $\mathrm{OGr}(n, 2n)$ is either ± 1 if $n + \#S$ is even and $\pm i$ otherwise. Here S is the set of $-$ in the signature of the quadratic form $(\pm, \ldots, \pm)$.*

Proof. Suppose $I, J \subset [2n]$ are disjoint, and consider some $i \in I$ and $j \in J$. Then the orthogonal relation coming from the sets $I \smallsetminus i, J \smallsetminus j$ is given by

$$p_I p_{J+i-j} \pm p_{I+j-i} p_J = 0,$$

where the sign is determined by the form and by I, J, i, j. This relation tells us that

$$\frac{p_I}{p_J} = \pm \frac{p_{I+j-i}}{p_{J+i-j}}.$$

Thus, for two complementary sets I, J the ratio of their Plücker coordinates is equal, up to sign, to the ratio of the Plücker coordinates of two new complementary sets obtained by swapping one element of I with one element of J. We can swap elements n times and get a chain of such equalities that ultimately yields

$$\frac{p_I}{p_J} = \pm \frac{p_J}{p_I}.$$

If the sign is positive, this means the ratio is ± 1, while if it is negative, the ratio is $\pm i$, where $i = \sqrt{-1}$. Moreover, note that any ratio of complementary Plücker coordinates can be

obtained as a result of exchanging elements of I and J, so if $\frac{p_I}{p_J} = \pm 1$, then this is true for all complementary Plücker coordinates. We now show that this is determined by the parity of $n + \#S$.

As noted above, since any pair of complementary sets can be obtained by exchanging elements from a different pair, it is sufficient to consider $\frac{p_I}{p_J}$ for just one pair I, J. Let $I = \{1, 3, \ldots, 2n - 1\}$ and $J = \{2, 4, \ldots, 2n\}$. Then, to swap the sets we proceed to iteratively exchange the smallest odd element of I with the smallest even element of J. Observe that, as a result of our choice of sets and exchanged elements, we have $\varepsilon(\tilde{I}k)\varepsilon(\tilde{J}k) = 1$ for any $\tilde{I}, \tilde{J}$ obtained as a result of partially completing the exchange process. $\qquad \square$

Then, for any signature such that $n + \#S$ is even, the positive orthogonal Grassmannian $\mathrm{OGr}_{\geq 0}(n, 2n)$ is the component of $\mathrm{OGr}(n, 2n)$ where the ratios of complimentary Plücker coordinates are 1.

Proposition 4.2.5. *The two ideals given by the sets of equations below both cut out the positive orthogonal Grassmannian* $\mathrm{OGr}_{\geq 0}^{(n,n)}(n, 2n)$:

1. *The Plücker relations, given by*

$$\sum_{j \in J \cap \bar{I}} \varepsilon(I, J, j) p_{Ij} p_{J \smallsetminus j} = 0,$$

   for all sets, $I \in \binom{[2n]}{n-1}, J \in \binom{[2n]}{n+1}$ and the complement relations, given by

$$p_I - p_{\bar{I}} = 0,$$

   for all $I \in \binom{[2n]}{n}$.

2. *The orthogonal relations (4.3)*

$$\sum_{k=1}^{n} \varepsilon(Ik)\varepsilon(Jk) \, p_{Ik} p_{Jk} = 0, \quad \text{for ordered sets } I, J \in \binom{[n]}{k-1}.$$

   and the complement relations

$$p_I - p_{\bar{I}} = 0,$$

   for all $I \in \binom{[2n]}{n}$.

Proof. We show that the two ideals are the same. Then the fact that they both cut out the positive orthogonal Grassmannian follows. We will show that, using the complement relations, a Plücker relation can be transformed into an orthogonal relation and vice-versa.

Consider general $I \in \binom{[2n]}{n-1}, J \in \binom{[2n]}{n+1}$. Suppose they have m elements in common. Then we may write $I = \{i_1, \ldots, i_{n-1}\}$ and $J = \{i_1, \ldots, i_m, j_1, \ldots, j_{n-m+1}\}$. Then, the orthogonal relation with I and $\bar{J} = \{j_{n-m+2}, \ldots, j_{n+1}, i_{m+1}, \ldots, i_{n-1}\}$ is given by

$$\sum_{l=1}^{n-m+1} p_{Ij_l} p_{\bar{J}j_l} \varepsilon(I\bar{J}l).$$

Using the complement relation to replace $p_{\overline{J}j_l}$ with $p_{J \smallsetminus j_l}$, and checking that the signs $\varepsilon(I\overline{J}l) = \varepsilon(IJl)$, we obtain exactly the Plücker relation for I, J. Thus we can derive the Plücker relations from the orthogonal relations and complement relations. The same process can be followed backwards to derive the orthogonal relations from the complement and Plücker relations.

$\square$

4.3 $\mathrm{OGr}_{\geq 0}(1, n)$

Restricting to the case $k = 1$, we now consider the positive orthogonal Grassmannian with a quadratic form $Q = (\pm 1, \cdots \pm 1)$ with *signature* (p, q), meaning p of the entries in Q are $+1$ and q are -1. We denote this by $\mathrm{OGr}_{\geq 0}^{(p,q)}(1, n)$. It is the set of points $\{v \in \mathbb{R}^n : vQv = 0$ and $v_i \geq 0$ for all $i\}$.

Theorem 4.3.1. *The positive orthogonal Grassmannian* $\mathrm{OGr}_{\geq 0}^{(p,q)}(1, n+1)$ *in signature* (p, q) *is combinatorially isomorphic to* $\Delta_{p-1} \times \Delta_{q-1}$. *Moreover it is a positive geometry with canonical form:*

$$\Omega^{(p,q)} = \left(1 + u_{1,0}^2 + \cdots + u_{p,0}^2\right) \frac{du_{1,0} \wedge du_{2,0} \wedge \cdots \wedge du_{n-1,0}}{u_{1,0} \; u_{2,0} \; \cdots \; u_{n-1,0} \; u_{n,0}^2}$$

where $u_{i,j}$ denotes the rational function x_i/x_j in the coordinates $(x_0 : \cdots : x_n)$ of $\mathbb{P}^n$.

Proof. We begin by examining the combinatorial structure of $\mathrm{OGr}_{\geq 0}^{(p,q)}(1, n + 1)$. It is a simplex cut by the hypersurface X given by $x^\top Q x = 0$. By permuting the coordinates, we see that any form with signature (p, q) will define the same hypersurface, up to relabeling, as the form $Q = (1, \ldots, 1, -1, \ldots, -1)$ with all positive signs coming before all negative ones. The combinatorial structure of $\mathrm{OGr}_{\geq 0}^{(p,q)}(1, n+1)$ can be seen by building up from the intersections of X with lower-dimensional boundaries of the simplex. Indeed, note that, setting $x_i = 0$ for some $i < p$, the resulting boundary of $\mathrm{OGr}_{\geq 0}^{(p,q)}(1, n + 1)$ is isomorphic to $\mathrm{OGr}_{\geq 0}^{(p-1,q)}(1, n)$. Similarly, setting $x_i = 0$ for some $i > p$ gives a copy of $\mathrm{OGr}_{\geq 0}^{(p,q-1)}(1, n)$. Observe that if either p or q are 0, it is clear that $\mathrm{OGr}_{\geq 0}^{(p,q)}(1, p + q)$ is empty, since the form Q is setting a sum of squares of projective coordinates to 0. On the other hand, we have $\mathrm{OGr}_{\geq 0}^{(1,1)}(1, 2) = \{x \in [0, 1] : x^2 - (1 - x)^2 = 0\} = \{1/2\}$, or a single point i.e. a zero-dimensional simplex. Building up inductively, every restriction to a boundary simplex $S = \mathrm{conv}(\{e_i : 1 \leq i \leq p+1\})$, where e_i is the ith standard with arbitrary $p \geq 1$ and $q = 1$ yields a (shape combinatorially equivalent to a) $p - 1$ simplex with vertices given by the midpoints of the edges of S which connect e_i to e_{p+1} for $1 \leq i \leq p$. The case with q arbitrary and $p = 1$ is the same. Now building by induction we find that the unique shape with boundaries given by $\Delta_{p-1} \times \Delta_{q-2}$ on each boundary given by $x_i = 0$, for some $i > p$ and $\Delta_{p-2} \times \Delta_{q-1}$ on each boundary given by $x_i = 0$, for some $i \leq p$ is exactly the product $\Delta_{p-1} \times \Delta_{q-1}$, as desired. We remark that this is combinatorially equivalent to the convex hull of all the points which are given by an $\mathrm{OGr}_{\geq 0}^{(1,1)}(1, 2)$, i.e taking

one coordinate corresponding to a positive p index and one from the negative q. This yields the product of a $(p-1)$-simplex and a $(q-1)$-simplex.

Now we show that $\Omega^{(p,q)}$ as given above is a canonical form for $\mathrm{OGr}^{(p,q)}_{\geq 0}(1, n+1)$. Setting $x_0 = 1$ sends the boundary corresponding to $x_0 = 0$ to infinity (we shall check different gauge choice later). For ease of notation, we can then write u_i for $u_{i,0}$, and note that these are given by the x_i. In the way the form $\Omega^{(p,q)}$ is defined, it is clear that for $p+1 \leq i \leq n-1$

$$\mathrm{Res}_{u_i=0}(\Omega^{(p,q)}) = (-1)^{i+1}(1 + u_1^2 + \cdots + u_p^2)\frac{du_1 \wedge \cdots \wedge \widehat{du_i} \wedge \cdots \wedge du_{n-1}}{u_1 \ldots \widehat{u_i} \ldots u_{n-1}u_n^2}$$

For $1 \leq i \leq p$, since $1 + u_1^2 + \ldots u_p^2 - u_{p+1}^2 - \cdots - u_n^2 = 0$, we can rewrite $\Omega^{(p,q)}$ as

$$\Omega^{(p,q)} = (-u_{p+1}^2 - \cdots - u_n^2)\ \frac{du_1 \wedge du_2 \wedge \cdots \wedge du_{n-1}}{u_1\ u_2\ \cdots\ u_{n-1}\ u_n^2}$$

and then

$$\mathrm{Res}_{u_i=0}(\Omega^{(p,q)}) = (-1)^{i+1}(-u_{p+1}^2 - \cdots - u_n^2)\frac{du_1 \wedge \cdots \wedge \widehat{du_i} \wedge \cdots \wedge du_{n-1}}{u_1 \ldots \widehat{u_i} \ldots u_{n-1}u_n^2}$$

For the boundary corresponding to $u_n = 0$ note that since $1 + u_1^2 + \ldots u_p^2 - u_{p-1}^2 \cdots - u_n^2 = 0$ we have

$$u_1 du_1 + \cdots + u_p du_p - u_{p+1}du_{p+1} - \cdots - u_n du_n = 0.$$

Taking the wedge on the right with $du_2 \wedge \cdots \wedge du_{n-1}$ we get

$$u_1 du_1 \wedge \cdots \wedge du_{n-1} \pm u_n du_n \wedge du_2 \wedge \cdots \wedge du_{n-1} = 0$$

so we deduce that

$$\Omega^{(p,q)} = (1 + u_{1,0}^2 + \cdots + u_{p,0}^2)\ \frac{du_{1,0} \wedge du_{2,0} \wedge \cdots \wedge du_{n-1,0}}{u_{1,0}\ u_{2,0}\ \cdots\ u_{n-1,0}\ u_{n,0}^2}$$

$$= \pm(1 + u_{1,0}^2 + \cdots + u_{p,0}^2)\ \frac{du_n \wedge du_2 \wedge \cdots \wedge du_{n-1}}{u_1^2 u_2 \ldots u_{n-1}u_n}.$$

So we get

$$\Omega^{(p,q)} = \frac{du_n}{u_n} \wedge \pm(1 + u_{1,0}^2 + \cdots + u_{p,0}^2)\ \frac{du_2 \wedge \cdots \wedge du_{n-1}}{u_1^2 u_2 \ldots u_{n-1}}.$$

We then get the residue at $u_n = 0$:

$$\mathrm{Res}_{u_n=0}(\Omega^{(p,q)}) = \pm(1 + u_{1,0}^2 + \cdots + u_{p,0}^2)\ \frac{du_2 \wedge \cdots \wedge du_{n-1}}{u_1^2 u_2 \ldots u_{n-1}}.$$

This covers all the boundaries of $\mathrm{OGr}^{1,q}(1, n)$ and since the residue at each boundary gives the same form for a lower dimensional positive orthogonal Grassmannian $\mathrm{OGr}^{(p-1,q)}_{\geq 0}(k, n)$ or $\mathrm{OGr}^{(p,q-1)}_{\geq 0}(k, n)$, we can carry on taking residues for lower dimensional boundaries. $\square$

Example 4.3.2 ($\mathrm{OGr}_{\geq 0}(1,4)$). We work in the signature $(+,+,-.-)$. The points $(x_0 : x_1 : x_2 : x_3)$ in the positive orthogonal Grassmannian $\mathrm{OGr}_{\geq 0}(1,4)$ in $\mathbb{P}^3$ are those such that:

$$x_0^2 + x_1^2 - x_2^2 - x_3^2 = 0 \text{ and } x_0, x_1, x_2, x_3 \geq 0.$$

We can see in this case that $\mathrm{OGr}_{\geq 0}(1,4)$ is a curvy quadrilateral inside the 3-simplex in $\mathbb{P}^3$ depicted in Figure 4.1.
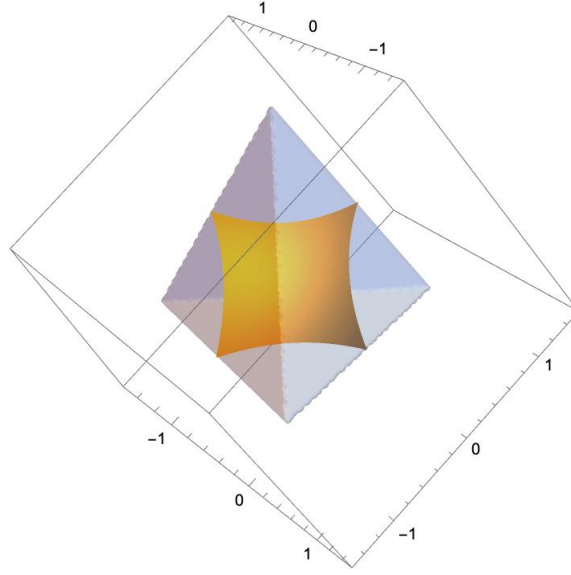
Figure 4.1: The positive Grassmannian $\mathrm{OGr}(1,4)_{\geq 0}$ in $\mathbb{P}^3$.

To show that this is a positive geometry, we now describe the canonical form. For $0 \leq i \neq j \leq 3$ denote by $u_{i,j}$ the rational function x_i/x_j. The equation above becomes:

$$1 + u_{1,0}^2 - u_{2,0}^2 - u_{3,0}^2.$$

Now consider the form:

$$\Omega = (1+u_{1,0}^2)\,\frac{du_{1,0} \wedge du_{2,0}}{u_{1,0}\ u_{2,0}\ u_{3,0}^2} = (1+u_{0,1}^2)\,\frac{du_{2,1} \wedge du_{0,1}}{u_{0,1}\ u_{2,1}\ u_{3,1}^2} = (1+u_{3,2}^2)\,\frac{du_{0,2} \wedge du_{1,2}}{u_{0,2}\ u_{1,2}\ u_{3,2}^2} = (1+u_{2,3}^2)\,\frac{du_{0,3} \wedge du_{1,3}}{u_{0,3}u_{1,3}u_{2,3}^2}.$$

We then see that

$$\mathrm{Res}_{u_{1,0}=0}(\Omega) = \frac{du_{2,0}}{u_{2,0}(1 - u_{2,0}^2)}$$

$$\mathrm{Res}_{u_{0,1}=0}(\Omega) = -\frac{du_{2,1}}{(1 - u_{2,1}^2)u_{2,1}}.$$

Example 4.3.3 ($\mathrm{OGr}_{\geq 0}(1,5)$)**.** Again we work with $(+,+,+,-,-)$ and for this case we use a rational parametrization of $X \subset \mathrm{OGr}(1,5)$ in $\mathbb{P}^4$ where X is cut out by the equation

$$x_0^2 + x_1^2 + x_2^2 - x_3^2 - x_4^2.$$

The canonical form is:

$$\Omega = \left(1 + u_{1,0}^2 + u_{2,0}^2\right) \frac{du_{1,0} \wedge du_{2,0} \wedge du_{3,0}}{u_{1,0} \; u_{2,0} \; u_{3,0} \; u_{4,0^2}}.$$

4.4 Concluding remarks

A natural next step is to investigate $\mathrm{OGr}_{\geq 0}(2,n)$ and determine whether it is a positive geometry. We intend to study this and (more ambitiously) to extend this to general (k,n).

Another interesting direction is to study $\mathrm{OGr}(n, 2n+1)$ and its positive part in the alternating signature. This would be analogous to work done in [53] which was for $\mathrm{OGr}(n, 2n)$.

Chapter 5

Grasstopes

This chapter is based on the paper, "Combinatorics of $m = 1$ Grasstopes" [85], which is joint with Dmitrii Pavlov and Lizzie Pratt.

5.1   Introduction

The (tree) amplituhedron, introduced by Arkani-Hamed and Trnka in [11], is a geometric object playing an important role in calculations of scattering amplitudes in planar $N = 4$ Super-Yang-Mills theory. It is defined as the image of the totally nonnegative Grassmannian $\mathrm{Gr}_{\geq 0}(k, n)$ under a totally positive linear map $\tilde{Z} : \mathrm{Gr}(k, n) \dashrightarrow \mathrm{Gr}(k, k + m)$ given by an $n \times (k + m)$ matrix Z. While immediate physical relevance of the amplituhedron becomes manifest at $m = 4$, it is an object of independent mathematical interest for any m. It is known that when $k = 1$, it is a cyclic polytope [105] and when $k + m = n$, it is isomorphic to the totally nonnegative Grassmannian $\mathrm{Gr}_{\geq 0}(k, n)$.

In recent years, the amplituhedron has been studied extensively from the point of view of algebraic combinatorics for $m = 1, 2, 4$ (see [42, 52, 71, 72, 84, 92]). The structure of the amplituhedron in the $m = 1$ case is particularly simple: Karp and Williams [72] show that it is linearly homeomorphic to the complex of bounded cells of an affine hyperplane arrangement and therefore is homeomorphic to a closed ball.

One reason that the amplituhedron is so amenable to combinatorial study is that the totally nonnegative Grassmannian itself has a rich combinatorial structure. In particular, $\mathrm{Gr}_{\geq 0}(k, n)$ admits a stratification by positroid cells, which are all homeomorphic to open balls [93]. However, amplituhedra are images of very special linear maps, just as cyclic polytopes are very special polytopes. From this point of view, it makes sense to consider images of the totally nonnegative Grassmannian under arbitrary linear maps. In [81], Lam considers the images of positroid cells under arbitrary linear maps, and calls them *Grassmann polytopes*. Images of the whole totally nonnegative Grassmannian are referred to as *full Grassmann polytopes*.

While amplituhedra have attracted significant attention from the mathematical commu-

nity, many results in this area rely on the total positivity of the map $\tilde{Z}$, and much less is known about more general Grassmann polytopes. Most of the known results are assembled in [81, Part 2]. Many of them are limited to the case when $\tilde{Z}$ does not have base points on the totally nonnegative Grassmannian, i.e. is regular (well-defined) on $\mathrm{Gr}_{\geq 0}(k, n)$.

In this chapter, we initiate the study of general full Grassmann polytopes (*Grasstopes*) and focus on the case of $m = 1$, when the ambient Grassmannian is the dual projective space $(\mathbb{P}^k)^\vee$. We extend the results of [72], showing that when $\tilde{Z}$ is regular on $\mathrm{Gr}_{\geq 0}(k, n)$, the resulting Grasstope is a union of cells of a projective hyperplane arrangement satisfying a certain sign variation condition. This, in particular, implies that Grasstopes arising from such $\tilde{Z}$ are closed and connected, in accordance with [81, Proposition 15.2]. When there are no additional restrictions on $\tilde{Z}$, we show that the image of the totally positive Grassmannian $\mathrm{Gr}_{>0}(k, n)$ can still be characterized in terms of sign changes, although the image of $\mathrm{Gr}_{\geq 0}(k, n)$ might have irregular boundary. We also show that, unlike amplituhedra, general $m = 1$ Grasstopes are not necessarily homeomorphic to closed balls or even contractible.

This chapter is organized as follows. In Section 5.2, we define Grassmannians, their totally nonnegative and totally positive parts, and Grasstopes. We divide Grasstopes into three categories (tame, wild, and rational) based on the properties of the map $\tilde{Z}$. We introduce the concepts necessary for the sign variation characterization of $m = 1$ Grasstopes and prove some auxiliary results about general Grasstopes. In Section 5.3, we study the combinatorics and geometry of Grasstopes for $m = 1$ and prove the sign variation characterization results for tame and wild Grasstopes, as well as for open rational Grasstopes. Section 5.4 is devoted to examples. In Section 5.5, we give background on oriented matroids, which is useful for Section 5.6. Finally, in Section 5.6 we investigate how many regions of a hyperplane arrangement can be in an $m = 1$ Grasstope, and, based on the sign variation characterization, suggest a definition of the Grasstope of a (not necessarily realizable) oriented matroid.

5.2 Preliminaries

Recall that the *real Grassmannian* $\mathrm{Gr}(k, n)$ is the variety parameterizing k-dimensional subspaces of an n-dimensional vector space $\mathbb{R}^n$. It is realized as a subvariety of $\mathbb{P}^{\binom{n}{k}-1}$ via the Plücker embedding, such that a vector space is represented by a vector of maximal minors of a matrix representative.

The *totally nonnegative Grassmannian* $\mathrm{Gr}_{\geq 0}(k, n)$ is the subset of $\mathrm{Gr}(k, n)$ consisting of the elements whose non-zero Plücker coordinates all have the same sign. The *totally positive Grassmannian* $\mathrm{Gr}_{>0}(k, n)$ is a subset of the totally nonnegative Grassmannian consisting of the elements whose Plücker coordinates are all non-zero. Elements of $\mathrm{Gr}_{>0}(k, n)$ can be represented by $k \times n$ matrices with strictly positive maximal minors (such matrices are called *totally positive*). For more information and references about the Grassmannian and the positive Grassmannian we direct the reader back to Section 1.3.

Let Z be a real $n \times (k + m)$ matrix of full rank, where $k + m \leq n$. The matrix Z defines a rational map $\tilde{Z} : \mathrm{Gr}(k, n) \dashrightarrow \mathrm{Gr}(k, k + m)$ by $[A] \mapsto [AZ]$, where $[A]$ is the class in $\mathrm{Gr}(k, n)$

of a matrix A.

Definition 5.2.1 (Grasstopes)**.** The image $\tilde{Z}(\mathrm{Gr}_{\geq 0}(k, n)) \subseteq \mathrm{Gr}(k, k + m)$ is called the (n, k, m)-*Grasstope* of Z and is denoted by $\mathcal{G}_{n,k,m}(Z)$.

The totally nonnegative Grassmannian $\mathrm{Gr}_{\geq 0}(k, n)$ is a semialgebraic set (that is, it can be described by polynomial equations and inequalities) and $\mathcal{G}_{n,k,m}(Z)$ is its image under a polynomial map. Thus, it follows from the Tarski-Seidenberg theorem [13, Theorem A.49] that $\mathcal{G}_{n,k,m}(Z)$ is also semialgebraic.

In [81], the sets $\mathcal{G}_{n,k,m}(Z)$ are called *full Grassmann polytopes*. When Z is a totally positive matrix, one recovers the definition of the *(tree) amplituhedron* $\mathcal{A}_{n,k,m}(Z)$ [11], a geometric object of fundamental importance to calculating scattering amplitudes in particle physics.

Note that the matrix AZ defines an element in $\mathrm{Gr}(k, k + m)$ if and only if AZ has full rank. It is a priori not guaranteed that the map $\tilde{Z}$ is *well-defined* on $\mathrm{Gr}_{\geq 0}(k, n)$, that is, that AZ has full rank for any totally nonnegative $k \times n$ matrix A. In general, the map $\tilde{Z}$ has base locus

$$\mathcal{B}(\tilde{Z}) \coloneqq \{V : \dim(V \cap \ker Z^T) \geq 1\} \subset \mathrm{Gr}(k, n),$$

which may or may not intersect $\mathrm{Gr}_{\geq 0}(k, n)$. Note that the $\mathcal{B}(\tilde{Z})$ is a Schubert variety, so in particular, it is closed in $\mathrm{Gr}(k, n)$ [81, Section 17]. We will often view $\mathrm{Gr}_{\geq 0}(k, n)$ as a parameter space of $(k-1)$-dimensional subspaces of $\mathbb{P}^{n-1}$, in which case the base locus is all projective subspaces which are not disjoint from $\mathbb{P}(\ker Z^T)$.

Finding combinatorial conditions for $\tilde{Z}$ to be well-defined on $\mathrm{Gr}_{\geq 0}(k, n)$ had been an active area of research for several years. In [81, Proposition 15.2] Lam proved that if $\tilde{Z}$ is well-defined on $\mathrm{Gr}_{\geq 0}(k, n)$, then $\mathcal{G}_{n,k,m}(Z)$ is closed and connected. In the same proposition he showed that the following condition is sufficient for $\tilde{Z}$ to be well-defined.

There exists a $(k + m) \times k$ matrix M such that all $k \times k$ minors of ZM are positive. (5.1)

Geometrically, condition (5.1) means that the element of $\mathrm{Gr}(k + m, n)$ represented by Z contains a totally positive k-dimensional subspace, that is, an element of $\mathrm{Gr}_{>0}(k, n)$. Lam also conjectured that this condition is necessary for $\tilde{Z}$ to be well-defined on $\mathrm{Gr}_{\geq 0}(k, n)$. This conjecture turned out to be false, with a counterexample given by Galashin (see [72, Remark 9.3] and Example 5.4.2). A combinatorial criterion was given in [70, Theorem 4.2]. Lam's conjecture gives rise to the following definition.

Definition 5.2.2 (Tame Grasstope)**.** The Grasstope $\mathcal{G}_{n,k,m}(Z)$ is called *tame* if Z satisfies (5.1).

Let $\phi : V \to W$ be a map of vector spaces. We define its kth exterior power $\wedge^k \phi : \bigwedge^k V \to \bigwedge^k W$ by $v_1 \wedge \ldots \wedge v_k \mapsto \phi(v_1) \wedge \ldots \wedge \phi(v_k)$. If M is a matrix representing ϕ in bases $\{e_i\}$ of V and $\{\tilde{e}_j\}$ of W, we denote the matrix representing $\wedge^k \phi$ in the induced bases of $\bigwedge_k V$ and $\bigwedge_k W$ by $\wedge_k M$. Then the matrix of $\tilde{Z}$ is $\wedge^k Z$, where we use the standard embedding

$\mathrm{Gr}(k,n) \to \wedge^k(\mathbb{R}^n)$, $\mathrm{Span}\{v_1, \dots, v_k\} \mapsto v_1 \wedge \dots \wedge v_k$. Concretely, the entries of $\wedge^k M$ are the $k \times k$ minors of M. Those minors are ordered by multi-indices in reverse lexicographic order (according to `Macaulay2` convention).

We now give a simple geometric criterion of tameness. Although well-known to specialists in this area, this result seems to have not appeared in the literature yet. In what follows, for the sake of simplicity, we slightly abuse notation and write $\mathcal{G}_{n,k,m}(Z)$ both for the Grasstope as a subset of $\mathrm{Gr}(k, k+m)$ and its image under the Plücker embedding.

Proposition 5.2.3. *An $n \times (k+m)$ matrix Z satisfies* (5.1) *(i.e. $\mathcal{G}_{n,k,m}(Z)$ is tame) if and only if there exists a hyperplane in $\mathbb{P}^{\binom{k+m}{k}-1}$, whose coefficients satisfy the Plücker relations, which does not intersect $\mathcal{G}_{n,k,m}(Z)$.*

Proof. Any $(k+m) \times k$ matrix M defines a hyperplane in $\mathbb{P}^{\binom{k+m}{k}-1}$ by its Plücker coordinates: a point $p \in \mathbb{P}^{\binom{k+m}{k}-1}$ lies on the hyperplane defined by M if and only if $(\wedge_k M)^T p = 0$. Suppose that Z satisfies (5.1) and M is a $(k+m) \times k$ matrix such that ZM is totally positive. Suppose that a point in $\mathcal{G}_{n,k,m}(Z)$ lies on the hyperplane defined by M. Then, for some $A \in \mathrm{Gr}_{\geq 0}(k,n)$, it holds that $(\wedge_k M)^T (\wedge_k AZ)^T = 0$, which implies that $(\wedge_k (ZM))^T (\wedge_k A)^T = 0$. Since all $k \times k$ minors of A are non-negative, and at least one is nonzero, it is not possible for all $k \times k$ minors of ZM to have the same sign. Thus, if there exists M such that ZM has all positive (or negative) $k \times k$ minors, then the image $\mathcal{G}_{n,k,m}(Z)$ does not intersect the hyperplane defined by M.

Now suppose that Z does not satisfy (5.1), that is, for any M the matrix ZM has either a zero $k \times k$ minor or at least one positive and one negative $k \times k$ minor. We will show that there exists a matrix $A \in \mathrm{Gr}_{\geq 0}(k,n)$ such that $(\wedge_k (ZM))^T (\wedge_k A)^T = 0$, so that the hyperplane defined by M intersects $\tilde{Z}(\mathrm{Gr}_{\geq 0}(k,n))$.

In the first case, when ZM has a zero minor in the ith Plücker coordinate, one can find an element $A \in \mathrm{Gr}_{\geq 0}(k,n)$ which has all Plücker coordinates equal to zero except for the ith one. In this case, $(\wedge_k (ZM))^T (\wedge_k A)^T = 0$.

Now consider the second case, in which ZM has at least one positive and one negative $k \times k$ minor. By the pigeonhole principle, there exists a set of column indices $I = \{i_1, \dots, i_{k-1}\}$ such that two Plücker coordinates involving I (which we label $p_{I \cup \{i\}}$ and $p_{I \cup \{j\}}$) have different signs. Then, take $(q_{1,\dots k} : \dots : q_{n-k+1,\dots,n}) \in \mathbb{P}^{\binom{n}{k}-1}$ such that all coordinates except for $q_{I \cup \{i\}}, q_{I \cup \{j\}}$ are zero, and $q_{I \cup \{i\}} = |p_{I \cup \{j\}}|$ and $q_{I \cup \{j\}} = |p_{I \cup \{i\}}|$. Then, all Plücker relations are satisfied so this point represents an element $A \in \mathrm{Gr}_{\geq 0}(k,n)$. We have $(\wedge_k (ZM))^T (\wedge_k A)^T = 0$, so the hyperplane given by M intersects the Grasstope $\mathcal{G}_{n,k,m}(Z)$. $\square$

Note than when $m = 1$, all hyperplanes in $\mathbb{P}^k$ have coordinates satisfying the Plücker relations. By choosing a hyperplane disjoint from $\mathcal{G}_{n,k,m}(Z)$ to be the hyperplane at infinity, we arrive at the following result.

Corollary 5.2.4. *The Grasstope $\mathcal{G}_{n,k,1}(Z)$ is tame if and only if its image under the Plücker embedding is contained in some affine chart of $\mathbb{P}^k$.*

Tame Grasstopes share many nice properties with amplituhedra. In particular, for $m = 1$ they are homeomorphic to closed balls and can be described as complexes of bounded cells of affine hyperplane arrangements [72, Section 9]. The focus of this chapter, however, is to take a step away from the tame case and study Grasstopes that behave somewhat less regularly.

Definition 5.2.5 (Wild Grasstope). If the map $\tilde{Z}$ is well-defined on $\mathrm{Gr}(k,n)_{\geq 0}$ but Z does not satisfy (5.1), then the Grasstope $\mathcal{G}_{n,k,m}(Z)$ is called *wild*.

Even though $\tilde{Z}$ might not be well-defined on $\mathrm{Gr}_{\geq 0}(k,n)$, it still makes sense to consider the image of $\mathrm{Gr}_{\geq 0}(k,n) \smallsetminus (\mathcal{B}(\tilde{Z}) \cap \mathrm{Gr}_{\geq 0}(k,n))$, where $\mathcal{B}(\tilde{Z})$ is the base locus of $\tilde{Z}$. In this case, we will still write $\tilde{Z}(\mathrm{Gr}_{\geq 0}(k,n))$ for this image.

Definition 5.2.6 (Rational Grasstope). Suppose the map $\tilde{Z}$ is not well-defined on $\mathrm{Gr}(k,n)_{\geq 0}$. Then the image $\mathcal{G}_{n,k,m}(Z) = \tilde{Z}(\mathrm{Gr}(k,n)_{\geq 0})$ is called a *rational* Grasstope. The image $\mathcal{G}^{\circ}_{n,k,m}(Z) = \tilde{Z}(\mathrm{Gr}(k,n)_{>0})$ of the totally positive Grassmannian is called an *open rational* Grasstope. This is indeed an open set, as shown in Proposition 5.3.4.

The definitions and names for "tame" and "wild" Grasstopes were suggested by Lam. This is in contrast to Definition 5.2.6 above, which is new.

We conclude this section with technical results that will prove useful in the characterization of $m = 1$ Grasstopes in Section 5.3. Given a point u in $\mathbb{P}^n$, we associate a sign pattern $\sigma = (\sigma_0, \ldots, \sigma_n) \in \{+, -, 0\}^{n+1}$ to u in the following way. Pick i such that $u_i \neq 0$ and set $\sigma_i := +$. Then $\sigma_j := \mathrm{sign}(u_i u_j)$, which is a well-defined function of homogeneous coordinates of u. Since we associate sign labels to points in projective space, we will identify sign labels σ and $-\sigma$. Each orthant of the $\mathbb{P}^n$ consists of the points with the same sign pattern. For instance, the sign pattern $(+ : + : - : +)$ for a point in $\mathbb{P}^3$ represents the orthant defined by

$$\{u_0 u_1 > 0, u_0 u_2 < 0, u_0 u_3 > 0, u_1 u_2 < 0, u_1 u_3 > 0, u_2 u_3 < 0\}.$$

Given a point $x \in \mathbb{P}^k$ being the image of a hyperplane $X = \mathrm{Span}\{w_1, ..., w_k\}$ under the Plücker embedding of $\mathrm{Gr}(k, k+1)$, and any point $v \in \mathbb{P}^k$, one may consider the bilinear map

$$T : \mathbb{P}^k \times \mathbb{P}^k \to \mathbb{R}, \quad x, v \mapsto \det \begin{bmatrix} | & & | & | \\ w_1 & \cdots & w_k & v \\ | & & | & | \end{bmatrix} = \sum_{j=1}^{k} (-1)^j p_{1...\hat{j}...k} v_j. \tag{5.2}$$

Then $T(x, v) = 0$ if and only if v is contained in X. If $v = Z_i$ for some row Z_i of Z, then $T(x, Z_i)$ is commonly called a *twistor coordinate of X with respect to Z* [114, Definition 4.5].

Remark 5.2.7. One may also fix either argument x or v of T to get a linear form on $\mathbb{P}^k$. In this paper we will consider the twistor coordinates as functions of x by setting $v = Z_i$ and denote the resulting forms by $l_i(x)$. We will see in Theorem 5.3.1 that the vanishing loci of the l_i's are exactly the hyperplanes which contain the boundaries of $\mathcal{G}_{n,k,m}(Z)$.

We now recall the definition of sign variation from [72].

Definition 5.2.8 (Sign variation). Given a sequence v of n real numbers, let $var(v)$ be the number of sign changes in v (zeros are ignored). Let $\overline{var}(v) := \max\{var(w) : w \in \mathbb{R}^n$ such that $w_i = v_i$ for all $i \in [n]$ with $v_i \neq 0\}$, i.e. $\overline{var}(v)$ is the maximum number of sign changes in v after a sign for each zero component is chosen. Note that both var and $\overline{var}$ are well-defined functions in the homogeneous coordinates of a point in $\mathbb{P}^{n-1}$.

We call a $(k-1)$-dimensional subspace of $\mathbb{P}^{n-1}$ *positive* if it is a point in $\mathrm{Gr}_{\geq 0}(k, n)$ and *totally positive* if it is a point in $\mathrm{Gr}_{>0}(k, n)$. Given a point $u \in \mathbb{P}^{n-1}$, we define the *hyperplane* H_u *given by* u to be the hyperplane orthogonal to u with respect to the standard dot product, i.e. $H_u := \{v \in \mathbb{P}^{n-1} : u \cdot v = 0\}$. Then we have the following proposition.

Proposition 5.2.9. *Let H_u be the hyperplane given by $u \in \mathbb{P}^{n-1}$.*

1. *H_u contains a positive subspace of dimension $k-1$ if and only if $\overline{var}(u) \geq k$.*

2. *H_u contains a totally positive susbspace of dimension $k-1$ if and only if $var(u) \geq k$.*

Proof. We start by proving the first statement. A hyperplane H_u contains a positive subspace of dimension k if and only if u is in the kernel of some matrix of the form $\left(\dfrac{A}{B}\right)$ where $A \in \mathrm{Gr}_{\geq 0}(k, n)$, and $B \in \mathrm{Gr}(n-k-1, n)$. Here A represents the positive subspace, and B the additional points to define a hyperplane. Note that $u \in \ker\left(\dfrac{A}{B}\right)$ if and only if $u \in \ker(A)$ and $u \in \ker(B)$. Then, the "only if" direction follows directly from [55, Theorems V1 and V6] (also [72, Theorem 3.4(i)]). The "if" direction also follows, with the note that one can always find $n-k-1$ additional points to form the matrix B such that $u \in \ker(B)$. The second statement is proved analogously, with replacing $\mathrm{Gr}_{\geq 0}(k, n)$ by $\mathrm{Gr}_{>0}(k, n)$ and using [72, Theorem 3.4(ii)]. $\square$

5.3 Grasstopes for $m = 1$: tame, wild, and rational

We begin by stating our main theorem which describes any $m = 1$ Grasstope $\mathcal{G}_{n,k,1}(Z)$ arising from a well-defined map $\tilde{Z}$ as a subset of $\mathbb{P}^k \cong \mathrm{Gr}(k, k+1)$. This theorem recovers and generalizes many of the results of Karp and Williams describing $m = 1$ amplituhedra and tame Grasstopes ([72, Section 6]).

Theorem 5.3.1. *Suppose $\tilde{Z} : Gr(k, n) \dashrightarrow Gr(k, k+1)$ is well-defined on $Gr_{\geq 0}(k, n)$. Then the Grasstope $\mathcal{G}_{n,k,1}(Z)$ consists of the points $\mathbf{x} \in \mathbb{P}^k$ such that $\overline{var}(L(\mathbf{x})) \geq k$, where $L(\mathbf{x})$ is the vector of twistor coordinates of $\mathbf{x}$ with respect to Z.*

Proof. Let $L(\mathbf{x}) = (l_1(\mathbf{x}) : \dots : l_n(\mathbf{x})) \in \mathbb{P}^{n-1}$ (see Remark 5.2.7). By Proposition 5.2.9, it suffices to show that $H_{L(\mathbf{x})}$ contains a positive subspace if and only if $X \in \mathcal{G}_{n,k,1}(Z)$.

For the "if" direction, suppose that $A \in \mathrm{Gr}_{\geq 0}(k, n)$ and $\mathbf{x}$ is the vector of Plücker coordinates of $[AZ]$. Then for each row A_i of A, we have

$$L(\mathbf{x}) \cdot A_i = \sum_{j=1}^{n} T(\mathbf{x}, Z_j) A_{ij} = T(\mathbf{x}, \sum_{j=1}^{n} A_{ij} Z_j) = 0,$$

since $\sum A_{ij} Z_j$ is a row of AZ. Thus $H_{L(\mathbf{x})}$ contains A.

For the "only if" direction, suppose that $H_{L(\mathbf{x})}$ contains a positive subspace A, and let $v \in \ker Z^T$. Then

$$L(\mathbf{x}) \cdot v = \sum_{i=1}^{n} T(\mathbf{x}, Z_i) v_i = T(\mathbf{x}, \sum_{i=1}^{n} Z_i v_i) = T(\mathbf{x}, 0) = 0.$$

So $H_{L(\mathbf{x})}$ contains $\mathbb{P}(\ker Z^T)$. Since $\mathbb{P}(\ker Z^T) \cap A = \varnothing$ by regularity of $\tilde{Z}$ on $\mathrm{Gr}_{\geq 0}(k, n)$, we have by dimension considerations that any two hyperplanes containing A and $\mathbb{P}(\ker Z^T)$ must be equal. However, by the "if" direction, if $\mathbf{a}$ is the vector of Plücker coordinates of $[AZ]$, then $H_{L(\mathbf{a})}$ contains A. In addition, $H_{L(\mathbf{a})}$ contains $\mathbb{P}(\ker Z^T)$. Therefore $H_{L(\mathbf{x})} = H_{L(\mathbf{a})}$. Since $u \mapsto H_u$ is injective, we obtain $\mathbf{x} = \mathbf{a}$.

$\square$

Note that in the proof of Theorem 5.3.1, the well-defined condition is necessary, since otherwise there might be positive subspaces which intersect $\mathbb{P}(\ker Z^T)$. In this case, there is no guarantee that a hyperplane containing a positive subspace also contains a positive subspace disjoint from $\mathbb{P}(\ker Z^T)$, which might present problems on the boundary of the Grasstope.

However, as we show in the following results, we can still describe the open rational Grasstope in the case that the map $\tilde{Z}$ is not well-defined on $\mathrm{Gr}_{\geq 0}(k, n)$. We first need the following lemma about totally positive subspaces to show that intersection with $\mathbb{P}(\ker Z^T)$ does not cause issues.

Lemma 5.3.2. *Let H be a hyperplane in $\mathbb{P}^{n-1}$ containing an $(n-k-1)$-dimensional subspace P. If H contains a totally positive $(k-1)$-dimensional subspace, then it contains a totally positive $(k-1)$-dimensional subspace disjoint from P.*

Proof. Let $V \subset H$ be a totally positive $(k-1)$-dimensional subspace. Let $l = \dim(V \cap P)$. Then $\dim(V + P) = n - l - 2$ and $V + P \subset H$. In particular, the codimension of $V + P$ inside H is equal to l. Pick $l + 1$ points $q_1, \ldots, q_{l+1}$ in general position in $H \smallsetminus (V + P)$. Let M be a matrix representing $V + P \in \mathrm{Gr}(n - l - 1, n)$ such that the first $k + 1$ rows of M represent $V \in \mathrm{Gr}_{>0}(k, n)$ and there is a subset of rows $r_1, \ldots, r_{l+1}$ of M representing $V \cap P \in \mathrm{Gr}(l, n)$. Denote by B the submatrix of M given by its first $k + 1$ rows. Note that the $k - l$ rows $s_1, \ldots, s_{k-l}$ of B that are not $r_1, \ldots, r_{l+1}$ span a subspace W disjoint from P. Consider a matrix M' obtained from M by replacing r_i with $r_i + \varepsilon_i \tilde{q}_i$ for $i = 1, \ldots, l + 1$, where $\varepsilon_i > 0$ and $\tilde{q}_i$ is a vector of homogeneous coordinates of the point q_i. Since the points $q_1, \ldots, q_{l+1}$ are in general position in $H \smallsetminus (V + P)$, the matrix M' has full rank and represents an $(n - l - 2)$-dimensional subspace of H. Denote

the first $k+1$ rows of M' by B'. Then, for $\varepsilon_1, \ldots, \varepsilon_{l+1}$ small enough, B' represents a subspace $V' \in \mathrm{Gr}_{>0}(k, n)$. We claim that V' is disjoint from P. To show this, consider the matrix D obtained by stacking B' below a matrix C representing P. Note that D represents the projective subspace $V' + P$. Since the points in $\mathbb{P}^{n-1}$ defined by rows $r_1, \ldots, r_{l+1}$ are in P, by performing row operations on D, one can reduce it to the form $D' = \begin{pmatrix} C \\ \hline Q \end{pmatrix}$, where Q consists of the rows $s_1, \ldots, s_{k-l}, \tilde{q}_1, \ldots, \tilde{q}_{l+1}$. Due to the choice of $q_1, \ldots, q_{l+1}$ and the fact that W is disjoint from P, D' has full rank. This means that $\dim(V' + P) = \dim(V') + \dim(P)$, so V' and P are disjoint. $\qquad\square$

Following Lemma 5.3.2, we are ready to describe the open rational Grasstope $\tilde{Z}(\mathrm{Gr}_{>0}(k, n))$. Recall that $\mathcal{B}(\tilde{Z})$ denotes the set of base points of $\tilde{Z}$.

Proposition 5.3.3. *For a map $\tilde{Z} : Gr_{\geq 0}(k, n) \dashrightarrow Gr(k, k+1)$ given by a matrix Z the open Grasstope $\tilde{Z}(Gr_{>0}(k, n))$ consists of the points $\mathbf{x} \in \mathbb{P}^k$ such that $var(L(\mathbf{x})) \geq k$, where $L(\mathbf{x})$ is the vector of twistor coordinates of $\mathbf{x}$ with respect to Z.*

Proof. We will prove this statement by slightly modifying the proof of Theorem 5.3.1. Fix a totally positive matrix $A \in \mathrm{Gr}_{>0}(k, n) \smallsetminus \mathcal{B}(\tilde{Z})$ and let $\mathbf{x}$ be the vector of Plücker coordinates of $[AZ]$. Then the hyperplane $H_{L(\mathbf{x})}$ contains $\mathbb{P}(\ker Z^T)$ and the totally positive subspace A. Conversely, if a hyperplane H contains $\mathbb{P}(\ker Z^T)$ and a totally positive subspace A, then by Lemma 5.3.2 H contains a totally positive subspace A' disjoint from $\mathbb{P}(\ker Z^T)$ (thus, $A' \notin \mathcal{B}(\tilde{Z})$). The hyperplane is then uniquely determined by its containment of $\mathbb{P}(\ker Z^T)$ and A', so it must be $H_{L(\mathbf{x})}$, where $\mathbf{x}$ is the vector of Plücker coordinates of $[A'Z]$. We now use the second part of Proposition 5.2.9 to conclude that the open Grasstope $\tilde{Z}(\mathrm{Gr}_{>0}(k, n))$ consists of the points in $\mathbf{x} \in \mathbb{P}^k$ such that $var(L(\mathbf{x})) \geq k$.

$\qquad\square$

Proposition 5.3.4. *The open rational Grasstope of Z is open and, if Z has no zero rows, the rational Grasstope of Z is contained in the closure of the open rational Grasstope of Z.*

Proof. Let Z define a rational Grasstope and consider a point $\mathbf{x}$ with $var(L(\mathbf{x})) \geq k$, where $L(\mathbf{x})$ is the vector of twistor coordinates of $\mathbf{x}$ with respect to Z. Then for all points $\mathbf{x}'$ in a sufficiently small neighborhood around it, $L(\mathbf{x}')$ has the same signs as $L(\mathbf{x})$ in all the indices of the nonzero entries of $L(\mathbf{x})$. Since changing the zero entries cannot decrease the sign variation, the neighborhood is contained in the open rational Grasstope.

Similarly to the reasoning of Theorem 5.3.1, it follows from the second part of Proposition 5.2.9 that the rational Grasstope of Z must be contained in the set $C := \{\mathbf{x} : \overline{var}(L(\mathbf{x})) \geq k\}$. We show that when Z has no zero rows, C is the closure of the open rational Grasstope of Z. First, we show that the complement of C, the set $\{\mathbf{x} : \overline{var}(L(\mathbf{x})) < k\}$, is open. Let $\mathbf{x}$ be such that $\overline{var}(L(\mathbf{x})) < k$. Then for all points $\mathbf{x}'$ in a sufficiently small neighborhood around $\mathbf{x}$, $L(\mathbf{x}')$ has the same signs as $L(\mathbf{x})$ in all the indices of the nonzero entries of $L(\mathbf{x})$. Since changing the values of the zero entries cannot increase $\overline{var}$, we know $\overline{var}(L(\mathbf{x}')) < k$. Therefore C is closed.

Now consider a point $\mathbf{x} \in C$ and an open neighborhood N of points around it. We will show that there is some $\mathbf{x}' \in N$ with $var(L(\mathbf{x}')) \geq k$, which is sufficient to conclude that C is the closure of the open rational Grasstope of Z. Since Z has no zero rows, each zero entry of $L(\mathbf{x})$ corresponds to containment of $\mathbf{x}$ in a hyperplane. Any open neighborhood around $\mathbf{x}$ contains points on either side of the hyperplane. Similarly, if $\mathbf{x}$ lies in the intersection of several hyperplanes, any open neighborhood of $\mathbf{x}$ contains points in each orthant defined by these hyperplanes, so any sign pattern can be achieved in the entries which are zero in $L(\mathbf{x})$. In particular, this means that there is a point $\mathbf{x}'$ with signs in the nonzero entries of $L(\mathbf{x})$ equal to the signs of the corresponding entries of $L(\mathbf{x}')$ (since we can restrict N to be small enough such that the signs in the nonzero entries of $L(\mathbf{x})$ are unchanged), and signs of the zero entries replaced by the signs which ensure that $var(L(\mathbf{x}')) \geq k$. $\qquad \square$

In Section 5.4, we show that the rational Grasstope may be equal to the closure of the open rational Grasstope. However, we do not know if this holds in general, since as far as we can tell, it might be possible for points in the boundary to be missing. Thus the question of fully describing which parts of the boundary are contained in $m = 1$ rational Grasstopes remains open.

5.4   Examples

In this section we provide examples of the families of Grasstopes we considered. We begin with an example of a tame Grasstope.

Example 5.4.1 (A tame Grasstope). Let

$$Z = \begin{bmatrix} 1 & 0 & -1 & -3 & -2 \\ 0 & 1 & 1 & 2 & 1 \\ 0 & 0 & 1 & -1 & -2 \end{bmatrix}^T.$$

This matrix is not totally positive, since $p_{123} = 1$ and $p_{124} = -1$. However, the first two rows of Z^T span a totally positive line, so Z satisfies (5.1) with the matrix M being

$$\begin{bmatrix} 1 & 0 & 0 \\ 0 & 1 & 0 \end{bmatrix}^T.$$

Therefore the resulting Grasstope is tame but is not an amplituhedron. The rows of Z define 5 linear forms, as noted in Remark 5.2.7:

$$l_1 = z, \quad l_2 = -y, \quad l_3 = x - y - z, \quad l_4 = -x - 2y - 3z, \quad l_5 = -2x - y - 2z.$$

Not every affine chart that we choose results in a bounded picture. For instance, if we map $(x : y : z) \mapsto (x + y : y : z)$ and dehomogenize with respect to the first coordinate, the resulting picture is unbounded. However, as predicted by Corollary 5.2.4, there are lines
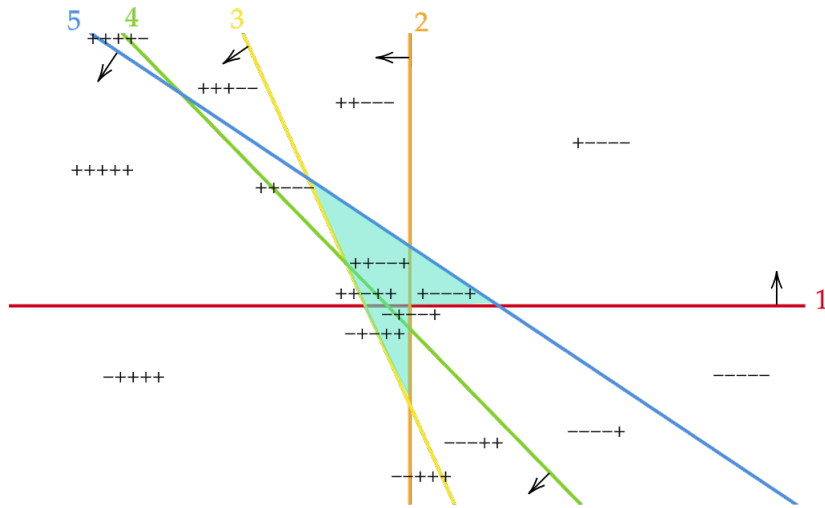
Figure 5.1: Affine chart in which the tame Grasstope is bounded.

disjoint from the Grasstope. One of them is $\{-4x + z = 0\}$ in $\mathbb{P}^2$. By picking it to be the line at infinity (that is, by mapping $(x : y : z) \mapsto (-4x + z : y : z)$ and dehomogenizing with respect to the first coordinate), we obtain affine lines given by the linear forms

$$\tilde{l}_1 = \tilde{y}, \quad \tilde{l}_2 = -\tilde{x}, \quad \tilde{l}_3 = \frac{-1 - 4\tilde{x} - 3\tilde{y}}{4}, \quad \tilde{l}_4 = \frac{-1 - 8\tilde{x} - 13\tilde{y}}{4}, \quad \tilde{l}_5 = \frac{1 - 2\tilde{x} - 5\tilde{y}}{2}.$$

Each line has an orientation, with the positive half-space given by the points $(\tilde{x}, \tilde{y})$ for which $\tilde{l}(\tilde{x}, \tilde{y}) \geq 0$. The lines divide the affine plane into regions, each of which has a corresponding sign vector with i^{th} coordinate being + if $\tilde{l}_i(\tilde{x}, \tilde{y}) > 0$ for all $(\tilde{x}, \tilde{y})$ in the region, and − if $\tilde{l}_i(\tilde{x}, \tilde{y}) < 0$. The Grasstope of Z consists exactly of those points in the regions for which $\overline{var}(u) \geq 2$, as can be seen in Figure 5.1. The six lines corresponding to the rows of Z are colored red, orange, yellow, green, and blue, in order, with orientations given by arrows. The shaded portion of the figure is the Grasstope, which consists exactly of the regions with at least two sign changes.

Example 5.4.2 (A wild Grasstope)**.** Let

$$Z = \begin{bmatrix} 2 & 2 & 0 & -1 & 1 & 0 \\ 2 & 3 & 1 & 0 & 2 & 0 \\ 2 & 2 & 0 & 0 & 2 & 1 \end{bmatrix}^T.$$

This is the example found by Galashin (and communicated to us by Lam [80]) to show that wild Grasstopes exist. Indeed, suppose there exists a 3×2 matrix M such that ZM has

positive 2×2 minors. The 2×2 minors of ZM are the entries of $\wedge_2(ZM) = \wedge_2(Z) \times \wedge_2(M) =$

$$
= \begin{bmatrix} 2 & 2 & 2 & 2 & 3 & 1 & 2 & 1 & -1 & -2 & 0 & 0 & 0 & 0 & 0 \\ 0 & 0 & 0 & 2 & 2 & 0 & 2 & 2 & 0 & -2 & 2 & 2 & 0 & -1 & 1 \\ -2 & -2 & -2 & 0 & 0 & 0 & 0 & 2 & 2 & 0 & 2 & 3 & 1 & 0 & 2 \end{bmatrix}^T \begin{bmatrix} p_{12} \\ p_{13} \\ p_{23} \end{bmatrix},
$$

where p_{12}, p_{13}, p_{23} are the minors of M. Then, column 4 of $(\wedge_2 Z)^T$ tells us that $p_{12} + p_{13} > 0$ but column 10 tells us that $p_{12} + p_{13} < 0$, so no such matrix M can exist.

The six rows of Z correspond to the six linear forms

$$
\begin{array}{lll}
l_1 = 2x - 2y + 2z, & l_2 = 2x - 3y + 2z, & l_3 = -y \\
l_4 = -z, & l_5 = 2x - 2y + z, & l_6 = x.
\end{array}
$$

Mapping $(x : y : z) \mapsto (x + y : y : z)$ and dehomogenizing with respect to the first coordinate, we obtain affine lines given by the linear forms

$$
\begin{array}{lll}
\tilde{l}_1 = 2\tilde{y} - 4\tilde{x} + 2, & \tilde{l}_2 = 2\tilde{y} - 5\tilde{x} + 2, & \tilde{l}_3 = -\tilde{x}, \\
\tilde{l}_4 = -\tilde{y}, & \tilde{l}_5 = \tilde{y} - 4\tilde{x} + 2, & \tilde{l}_6 = -\tilde{x} + 1.
\end{array}
$$

We draw these in the affine plane and color them (in order) red, orange, yellow, green, blue, and purple. We also give the lines orientations with the positive half-space given by the points $(\tilde{x}, \tilde{y})$ for which $\tilde{l}(\tilde{x}, \tilde{y}) > 0$. Then the Grasstope of Z consists exactly of those points in the regions between the lines for which $\overline{var}(u) \geq 2$, as can be seen in Figure 5.2. The six lines corresponding to the rows of Z are pictured as described above, with orientations given by the arrows. The regions are labelled by sign patterns. The shaded portion of the figure is the Grasstope, and it consists exactly of those regions with at least two sign changes.

Example 5.4.3 (A rational Grasstope with closed boundary and Möbius strip topology). Let

$$
Z = \begin{bmatrix} 1 & 0 & 0 & -1 & 0 & 0 \\ 0 & 1 & 0 & -1 & 1 & -1 \\ 0 & 0 & 3 & 0 & -2 & -1 \end{bmatrix}^T .
$$

Note that $(1, 1, 1, 1, 1, 1) \in \ker(Z^T)$, so the map $\tilde{Z}$ has base points on $\mathrm{Gr}_{\geq 0}(2, 6)$. Following Proposition 5.3.3 we can still describe its open Grasstope. As in the previous examples, we find 6 dehomogenized linear forms corresponding to six affine lines

$$
\begin{array}{lll}
\tilde{l}_1 = \tilde{y}, & \tilde{l}_2 = -\tilde{x}, & \tilde{l}_3 = -3\tilde{x} + 3, \\
\tilde{l}_4 = \tilde{x} - \tilde{y}, & \tilde{l}_5 = \tilde{x} - 2, & \tilde{l}_6 = 2\tilde{x} - 1.
\end{array}
$$

Then we can find the open rational Grasstope of Z as in Figure 5.3. The six lines corresponding to the rows of Z are pictured as described above, with orientations given by the arrows. The regions can then be labelled by sign patterns. The shaded portion of the figure
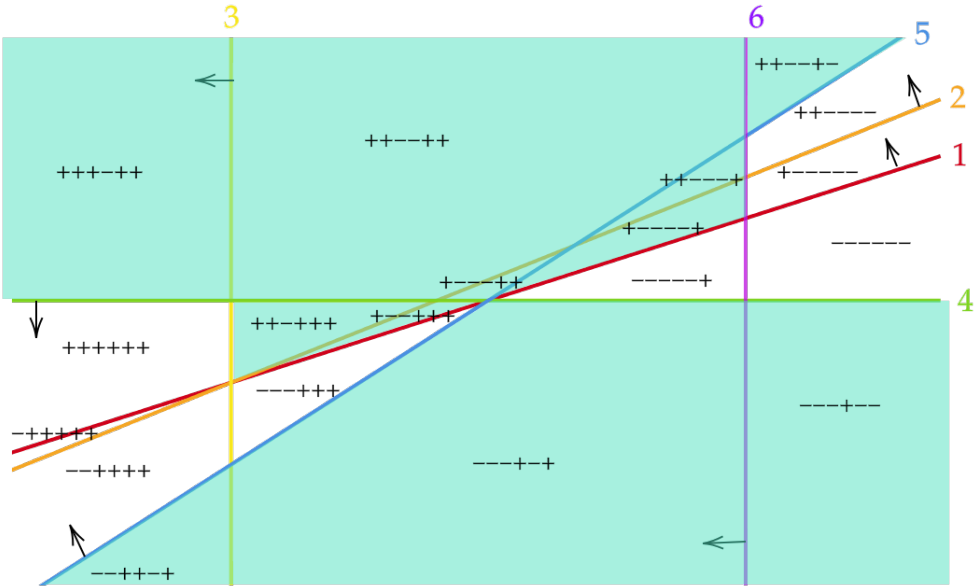
Figure 5.2: A wild Grasstope. It meets every line in $\mathbb{P}^2_{\mathbb{R}}$
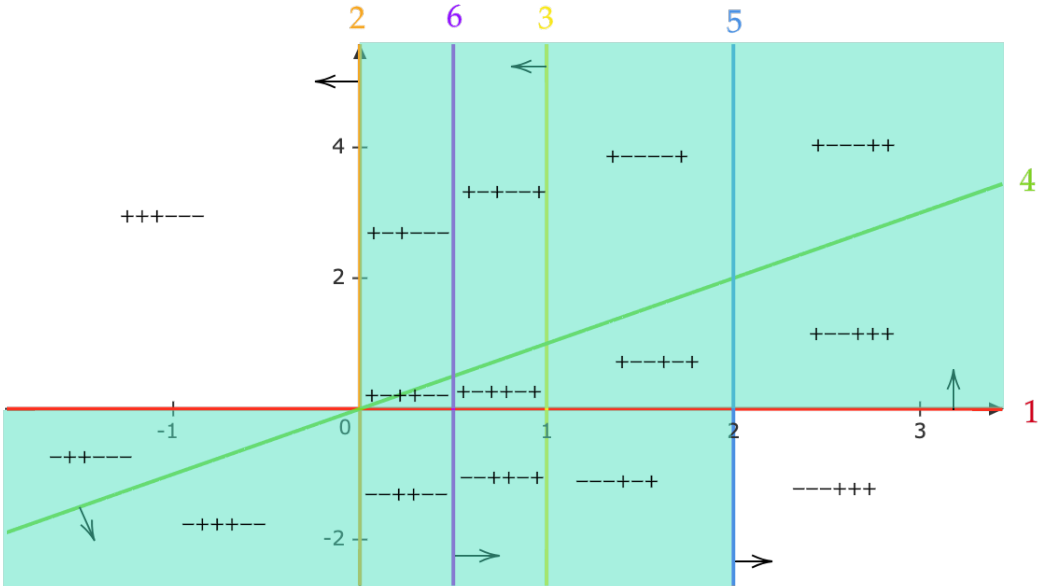
Figure 5.3: A rational Grasstope. The shaded region has the topology of a Möbius strip.

is the Grasstope, and it consists exactly of those regions with at least two sign changes. In this case, the shaded region is a Möbius strip.

We claim that the rational Grasstope of Z is the closure of the open rational Grasstope. One can check this by directly finding Plücker coordinates for some $M \in \mathrm{Gr}_{\geq 0}(2,6)$ which map to the points that lie on the boundary. For example, to find such M for any point of the form $(0, a)$ with $a \geq 0$, we solve $\wedge_2(Z) \times \wedge_2(M) = (1 : 0 : a)$. Then $\wedge_2(M)$ must have nonnegative entries which satisfy the Plücker relations. This process is made easier if one recalls that the Plücker relations are trivially satisfied if all entries are zero except for ones which correspond to pairwise overlapping submatrices, that is any two nonzero minors come from submatrices which share a column. In this case, since

$$
\wedge_2(Z) = \begin{bmatrix} 1 & 0 & 0 & -1 & 1 & 0 & 1 & 0 & 0 & -1 & -1 & 0 & 0 & 1 & 0 \\ 0 & 3 & 0 & 0 & 0 & 3 & -2 & 0 & 0 & 2 & -1 & 0 & 0 & 1 & 0 \\ 0 & 0 & 3 & 0 & 0 & 3 & 0 & -2 & -3 & 2 & 0 & -1 & 3 & 1 & -3 \end{bmatrix}^T,
$$

we find that the point $(1 : 0 : a)$ is given by $\wedge_2(M) = (0 : 0 : a/3 : 0 : 1 : 0 : 0 : 0 : 0 : 0 : 0 : 0 : 0 : 0 : 0)$. Since the only nonzero entries correspond to the minors p_{23} and p_{24}, the Plücker relations are satisfied. Thus the portion of the boundary line $x = 0$ with $y \geq 0$ is part of the rational Grasstope of Z. One can similarly check that all other parts of all six lines are included. Therefore the rational Grasstope of Z is closed. Furthermore, topologically, as one can see from Figure 5.3, it is a Möbius strip. Indeed, since it is a projective picture, the "positive" orthant and the "negative" orthant connect, but with a twist to account for the sign inversion.

5.5 Background on oriented matroids

Much of the material on hyperplane arrangements can be naturally generalized to oriented matroids [12]. In this section, we review the basics of oriented matroid theory and recall a dictionary between hyperplane arrangements and oriented matroids. This will prove useful in algorithmically counting the number of regions in a given Grasstope (see Section 5.6). We begin by discussing signed circuits, which we will often abbreviate as circuits if the meaning is clear from context.

Definition 5.5.1 (Signed circuit axioms)**.** An oriented matroid consists of a ground set $\mathcal{E}$ and a collection $\mathcal{C}$ of tuples of the form $X = (X^+, X^-)$ called *circuits*, where X^+, X^- are disjoint subsets of $\mathcal{E}$ satisfying

1. $\varnothing$ is not a circuit.

2. If X is a circuit, then so is $-X = (X^-, X^+)$.

3. No proper subset of a circuit is a circuit.

4. (Elimination). If X_0 and X_1 are two signed circuits with $X_0 \neq X_1$ and $e \in X_0^+ \cap X_1^-$, then there is a third circuit $X \in \mathcal{C}$ with $X^+ \subset (X_0^+ \cup X_1^+) \smallsetminus \{e\}$ and $X^- \subset (X_0^- \cup X_1^-) \smallsetminus \{e\}$.

We can obtain the oriented matroid of a matrix as follows.

Definition 5.5.2 (Oriented matroid of a matrix)**.** Fix a matrix A and let $\sum_i \lambda_i v_i$ be a minimal linear dependency among its rows. Associate to this dependency the signed set $X = (X^-, X^+)$, where

$$X^- = \{i : \lambda_i < 0\}$$
$$X^+ = \{i : \lambda_i > 0\}.$$

Then the *oriented matroid* $\mathcal{M}_A$ associated to A has as its signed circuits the signed sets coming from minimal linear dependencies.

One can check that oriented matroids of matrices satisfy the signed circuit axioms.

Example 5.5.3 (Matroid of a matrix A)**.** Consider the matrix

$$A = \begin{bmatrix} 1 & 0 & 0 \\ 0 & 1 & 0 \\ 0 & 0 & 1 \\ 2 & -3 & 4 \end{bmatrix}.$$

Then the only linear dependency up to scaling is $v_4 - 4v_3 + 3v_2 - v_1 = 0$. Thus the only circuit (when only one of $X, -X$ is considered) is $24\overline{1}\overline{3}$, where we use a more compact notation in which the bar indicates being in the negative part of the signed set.

Remark 5.5.4. One can also define $\mathcal{M}_A$ by signed bases; the matroid is the map which assigns to each size k subset $I \subset [n]$ the sign of the determinant of A_I. This definition is called the *chirotope definition* [12, page 6] and satisfies the *chirotope axioms,* which we do not describe here. In particular, the database [48] used in Section 5.6 indexes oriented matroids by their chirotope.

We recall a few definitions we will need to explain how a hyperplane arrangement can be viewed as an oriented matroid.

Definition 5.5.5 (Composition)**.** Let $X = (X^+, X^-)$ and $Y = (Y^+, Y^-)$ be signed sets. Then their *composition* $X \circ Y$ is $(X^+ \cup (Y^+ \smallsetminus X^-), X^- \cup (Y^- \smallsetminus X^+))$.

Definition 5.5.6 (Orthogonality)**.** Let $X = (X^+, X^-)$ and $Y = (Y^+, Y^-)$ be signed sets. Define $S(X, Y) = (X^+ \cap Y^-) \cup (X^- \cap Y^+)$. We say X and Y are *orthogonal* if $S(X, Y)$ and $S(X, -Y)$ are both empty or both non-empty.

We define *vectors* as compositions of circuits, and *cocircuits* and *covectors* as the circuits and vectors of the dual matroid [12, page 4], respectively. An equivalent definition which is easier for computing is that the covectors of $\mathcal{M}$ are the signed sets which are orthogonal to all vectors of $\mathcal{M}$. For more detail, see [12, Chapter 1]. There is yet another definition in the case of vector configurations.

Definition 5.5.7 (Oriented matroid of a vector configuration)**.** One can also view the rows v_i of the matrix A as vectors in $\mathbb{R}^k$. For such a vector configuration, the covectors can be defined as the set of tuples $Y_H = (Y_H^+, Y_H^-)$ as H runs over oriented hyperplanes, where Y_H^+ is the set of vectors in the positive halfspace defined by H, and Y_H^- is the set of vectors in the negative halfspace. The *cocircuits* are the minimal covectors. They arise from hyperplanes that are spanned by subsets of $\{v_1, ..., v_n\}$.

Definition 5.5.8 (Oriented matroid of a hyperplane arrangment)**.** Let H_i be the hyperplane given by the vanishing of $l_i(x) = a_i \cdot x$. Then the oriented matroid of the arrangement $\{H_i\}_{i=1}^n$ is the matroid of the vector configuration given by $a_1, ..., a_n$, or equivalently, the oriented matroid of the matrix with rows $a_1, ..., a_n$.

Remark 5.5.9. Faces of a hyperplane arrangement correspond to covectors of its oriented matroid, and regions correspond to maximal covectors. The *rank* (denoted by r) of the oriented matroid is $k + 1$, where k is the dimension of the ambient space [12, Chapter 1].

Example 5.5.10 (Matroid of a matrix A)**.** Let A be the matrix

$$A = \begin{bmatrix} 1 & 0 & 0 \\ 0 & 1 & 0 \\ 0 & 0 & 1 \\ 2 & -3 & 4 \end{bmatrix}$$

as in Example 5.5.3. The cocircuits are given considering hyperplanes H spanned by pairs of rows. For example, if $H = \text{Span}\{a_1, a_3\} = \{y = 0\}$, then a_2 is in the positive halfspace (since the y-coordinate is 1) and a_4 is in the negative halfspace (since the y coordinate is -3). Thus we obtain the cocircuit $2\bar{4}$.

The total set of cocircuits (not including negations) is $\{2\bar{4}, 34, 23, 14, 3\bar{1}, 12\}$. In the previous sections we have used sign vector notation; that is, to each signed set we associate a length n vector with $\pm$ at index i if i is in $X^\pm$ and 0 otherwise. Applying this convention, one can check that the covectors are exactly the sign vectors with fewer than 3 sign changes. For example, $2\bar{4} \circ 3\bar{1} = 23\overline{14}$, which corresponds to $(- + +-)$.

Definition 5.5.11. A matroid is *realizable* if it arises from a hyperplane arrangement over $\mathbb{R}$.

5.6 Extremal counts and oriented matroid Grasstopes

Given an $n \times (k + 1)$ matrix Z, one may ask questions about the topology of the resulting $m = 1$ Grasstope. For instance, is it closed, connected, contractible? How many regions of

the hyperplane arrangement does it contain? For the $m = 1$ amplituhedron, the answer to the first three questions is "yes" [72, Corollary 6.18]. As for the latter, the $m = 1$ amplituhedron contains as few regions as possible, that is, all possible sign vectors with $var < k$ appear as labels of regions in the corresponding arrangement [72, Proposition 6.14]. In this section, we investigate this last question for more general $m = 1$ Grasstopes.

Definition 5.6.1. A *region* of a hyperplane arrangement is a connected component of the complement of the union of hyperplanes in the arrangement.

In [116], Zaslavsky gives the following formulae for the number of total regions $t(\mathcal{A})$ and bounded regions $b(\mathcal{A})$ of an affine arrangement $\mathcal{A}$ of n generic hyperplanes in $\mathbb{A}^k$:

$$t(\mathcal{A}) = 1 + n + \binom{n}{2} + \ldots + \binom{n}{k},$$
$$b(\mathcal{A}) = \binom{n-1}{k}.$$

Note that since intersections of two hyperplanes in any projective arrangement $\mathcal{P}$ have codimension two in $\mathbb{P}^k$ and there are a finite number of them, we can always find some hyperplane avoiding them, and hence an an affine chart which contains all of them (see Figure 5.4). A projective arrangement $\mathcal{P}$ naturally induces an affine arrangement $\mathcal{A}$ in this affine chart. If a region of $\mathcal{P}$ intersects the chosen hyperplane at infinity, it induces two unbounded regions of $\mathcal{A}$. Otherwise it induces a single bounded region. Thus, the total number of regions in $\mathcal{P}$ is

$$r(\mathcal{P}) = b(\mathcal{A}) + \frac{t(\mathcal{A}) - b(\mathcal{A})}{2}. \tag{5.3}$$

Definition 5.6.2. Let $\mathcal{P}$ be an arrangement of n hyperplanes in $\mathbb{P}^k$. Then $\mathcal{P}$ is called *simple* if the intersection of any i hyperplanes in $\mathcal{P}$ has codimension i in $\mathbb{P}^k$ for all $i \leq k$, and is empty for $i > k$.

We write $\beta(k, n)$ for the number of possible sign patterns of length n with sign variation less than k and $\gamma(k, n)$ for the number of sign patterns with variation greater or equal than k (we identify sign patterns σ and $-\sigma$). Note that $\beta(k, n) = 1 + \binom{n-1}{2} + \ldots + \binom{n-1}{k}$, and $\gamma(k, n) = 2^{n-1} - \beta(k, n)$. Theorem 5.3.1 and Proposition 5.3.4 then give the lower bound $r(\mathcal{P}) - \beta(k, n)$ for the number of regions in $\mathcal{G}_{n,k,1}(Z)$, where $\mathcal{P}$ is the hyperplane arragement defined by Z. An upper bound is given by the minimum of $\gamma(k, n)$ and $r(\mathcal{P})$.

The database [48] contains a catalog of isomorphism classes of oriented matroids [47, Section 6]. Each matroid is indexed by a vector of signs of its bases and each hyperplane arrangement corresponds to a realizable matroid, as explained in the previous section. An arrangement is simple if the vector of signs of bases of its matroid does not contain zeros, that is, the matroid is uniform.
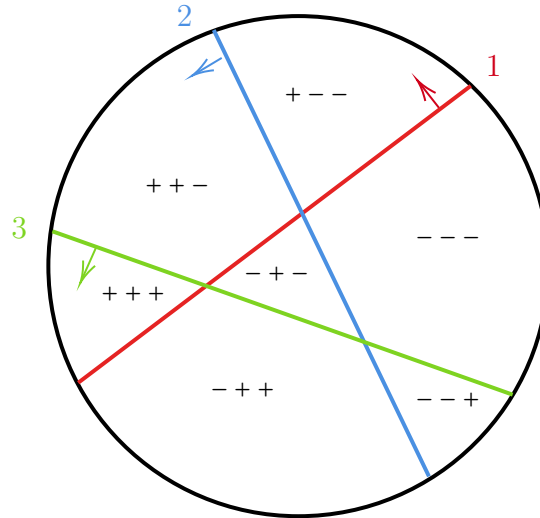
Figure 5.4: An oriented hyperplane arrangement and its sign labels.

We iterate over all uniform oriented matroid isomorphism classes in this catalog for small values of k and n. Note that, for all the values of k and n which we consider, all uniform matroids are realizable [51], that is, arise from hyperplane arrangements. Within each isomorphism class, we iterate over all possible reorderings of the ground set and reorientations. If the matroid is realizable, at the level of the matrix Z defining the arrangement as described in Section 5.2, reorderings correspond to permuting the rows and reorientations to negating certain rows. For each isomorphism class, ordering of the hyperplanes, and a choice of orientation, we compute the number of regions in the corresponding Grasstope (that is, the number of maximal covectors with sign variation greater or equal than k; see Remark 5.5.9). It turns out that for many values of k and n the minimal and maximal number of regions in the Grasstope when iterating over reorderings and reorientations does not depend on the oriented matroid isomorphism class. The minimal and maximal number of regions in the Grasstope for these values of k and n are presented in Table 5.1. The `Python` code used to extract this data is available at https://mathrepo.mis.mpg.de/Grasstopes. We therefore have a computational proof of the following statement.

Proposition 5.6.3. *For each pair of values of k and n in Table 5.1 the minimal and maximal possible number of regions in a Grasstope arising from a simple arrangement of n hyperplanes in $\mathbb{P}^k$ do not depend on the choice of arrangement.*

Out of the entries in Table 5.1, note that for $k = 2$ and the pairs $(3, 5)$ and $(4, 6)$, there is only one oriented matroid up to isomorphism [48]. For $k = 2$, this is because any matrix may be turned into a totally positive matrix by permuting the rows. This can be done by viewing rows as vectors in the plane and arranging them in counterclockwise position.

k, n	Minimal	Maximal	$r(\mathcal{P})$	$\beta(k,n)$	$\gamma(k,n)$
2, 6	10	16	16	6	26
2, 7	15	22	22	7	57
3, 5	4	5	15	11	5
3, 6	10	16	26	16	16
4, 6	5	6	31	26	6
4, 7	15	22	57	42	22

Table 5.1: Minimal and maximal possible number of regions in a Grasstope.

The pair $(3, 7)$ does not appear in Table 5.1. This is the first time we see variation depending on which simple arrangement we choose, with the maximal number of regions ranging from 38 to 42. The reorientations and reorderings of a totally positive matrix (i.e. the amplituhedron case) give at most 42 regions, while all other oriented matroid classes achieve fewer. We can see the maximal numbers of regions for other small k, n in Table 5.2. It would be interesting to see whether the maximal number of regions attained by reorienting and reordering a totally positive matrix attains the upper bound in general.

k, n	Maximal	$r(\mathcal{P})$	$\gamma(k,n)$
3, 7	42	42	42
3, 8	64	64	99
4, 8	64	99	64
5, 8	29	120	29
2, 9	37	37	247
3, 9	93	93	219
4, 9	163	163	163

Table 5.2: Maximal number of regions from reorienting and reordering a positive matrix.

Example 5.6.4. Any totally positive 6×3 matrix with the second and fourth rows negated yields a Grasstope which includes all 16 regions counted by Equation (5.3). The resulting hyperplane arrangement is cyclic, with just two orientations flipped. See Figure 5.5 to see all of the regions labelled with sign patterns. The six lines are cyclically ordered with orientations indicated by arrows. Every region has at least two sign changes, so the Grasstope is all of $\mathbb{P}^2$.

Example 5.6.5. An example of a 6×3 matrix whose Grasstope has 16 regions is any totally positive matrix with the 2nd and 4th rows swapped. For examples of totally positive
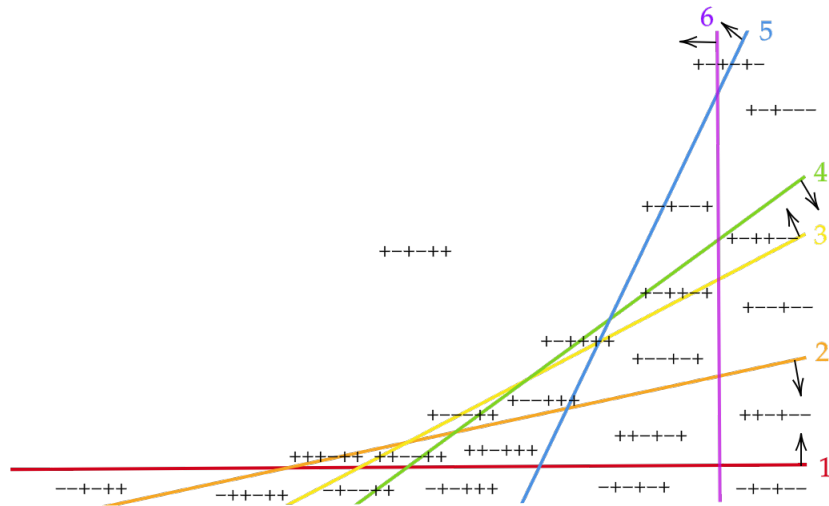
Figure 5.5: The Grasstope of a totally positive matrix with two rows negated is all of $\mathbb{P}^2$.

matrices, one can take the Vandermonde matrix

$$
\begin{bmatrix}
1 & 1 & 1 & 1 & 1 & 1 \\
d_1 & d_2 & d_3 & d_4 & d_5 & d_6 \\
d_1^2 & d_2^2 & d_3^2 & d_4^2 & d_5^2 & d_6^2
\end{bmatrix}^T .
$$

with $0 < d_1 < \ldots < d_6$.

Note that the lower bound $r(\mathcal{P}) - \beta(k, n)$ for the number of regions in a Grasstope is actually attained for all k and n, by the $m = 1$ amplituhedron [72, Proposition 6.14, Theorem 6.16]. The upper bound is also attained by starting from the $m = 1$ amplituhedron and negating some rows of the defining totally positive matrix, for the values in Tables 5.1 and 5.2. One interesting question to study is to determine whether this holds in general, and to describe all oriented matroids achieving this upper bound.

The dictionary between hyperplane arrangements and oriented matroids (Remark 5.5.9) guides us to generalize our definition of a Grasstope to oriented matroids that are not necessarily realizable, such that the definitions agree when $\mathcal{M} = \mathcal{M}_Z$.

Definition 5.6.6 (Grasstope of an oriented matroid)**.** Let $\mathcal{M}$ be an oriented matroid of rank r, and $<$ be a total order on the ground set $\mathcal{E}$ of $\mathcal{M}$. Then we define the *Grasstope* $\mathcal{G}(\mathcal{M}, <)$ to be the subset of covectors $\{v : \overline{var}(v) \geq r - 1\}$, where r is the rank of $\mathcal{M}$ and the variation is with respect to $<$.

Note that by Topological Representation Theorem [49, Theorem 20], every rank 3 oriented matroid arises from a pseudoline arrangement, with covectors labelling the cells of this arrangement. In particular, the Grasstope $\mathcal{G}(\mathcal{M}, <)$ can be identified with the union of cells

of a pseudoline arrangement that satisfy the sign variation condition from Definition 5.6.6. Therefore, Grasstopes of oriented matroids are meaningful geometric objects, and topological concepts such as connectedness and contractibility generalize naturally to them. Studying their topological properties is an interesting topic for future research.

Finally, we use our code to analyze a non-realizable example, which does not attain the upper bound.

Example 5.6.7. Consider the non-realizable matroid FMR(8) of rank 4 on 8 elements, whose signed cocircuits are given in [96, Table 1]. Reorientations and reorderings give at least 34 and at most 63 regions. Thus, unlike the amplituhedron, FMR(8) does not achieve the upper bound of 64.

In conclusion, there are many questions arising from our study of Grasstopes. These are combinatorially and algebraically interesting objects with structure which becomes progressively more complicated as we increase the parameters k, n, m. In addition to the open problems listed throughout this chapter, a natural next step would be to study Grasstopes for $m = 2$ and in particular, see if results for the $m = 2$ amplituhedron such as in [92] can be extended. Oriented matroid Grasstopes are also appealing objects to study and may yield insights that end up having relevance to physics. In particular, we would like to know if and how other topological concepts such as contractibility of $\mathcal{G}_{n,k,m}(Z)$ can be detected from the oriented matroid. This would be an interesting problem for computational algebraic topology.

Part III

Classical problems revisited

Chapter 6

Crossing the transcendental divide

This chapter is based on the publication "Crossing the transcendental divide: from translation surfaces to algebraic curves" [26], joint with Türkü Özlüm Çelik and Samantha Fairchild.

6.1   Introduction

We present an algorithm with numerical experiments as a step in bridging the *transcendental divide* between Riemann surfaces and algebraic curves. The classical equivalence of Riemann surfaces and algebraic curves leaves a divide in the sense that it is non-trivial to determine the exact curve associated to a Riemann surface. This becomes transcendental as connecting a Riemann surface to an algebraic curve utilizes Riemann theta functions. In our case we use discrete harmonic functions to approximate the Jacobian variety of the algebraic curve of a translation surface and the theta functions to understand these approximations.

A translation surface is obtained by identifying edges of finitely many polygons in the plane with complex translations. This identification of polygons builds a Riemann surface X, or equivalently a complex algebraic curve. The surface X naturally comes equipped with a nonzero holomorphic 1-form ω, given locally by dz, with $2g - 2$ zeroes located at the vertices of the polygons, where g is the genus of X. One method to obtain an equation for the underlying algebraic curve of a translation surface is to first find a basis of the space of holomorphic one-forms on X. This space identifies a canonical model of the curve in some projective space. For instance, if the translation surface has extra automorphisms the basis of holomorphic one-forms can be determined exactly [39, 95, 101]. Instead of requiring extra symmetries, we here aim to construct an algebraic curve explicitly from a translation surface by approximating the Riemann matrix.

Recall that a Riemann matrix τ associated to an algebraic curve $\mathcal{C}$ is defined by integrating a canonical basis of holomorphic differentials over the cycles forming a homology basis for the curve. The matrix τ data defines the Jacobian variety of $\mathcal{C}$, namely the quotient $\mathbb{C}^g/(\mathbb{Z}^g + \tau\mathbb{Z}^g)$. The Torelli theorem states that the curve $\mathcal{C}$ is determined by its Jacobian variety. In practice, one can construct Riemann matrices given an algebraic curve [33], and, less trivially,

given τ reconstruct the algebraic curve at least in low genus [2]. We will approximate the Riemann matrix from a translation surface and then utilize tools from numerical algebraic geometry to approximate the underlying curve.

The key instruments of our approach are discrete Riemann surfaces. They can be thought as discrete counterparts of the Riemann surfaces in discrete complex analysis [102]. All notions such as Riemann matrices and holomorphic differential forms have corresponding discretizations. An important result in the literature of discrete Riemann surfaces, which is fundamental for the present study, uses discrete energies to prove convergence of the discrete Riemann surfaces to the underlying Riemann surface. In particular the discrete Riemann matrices converge to a Riemann matrix [14, 15] of the Riemann surface. Our experiments employ compact Riemann surfaces given by quadrangulations based on theory developed in [17]. In the case of [17], convergence of the discrete Riemann matrices to a Riemann surface is not known in full generality, but our results give evidence for a potential result on convergence of the period matrices of [17].

A fairly technical algorithm to compute discrete Riemann matrices when the discrete complex structure is given by triangulations was presented in [18]. In contrast to the previous work, we present Algorithm 6.3 to be accessible to a large variety of mathematical audiences. Algorithm 6.3 inputs a translation surface as a polygon, a level of approximation, and outputs the associated discrete Riemann matrix. The given polygon must be able to be divided into squares. Moreover one must place an initial bipartite graph on the square tiled polygons, which means that the vertices are either black and white, and no two vertices of the same color are connected by an edge. The bipartite graph must be chosen so that all identified vertices of the translation surface are the same color. The rest is to find the correct basis of homology which respects the pairings given in the translation surface.

We present two concrete implementations of Algorithm 6.3. In Algorithm 6.3 we consider a family of symmetric L shaped polygons which are all genus 2 Riemann surfaces. The L shapes are highly symmetric, so they serve as a good test case where the exact underlying algebraic curve is known [101]. Another benefit of the L shapes is that they allow us to experiment with convergence to polygons which cannot be square tiled e.g., shapes with an irrational side length, by closer approximations of square tiled polygons.

We also present Algorithm 6.3, which gives a natural family of square tiled translation surfaces, called Jenkins–Strebel differentials, for any genus $g \geq 2$. When working with any genus, the step of Algorithm 6.3 where we must choose a homology basis respecting the identifications requires care. We explain our difficulties, and explain how we overcame these difficulties. This algorithm leads to two interesting experiments. First we approximate the Riemann matrix in a case where the underlying curve is not yet known. In genus 2, we can numerically compute the hyperelliptic curve, leading to some conjectures on the structure of the underlying curves. Further, we can do experiments in genus $g = 3, 4$, and 5, to understand how the discrete matrices approach along the Schottky locus of $g \times g$ matrices which are associated to an algebraic curve.

In Section 6.2, we give history, definitions, and examples for algebraic curves, translation surfaces, and discrete Riemann surfaces. In Section 6.3, we present the algorithms and

numerical experiments introduced above. Namely in Algorithm 6.3 we give the algorithm for any translation surface. Given a translation surface via its defining polygons, we approximate its Riemann matrix through a family of discrete Riemann surfaces, which are expressed in terms of subdivisions of the polygons. We then run experiments in two specific cases. In Section 6.3 we describe the algorithm in details and discuss convergence to the underlying Riemann surface for the case of the L. In Section 6.3 we again give specifics of the algorithm for the family of Jenkins-Strebel differentials, and we use theta functions to approximate an equation of the algebraic curve from the estimated matrix. Finally in Section 6.4 we give tables of values for approximating discrete Riemann matrices. The code can be found at our `MathRepo` page via the link

$$\text{https://mathrepo.mis.mpg.de/Tsurfaces2Acurves.} \tag{6.1}$$

6.2 Background

We aim here to recall some background which we need to reconstruct algebraic curves from their translation surfaces. This includes some preliminaries for Riemann surfaces and theta functions, translation surfaces, and discrete Riemann surfaces. Each topic is a well studied and interesting subject in its own right, so we provide references for their underlying theories.

Riemann Surfaces, analytic and algebraic

Riemann surfaces are one-dimensional complex manifolds, among which the compact ones are complex smooth algebraic curves. As discussed in the introduction, among central objects underlying the connection between the analytic side and the algebraic side are *theta functions* (1.1). We refer the reader to Section 1.2 to recall the relevant definitions of Riemann matrix, theta functions, theta constants, and the Schottky problem.

The theta functions play a central role in the literature of the Schottky problem and the Torelli theorem [61]. When $g = 4$, the Schottky-Igusa modular form defines an analytic hypersurface [68, Theorem 1] in terms of theta functions, which describes Riemann matrices in the Siegel upper half space that are of algebraic curves, the *Schottky locus*. For higher genus, there are analytical equations in terms of theta functions defining a locus containing the Schottky locus. In the context of the Torelli theorem, we suggest the reader to see [62, Theorem 8.1] for hyperelliptic curves and see [63, Theorem 1.1] for genus 3 non-hyperelliptic curves. These rely on the classical formulae going back to Riemann, namely the Thomae formula and the Weber formula [94, 109, 113] with their generalizations to any genus [25], which relate the extrinsic and intrinsic sides of geometry of the underlying curve. For instance, the vanishing theta constants i.e., the theta constants that are zero, are well-understood when the curve is hyperelliptic [89]. Actually, the theta constants express certain divisors of the curve $\mathcal{C}$, e.g. theta characteristic divisors (semi-canonical divisors), which recover the curve itself. More precisely, the choice of the basis $\omega_1, \ldots, \omega_g$ of the holomorphic differentials on $\mathcal{C}$

gives a map, namely the *canonical map* of $\mathcal{C}$:

$$\Phi : \mathcal{C} \to \mathbb{P}^{g-1}$$
$$P \mapsto (\omega_1(P), \ldots, \omega_g(P)).$$

An important note is that the canonical image $\Phi(\mathcal{C})$ is defined over a field over which the differential forms are defined. The following statement formulates the theta characteristic divisors in terms of the canonical model:

Theorem 6.2.1 (Theorem 2.2, [62]). *Let τ_1 be the first $g \times g$ part of the period matrix (1.2). Let D be an effective theta characteristic divisor of degree $g - 1$ with $\dim \mathrm{H}^0(\mathcal{C}, D) = 1$. The corresponding equations of the hyperplanes spanned by $\Phi(D)$ are given by:*

$$\left(\theta_1^{\varepsilon,\delta} \quad , \ldots, \quad \theta_g^{\varepsilon,\delta} \right) \cdot \tau_1^{-1} \cdot \begin{pmatrix} x_1 \\ \vdots \\ x_g \end{pmatrix} = 0, \tag{6.2}$$

where the characteristic $\begin{bmatrix} \varepsilon \\ \delta \end{bmatrix}$ ranges over the odd ones.

The values of the theta constants are nothing but the branch points for the case of hyperelliptic curves, which directly deliver the image of the canonical map. In the case of non-hyperelliptic curves, (6.2) gives the so-called *multitangent hyperplanes* of the canonical model in $\mathbb{P}^{g-1}$. For instance, the 28 bitangent lines of smooth plane quartics in genus 3, or the 120 tritangent planes of smooth space sextics in genus 4. It has been proven that the odd theta characteristics recover its algebraic curve [23]. For explicit reconstructions the algebraic curve from their multitangent hyperplanes for small genera see [27, 82, 83].

Algebro-geometric solutions of integrable systems contribute solutions to the Torelli and the Schottky problems in any genus [38, 78], where fundamental objects are again the theta functions (1.3) (see Chapter 3 for more discussion). For our experiments, we use an implementation presented in [2] that follows these studies to recover curves from their Riemann matrices. Mathematical software packages are available to compute with theta functions, such as [6, 32, 50, 54], which enable us to carry out our experiments.

Translation surfaces

We will give two equivalent definitions of a translation surface, introduce the two families of examples considered in this chapter, and conclude by discussing the connection to algebraic curves.

Fix a Riemann surface X of genus g. Recall that ω is a *holomorphic 1-form* (also called an *abelian differential*) if for every $x \in X$ there is a holomorphic function f_x so that in local coordinates $\omega = f_x(z)\, dz$ with the condition that a transition map T between charts with $f(z)$ and $g(z)$ as holomorphic function satisfies $f(T(z))T'(z) = g(z)$. In other words ω is a global section of the cotangent bundle of X.

Definition 6.2.2. A *translation surface* is:

1. a pairing (X, ω) where X is a Riemann surface and ω is a holomorphic 1-form. Two translation surfaces (X, ω) and (Y, η) are equivalent if there exists a holomorphic diffeomorphism $\phi : X \to Y$ so that $\phi^* \eta = \omega$.

2. collections of polygons up to an equivalence relation: $\mathcal{P}/\sim$. In particular $\mathcal{P}$ is a finite collection of polygons $\mathcal{P}$ in the plane so that all sides come in pairs of equal length with opposite orientations on the boundary of the polygons. Identifying these sides gives a compact finite genus Riemann surface. Given such collections of polygons $\mathcal{P}$ and $\mathcal{Q}$, we say $\mathcal{P} \sim \mathcal{Q}$ if elements of $\mathcal{P}$ can be cut into pieces along straight lines (where a cut produces two new boundary components that are paired) and these pieces can be translated and re-glued (where gluing only occurs along paired edges) to $\mathcal{Q}$.

For more background on translation surfaces see [86, 115].

Remark 6.2.3. If X has genus g then any holomophic 1-form ω has $2g - 2$ zeros with multiplicity. Away from the zeroes, $\omega = dz$, and if z is a point where ω has a zero of order k, then we can write $\omega = z^k dz$.

Example 6.2.4. The square torus $\mathcal{P} = [0, 1]^2$ on the right and the torus $\mathcal{Q}$ on the left with vertices given by $(0, 0), (1, 0), (1, 1), (2, 1)$ are equivalent via the cut and paste operation shown below.
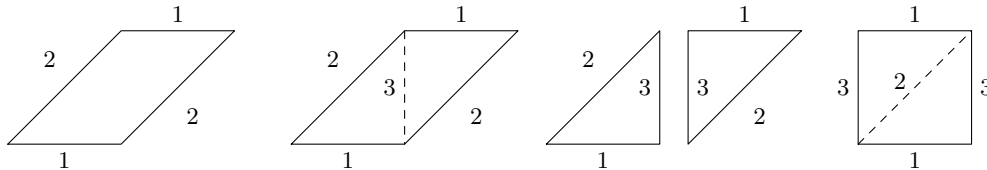
The first definition of a translation surface is very concise, but the second definition is useful for constructing examples, and we will use these as our source of examples for this paper. As mentioned in Remark 6.2.3, there are $2g - 2$ zeroes with multiplicity [115, Theorem 1.2]. If we label the zeroes by a multi-index $\alpha = (\alpha_1, \ldots, \alpha_k)$, then k is the number of distinct zeroes, each with multiplicity α_k, and $\sum_k \alpha_k = 2g - 2$.

Definition 6.2.5. The set of translation surfaces with orders of zeroes given by a multi-index α is the *stratum* $\mathcal{H}(\alpha)$. When $k = 2g - 2$ and thus for each $1 \le i \le 2g - 2$, $\alpha_i = 1$, then the stratum is called the *principal stratum*.

Example 6.2.6. Consider the L shaped polygon of Figure 6.1, which lives in the stratum $\mathcal{H}(2)$. For a general symmetric L shape fix $\lambda > 1$. Let 1 be the length of sides 4 and 1, and let $\lambda - 1$ be the length of sides 2 and 3. Figure 6.1 shows $\lambda = 2$. The sides given by the numbers $1, 2, 3, 4$ are identified by complex translations $z \mapsto z \pm \mathbf{i}\lambda$, $z \mapsto z \pm \mathbf{i}$, $z \mapsto z \pm 1$, and $z \mapsto z \pm \lambda$, respectively. Under these edge identifications, the corners are all mapped to a
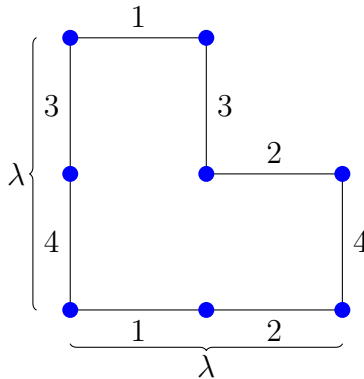
Figure 6.1: The L shape: a symmetric genus two translation surface with opposite sides identified by complex translation.

single point, which is a zero with angle $6\pi = (1+2)(2\pi)$. An angle of 6π is a zero of order 2 since it contains 2 full circles of excess angle. This can also be seen in the local charts from $\mathbb{C}$ into the Riemann surface $z \mapsto z^3$, for which the differential is $3z^2\,dz$, giving the zero of order 2. Since there are $2g - 2$ zeroes of ω with multiplicity, this implies that the genus should be 2. We can also see this via the Euler characteristic $2 - 2g = V - E + F = 1 - 4 + 1$, since there is 1 vertex under identification, 4 edges, and a single facet.

Example 6.2.7. The other primary examples we will work with are a family of curves in the principal stratum, so the $2g - 2$ zeros are all distinct zeroes of order 1, namely the *Jenkins–Strebel differentials*, which are formed by a single horizontal rectangle of length $4g-4$ and height 1 [117]. In Section 6.3, we review these objects in more detail. By considering horizontal lines connecting two zeros, there are at most $4g - 4$ total parallel lines connecting all of the zeroes as explained in Remark 6.3.5. In this example, the edge identifications are given through a permutation identifying the edges on the top of the rectangle to the bottom edges, as well as the horizontal translation identifying the vertical sides. For example in Figure 6.2, the translation surface J_2 is composed of a 1×4 rectangle where the numbers indicate the sides identified by translation. There are 4 horizontal sides on the top and bottom, and the sides are glued by taking a permutation of the top sides to glue to the bottom sides. In this particular figure, the associated permutation is $\pi_{J_2} = \begin{pmatrix} 1 & 2 & 3 & 4 \\ 2 & 1 & 4 & 3 \end{pmatrix}$. By an Euler characteristic argument, we can verify that there are 2 vertices, 5 edges, and 1 facet, resulting in a genus 2 surface. Thus $J_2 \in \mathcal{H}(1,1)$. Higher genus examples will be constructed in Section 6.3

By varying the edge lengths, we can move from J_2 through a family of curves which are all Jenkins–Strebel differentials of the same genus, similar to how λ formed a one-parameter family of curves in $\mathcal{H}(2)$. In order to preserve some of the symmetries, we will only allow two parameters to change. Given $\lambda, \mu \in (0, \infty)$, let 0 have side length λ, side 1 has side length

μ, and sides $2, 3$ and 4 each have length 1. This now gives a 2 dimensional family of curves $J_2(\lambda, \mu) \in \mathcal{H}(1, 1)$.
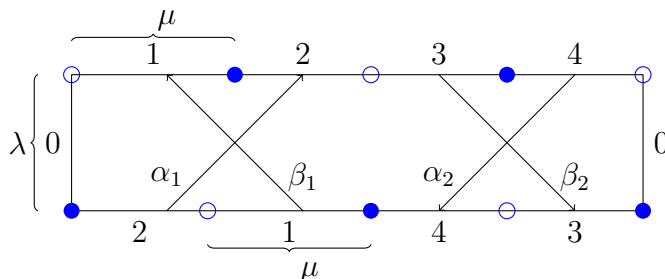
Figure 6.2: Above is $J_2(\lambda, \mu)$ associated to the permutation $\pi_{J_2} = (1, 2)(3, 4)$. The paths α_j, β_j for $j = 1, 2$ form a symplectic basis of homology.

For the Jenkins–Strebel differentials, we do not know the underlying Riemann surface. However in the case of the L, we can use symmetries of the polygon to determine a second linearly independent 1-form. This was done by [101, 95] in the case of the L using the order 4 symmetry to show that the underlying Riemann matrix is given by

$$\tau_\lambda = \frac{\mathbf{i}}{2\lambda - 1} \begin{pmatrix} 2\lambda^2 - 2\lambda + 1 & -2\lambda(\lambda - 1) \\ -2\lambda(\lambda - 1) & 2\lambda^2 - 2\lambda + 1 \end{pmatrix}. \tag{6.3}$$

Moreover, since we are in genus 2 and thus hyperelliptic, the equation of the underlying curve is given by

$$y^2 = x(x^2 - 1)(x - a)(x - 1/a) \text{ for } a \neq -1, 0, 1.$$

The values of a are computed in [101] for certain values of λ, in particular for the examples computed in this paper that when $\lambda = 2$, then $a = 7 + 4\sqrt{3}$. Other families of surfaces where the symmetries are used to compute the underlying curve can be found in [39].

We close our section with an example that illustrates reconstructing an algebraic curve from its translation surface via numerical computations relying on methods in Section 6.2.

Example 6.2.8. We take the Riemann matrix τ as $\mathbf{i} \begin{pmatrix} \frac{5}{3} & -\frac{4}{3} \\ -\frac{4}{3} & \frac{5}{3} \end{pmatrix}$ for certain λ in Equation (6.3). Section 6.2 contains more details about this example and its underlying translation surface. We use `SageMath` [54], computing with 100 bits of precision, we approximate the six branch points as follows via the six theta constants with odd characteristics:

$$-2.000000000000000000000000000 + \mathbf{i}6.411286979214040659776726185 \cdot 10^{-62},$$
$$-1.024253776455594926565578238 + \mathbf{i}4.639877849808649990904308178 \cdot 10^{-64},$$
$$-0.500000000000000000000000001 - \mathbf{i}3.073006847790767124807473878 \cdot 10^{-62},$$
$$-0.976320539876821811521789953 - \mathbf{i}3.817307044999267629996566930 \cdot 10^{-64},$$
$$1.241736035129527995762367152 + \mathbf{i}1.269499193911240271497034929 \cdot 10^{-61},$$
$$0.805324136297363697499801628 + \mathbf{i}1.157774094497279693874584809 \cdot 10^{-62}.$$

In fact, the branch points are nothing but the quotients of the six theta constants $-\theta_1^{\varepsilon,\delta}/\theta_2^{\varepsilon,\delta}$ among all the even characteristics with the notation (1.4). To verify that this curve is isomorphic to the curve exhibited in (6.3) one can compute their absolute Igusa invariants in a `SageMath` class [98] and note that the absolute Igusa invariants of both curves coincide up to a numerical round-off.

Discrete Riemann surfaces and discrete period matrices

The section aims to assist the reader in the literature on discrete Riemann surfaces. Our references are [17, 87]. We here skip recalling the vast amount of technical background on the topic and pinpoint the related results in the references instead.

Given a surface X, namely a two real-dimensional manifold, one discretizes the surface by considering it via one of its cellular decompositions, say Λ together with a discrete complex structure. Here, the discrete complex structure is introduced with the consideration of the dual cell decomposition of Λ, denoted by $\Lambda^\star$. Note that [17] encodes these objects, namely Λ and $\Lambda^\star$, by the colors black and white, respectively. Set $\Gamma := \Lambda \cup \Lambda^\star$, which is called the double of the cell decomposition Λ. This is to set a theoretical framework for *discrete complex analysis*, that is to say the discrete theory of complex analytic functions.

First and foremost, the discretization of the Cauchy-Riemann equation is formulated in terms of combinatorial elements of Λ and its dual $\Lambda^\star$, namely the sub-cells. In particular, for a complex valued function f defined on the 0-cells of Γ to satisfy the Cauchy-Riemann equation means certain compatibility between the proportions of the 0-cells of Λ and $\Lambda^\star$ and their values under f, see [17, Section 3].

In the development of this theory, one fundamental concept is the discrete theory of Riemann surfaces. In fact, many results in the classical theory have discrete counterparts, which includes period matrices, Abelian integrals, and so forth. Bobenko and Günther use a medial graph approach to the discrete theory of Riemann surfaces on quad-decompositions, which was introduced as a perspective to discrete complex analysis in [16]. Mercat makes use of the tool of deRham cohomology to introduce standard notions in discrete exterior calculus [87]. A *discrete one-form* ω is defined as a complex function on the one-cells of Γ. The evaluation of ω at an oriented edge is nothing but the discrete integral $\int_e \omega$, via which one defines the *discrete integral* over a directed path by means of the oriented edges forming the path.

Suppose that X is a compact Riemann surface of genus g. Its discretization is given a cell decomposition of X. We follow [17] for the notion of discrete Riemann matrix, where the authors note that their object coincides with [87]. Fix a symplectic basis $\alpha_1, \ldots, \alpha_g, \beta_1, \ldots, \beta_g$ of $\mathrm{H}_1(X, \mathbb{Z})$. One defines the A and B periods of a given discrete differential by taking the integrals over the α_j and β_j, respectively. These cycles induce closed paths on Λ and $\Lambda^\star$, which are distinguished with the colors, white and black, labeling the cell decompositions. This yields the notions of black or white A or B periods.

For a discrete differential, the $4g$ discrete black and white *periods* are defined as the integrals that are over the induced black and white closed paths. For technical details

of the cycles and the periods, see [17, Section 5.1]. It turns out that there is a unique holomorphic differential such that the black and white A and B periods match a given set of $4g$ complex values [17, Theorem 6.3]. It follows that the *canonical basis* of holomorphic one-forms $\omega_1, \ldots, \omega_g$ [17, §6.3 Definition] is well defined where the black and white A periods are chosen to be equal with integration against the curves $\alpha_1, \ldots, \alpha_g$ is the identity matrix. The $g \times g$ *discrete period matrix* entries are the B periods with respect to the canonical basis. This is somewhat mimicking the normalization of the $g \times 2g$ period matrix in the classical setting. Abusing the notation, we will call the discrete period matrix as *discrete Riemann matrix* by referring its second $g \times g$ part.

There is another notion of a period matrix called the *complete discrete period matrix*, which is a $2g \times 2g$ block matrix made of four $g \times g$ matrices. These $g \times g$ matrices are formed by not imposing that the white and black A periods are equal, and instead considering $g \times g$ matrices formed according to the relationship of black and white periods. Note that the discrete period matrix can be computed from the complete one [17, Remark at Page 917].

Computing the (complete) discrete period matrix amounts to computing the discrete periods. The periods are the values of the discrete differentials at the edges of the closed paths arising from the fixed symplectic basis. In order to compute these values, one may use the condition of being holomorphic for the discrete differentials by the discrete Cauchy-Riemann relations. This gives a linear system of equations, which we call *holomorphicity equations*.

In our algorithm we also construct the so-called *periodicity equations*, which are given by the presentation of our underlying surface as a translation surface. Translation surfaces are an example of a *polyhedral surface*, which consists of planar polygons that are glued together along edges. It turns out that this is yet another characterization of a compact Riemann surface [20]. This perspective might be more convenient for explicit computations involving discrete surfaces, in particular while considering the discrete complex structure on the decomposition of the surface. For the case of computing the discrete period matrices, the edges being glued adds linear equations to the holomoprhicity equations, namely the periodicity equations.

As the decomposition into cells gets finer, one expects that the discrete period matrix converges to a Riemann matrix of the underlying Riemann surface. At this point the convergence of discrete Riemann surfaces to their continuous counterparts in full generality remains open. When one decomposes the surface into a Delaunay triangulation, convergence of the period matrices is proved.

Theorem 6.2.9 (Theorem 2.5, [15])**.** *For a sequence of triangulations of a compact Riemann surface X with the maximal edge length tending to zero and with face angles bounded from zero, the discrete period matrices converge to a Riemann matrix of X.*

The techniques of [15] led to the suggestion that one builds the discrete complex structure via quad-decompositions with orthogonal diagonals. The study [17] put the suggestion in place and examined related fundamental notions of such discrete Riemann surfaces. Another

convergence result of [14, Theorem 3] considers compact Riemann surfaces in terms of their branched covers of the Riemann spheres. Our experiments, which employ compact Riemann surfaces given by quadrangulations, give evidence for a potential result on convergence of the period matrices of [17].

The convergence rate is given by looking at particular triangulations as the longest edge length l goes to zero. For translation surfaces, the convergence rate [15, Theorem 2.5], is proportional to l when the genus $g = 1$. When $g \geq 2$, the rate is $l|\log(l)|$ when the $2g - 2$ zeroes are all distinct, and at worst $l^{\frac{2}{2g-1}}$ which corresponds to the case when there is a single zero of order $2g - 2$. In [14, Theorem 2.4], when working with ramified coverings of the sphere and carefully choosing an optimal triangulation, the convergence rate is always proportional to l. We consider square quadrangulations instead of triangulations for two primary reasons. First, not every surface can be split into quadrilaterals, but when this is possible, the computational ease of parameterizing the quadrangulation, subdivision of the quadrilaterals, and elementary linear algebra needed to compute the matrices makes it more effective. Moreover, after discussions with Felix Günther, we expect similar convergence rates to [15]. The key idea is that by dividing the squares along the diagonal, the resulting triangulation is sufficiently regular to fit into the framework of [15].

6.3   Algorithms

In the following section, we will present algorithms for constructing discrete Riemann matrices associated to two families of translation surfaces: The L shape in Section 6.3 and the Jenkins–Strebel representatives in Section 6.3. In the first case, we aim to construct the associated discrete Riemann matrices when approximating the shape by squares and observe the convergence to the known underlying algebraic curve. In the second case we observe convergence and show experiments indicating what we expect from the underlying curve.

Definition 6.3.1. Given a translation surface P, the *0th level discrete approximation* P_0 is the discrete Riemann surface defined by the smallest bipartite square quadrangulation of the surface which respects the identifications of the vertices in P. The nth level discrete approximation P_n for $n \in \mathbb{N}_{\geq 1}$ is defined to be the discrete Riemann surface defined by the bipartite square quadrangulation which subdivides each square of the $n = 0$ level into 3^{2n} squares.

We give an algorithm for obtaining the discrete Riemann matrix associated to P_n.

General polygon algorithm

Input: A polygon P in $\mathbb{R}^2$ with fixed side lengths, and side identifications which gives a translation surface, and a level $n \in \mathbb{N}_{\geq 0}$.
Output: The discrete Riemann matrix associated to P_n.

1. **Constructing an initial bipartite quadrangulation.** We first divide the given translation surface into a bipartite quadrangulation, note that the bipartite quadrangulation must also respect the identifications of the vertices under the identifications in the given translation surface.

2. **Quadrangulations for further levels of approximation.** In order to preserve the bi-coloring, we must divide each square into an odd number of squares, for which we will choose 3. So each square of side length s will be divided into 3^{2n} squares, and so the nth level approximation will consist of squares of size $s/3^n$.

3. **Labelling vertices.** Placing the bottom left corner of the given polygon at the origin, we label the the vertices by their location in the plane, where we will move freely between complex notation and vector notation:

$$x_{i,j} = \left(i\frac{s}{3^n}, j\frac{s}{3^n} \right) = i\frac{s}{3^n} + j\frac{s}{3^n}\mathbf{i}.$$

The vertex $x_{i,j}$ corresponds to the bottom left corner of the square which is $(i+1)$ from the left and $(j+1)$ from the bottom.

4. **Holomorphicity equations.** For each square with coordinate $x_{i,j}$ in the bottom left, we have the holomorphicity relation

$$\mathbf{i}(x_{i+1,j+1} - x_{i,j}) = x_{i,j+1} - x_{i+1,j}. \tag{6.4}$$

See Figure 6.3 for a visual description of these relations.
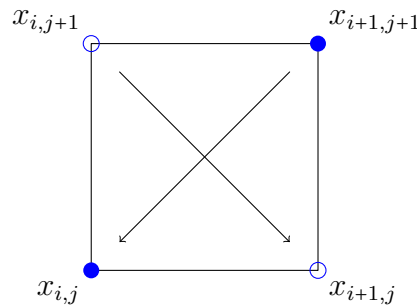
Figure 6.3: Representation of the holomorphicity equations at the ij square.

By [17, Proposition 2.1] and the discrete Cauchy Riemann equations, a discrete Riemann surface tiled by squares with given orientation in Figure 6.3 should indeed satisfy (6.4). When $x_{i,j}$ is instead a white vertex, [17] gives

$$\mathbf{i} = \frac{x_{i+1,j+1} - x_{i,j}}{x_{i+1,j} - x_{i,j+1}} = \frac{x_{i+1,j+1} - x_{i,j}}{-(x_{i,j+1} - x_{i+1,j})}$$

which is equivalent to (1.3).

5. **Periodicity.** We choose a symplectic basis of homology $\alpha_1, \ldots, \alpha_g, \beta_1, \ldots, \beta_g$, and the associated $4g$ discrete periods are given by $A_k^w, A_k^b, B_k^w, B_k^b$ for $k = 1, \ldots, g$, and the superscripts w, b representing the white and black periods, respectively. The periodicity relationships are constructed in order to make edge identifications for the given polygon in the plane. So for each edge identification, the identified vertices have difference given by the correct associated vector, and the coloring is found through checking the parity of i and j.

6. **Final Normalizations.** To make a well-determined system, we make the following normalizations:

   - Fix the first values of the holomorphic function, one one black and one one white vertex: $x_{0,0} = x_{1,0} = 0$. This comes from the fact that the associated holomorphic function is only defined up to a constant, so we normalize the constant to be zero at the origin.

   - In order to construct the canonical basis of discrete holomorphic differentials, we set the black and white values to be the same, and for each $k = 1, \ldots, g$, the differential ω_k is determined by the following equations for $j = 1, \ldots, g$:

   $$A_j^w = A_j^b \quad \text{and} \quad A_j^w = \begin{cases} 1 & j = k \\ 0 & \text{else.} \end{cases}$$

7. **Solving a system of equations for the discrete approximation.** Now for each $k = 1, \ldots, g$, the kth row of the discrete period matrix is given by

   $$\frac{1}{2}(B_1^w + B_1^b, \ldots, B_g^w + B_g^b).$$

Riemann matrix of the L

In this section we find numerical approximations to a family of translation surfaces for which we already know the Riemann matrix. Namely, consider a symmetric L shape with side length $\lambda \in (1, \infty)$ with opposite sides identified as in Figure 6.1. We aim to construct the associated discrete Riemann matrices when approximating the shape by squares, and observe the convergence towards τ_λ in Equation (6.3), which is guaranteed by [17].

As mentioned in Section 6.2, to construct the discrete Riemann matrix, we must solve a system of linear equations given by holomorphicity relations between vertices of squares in the polygonal subdivision, and by periodicity relations obtained from identifications of points on the boundary of the shape. We now describe an algorithm which constructs for us this system of equations. See [17] for more details on this construction. We used `Matlab` for the implementation of the algorithm.

Algorithm for symmetric L

Input: Let $\lambda = p/q$ be rational and reduced so that $\gcd(p, q) = 1$. Let $n \in \mathbb{N} \cup \{0\}$ be the level of approximation.
Output: Discrete Riemann matrix of the nth level approximation for symmetric L with side length λ.

1. **Constructing an initial bipartite quadrangulation.** Refer to Figure 6.4 for an example of the level 0 approximation. To divide the entire shape into squares, the sizes of the squares must divide $1/q$. In order to bi-color the square tiling and maintain the vertex identifications, there must be an even number of squares on each side length. Hence we define the step size to be $s_\lambda = \mathrm{lcm}(q, 2)$. The shape L can be bi-colored by being divided into squares of size $1/s_\lambda$.

2. **Quadrangulations for further levels of approximation.** Each square of side length $1/s_\lambda$ will be divided into 3^{2n} squares, and so the nth level approximation will consist of squares of size $1/(3^n s_\lambda)$.

3. **Labelling vertices.** We label the vertices with the following bounds to match the L shape:

$$x_{i,j} = \left(\frac{i}{3^n s_\lambda}, \frac{j}{3^n s_\lambda} \right) \quad \text{for} \quad \begin{cases} 0 \le i \le 3^n s_\lambda & 0 \le j \le \lambda 3^n s_\lambda, \\ 3^n s_\lambda + 1 \le i \le \lambda 3^n s_\lambda & 0 \le j \le 3^n s_\lambda. \end{cases}$$

4. **Holomorphicity equations.** For each bottom left of a square, we have a new holomorphicity equation. So in this case, we have a total of $3^{2n}(s_\lambda)^2(2\lambda - 1)$ equations with indices given by

$$\begin{cases} 0 \le i \le 3^n s_\lambda - 1 & 0 \le j \le \lambda 3^n s_\lambda - 1, \\ 3^n s_\lambda \le i \le \lambda 3^n s_\lambda - 1 & 0 \le j \le 3^n s_\lambda - 1. \end{cases}$$

5. **Periodicity equations.** We first choose a symplectic basis of the underlying Riemann surface, as shown in Figure 6.4. To justify our choice, under the edge identifications, we select the closed loops α_1 and β_1 as the first two, and normalize the symplectic basis so that we travel from α_1 counterclockwise to β_1 for a positive intersection number. The choice of α_2 comes naturally by trying to find another curve parallel to α_1 which does not intersect β_1. The final step involves finding β_2. To do this, recall α_2 is also identified by travelling from $x_{2,0}$ to $x_{8,0}$. Now going counterclockwise from α_2, we travel around the vertex $x_{2,0}$, which is identified with $x_{2,8}$, so β_2 must travel from $x_{2,8}$ to $x_{2,2}$ in order to have the correct intersection number with α_2 and avoid intersecting β_1 or α_1.
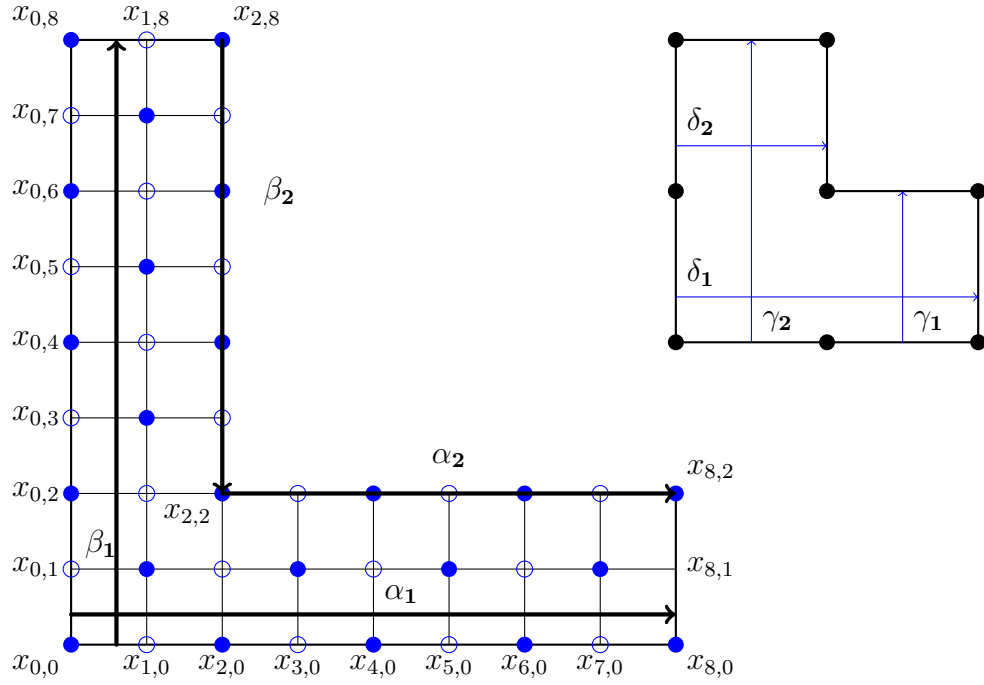
Figure 6.4: Some of the labels in the level 0 approximation of a symmetric L with $\lambda = 4$. On the right, we show a basis of homology $(\gamma_1, \gamma_2, \delta_1, \delta_2)$, which gives a symplectic basis of homology $(\gamma_1, \gamma_2 - \gamma_1, \delta_1, \delta_2)$. On the left is the basis of homology that we used in our algorithm (see Remark 6.3.2).

We now need to construct the period equations, so for example to travel from $x_{0,0}$ to $x_{8,0}$, we travel along the α_1 curve on black periods

$$A_1^b = \int_{\alpha_1} \omega_k = x_{8,0} - x_{0,0}.$$

For all the A periods we have the following equations where the parity p is determined by $p = b$ if $i + j \equiv 0 \pmod 2$ and $p = w$ otherwise:

$$\begin{cases} 0 \leq j \leq 3^n s_\lambda & x_{\lambda 3^n s_\lambda, j} - x_{0,j} = A_1^p \\ 3^n s_\lambda \leq j \leq \lambda 3^n s_\lambda & x_{3^n s_\lambda, j} - x_{0,j} = A_1^p - A_2^p. \end{cases}$$

We compute similar equations for the B periods,

$$\begin{cases} 0 \leq i \leq 3^n s_\lambda & x_{i, \lambda 3^n s_\lambda} - x_{i,0} = B_1^p \\ 3^n s_\lambda \leq i \leq \lambda 3^n s_\lambda & x_{i, 3^n s_\lambda} - x_{i,0} = B_1^p + B_2^p. \end{cases}$$

In total we have $2(\lambda 3^n s_\lambda + 1)$ equations.

6. **Final Normalizations.** In the final two normalizations we have the following number of equations:

   - 2 equations for normalization of holomorphic function.
   - For each $k = 1, 2$, there are 4 equations normalizing to the canonical basis.

7. **Solving a system of equations for the discrete approximation.** For the kth row of the period matrix with $k = 1, 2$, we obtain the equations by solving the system with:

   - Total of $9 + 3^{2n}(s_\lambda)^2(2\lambda - 1) + 2\lambda 3^n s_\lambda$ variables. With $(3^n s_\lambda + 1)(\lambda 3^n s_\lambda + 1) + (\lambda 3^n s_\lambda - 3^n s_\lambda)(3^n s_\lambda + 1)$ variables $x_{i,j}$, and 8 variables coming from B_j^p with $j = 1, 2$ and parity given by b and w.
   - Total of $10 + 3^{2n}(s_\lambda)^2(2\lambda - 1) + 2\lambda 3^n s_\lambda$ equations. With $3^{2n}(s_\lambda)^2(2\lambda - 1)$ holomorphicity equations, $2(\lambda 3^n s_\lambda + 2)$ periodicity equations, and 6 normalizing equations.

   Thus we have a system of linear equations overdetermined by 1 equation, and these are not conflicting with a unique solution, as guaranteed by [17, Theorem 6.8] since they are simply relations describing the unique holomorphic differential with the given initial conditions.

Remark 6.3.2. In our implementation, we choose the homology basis that is exhibited in Figure 6.4, namely $\alpha_1, \alpha_2, \beta_1, \beta_2$. This basis appears to be in relative homology, but this just reflects the representation of the L as a translation surface which includes a holomorphic one-form. Alternatively, in the same figure, we point out a different symplectic basis for the object given by $\delta_1, \delta_2, \gamma_1, \gamma_2 - \gamma_1$. The algorithm can be designed using the new basis by replacing the cases of the periodicity conditions as follows:

$$x_{3^n s_\lambda, j} - x_{0,j} = A_2^p,$$
$$x_{i,\lambda 3^n s_\lambda} - x_{i,0} = B_2^p + B_1^p,$$
$$x_{i,3^n s_\lambda} - x_{i,0} = B_1^p.$$

The matrix which results from $\delta_1, \delta_2, \gamma_1, \gamma_2 - \gamma_1$ can be obtained from the matrix resulting from $\alpha_1, \alpha_2, \beta_1, \beta_2$ by the transformation

$$\begin{bmatrix} x & y \\ y & z \end{bmatrix} \mapsto \begin{bmatrix} x + 2y + z & -y - z \\ -y - z & z \end{bmatrix}.$$

For each of the two the symplectic bases, we approximated the corresponding Riemann matrices and their curves for several examples. We compared the results via their invariants, which coincide up to 15 digits. Though the same curve is represented under this change of basis, we note that the experiments arising from $\alpha_1, \alpha_2, \beta_1, \beta_2$ coincide with the results following the algebraic computations of [101], whereas the computations from $\delta_1, \delta_2, \gamma_1, \gamma_2 - \gamma_1$ gives a matrix which is different from the one given by [101].

Example for $\lambda = 2$

Fix $\lambda = 2$, in Table 6.1 we demonstrate the convergence to the Riemann matrix for levels 0 through 7 as defined in Definition 6.3.1. Indeed, note that the accuracy of the matrix entries increases by about 1 digit with each additional level, resulting in accuracy up to 10^{-5} in level 7. The computation was unable to finish on the 8th level. Though the linear equations are very sparse (on the order of 4-5 nonzero coefficients each), due to the size of the system we were not able to push beyond level 8 for the computation. However, we believe there are ways to increase the efficiency of the computation, which may be worth attempting in future work.

An irrational λ

In this case, we first approximate the L surface up to a fixed tolerance via continued fractions. As we decrease the tolerance, the denominator of the continued fraction approximation grows, creating finer and finer quadrangulations as the size of the squares is dependent on the size of the denominator (See Table 6.2). We selected the value $\lambda = \frac{1+\sqrt{3}}{2}$ since the underlying algebraic curve is defined over the field of rational numbers, given in [101], by $y^2 = x(x^2 - 1)(x - 2)(x - \frac{1}{2})$.

Finally to demonstrate the further convergence, we fix a continued fraction approximation of $\frac{10864}{7953}$ (See Table 6.3). Since the 0th level already includes squares of size $\frac{1}{2(7953)}$, we were only able to run subdivisions of level 1 and level 2. For comparison we then include the numerical approximations of the Riemann matrices for the continued fraction as well as the original value of λ. In this case, similarly to the $\lambda = 2$ case, we find that the entries of the matrix are accurate to 10^{-6}, both for the matrix for the continued fraction and for the original irrational λ. The entries of the matrices for the continued fraction and for λ coincide up to 8 digits.

The Jenkins–Strebel representatives

Given an integer $g \geq 2$, the goal of this subsection is to use discrete approximations to estimate the curve underlying a Riemann surface of genus g for which we do not a priori know the underlying algebraic curve. Namely we will define J_g to be a square tiled Jenkins–Strebel (JS) representative of the principal stratum. We construct discrete approximations in low genera. Our construction of JS representatives for a holomorphic one-form with one cylinder follows the work of [117].

Constructing a Jenkins–Strebel representative

In this section we define the surface J_g for $g \geq 2$, with some background on how to obtain a Jenkins–Strebel representative of the principal stratum for each genus g and select basis curves for homology. Example 6.2.7 illustrates the surface when $g = 2$. In general we will construct a Jenkins–Strebel representative by taking a $1 \times (4g - 4)$ rectangle, identifying sides

by translation, where the top and bottom are identified via a permutation π_{J_g} of the $4g - 4$ horizontal edges and the single vertical side is identified. By varying the side lengths, we can move from J_g through a family of curves which are all Jenkins–Strebel differentials of the same genus. For the sake of tractable computations, we allow ourselves to vary only two parameters that label the vertical edge and the far left horizontal edge in our experiments. We insert the parameters in the parenthesis as $J_g(\lambda, \mu)$ if needed.

We say that π_{J_g} is the *permutation associated to J_g*.

Theorem 6.3.3 ([117] Proposition 2). *Given a genus $g \geq 2$, the Jenkins–Strebel representative associated to the principal stratum composed of unit squares is given by the permutation on $4g - 4$ elements where for $k = 1, \ldots, 4g - 4$,*

$$\pi_{J_g}(k) = \begin{cases} k + 1, & k \text{ is odd}, \\ k - 1, & k \equiv 2 \pmod 4, \\ k + 3 \pmod{4g - 4}, & k \equiv 0 \pmod 4. \end{cases}$$

Remark 6.3.4. We apply a shear by $\begin{bmatrix} 1 & -1/2 \\ 0 & 1 \end{bmatrix}$, and then perform a cut and paste operation moving the left square over to the right, and then relabel to obtain Theorem 6.3.3 from Proposition 2 of [117]

Remark 6.3.5. Notice that there are always $4g - 4$ elements in the permutation, which comes from the fact that at each singularity, there is an angle of 4π, so there are at most 4 parallel saddle connections. This gives a total of $4(2g - 2)$ possible saddle connections, but since each saddle connection has an incoming and outgoing direction, we have double counted. Thus there are $2(2g - 2) = 4g - 4$ possible parallel saddle connections.

Each JS differential is associated to a *ribbon graph*. Indeed we take the graph with vertices given by the $2g - 2$ singularities, and edges labelled by the $4g - 4$ parallel saddle connections. We then preserve the topological information by contracting the surface with boundary that follows the graph (c.f. Figure 6.5). The fact that we can do this on J_g comes from the fact that JS surfaces have closed horizontal leaves.

For any g, we obtain the ribbon graph by gluing $g - 1$ *pretzels* together. We define a pretzel to be a ribbon graph on two vertices, with 3 edges connecting the two vertices, and an open edge on each vertex. These pretzels are formed by the fact that 4π angle allows for a graph of degree 4 at each vertex. Then there are 3 parallel saddle connections between any two vertices, and the 4th at each pair of saddle connections is used to connect to other pretzels.

The ribbon graph has a top and bottom surrounding each edge. Following around the top edge starting at the top left in Figure 6.5, we start at $4g - 4$, then 1, then travel to 2, 3, 4, and continue in order. Now start at the bottom edge of $4g - 4$ on the left. The permutation is now $3, 2, 1, 4, 7, 6, 5$, and so on. For a concrete example, one can perform this exercise with $g = 3$ and edge numbers 1 through 8 to obtain the permutation as given in Figure 6.6a.
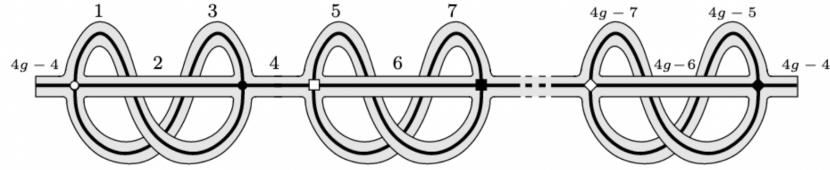
Figure 6.5: The ribbon graph associated to J_g. The first pretzel is given by the 1,2, and 3 edges, and then the two half edges $4g - 4$ and 4. There are a total of $g - 1$ pretzels.

The next step we must take is to fix a basis of homology to help in determining the periodicity equations. We first consider the topological picture, as in Figure 6.6b. We fix standard symplectic homology basis curves α_j, β_j for $j = 1, \ldots, g$ where the pairs α_i, β_i are oriented to have intersection number 1, and all other pairs have intersection zero. For higher genus, the picture is best seen when α_g, β_g are in the center, and all other attached tori are equally spread out and only attached to the α_g, β_g torus. The idea is each pretzel in the ribbon graph adds one torus and two zeros. Notice that the symplectic basis is less obvious in the polygonal picture. In Figure 6.6a, by removing the second reference to α_3 used for periodicity identifications, the set of curves are consistent in the intersection numbers to be a symplectic basis, and one can see the curves are not homologous by cutting the surface into g tori with boundary components formed by cutting vertically along the zeroes. The curves α_j, β_j then form the standard two symplectic basis vectors of homology of the torus excluding the basis curves relative to the boundary.

Next mark the $2g-2$ zeroes of the one-form, between the α_g, β_g torus and the corresponding numbers of that pretzel. For example in Figure 6.6b, the filled and unfilled circles belong to the first pretzel, and the filled and unfilled squares belong to the second pretzel. Next label each edge coming out of a vertex in the correct order. To determine the correct order, for example in Figure 6.6a, consider the unfilled circle. Starting at the 0 side, we travel in a circle with the unfilled circle vertex to our left. From side 0, we go to side 1, keep traveling with the circle on our left, cross side 2, then 3, and 8 before returning to side zero. This order matches the order seen in Figure 6.6b.

Now to connect edges, we have 3 cases. First we select the 1, 2 (mod 4) edges in the jth pretzel to be the edges crossing β_j, α_j, respectively. Next the 3 (mod 4) edges cross the β_g. Third, the 0 (mod 4) sides are either 0 and cross no homology curves, or cross α_g. In this manner, every homology curve is crossed by at least 1 edge. We then mark the respective homology curves and their directions in the polygonal picture by keeping track of directions. For example in 6.6b, as we travel along side 2 from open circle to filled circle α_1 crosses from left to right. Similarly α_3 crosses from left to right as we travel along side 8 from filled square to open circle, but this is exactly the opposite direction as side 2 in the polygonal picture Figure 6.6a, giving the marked directions of α_1 and α_3.

Remark 6.3.6. Notice that the choice of the principal stratum is for simplicity. To construct other orders of zeroes, [117] combines zeroes in the principal stratum. When the zeroes are
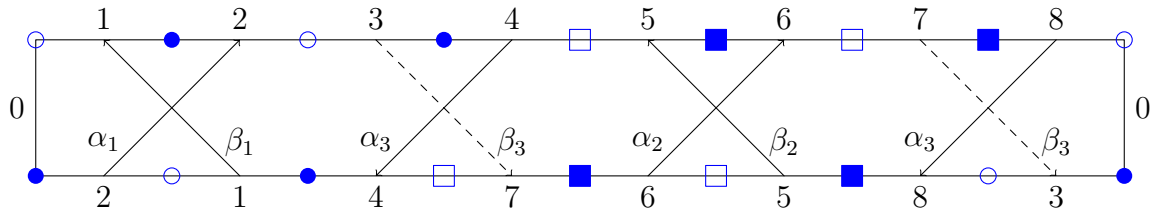
(a) Here is the polygonal representation of the JS surface for $g = 3$. The associated permutation is $\pi_{J_3} = \begin{pmatrix} 1 & 2 & 3 & 4 & 5 & 6 & 7 & 8 \\ 2 & 1 & 4 & 7 & 6 & 5 & 8 & 3 \end{pmatrix}$. The sides which are not 3 (mod 4) are labelled by the homology basis curve that is used for the periodicity equations in Algorithm 6.3. The curve β_3 is represented by a dashed line since more care must be taken to construct the periodicity equations. (See Algorithm 6.3.)
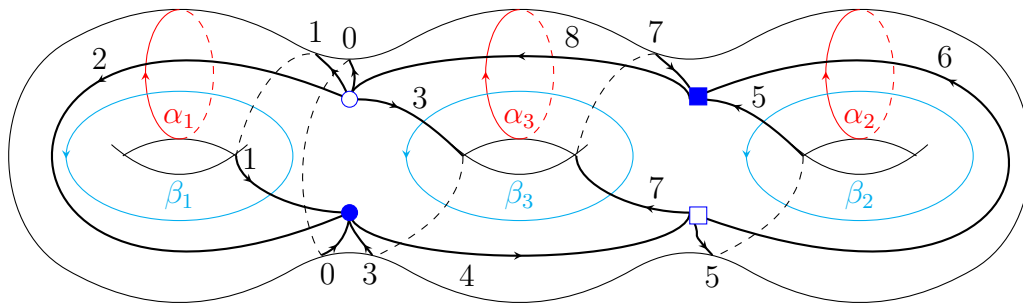
(b) Here is the topological representation of the polygonal surface for $g = 3$ keeping track of edge identifications and zeroes of the 1-form, and the intersections of the edges with the standard homology basis.

Figure 6.6: The polygonal representation and topological representation giving information of how homology vectors behave under identified sides of the JS surface for genus 3.

combined, the same method of carefully following edge identifications in the polygon and how they connect to the homology basis works as well.

In addition to computations for the two examples given in Figure 6.2 and Figure 6.6, we will also give examples in genus 4 and 5 (Figure 6.7), where the choice of homology basis follows the same strategy outlined above.
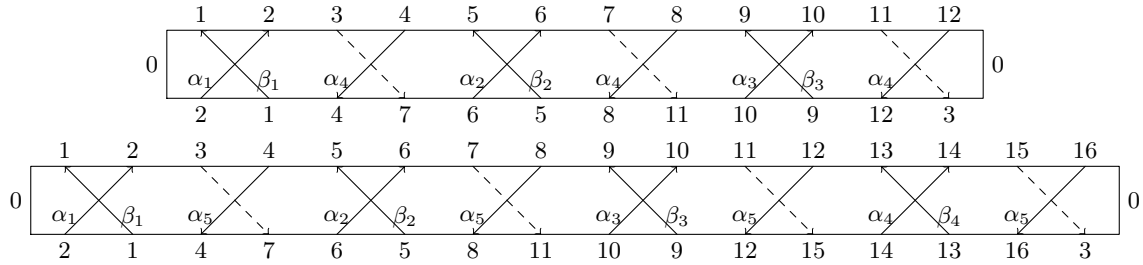
Figure 6.7: Surface representations of J_4 (above) and J_5 (below) with marked homology basis curves, the basis curve β_g is represented by the dashed line.

Algorithm for discrete approximation of JS surfaces

Let g be the genus of the JS representative. Let $n \in \mathbb{N} \cup \{0\}$ be the level of approximation. For simplicity of the description we here fix all side lengths to be 1, but implementation with varying side lengths can be found on our `MathRepo` page (6.1). We will note here, however, that the algorithm requires side lengths to be rational numbers, with odd numerator and denominator, due to the bicolored structure.

1. **Constructing an initial bipartite quadrangulation.** Since all the side lengths are 1, the shape is already divided into squares. In order to bi-color the square tiling and maintain the vertex identifications, there must be an even number of squares on each side length, which is always true since $4g - 4$ is always even. Hence we define the step size to be 1.

2. **Quadrangulations for further levels of approximation.** Each square of side length 1 will be divided into 3^{2n} squares, and so the nth level approximation will consist of squares of size $1/3^n$.

3. **Labelling vertices.** We label the vertices with the following bounds:
$$x_{i,j} = \left(\frac{i}{3^n}, \frac{j}{3^n} \right) \quad \text{for } 0 \leq i \leq 3^n(4g-4) \text{ and } 0 \leq j \leq 3^n.$$

4. **Holomorphicity equations.** For each bottom left of a square, we have a new holomorphicity equation. So in this case, we have a total of $3^{2n}(4g-4)$ equations with indices given by $0 \leq i \leq 3^n(4g-4) - 1$ and $0 \leq j \leq 3^n - 1$.

5. **Periodicity equations.** The basis of homology was chosen so that each edge aside from the 0 edge and the edges which are congruent to 3 (mod 4) is identifed via a single basis of homology vector. For all of the following periods, the parity p is determined by $p = b$ if $i + j \equiv 0 \pmod 2$ and $p = w$ otherwise, so we only need to determine the periodicity relationships.

- **A_{k+1} periods for $k = 0, \ldots, g - 2$.** We have $(g-1)(3^n + 1)$ equations where for each k there are $3^n + 1$ equations, and the basis vectors occur at $2 \pmod 4$ to give

$$A_{k+1}^p = x_{i+3^n, 3^n} - x_{i,0} \quad \text{for} \quad 4k3^n \leq i \leq 3^n(4k+1).$$

- **A_g periods.** We have $(g-1)(3^n + 1)$ equations where there are $3^n + 1$ equations occuring at each of the $0 \pmod 4$ sides given by

$$A_g^p = x_{i,0} - x_{i+3^n, 3^n} \quad \text{for} \quad 3^n(4k+2) \leq i \leq 3^n(4k+3).$$

- **B_k periods for $k = 1, \ldots, g - 1$.** We use the same indexing as the A_{k+1} periods to have $(g-1)(3^n + 1)$ equations given by

$$B_{k+1}^p = x_{i,3^n} - x_{i+3^n, 0} \quad \text{for} \quad 4k3^n \leq i \leq 3^n(4k+1).$$

- **B_g periods and $0 \pmod 4$ side identifications.** The homology curve is crossed by all of the sides $3 \pmod 4$, and the side 0 crosses no homology curve. To find the correct identifications, we construct relations from highest numbers to lowest numbers. The idea is for each unidentified edge, we follow all paths around vertices which identify the two possible sides, except for the side 3 which we choose to be the curve we follow around β_3. We go through this carefully following the identification in the example of $g = 3$ following the image in Figure 6.6b. We refer to the top and bottom of every edge by looking at the top and bottom in the polygonal representation of Figure 6.6a.

  - **Sides $3 \pmod 4$ bigger than 3.** On side 7, we describe the path travelling from 7_{bottom} to 7_{top}, by travelling around the filled square to the right. To do this we cross side 6 from bottom to top, which is identified via α_2. Next we cross side 5 top to bottom giving $-\beta_2$, and finally side 8 bottom to top giving a $-\alpha_3$. So all together,

$$7_{top} - 7_{bottom} = \alpha_2 - \beta_2 - \alpha_3.$$

    Following along a circle with the unfilled square to the left verifies the choice that side 4 is identified by α_3. In general working with $3 \pmod 4$ sides not equal to 3 we have $(g-2)(3^n + 1)$ equations of the form

$$x_{(i+3\cdot 3^n), 3^n} - x_{i,0} = A_{k+2} - B_{k+2} - A_g \quad \text{for} \quad \begin{cases} 0 \leq k \leq g - 3, \\ (4k+3)3^n \leq i \leq 3^n(4k+4). \end{cases}$$

  - **Side 3.** On the 3 side, travelling around the zeroes as in the 7 sides will be used to determine the identifications of the 0 sides. We choose the 3 side to encode the crossing information of β_g since it is included in all genus $g \geq 2$. When $g = 2$, the curve β_2 only is crossed by side 3. However for $g = 3$, we may

follow the image in Figure 6.6b. Starting at the bottom of 3, we travel in the direction of $-\beta_3$, crossing side 7 from top to bottom before we complete β_3 to return to the bottom of 3. Thus

$$3_{top} - 3_{bottom} = -\beta_3 + 7_{bottom} - 7_{top} = -\beta_3 + \alpha_3 - \alpha_2 + \beta_2.$$

For higher genus, there are $g - 2$ total 3 (mod 4) sides each contributing α_3 and some $\beta_k - \alpha_k$.
Setting

$$\iota = i + 3 \cdot 3^n \quad (\mathrm{mod}\ 3^n(4g-4))$$

we have $3^n + 1$ equations for identifying the top and bottom of side 3 given by

$$x_{\iota,3^n} - x_{i,0} = -B_g + (g-2)A_g + \sum_{j=2}^{g-1}(B_j - A_j) \quad \text{for } (4g-5)3^n \leq i \leq 3^n(4g-4).$$

– **Side 0.** We conclude by identifying the zero sides. We will travel around with the open circle on the left, and leave it to the reader to verify the same result holds for travelling around the closed circle to the right. We start at the left side of zero, crossing sides 1, 2, 3, 8. This gives

$$0_{right} - 0_{left} = -\beta_1 + \alpha_1 + 3_{bottom} - 3_{top} - \alpha_3 = \beta_3 - 2\alpha_3 + \alpha_2 - \beta_2 + \alpha_1 - \beta_1.$$

In general, we always follow the same crossing pattern, of $-\beta_1 + \alpha_1 - \alpha_3$, and then this must be combined with the information about the 3 side. This gives $3^n + 1$ equations of the form

$$x_{3^n(4g-4),j} - x_{0,j} = B_g - (g-1)A_g + \sum_{j=1}^{g-1}(B_j - A_j) \quad \text{for } 0 \leq j \leq 3^n.$$

6. **Final normalizations.** In the final two normalizations we have the following number of equations:

   • 2 equations for normalization of holomorphic function.

   • For each $k = 1, \ldots, g$, there are $2g$ equations normalizing to the canonical basis.

7. **Solving a system of equations for the discrete approximation.** For the kth row of the period matrix with $k = 1, \ldots, g$, we obtain the equations by solving the system with:

   • Total of $3^{2n}(4g-4)+3^n(4g-3)+4g+1$ variables. With $(3^n(4g-4)(3^n+1))+(3^n+1)$ variables $x_{i,j}$, and $4g$ variables coming from A_k^p, B_k^p with $k = 1, \ldots, g$ and parity given by b and w.

- Total of $3^{2n}(4g-4)+3^n(4g-3)+6g-1$ equations. With $3^{2n}(4g-4)$ holomorphicity equations, $(2g-2)(3^n+1)$ periodicity equations for the A periods, $(2g-2)(3^n+1)$ equations for the B periods and 3 (mod 4) sides, 3^n+1 equations for the 0 sides, and $2g+2$ normalizing equations.

Since $g \geq 2$, we have a system of linear equations overdetermined by $2g-2$ equations, and these are not conflicting with a unique solution, since they all describe the unique discrete holomorphic differential guaranteed to exist by [17, Theorem 6.8].

Experiments in low genus

We consider the JS respresentative for $g = 2, 3, 4, 5$ in the principal stratum. We only consider 2-parameter family $J_g(\lambda, \mu)$ as noted in the beginning of Section 6.3. When $g = 2$, such a surface has been exhibited in Example 6.2.7. Setting the side lengths to be $\lambda = \mu = 1$, we present our experiments of the discrete period matrix approximations up to level 7 in Table 6.4–6.8, which use our algorithm that has been described in Section 6.3. Our computations with the approximations in theta functions encourage us to make the following conclusions for low genus.

Genus 2. We now take the discrete Riemann matrix of level 7 from Table 6.4. As in Example 6.2.8, we compute the odd theta constants and then approximate the six branch points of the hyperelliptic curve corresponding the J_2 surface via the `SageMath` package [54]:

$$\alpha_1 := -3.55001177927944 + \mathbf{i} \cdot 9.27369555271397,$$
$$\alpha_2 := -0.0360027110167584 - \mathbf{i} \cdot 0.0940498797751955,$$
$$\alpha_3 := 0.603906137193071 + \mathbf{i} \cdot 3.24517640725254,$$
$$\alpha_4 := 0.0554252204362169 - \mathbf{i} \cdot 0.297835386410189,$$
$$\alpha_5 := 3.90800485599692 - \mathbf{i} \cdot 7.79154768793860,$$
$$\alpha_6 := 0.0514341663705383 + \mathbf{i} \cdot 0.102546382318450.$$

We observe that these values are pairwise reciprocal, more precisely $\alpha_1 \cdot \alpha_2 = \alpha_3 \cdot \alpha_4 = \alpha_5 \cdot \alpha_6 = 1$ up to a numerical round off, which can be sharpened by working with a higher precision complex field. Computing also the 10 even theta constants, we see that some of these values coincide up pairwise to numerical error. These pairs of the constants are in the following pairs of characteristics:

$$\left\{ \begin{bmatrix} 1 & 0 \\ 0 & 0 \end{bmatrix}, \begin{bmatrix} 0 & 1 \\ 0 & 0 \end{bmatrix} \right\}, \quad \left\{ \begin{bmatrix} 0 & 0 \\ 1 & 0 \end{bmatrix}, \begin{bmatrix} 0 & 0 \\ 0 & 1 \end{bmatrix} \right\}, \quad \left\{ \begin{bmatrix} 1 & 0 \\ 0 & 1 \end{bmatrix}, \begin{bmatrix} 0 & 1 \\ 1 & 0 \end{bmatrix} \right\}.$$

Concluding from similar computations as above, we observe that the reciprocity is respected for some other rational λ parameters and $\mu = 1$. On the other hand, this phenomenon does not occur if we change μ.

Therefore, our experiments suggest making the following conjecture:

Conjecture 6.3.7. The family of hyperelliptic curves corresponding to the family of the translation surfaces, $J_2(\lambda, 1)$ of genus 2, in the stratum $\mathcal{H}(1, 1)$, is given by the equation:

$$y^2 = (x - a)(x - 1/a)(x - b)(x - 1/b)(x - c)(x - 1/c) \tag{6.5}$$

for some complex parameters a, b, c.

A first remark about the conjecture is that the curve (6.5) can be transformed to the curve by a projective transformation of $\mathbb{P}^1$:

$$y^2 = x(x - 1)(x - A)(x - B)(x - B/(1 - A - B))$$

for some complex parameters A, B. The model (6.5) also manifests that this hyperelliptic curve has an extra involution, namely $(x, y) \mapsto (1/x, y)$. This suggests studying of the translation surface $J_2(\lambda, 1)$, in particular to reconstruct the underlying algebraic curve via exact computations, akin to the work of [101, 95] for the L-shape. We also remark that there are a total of 5 possible choices of side lengths when constructing J_2, and we do not expect the symmetry of Weierstrass points to hold for every choice. Indeed by restricting to only allowing λ to change, we observe Conjecture 6.5 still holds in the cases tested, whereas allowing μ to change no longer preserved the symmetries of the fixed points. Indeed the change in symmetry can already be seen on the diagonal entries as shown in Table 6.5, which by continuity, we expect similar results for irrational λ.

In [97], the author is able to construct algebraic equations for genus two curves by approximating the coefficients numerically to high precision with transcendental methods, and then deducing the algebraic numbers using their continued fraction expansions. Once one has the algebraic numbers, it is significantly easier to prove that the equations are correct. In our case, it appears that we need more digits to be able to draw conclusions from the continued fraction expansions. In particular, the methods in section 5 of [97] do not lead to any clear guesses as to what the algebraic numbers may be. An improvement to our algorithm's implementation, allowing one to compute further levels of subdivision, may lead to these methods becoming applicable.

Genus 3. We take the level 7 approximation in Table 6.6. Among the 36 even theta constants that we compute in `SageMath`, one of them gets closer to zero as the precision is increased. As the hyperelliptic curves of genus 3 are characterized with the condition of at least one vanishing even theta constant, we state Conjecture 6.3.8 for $g = 3$.

Genus 4. We first look for evidence that the discrete Riemann matrix estimates a Riemann matrix of an algebraic curve. So we evaluate the discrete Riemann matrix of level 7 from Table 6.7 in the Schottky-Igusa modular form [68] as the underlying precision increases. We observe the values approximate to zero. For references see Section 6.2. Similar to the case above, our computations in `SageMath` support that there are 10 vanishing even theta constants, which inspires us to state Conjecture 6.3.8 for $g = 4$.

Genus 5. Plugging the discrete period matrix of level 7 from Table 6.7 into the three equations [43, Proposition 1.2], we estimate each of the three values at zero. In addition,

we observe that the number of even theta constants that converge the zero is more than 10, which concludes Conjecture 6.3.8 for $g = 5$.

Conjecture 6.3.8. The surface $J_g(\lambda, 1)$ is hyperelliptic for $g = 3, 4, 5$.

One of the primary results of [117] was to give JS representatives in every connected component of every stratum, of which some of these connected components are called hyperelliptic. As stated in remark 3 of [77] we note that a hyperelliptic Riemann surface is not always contained in a hyperelliptic connected component. Thus we can expect these specific elements of the principal stratum to be hyperelliptic, but shouldn't expect that we keep a hyperelliptic involution once we allow less symmetries by allowing the $4g - 3$ side lengths to be changed.

6.4   Tables of (discrete) Riemann matrices

In the following tables, n denotes the level of approximation as given in Definition 6.3.1. The code is always run in `Matlab` with run time given in seconds.

L shape tables

n	Time	Approximation
0	0.02	$i\begin{pmatrix} 1.75 & -1.5 \\ -1.5 & 2.00 \end{pmatrix}$
1	0.05	$i\begin{pmatrix} 1.682276986822770 & -1.364553973645541 \\ -1.364553973645541 & 1.729107947291081 \end{pmatrix}$
2	0.37	$i\begin{pmatrix} 1.670169914926280 & -1.340339829852565 \\ -1.340339829852566 & 1.680679659705133 \end{pmatrix}$
3	3.92	$i\begin{pmatrix} 1.667472042082942 & -1.334944084165891 \\ -1.334944084165893 & 1.669888168331791 \end{pmatrix}$
4	28.23	$i\begin{pmatrix} 1.666852605322711 & -1.333705210645449 \\ -1.333705210645455 & 1.66741042129092 \end{pmatrix}$
5	255.10	$i\begin{pmatrix} 1.666709630962870 & -1.333419261925784 \\ -1.333419261925776 & 1.666838523851582 \end{pmatrix}$
6	2333.12	$i\begin{pmatrix} 1.666676596082551 & -1.333353192165260 \\ -1.33335319216523 & 1.666706384330567 \end{pmatrix}$
7	22786.59	$i\begin{pmatrix} 1.666668961530435 & -1.333337923061337 \\ -1.333337923061278 & 1.666675846122862 \end{pmatrix}$
∞	$i\begin{pmatrix} \frac{5}{3} & -\frac{4}{3} \\ -\frac{4}{3} & \frac{5}{3} \end{pmatrix}$	$i\begin{pmatrix} 1.66666666667 & -1.33333333333 \\ -1.33333333333 & 1.66666666667 \end{pmatrix}$

Table 6.1: Given the L shape as in Figure 6.1 for $\lambda = 2$, the table gives the successive approximations with the bottom row representing the Riemann matrix in the limit. Since we expect the real part to be zero, we only write down the imaginary parts of the matrix level. The real parts are on the order of at worst 10^{-14}.

Fraction	Tolerance	Time	0 level approximation
$\frac{15}{11}$	$1e-2$	0.33	$i\begin{pmatrix} 1.155267361944555 & -0.582252607292078 \\ -0.582252607292077 & 1.183447277345288 \end{pmatrix}$
$\frac{56}{41}$	$1e-3$	4.04	$i\begin{pmatrix} 1.15495696004714 & -0.578505984176023 \\ -0.57850598417602 & 1.159755674257178 \end{pmatrix}$
$\frac{209}{153}$	$1e-4$	56.96	$i\begin{pmatrix} 1.154756293461396 & -0.577572595239909 \\ -0.577572595239901 & 1.155583435806089 \end{pmatrix}$
$\frac{780}{571}$	$1e-5$	758.43	$i\begin{pmatrix} 1.154710996247692 & -0.577390320924590 \\ -0.577390320924568 & 1.154853829287965 \end{pmatrix}$
$\frac{780}{571}$	$1e-6$	758.43	$i\begin{pmatrix} 1.154710996247692 & -0.577390320924590 \\ -0.577390320924568 & 1.154853829287965 \end{pmatrix}$
$\frac{2911}{2131}$	$1e-7$	744.47	$i\begin{pmatrix} 1.15471099624769 & -0.577390320924590 \\ -0.577390320924568 & 1.154853829287965 \end{pmatrix}$
$\frac{10864}{7953}$	$1e-8$	774.37	$i\begin{pmatrix} 1.154710996247692 & -0.57739032092459 \\ -0.577390320924568 & 1.154853829287965 \end{pmatrix}$
$\frac{40545}{29681}$	$1e-9$	871.63	$i\begin{pmatrix} 1.154710996247692 & -0.577390320924590 \\ -0.577390320924568 & 1.154853829287965 \end{pmatrix}$
	Exact:	$\frac{i}{\sqrt{3}}\begin{pmatrix} 2 & -1 \\ -1 & 2 \end{pmatrix}$	$i\begin{pmatrix} 1.15470053838 & -0.57735026919 \\ -0.57735026919 & 1.15470053838 \end{pmatrix}$

Table 6.2: This table gives the successive approximations representing τ_λ for $\lambda = \frac{1+\sqrt{3}}{2}$. Since we expect the real part to be zero, we only keep track of the exponential parts of the real term which are on the order of 10^{-14}. We run a 0 level approximation, with the finer square tilings coming from increasing the tolerance according to the continued fraction expansion.

Level	Time	Approximation
0	774.37	$i\begin{pmatrix} 1.154710996247692 & -0.57739032092459 \\ -0.577390320924568 & 1.154853829287965 \end{pmatrix}$
1	7290.33	$i\begin{pmatrix} 1.154702501426855 & -0.577358617765855 \\ -0.577358617765802 & 1.154735511279386 \end{pmatrix}$
2	72388.83	$i\begin{pmatrix} 1.154700538230285 & -0.577351291004541 \\ -0.577351291004404 & 1.154708167385750 \end{pmatrix}$
∞	$\frac{10864}{7953}$	$i\begin{pmatrix} 1.15470053534 & -0.5773502631 \\ -0.5773502631 & 1.15470053534 \end{pmatrix}$
∞	$\frac{1+\sqrt{3}}{2}$	$i\begin{pmatrix} 1.15470053838 & -0.57735026919 \\ -0.57735026919 & 1.15470053838 \end{pmatrix}$

Table 6.3: This table gives an approximation of $\lambda = \frac{1+\sqrt{3}}{2}$ by the continued fraction expansion up to a tolerance of 10^{-8} which is $\frac{10864}{7953}$. Since we expect the real part to be zero, we only keep track of the exponential parts of the real term, which are on the order of 10^{-14}.

Jenkins–Strebel tables

n	Time	Approximation	
0	0.01	$\begin{pmatrix} i & 0 \\ 0 & i \end{pmatrix}$	
1	0.01	$-0.162162162162162 + 0.972972972972974i$ $-0.162162162162163 - 0.0270270270270272i$	$-0.162162162162161 - 0.0270270270270267i$ $-0.162162162162162 + 0.972972972972973i$
2	0.01	$-0.181145110935354 + 0.966032669224184i$ $-0.181145110935355 - 0.0339673307758161i$	$-0.181145110935353 - 0.0339673307758142i$ $-0.181145110935356 + 0.966032669224183i$
3	0.88	$-0.183154151609461 + 0.96524676973432i$ $-0.183154151609457 - 0.0347532302656803i$	$-0.183154151609459 - 0.0347532302656807i$ $-0.183154151609459 + 0.965246769734321i$
4	6.07	$-0.18337643045845 + 0.965159203662908i$ $-0.183376430458457 - 0.0348407963370859i$	$-0.183376430458463 - 0.0348407963370877i$ $-0.183376430458452 + 0.965159203662913i$
5	61.02	$-0.183401116934979 + 0.965149470930576i$ $-0.183401116934996 - 0.0348505290694234i$	$-0.183401116935002 - 0.0348505290694085i$ $-0.183401116934987 + 0.965149470930574i$
6	539.43	$-0.183403859739504 + 0.965148389476543i$ $-0.183403859739527 - 0.0348516105234329i$	$-0.183403859739557 - 0.0348516105233965i$ $-0.183403859739509 + 0.96514838947655i$
7	3969.65	$-0.183404164493817 + 0.965148269314438i$ $-0.183404164493896 - 0.0348517306854744i$	$-0.183404164494 - 0.0348517306853213i$ $-0.183404164493843 + 0.965148269314462i$

Table 6.4: The table gives the successive approximations of the Riemann matrix for $J_2(1,1)$, from the family of the Jenkins–Strebel differential of genus 2.

(λ,μ)	n	Approximation
$(3,1)$	6	$\begin{pmatrix} 0.391790821341348 + 0.799932604843609i & -0.408209178658656 + 0.199932604843692i \\ -0.40820917865866 + 0.199932604843639i & 0.391790821341349 + 0.799932604843633i \end{pmatrix}$
$(3/5,1)$	5	$\begin{pmatrix} -0.552067431042614 + 0.828028726521117i & -0.0814791957486144 - 0.0543242146552902i \\ -0.0814791957485449 - 0.0543242146553346i & -0.552067431042622 + 0.828028726521113i \end{pmatrix}$
$(5/7,1)$	4	$\begin{pmatrix} -0.435881709806809 + 0.891395736738509i & -0.111557385482526 - 0.0545502092073928i \\ -0.111557385482489 - 0.0545502092074161i & -0.435881709806802 + 0.891395736738513i \end{pmatrix}$
$(1,3)$	6	$\begin{pmatrix} -0.219850572165274 + 0.369151081713766i & -0.0705500626168651 - 0.0418472644071332i \\ -0.0705500626168283 - 0.0418472644071658i & -0.182947389640796 + 0.986855533802479i \end{pmatrix}$
$(1,3/5)$	5	$\begin{pmatrix} 0.0140501297786541 + 1.24511271092546i & -0.237782438362241 - 0.00109980530376883i \\ -0.237782438362194 - 0.00109980530385763i & -0.190005989628958 + 0.951563668084441i \end{pmatrix}$
$(1,5/7)$	4	$\begin{pmatrix} -0.0638935382171857 + 1.16061629684551i & -0.220568218021264 - 0.0143136795919605i \\ -0.220568218021245 - 0.0143136795919968i & -0.187013661219342 + 0.956221386346668i \end{pmatrix}$
$(3/5,5/7)$	3	$\begin{pmatrix} -0.553835613968335 + 1.13666373978695i & -0.110172300923 - 0.054295316550795i \\ -0.110172300922962 - 0.0542953165508437i & -0.550771147382289 + 0.825576938910713i \end{pmatrix}$

Table 6.5: The table gives some approximations in genus 2 for $J_2(\lambda,\mu)$ where we chose the level n so that the number of subdivided squares is approximately the same for each case.

n	Time	Approximation
0	0.01	$\begin{pmatrix} i & 0 & 0 \\ 0 & i & 0 \\ 0 & 0 & 2i \end{pmatrix}$
1	0.01	$\begin{pmatrix} -0.163636364 + 0.972727273i & 0.001474201 + 0.000245700i & -0.162162162 - 0.027027027i \\ 0.001474201 + 0.000245700i & -0.163636364 + 0.972727273i & -0.162162162 - 0.027027027i \\ -0.162162162 - 0.027027027i & -0.162162162 - 0.027027027i & -0.324324324 + 1.945945946i \end{pmatrix}$
2	0.01	$\begin{pmatrix} -0.181890640 + 0.965429514i & 0.000745530 + 0.000603155i & -0.181145111 - 0.033967331i \\ 0.000745530 + 0.000603155i & -0.181890640 + 0.965429514i & -0.181145111 - 0.033967331i \\ -0.181145111 - 0.033967331i & -0.181145111 - 0.033967331i & -0.362290222 + 1.932065338i \end{pmatrix}$
3	0.27	$\begin{pmatrix} -0.183837862 + 0.964626792i & 0.000683710 + 0.000619978i & -0.183154152 - 0.034753230i \\ 0.006837101 + 0.000619978i & -0.183837862 + 0.964626792i & -0.183154152 - 0.034753230i \\ -0.183154152 - 0.034753230i & -0.183154152 - 0.034753230i & -0.366308303 + 1.930493539i \end{pmatrix}$
4	2.65	$\begin{pmatrix} -0.184053419 + 0.964537638i & 0.000676988 + 0.000621565i & -0.183376430 - 0.034840796i \\ 0.000676988 + 0.000621565i & -0.1840534189 + 0.964537638i & -0.183376430 - 0.034840796i \\ -0.183376430 - 0.034840796i & -0.183376430 - 0.034840796i & -0.366752861 + 1.930318407i \end{pmatrix}$
5	38.37	$\begin{pmatrix} -0.184077360 + 0.964527733i & 0.000676243 + 0.000621738i & -0.183401117 - 0.034850529i \\ 0.000676243 + 0.000621738i & -0.184077360 + 0.964527733i & -0.183401117 - 0.034850529i \\ -0.183401117 - 0.034850529i & -0.183401117 - 0.034850529i & -0.366802234 + 1.930298942i \end{pmatrix}$
6	398.04	$\begin{pmatrix} -0.1840800120 + 0.964526632i & 0.000676160 + 0.000621757i & -0.183403860 - 0.034851611i \\ 0.000676160 + 0.000621757i & -0.1840800120 + 0.964526632i & -0.183403860 - 0.034851611i \\ -0.183403860 - 0.034851611i & -0.183403860 - 0.034851611i & -0.366807719 + 1.930296779i \end{pmatrix}$
7	3429.78	$\begin{pmatrix} -0.184080315 + 0.96452651i & 0.000676151 + 0.000621759i & -0.183404164 - 0.034851731i \\ 0.000676151 + 0.000621759i & -0.184080315 + 0.96452651i & -0.183404164 - 0.034851731i \\ -0.183404164 - 0.034851731i & -0.183404164 - 0.034851731i & -0.366808329 + 1.930296539i \end{pmatrix}$

Table 6.6: The table gives the successive approximations of the Riemann matrix for $J_3(1,1)$, a specific surface from the family of the Jenkins–Strebel differential of genus 3. Results are rounded to 9 decimal places.

n	Time	Approximation			
0	0.01	$\begin{pmatrix} i & 0 & 0 & 0 \\ 0 & i & 0 & 0 \\ 0 & 0 & i & 0 \\ 0 & 0 & 0 & 3i \end{pmatrix}$			
1	0.01	$\begin{pmatrix} -0.163639 + 0.972727i & 0.000739 + 0.000123i & 0.00073859 + 0.000123i & -0.162162 - 0.027027i \\ 0.000739 + 0.000123i & -0.163639 + 0.972727i & 0.000739 + 0.000123i & -0.162162 - 0.027027i \\ 0.000739 + 0.000123i & 0.000739 + 0.000123i & -0.163639 + 0.972727i & -0.162162 - 0.027027i \\ -0.162162 - 0.027027i & -0.162162 - 0.027027i & -0.162162 - 0.027027i & -0.486486 + 2.918919i \end{pmatrix}$			
2	0.02	$\begin{pmatrix} -0.181893 + 0.96543i & 0.000374 + 0.000301i & 0.000374 + 0.000301i & -0.181145 - 0.033967i \\ 0.000374 + 0.000301i & -0.181893 + 0.965430i & 0.000374 + 0.000301i & -0.181145 - 0.033967i \\ 0.000374 + 0.000301i & 0.000374 + 0.000301i & -0.181893 + 0.96543i & -0.181145 - 0.033967i \\ -0.181145 - 0.033967i & -0.181145 - 0.033967i & -0.181145 - 0.033967i & -0.543435 + 2.898098i \end{pmatrix}$			
3	.48	$\begin{pmatrix} -0.18384 + 0.964628i & 0.000343 + 0.00031i & 0.000343 + 0.00031i & -0.183154 - 0.034753i \\ 0.000343 + 0.00031i & -0.18384 + 0.964628i & 0.000343 + 0.00031i & -0.183154 - 0.034753i \\ 0.000343 + 0.00031i & 0.000343 + 0.00031i & -0.18384 + 0.964628i & -0.183154 - 0.034753i \\ -0.183154 - 0.034753i & -0.183154 - 0.034753i & -0.183154 - 0.034753i & -0.549462 + 2.89574i \end{pmatrix}$			
4	5.70	$\begin{pmatrix} -0.18384 + 0.964628i & 0.000343 + 0.00031i & 0.000343 + 0.00031i & -0.183154 - 0.034753i \\ 0.0003437 + 0.00031i & -0.18384 + 0.964628i & 0.000343 + 0.00031i & -0.183154 - 0.034753i \\ 0.000343 + 0.00031i & 0.000343 + 0.00031i & -0.18384 + 0.964628i & -0.183154 - 0.034753i \\ -0.183154 - 0.034753i & -0.183154 - 0.034753i & -0.183154 - 0.034753i & -0.549462 + 2.89574i \end{pmatrix}$			
5	89.00	$\begin{pmatrix} -0.184079 + 0.964529i & 0.000339 + 0.000310i & 0.000339 + 0.000310i & -0.183401 - 0.034851i \\ 0.000339 + 0.000310i & -0.184079 + 0.964529i & 0.000339 + 0.0003103i & -0.183401 - 0.034851i \\ 0.000339 + 0.000310i & 0.000339 + 0.000310i & -0.184079 + 0.964529i & -0.183401 - 0.034851i \\ -0.183401 - 0.0348518i & -0.183401 - 0.034851i & -0.183401 - 0.0348512i & -0.550203 + 2.895448i \end{pmatrix}$			
6	846.84	$\begin{pmatrix} -0.184082 + 0.9645278i & 0.0003396 + 0.000310i & 0.000339 + 0.000310i & -0.183404 - 0.034852i \\ 0.000339 + 0.000310i & -0.184082 + 0.964527i & 0.000339 + 0.000310i & -0.183404 - 0.034852i \\ 0.000339 + 0.000310i & 0.000339 + 0.000310i & -0.184082 + 0.964527i & -0.183404 - 0.034852i \\ -0.183404 - 0.034852i & -0.1834044 - 0.034852i & -0.183404 - 0.0348512i & -0.550212 + 2.895445i \end{pmatrix}$			
7	7997.04	$\begin{pmatrix} -0.184082 + 0.964527i & 0.000339 + 0.000310i & 0.000339 + 0.000310i & -0.1834043 - 0.03485125i \\ 0.000339 + 0.000310i & -0.184082 + 0.964527i & 0.000339 + 0.0003105i & -0.1834041 - 0.0348512i \\ 0.000339 + 0.000310i & 0.000339 + 0.000310i & -0.184082 + 0.964527i & -0.183404 - 0.034852i \\ -0.183404 - 0.034852i & -0.183404 - 0.034852i & -0.183404 - 0.034852i & -0.550212 + 2.895445i \end{pmatrix}$			

Table 6.7: The table gives the successive approximations of the Riemann matrix for $J_4(1,1)$ from the family of the Jenkins–Strebel differential of genus 4. Results rounded to 6 places.

n	Time	Approximation
0	0.01	$\begin{pmatrix} i & 0 & 0 & 0 & 0 \\ 0 & i & 0 & 0 & 0 \\ 0 & 0 & i & 0 & 0 \\ 0 & 0 & 0 & i & 0 \\ 0 & 0 & 0 & 0 & 4i \end{pmatrix}$
1	0.01	$\begin{pmatrix} -0.163639 + 0.972727i & 0.000737 + 0.000123i & 0.000003 & 0.000737 + 0.000123i & -0.162162 - 0.027027i \\ 0.000737 + 0.000123i & -0.163639 + 0.972727i & 0.000737 + 0.000123i & 0.000003 & -0.162162 - 0.027027i \\ 0.000003 & 0.000737 + 0.000123i & -0.163639 + 0.972727i & 0.000737 + 0.000123i & -0.162162 - 0.027027i \\ 0.000737 + 0.000123i & 0.000003 & 0.000737 + 0.000123i & -0.163639 + 0.972727i & -0.162162 - 0.027027i \\ -0.162162 - 0.027027i & -0.162162 - 0.027027i & -0.162162 - 0.027027i & -0.162162 - 0.027027i & -0.648649 + 3.891892i \end{pmatrix}$
2	0.03	$\begin{pmatrix} -0.181893 + 0.96543i & 0.000373 + 0.000302i & 0.000002 - 0.000001i & 0.0003731 + 0.000303i & -0.181145 - 0.033967i \\ 0.000373 + 0.000302i & -0.181893 + 0.96543i & 0.000373 + 0.000302i & 0.000002 - 0.000001i & -0.181145 - 0.033967i \\ 0.000002 - 0.000001i & 0.000373 + 0.000302i & -0.181893 + 0.965430i & 0.000373 + 0.000302i & -0.181145 - 0.033967i \\ 0.000373 + 0.000302i & 0.000002 - 0.000001i & 0.000373 + 0.000302i & -0.1818938 + 0.96543i & -0.181145 - 0.033967i \\ -0.181145 - 0.033967i & -0.181145 - 0.033967i & -0.181145 - 0.033967i & -0.181145 - 0.033967i & -0.72458 + 3.864131i \end{pmatrix}$
3	0.69	$\begin{pmatrix} -0.18384 + 0.964628i & 0.000342 + 0.00031i & 0.000002 - 0.0000001i & 0.000342 + 0.00031i & -0.183154 - 0.034753i \\ 0.000342 + 0.00031i & -0.18384 + 0.964628i & 0.000342 + 0.00031i & 0.000002 - 0.000001i & -0.183154 - 0.034753i \\ 0.000002 - 0.000001i & 0.000342 + 0.00031i & -0.18384 + 0.964628i & 0.000342 + 0.00031i & -0.183154 - 0.034753i \\ 0.000342 + 0.00031i & 0.000002 - 0.000001i & 0.000342 + 0.00031i & -0.18384 + 0.964628i & -0.183154 - 0.034753i \\ -0.183154 - 0.034753i & -0.183154 - 0.034753i & -0.183154 - 0.034753i & -0.183154 - 0.034753i & -0.732617 + 3.860987i \end{pmatrix}$
4	9.02	$\begin{pmatrix} -0.184055 + 0.964538i & 0.000338 + 0.000311i & 0.000002 - 0.000001i & 0.000338 + 0.000311i & -0.183376 - 0.034841i \\ 0.000338 + 0.000311i & -0.184055 + 0.964538i & 0.000338 + 0.000311i & 0.000002 - 0.000001i & -0.183376 - 0.034841i \\ 0.000001 - 0.000001i & 0.000338 + 0.000311i & -0.184055 + 0.964538i & 0.000338 + 0.000311i & -0.183376 - 0.034841i \\ 0.000338 + 0.000311i & 0.000001 - 0.000001i & 0.000338 + 0.000311i & -0.184055 + 0.964538i & -0.183376 - 0.034841i \\ -0.183376 - 0.034841i & -0.183376 - 0.034841i & -0.183376 - 0.034841i & -0.183376 - 0.034841i & -0.733506 + 3.860637i \end{pmatrix}$
5	94.25	$\begin{pmatrix} -0.184079 + 0.964529i & 0.000338 + 0.000311i & 0.000001 - 0.000001i & 0.000338 + 0.000311i & -0.183401 - 0.034851i \\ 0.000338 + 0.000311i & -0.184079 + 0.964529i & 0.000338 + 0.000311i & 0.000002 - 0.000001i & -0.183401 - 0.034851i \\ 0.000002 - 0.000001i & 0.000338 + 0.000311i & -0.184079 + 0.964529i & 0.000338 + 0.000311i & -0.183401 - 0.034851i \\ 0.000338 + 0.000311i & 0.000002 - 0.000001i & 0.000338 + 0.000311i & -0.184079 + 0.964529i & -0.183401 - 0.034851i \\ -0.183401 - 0.034851i & -0.183401 - 0.034851i & -0.183401 - 0.034851i & -0.183401 - 0.034851i & -0.733604 + 3.860598i \end{pmatrix}$
6	1051.54	$\begin{pmatrix} -0.184082 + 0.964527i & 0.000338 + 0.000311i & 0.000002 - 0.000001i & 0.000338 + 0.000311i & -0.183404 - 0.034852i \\ 0.000338 + 0.000311i & -0.184082 + 0.964527i & 0.000338 + 0.000311i & 0.000002 - 0.000001i & -0.183404 - 0.034852i \\ 0.000002 - 0.000001i & 0.000338 + 0.000311i & -0.184082 + 0.964527i & 0.000338 + 0.000311i & -0.183404 - 0.034852i \\ 0.000338 + 0.000311i & 0.000002 - 0.000001i & 0.000338 + 0.000311i & -0.184082 + 0.964527i & -0.183404 - 0.034852i \\ -0.183404 - 0.034852i & -0.183404 - 0.034852i & -0.183404 - 0.034852i & -0.183404 - 0.034852i & -0.733615 + 3.860594i \end{pmatrix}$
7	12739.99	$\begin{pmatrix} -0.184082 + 0.964527i & 0.000338 + 0.000311i & 0.000002 - 0.000001i & 0.000338 + 0.000311i & -0.183404 - 0.034852i \\ 0.000338 + 0.000312i & -0.184082 + 0.964527i & 0.000338 + 0.000311i & 0.000002 - 0.000001i & -0.183404 - 0.034852i \\ 0.000002 - 0.000001i & 0.000338 + 0.000311i & -0.184082 + 0.964527i & 0.000338 + 0.000311i & -0.183404 - 0.034852i \\ 0.000338 + 0.000311i & 0.000002 - -0.000001i & 0.000338 + 0.000311i & -0.184082 + 0.964527i & -0.183404 - 0.034852i \\ -0.183404 - 0.034852i & -0.183404 - 0.034852i & -0.183404 - 0.034852i & -0.183404 - 0.034852i & -0.733617 + 3.860593i \end{pmatrix}$

Table 6.8: The table gives the successive approximations of the Riemann matrix for $J_5(1,1)$ from the family of the Jenkins–Strebel differential of genus 5. Results rounded to 6 places.

Concluding remarks

The algorithms presented in this chapter are a step towards bridging the transcendental divide. They provide an explicit way to generate examples and conjectures, some of which are posed in Section 6.3. In addition, our study leads to yet another variant of the Schottky problem 1.2.1: the *discrete Schottky problem*. It asks to classify the discrete Schottky locus in relation to the classical Schottky locus. Concretely, it asks whether the sequence of discrete Riemann matrices lies entirely in the Schottky locus, or whether it is possible for it to converge inside the Schottky locus while starting outside.

Chapter 7

Pencils of quadrics

This chapter is based on the article "Pencils of quadrics: old and new" [46], which is joint with Claudia Fevola and Bernd Sturmfels. In it we revisit the classical study of pencils of quadrics dating back to Weierstrass and Segre. We use the classification by Segre symbols, in addition to computational methods, to answer questions motivated by algebraic statistics and optimization.

7.1   Introduction

A pencil of quadrics is a two-dimensional linear subspace $\mathcal{L}$ in the space $\mathbb{S}^n$ of (real or complex) symmetric $n \times n$ matrices. It is a point in the Grassmannian $\mathrm{Gr}(2, \mathbb{S}^n)$, and it specifies a line $\mathbb{P}\mathcal{L}$ in the projective space $\mathbb{P}(\mathbb{S}^n) \simeq \mathbb{P}^{\binom{n+1}{2}-1}$. The group GL_n acts on $\mathbb{S}^n$ by congruence and this induces an action on $\mathrm{Gr}(2, \mathbb{S}^n)$. We say that two pencils are *isomorphic* if they lie in the same GL_n-orbit.

Fix a pencil $\mathcal{L}$ with basis $\{A, B\}$. The determinant $\det(\mathcal{L}) = \det(\lambda A + \mu B)$ is well-defined up to the action of GL_2 by changing basis in $\mathcal{L}$. The zeros of this binary form are a multiset of size n in the line $\mathbb{P}^1$, well-defined up to isomorphism of $\mathbb{P}^1$. We exclude pencils $\mathcal{L}$ that are *singular*, meaning that $\det(\mathcal{L}) = 0$.

The singular pencils form a subvariety $\mathrm{Gr}(2, \mathbb{S}^n)^{\mathrm{sing}}$ in the Grassmannian. We are interested in a natural stratification of the open set of all regular pencils:

$$\mathrm{Gr}(2, \mathbb{S}^n)^{\mathrm{reg}} \;=\; \mathrm{Gr}(2, \mathbb{S}^n) \setminus \mathrm{Gr}(2, \mathbb{S}^n)^{\mathrm{sing}}.$$

Each stratum is indexed by a *Segre symbol* σ. This is a multiset of partitions whose parts add up to n in total. One exception: the singleton $[(1, 1, \ldots, 1)]$ is not a Segre symbol. The number $S(n)$ of Segre symbols was already of interest to Arthur Cayley in 1855. In [24, p. 316], he derived the generating function

$$\sum_{n=1}^{\infty} S(n) x^n \;=\; \prod_{k \geq 1} \frac{1}{(1 - x^k)^{P(k)}} \;-\; \frac{1}{1-x} \;=\; 2x^2 + 5x^3 + 13x^4 + 26x^5 + 57x^6 + 110x^7 + \cdots,$$

where $P(k)$ is the number of partitions of the integer k. The two Segre symbols for $n = 2$ are $[1, 1]$ and $[2]$. For $n = 3$ and $n = 4$ they are shown in Figure 7.1.

The Segre symbol $\sigma = \sigma(\mathcal{L})$ of a given pencil $\mathcal{L}$ can be computed as follows. Pick a basis $\{A, B\}$ of $\mathcal{L}$, where B is invertible, and find the Jordan canonical form of AB^{-1}. Each eigenvalue of AB^{-1} determines a partition, according to the sizes of its Jordan blocks. Then σ is the associated multiset of partitions. It turns out that σ does not depend on the choice of basis $\{A, B\}$. For the relevant background in linear algebra see [37, 110, 111] and Section 7.2 below.

The role of Segre symbols in projective geometry can be stated as follows.

Theorem 7.1.1 (Weierstrass-Segre). *Two pencils of quadrics in $\mathbb{S}^n$ are isomorphic if and only if their Segre symbols agree and their determinants define the same multiset of n points on the projective line $\mathbb{P}^1$, up to isomorphism of $\mathbb{P}^1$.*

Example 7.1.2 ($n = 2$). All pencils $\mathcal{L}$ are regular. There are two GL_2-orbits, given by the rank of a matrix X that spans $\mathcal{L}^\perp = \{X \in \mathbb{S}^2 : \mathrm{trace}(AX) = \mathrm{trace}(BX) = 0\}$. If X has rank 2 then $\det(\mathcal{L})$ has two distinct roots in $\mathbb{P}^1$ and the Segre symbol is $\sigma(\mathcal{L}) = [1, 1]$. If X has rank 1 then it is a double root in $\mathbb{P}^1$ and $\sigma(\mathcal{L}) = [2]$.

We learned about Theorem 7.1.1 from an unpublished note by Pieter Belmans, titled *Segre symbols*, which credits the 1883 PhD thesis of Corrado Segre. It appears in the textbooks on algebraic geometry by Dolgachev [36, §8.6.1] and Hodge-Pedoe [65, §XIII.10]. The idea goes back to at least the 1850s, in works of Cayley [24] and Sylvester [108]. One aim of this chapter is to revisit this history.

We begin in Section 7.2 with a linear algebra perspective on Theorem 7.1.1. In Section 7.3 we study the reciprocal curve $\mathbb{P}\mathcal{L}^{-1}$ of a pencil $\mathcal{L} \in \mathrm{Gr}(2, \mathbb{S}^n)^{\mathrm{reg}}$. This curve lives in $\mathbb{P}(\mathbb{S}^n)$, and it is parametrized by the inverses of all invertible matrices in $\mathcal{L}$. We prove that $\mathbb{P}\mathcal{L}^{-1}$ is a rational normal curve. We express its degree in terms of the Segre symbol $\sigma(\mathcal{L})$, and we determine its prime ideal.

In Section 7.2 we turn to maximum likelihood estimation for Gaussians. A pencil $\mathcal{L}$ plays two different roles in statistics, depending on whether it lives in the space of concentration matrices (as in [107]) or in the space of covariance matrices (as in [31]). This yields two numerical invariants, the ML degree $\mathrm{mld}(\mathcal{L})$ and the reciprocal ML degree $\mathrm{rmld}(\mathcal{L})$. We compute these in Theorem 7.4.2.

In Section 7.5 we study the constructible set defined by a fixed Segre symbol:

$$\mathrm{Gr}_\sigma = \left\{ \mathcal{L} \in \mathrm{Gr}(2, \mathbb{S}^n)^{\mathrm{reg}} : \sigma(\mathcal{L}) = \sigma \right\}. \tag{7.1}$$

Its closure $\overline{\mathrm{Gr}}_\sigma$ is a variety. We study these varieties and their poset of inclusions, seen in Figure 7.1. This extends the stratification of $\mathrm{Gr}(2, \mathbb{R}^n)$ by matroids.

Example 7.1.3 $(n = 3)$**.** There are five strata Gr_σ in the Grassmannian $\mathrm{Gr}(2, \mathbb{S}^3)$:

symbol	codim	degrees	P	Q	variety in $\mathbb{P}^2$
$[1,1,1]$	0	$(2,2,3)$	$ax^2+by^2+cz^2$	$x^2+y^2+z^2$	*four reduced points*
$[2,1]$	1	$(2,1,2)$	$2axy+y^2+bz^2$	$2xy+z^2$	*one double point, two others*
$[3]$	2	$(2,0,1)$	$2axz+ay^2+2yz$	$2xz+y^2$	*one triple point, one other*
$[(1,1),1]$	2	$(1,1,1)$	$ax^2+ay^2+bz^2$	$x^2+y^2+z^2$	*two double points*
$[(2,1)]$	3	$(1,0,0)$	$2axy+y^2+az^2$	$2xy+z^2$	*quadruple point*

For each Segre symbol σ, we display $\mathrm{codim}(\mathrm{Gr}_\sigma)$, the triple of degrees

$$\big(\deg(\mathcal{L}^{-1}), \mathrm{mld}(\mathcal{L}), \mathrm{rmld}(\mathcal{L})\big),$$

the basis $\{P, Q\}$ from Section 7.2, and its variety in $\mathbb{P}^2$. Here, x, y, z are coordinates on $\mathbb{P}^2$, and a, b, c are distinct nonzero reals. This accounts for all regular pencils. A pencil is singular if P and Q share a linear factor. One such $\mathcal{L}$ is spanned by xy and xz. This defines a line and a point in $\mathbb{P}^2$. We conclude that $\mathrm{Gr}(2, \mathbb{S}^3)^{\mathrm{sing}}$ is an irreducible variety of dimension 4.

7.2 Canonical representatives

We identify symmetric $n \times n$ matrices A with quadratic forms $\mathbf{x}A\mathbf{x}^T$ in unknowns $\mathbf{x} = (x_1, \ldots, x_n)$. We fix the field to be $\mathbb{C}$. The $\binom{n+1}{2}$-dimensional vector space $\mathbb{S}^n$ is equipped with the trace inner product $(A, B) \mapsto \mathrm{trace}(AB)$. The group GL_n acts on quadratic forms by linear changes of coordinates, via $\mathbf{x} \mapsto \mathbf{x}g$. This corresponds to the action of GL_n on symmetric matrices by congruence:

$$\mathrm{GL}_n \times \mathbb{S}^n \to \mathbb{S}^n, \quad (g, A) \mapsto gAg^T.$$

Let $\mathcal{L} = \mathbb{C}\{A, B\}$ be a regular pencil in $\mathrm{Gr}(2, \mathbb{S}^n)$, with $\det(B) \neq 0$. The polynomial ring $\mathbb{C}[\lambda]$ in one variable λ is a principal ideal domain. The cokernel of the matrix $A - \lambda B$ is a module over this PID. Consider its *elementary divisors*

$$(\lambda - \alpha_1)^{e_1}, (\lambda - \alpha_2)^{e_2}, \ldots, (\lambda - \alpha_s)^{e_s}. \tag{7.2}$$

Here $e_1, \ldots, e_s$ are positive integers whose sum equals n. The list (7.2) is unordered and its product is $\det(\mathcal{L}) = \pm\det(A - \lambda B)$. The complex numbers α_i are the *eigenvalues* of the pair (A, B). They form a multiset of cardinality n in $\mathbb{P}^1$.

Suppose there are r distinct eigenvalues α_i. We have $r \leq s \leq n$. The exponents e_i corresponding to one fixed eigenvalue form a partition. This gives a multiset of r partitions, with s parts in total, where the sum of all parts is n. This multiset of partitions is the Segre symbol $\sigma = \sigma(\mathcal{L})$. It is thus visible in (7.2). We now paraphrase Theorem 7.1.1 using the elementary divisors of the matrix $A - \lambda B$.

Corollary 7.2.1. *Consider two quadrics $\mathbf{x}A\mathbf{x}^T$ and $\mathbf{x}B\mathbf{x}^T$ with $\det(B) \neq 0$. There exists a change of coordinates $\mathbf{x} \mapsto \mathbf{x}g$ which transforms them to $\mathbf{x}C\mathbf{x}^T$ and $\mathbf{x}D\mathbf{x}^T$ if and only if the matrices $A - \lambda B$ and $C - \lambda D$ have the same elementary divisors.*

Proof. For a textbook proof of this classical fact see [65, Theorem 1, p. 278]. □

Corollary 7.2.1 is used to construct a canonical form for pencils. For $e \in \mathbb{N}$ and $\alpha \in \mathbb{C}$, we define a pair of symmetric $e \times e$ matrices by filling their antidiagonals:

$$P_e(\alpha) = \begin{pmatrix} 0 & 0 & \cdots & 0 & \alpha \\ 0 & 0 & \cdots & \alpha & 1 \\ \vdots & \vdots & \ddots & \ddots & \vdots \\ 0 & \alpha & 1 & \vdots & 0 \\ \alpha & 1 & \cdots & 0 & 0 \end{pmatrix} \quad \text{and} \quad Q_e = \begin{pmatrix} 0 & \cdots & 0 & 0 & 1 \\ 0 & \cdots & 0 & 1 & 0 \\ 0 & \cdots & 1 & 0 & 0 \\ \vdots & \ddots & \vdots & \vdots & \vdots \\ 1 & \cdots & 0 & 0 & 0 \end{pmatrix}. \tag{7.3}$$

The $e \times e$ matrix $P_e(\alpha) - \lambda Q_e$ has only one elementary divisor, namely $(\lambda - \alpha)^e$.

Let us now start with the list in (7.2). For each elementary divisor $(\lambda - \alpha_i)^{e_i}$ we form the $e_i \times e_i$ matrices in (7.3), and we aggregate these blocks as follows:

$$P = \begin{pmatrix} P_{e_1}(\alpha_1) & 0 & \cdots & 0 \\ 0 & P_{e_2}(\alpha_2) & \cdots & 0 \\ \vdots & \vdots & \ddots & \vdots \\ 0 & 0 & \cdots & P_{e_s}(\alpha_s) \end{pmatrix} \quad \text{and} \quad Q = \begin{pmatrix} Q_{e_1} & 0 & \cdots & 0 \\ 0 & Q_{e_2} & \cdots & 0 \\ \vdots & \vdots & \ddots & \vdots \\ 0 & 0 & \cdots & Q_{e_s} \end{pmatrix}. \tag{7.4}$$

The matrices $A - \lambda B$ and $P - \lambda Q$ have the same elementary divisors. Hence, by Corollary 7.2.1, the pair $(\mathbf{x}A\mathbf{x}^T, \mathbf{x}B\mathbf{x}^T)$ is isomorphic to $(\mathbf{x}P\mathbf{x}^T, \mathbf{x}Q\mathbf{x}^T)$ under the action by GL_n. As in Example 7.1.3, every regular pencil $\mathcal{L} \in \mathrm{Gr}(2, \mathbb{S}^n)$ has a normal form $\mathbb{C}\{P, Q\}$, where the matrices P and Q are defined by the unordered list (7.2). Given any Segre symbol σ, its canonical representative is $\mathcal{L} = \mathbb{C}\{P, Q\}$ where $\alpha_1, \ldots, \alpha_r$ are parameters. In what follows, we often use index-free notation for unknowns, like $\mathbf{x} = (x, y, z)$ and $(\alpha_1, \alpha_2, \alpha_3) = (a, b, c)$.

Example 7.2.2 ($n = 5$). Let $\sigma = [(2, 1), 2]$. The list of elementary divisors equals

$$(\lambda - a)^2, \ (\lambda - a), \ (\lambda - b)^2.$$

Our canonical representative (7.4) for this class of pencils $\mathcal{L}$ is the matrix pair

$$P = \begin{pmatrix} 0 & a & 0 & 0 & 0 \\ a & 1 & 0 & 0 & 0 \\ 0 & 0 & a & 0 & 0 \\ 0 & 0 & 0 & 0 & b \\ 0 & 0 & 0 & b & 1 \end{pmatrix} \quad \text{and} \quad Q = \begin{pmatrix} 0 & 1 & 0 & 0 & 0 \\ 1 & 0 & 0 & 0 & 0 \\ 0 & 0 & 1 & 0 & 0 \\ 0 & 0 & 0 & 0 & 1 \\ 0 & 0 & 0 & 1 & 0 \end{pmatrix}.$$

The quadrics $P = 2axy + y^2 + az^2 + 2buv + v^2$ and $Q = 2xy + z^2 + 2uv$ define a degenerate del Pezzo surface of degree four in $\mathbb{P}^4$. This surface has two singular points, $(0:0:0:1:0)$ and $(1:0:0:0:0)$; their multiplicities are one and three.

Remark 7.2.3. To appreciate Theorem 7.1.1 and Corollary 7.2.1, it helps to distinguish the two geometric figures associated with a pencil of quadrics, and how the groups GL_2 and GL_n act on these. First, there is the configuration of n points in $\mathbb{P}^1$ defined by $\det(\mathcal{L})$. This configuration undergoes projective transformations via GL_2 but it is left invariant by GL_n. Second, there is the codimension 2 variety in $\mathbb{P}^{n-1}$ defined by the quadrics in $\mathcal{L}$. This variety undergoes projective transformations via GL_n but it is left invariant by GL_2.

In this section, pencils $\mathcal{L} = \mathbb{C}\{A, B\}$ are studied by linear algebra over a PID. We use the relationship between elementary divisors and invariant factors. One can compute these with the *Smith normal form* algorithm over $\mathbb{C}[\lambda]$. We apply this to a specific torsion module, namely the cokernel of our matrix $A - \lambda B$.

Fix n and a Segre symbol $\sigma = [\sigma_1, \ldots, \sigma_r]$, where each entry is now a weakly decreasing vector $\sigma_i = (\sigma_{i1}, \sigma_{i2}, \ldots, \sigma_{in})$ of nonnegative integers. With this convention, the Segre symbol $\sigma = [\sigma_1, \sigma_2]$ in Example 7.2.2, with $n = 5, s = 3, r = 2$, has $\sigma_1 = (2, 1, 0)$ and $\sigma_2 = (2, 0, 0)$. Write $\alpha_1, \ldots, \alpha_r \in \mathbb{C}$ for the distinct roots of $\det(A - \lambda B)$. Then the elementary divisors are $(\lambda - \alpha_i)^{\sigma_{ij}}$ for $i = 1, \ldots, r$ and $j = 1, \ldots, n$. Only s of these are different from 1. The invariant factors are

$$d_j \; := \; \prod_{i=1}^{r}(\lambda - \alpha_i)^{\sigma_{ij}} \quad \text{for } j = 1, \ldots, n.$$

Note that $d_n | d_{n-1} | \cdots | d_2 | d_1$. The number of nontrivial invariant factors is the maximum number of parts among the r partitions σ_i. For instance, in Example 7.2.2, the invariant factors are $d_1 = (\lambda - a)^2(\lambda - b)^2$, $d_2 = \lambda - a$, $d_3 = d_4 = d_5 = 1$.

The ideal of $k \times k$ minors of $A - \lambda B$ is generated by the greatest common divisor D_k of these minors. The theory of modules over a PID tells us that

$$D_k \quad := \quad \prod_{j=1}^{k} d_{n+1-j} \quad = \quad \prod_{i=1}^{r}(\lambda - \alpha_i)^{\sigma_{i,n-k+1}+\cdots+\sigma_{i,n-1}+\sigma_{i,n}}. \tag{7.5}$$

The Segre symbol of a pencil $\mathcal{L} = \mathbb{C}\{A, B\}$ is determined by the ideal of $k \times k$ minors of $A - \lambda B$ for $k = 1, \ldots, n$. In practice, we use the Smith normal form of $A - \lambda B$. In Section 7.1 we proposed a different method, namely the Jordan canonical form of AB^{-1}. This computation uses only linear algebra over $\mathbb{C}$, unlike the Smith normal form. To see that the Jordan canonical form of AB^{-1} reveals the Segre symbol, consider the transformation from (A, B) to (P, Q) in Corollary 7.2.1. This preserves the conjugacy class of AB^{-1}. Therefore, AB^{-1} and PQ^{-1} have the same Jordan canonical form. We see in (7.4) that Q is a permutation matrix, and hence so is Q^{-1}. Furthermore, P is already in Jordan canonical form, after permuting rows and columns, and σ is clearly visible in P.

7.3 The reciprocal curve

For any regular pencil $\mathcal{L}$, we are interested in the reciprocal curve $\mathbb{P}\mathcal{L}^{-1}$. We write $\deg(\mathcal{L}^{-1})$ for the degree of this curve in $\mathbb{P}(\mathbb{S}^n)$. In Example 7.1.3, we have $\deg(\mathcal{L}^{-1}) = 2$ in three

cases, so $\mathbb{P}\mathcal{L}^{-1}$ is a plane conic. In the other two cases, $\mathbb{P}\mathcal{L}^{-1}$ is a line in $\mathbb{P}^5$. Here are the homogeneous prime ideals of these curves:

Segre symbol	Ideal of the reciprocal curve $\mathbb{P}\mathcal{L}^{-1}$	mingens
$[1,1,1]$	$\langle x_{12}, x_{13}, x_{23}, (c{-}b)x_{11}x_{22} + (a{-}c)x_{11}x_{33} + (b{-}a)x_{22}x_{33}\rangle$	$(3,1)$
$[2,1]$	$\langle x_{13}, x_{22}, x_{23}, x_{12}^2 + (c-a)x_{11}x_{33} - 2x_{12}x_{33}\rangle$	$(3,1)$
$[3]$	$\langle x_{23}, x_{33}, x_{13} - 2x_{22}, x_{12}^2 - x_{11}x_{22}\rangle$	$(3,1)$
$[(1,1),1]$	$\langle x_{12}, x_{13}, x_{23}, x_{11} - x_{22}\rangle$	$(4,0)$
$[(2,1)]$	$\langle x_{13}, x_{22}, x_{23}, x_{12} - 2x_{33}\rangle$	$(4,0)$

The column "mingens" gives the numbers of linear and quadratic generators.

Example 7.3.1 ($n = 4$). Two quadrics P and Q in $\mathbb{P}^3$ meet in a quartic curve. There are 13 cases, one for each Segre symbol. Here, x, y, z, u are coordinates on $\mathbb{P}^3$.

symbol	codims	degrees	mingens	quadrics P, Q	variety in $\mathbb{P}^3$
$[1,1,1,1]$	$0,0,0$	$(\mathbf{3},3,5)$	$(6,3)$	$ax^2+by^2+cz^2+du^2$ $x^2+y^2+z^2+u^2$	elliptic curve
$[2,1,1]$	$1,1,1$	$(\mathbf{3},2,4)$	$(6,3)$	$2axy+y^2+cz^2+du^2$ $2xy+z^2+u^2$	nodal curve
$[(1,1),1,1]$	$3,2,2$	$(\mathbf{2},2,3)$	$(7,1)$	$a(x^2+y^2)+cz^2+du^2$ $x^2+y^2+z^2+u^2$	two conics meet twice
$[3,1]$	$2,2,2$	$(\mathbf{3},1,3)$	$(6,3)$	$2axz+ay^2+2yz+du^2$ $2xz+y^2+u^2$	cuspidal curve
$[2,2]$	$2,2,2$	$(\mathbf{3},1,3)$	$(6,3)$	$2axy+y^2+2bzu+u^2$ $2xy+2zu$	twisted cubic with secant
$[(2,1),1]$	$4,3,3$	$(\mathbf{2},1,2)$	$(7,1)$	$2axy+y^2+az^2+du^2$ $2xy+z^2+u^2$	two tangent conics
$[4]$	$3,3,3$	$(\mathbf{3},0,2)$	$(6,3)$	$2axu+2ayz+2yu+z^2$ $2xu+2yz$	twisted cubic with tangent
$[2,(1,1)]$	$4,3,3$	$(\mathbf{2},1,2)$	$(7,1)$	$2axy+y^2+c(z^2+u^2)$ $2xy+z^2+u^2$	conic meets two lines
$[(3,1)]$	$5,4,4$	$(\mathbf{2},0,1)$	$(7,1)$	$2axz+ay^2+2yz+au^2$ $2xz+y^2+u^2$	conic and two lines concur
$[(1,1),(1,1)]$	$6,4,4$	$(\mathbf{1},1,1)$	$(8,0)$	$a(x^2+y^2)+c(z^2+u^2)$ $x^2+y^2+z^2+u^2$	quadrangle of lines
$[(1,1,1),1]$	$8,5,5$	$(\mathbf{1},1,1)$	$(8,0)$	$a(x^2+y^2+z^2)+du^2$ $x^2+y^2+z^2+u^2$	double conic
$[(2,2)]$	$7,5,5$	$(\mathbf{1},0,0)$	$(8,0)$	$2axy+y^2+2azu+u^2$ $2xy+2zu$	double line and two lines
$[(2,1,1)]$	$9,6,6$	$(\mathbf{1},0,0)$	$(8,0)$	$2axy+y^2+a(z^2+u^2)$ $2xy+z^2+u^2$	two double lines

We see that $\mathbb{P}\mathcal{L}^{-1} \subset \mathbb{P}^9$ is either a line, a plane conic, or a twisted cubic curve. This is explained by the next theorem, which is our main result in Section 7.3.

Theorem 7.3.2. *Let $\mathcal{L}$ be a regular pencil in $\mathbb{S}^n$ with Segre symbol $\sigma = [\sigma_1, \ldots, \sigma_r]$. Then $\mathbb{P}\mathcal{L}^{-1}$ is a rational normal curve of degree d in $\mathbb{P}(\mathbb{S}^n)$, where $d = \sum_{i=1}^{r} \sigma_{i1} - 1$ is one less than the sum of the first parts of the partitions in σ. The ideal of $\mathbb{P}\mathcal{L}^{-1}$ is generated by $\binom{n+1}{2} - d - 1$ linear forms and $\binom{d}{2}$ quadrics in $\binom{n+1}{2}$ unknowns.*

Proof. The curve $\mathbb{P}\mathcal{L}^{-1}$ is parametrized by $\binom{n+1}{2}$ rational functions in one unknown λ, namely the entries in the inverse of matrix $P - \lambda Q$ in Section 7.2. We scale each entry by $D_n = \pm\det(P - \lambda Q)$ to get a polynomial parametrization by the adjoint of $P - \lambda Q$. This is an $n \times n$ matrix whose entries are the $(n-1) \times (n-1)$ minors of $P - \lambda Q$. These are polynomials of degree $\leq n - 1$ in λ, which are divisible by the invariant factor D_{n-1}. Note that D_{n-1} has degree $\sum_{i=1}^{r} \sum_{j=2}^{n} \sigma_{ij}$ in λ. Subtracting this from the expected degree $n - 1$, we obtain $d = \sum_{i=1}^{r} \sigma_{i1} - 1$. We remove the factor D_{n-1} from each entry of the adjoint. The resulting matrix $(D_n/D_{n-1}) \cdot (P - \lambda Q)^{-1}$ also parametrizes $\mathbb{P}\mathcal{L}^{-1}$. The entries of that matrix are polynomials in λ of degree $\leq d$. As a key step, we will show that these span the $(d+1)$-dimensional space $\mathbb{C}[\lambda]_{\leq d}$ of all polynomials in λ of degree $\leq d$.

The inverse of $P - \lambda Q$ is a block matrix, where the blocks are the inverses of the $e \times e$ matrices $P_e(\alpha) - \lambda Q_e$ in (7.3), one for each elementary divisor. A computation shows that the entry of $(P_e(\alpha) - \lambda(Q_e))^{-1}$ in row i and column j is

$$-(\lambda - \alpha)^{i+j-e-2} \quad \text{if } i + j \leq e + 1 \qquad \text{and} \qquad 0 \quad \text{if } i + j \geq e + 2. \tag{7.6}$$

It follows that the distinct nonzero entries in the $n \times n$ matrix $(P - \lambda Q)^{-1}$ are

$$\pm(\lambda - \alpha_i)^{-k} \quad \text{where } 1 \leq k \leq \sigma_{i1} \text{ and } 1 \leq i \leq r. \tag{7.7}$$

The common denominator of these $d + 1 = \sum_{i=1}^{r} \sigma_{i1}$ rational functions in λ is equal to $D_n/D_{n-1} = \prod_{i=1}^{r}(\lambda - \alpha_i)^{\sigma_{i1}}$. Multiplying by that common denominator, we obtain $d + 1$ polynomials in λ of degree $\leq d$. Lemma 7.3.3 below tells us that these polynomials are linearly independent. Hence they span $\mathbb{C}[\lambda]_{\leq d} \simeq \mathbb{C}^{d+1}$.

The proof of Theorem 7.3.2 now concludes as follows. By recording which entries of $(P - \lambda Q)^{-1}$ are zero, and which pairs of entries are equal, we obtain $\binom{n+1}{2} - d - 1$ independent linear forms that vanish on $\mathbb{P}\mathcal{L}^{-1}$. We know that there exist linear forms u_i in the matrix entries which evaluate to λ^i for $i = 0, 1, 2, \ldots, d$. The $\binom{d}{2}$ quadrics that vanish on $\mathbb{P}\mathcal{L}^{-1}$ are the 2×2 minors of the $2 \times d$ matrix

$$\begin{pmatrix} u_0 & u_1 & u_2 & \cdots & u_{d-1} \\ u_1 & u_2 & u_3 & \cdots & u_d \end{pmatrix}. \tag{7.8}$$

We have thus constructed an isomorphism between our curve $\mathbb{P}\mathcal{L}^{-1}$ and the rational normal curve $\{(1 : \lambda : \cdots : \lambda^d)\}$, whose prime ideal is given by (7.8). $\qquad \square$

Lemma 7.3.3. *A finite set of distinct rational functions* $(\lambda - \alpha_j)^{-s_{ij}}$, *each a negative power of one of the expressions* $\lambda - \alpha_1, \ldots, \lambda - \alpha_r$, *is linearly independent.*

Proof. We use induction on r. The base case is $r = 1$. We claim that $(\lambda-\alpha)^{-s_1}, \ldots, (\lambda-\alpha)^{-s_n}$ are linearly independent when $0 < s_1 < \cdots < s_n$. Suppose

$$k_1(\lambda - \alpha)^{-s_1} + \cdots + k_n(\lambda - \alpha)^{-s_n} = 0 \qquad \text{for some } k_1, \ldots, k_n \in \mathbb{C}.$$

Clearing denominators, we obtain $k_1(\lambda - \alpha)^{s_n - s_1} + \cdots + k_n = 0$. Setting $\lambda = \alpha$ we find $k_n = 0$. Repeating this computation n times, we conclude $k_1 = k_2 = \cdots = k_n = 0$.

For the induction step from $r-1$ to r, we consider distinct negative powers

$$
\begin{array}{cccc}
(\lambda-\alpha_1)^{-s_{1,1}}, & (\lambda-\alpha_1)^{-s_{1,2}}, & \ldots, & (\lambda-\alpha_1)^{-s_{1,n_1}}, \\
\vdots & \vdots & & \vdots \\
(\lambda-\alpha_r)^{-s_{r,1}}, & (\lambda-\alpha_r)^{-s_{r,2}}, & \ldots, & (\lambda-\alpha_r)^{-s_{r,n_r}},
\end{array}
\tag{7.9}
$$

where $0 \le s_{i,j} < s_{i,j+1}$ for $i = 1,...,r$ and $j = 1,...,n_i$. Consider a linear combination of (7.9) with coefficients $k_{1,1},\ldots,k_{r,n_r}$. Multiplying by $(\lambda-\alpha_r)^{s_{r,n_r}}$ and setting $\lambda = \alpha_r$, we find $k_{r,n_r} = 0$. Repeating with $(\lambda-\alpha_r)^{s_{r,i}}$ for $i = n_r-1, n_r-2,\ldots,1$, we get $k_{r,1} = \cdots = k_{r,n_r} = 0$. By the induction hypothesis, the first $r-1$ rows of (7.9) are linearly independent. This proves that all k_{ij} are zero. Lemma 7.3.3 follows. $\qquad\square$

The last paragraph in the proof of Theorem 7.3.2 gives an algorithm for computing generators of the ideal of $\mathbb{P}\mathcal{L}^{-1}$. We show this for our running example.

Example 7.3.4. Let $\sigma = [(2,1),2]$ as in Example 7.2.2. We have $d = \sigma_{11} + \sigma_{21} - 1 = 3$, so $\mathbb{P}\mathcal{L}^{-1}$ is a twisted cubic curve in $\mathbb{P}^{14}$. The inverse of $P-\lambda Q$ satisfies the $\binom{6}{2}-3-1 = 11$ linear forms $x_{13}, x_{14}, x_{15}, x_{22}, x_{23}, x_{24}, x_{25}, x_{34}, x_{35}, x_{55}, x_{12}-x_{33}$. The quadratic ideal generators are $u_0u_2 - u_1^2$, $u_0u_3 - u_1u_2$ and $u_1u_3 - u_2^2$, where

$$
\begin{array}{rl}
u_0 =& (a-b)x_{11} - 2x_{12} + (a-b)x_{44} + 2x_{45}, \\
u_1 =& (a^2-ab)x_{11} - (a+b)x_{12} + (ab-b^2)x_{44} + (a+b)x_{45}, \\
u_2 =& (a^3-a^2b)x_{11} - 2abx_{12} + (ab^2-b^3)x_{44} + 2abx_{45}, \\
u_3 =& (a^4-a^3b)x_{11} + (a^3-3a^2b)x_{12} + (ab^3-b^4)x_{44} + (3ab^2-b^3)x_{45}.
\end{array}
$$

Note that $x_{11} = -(\lambda-a)^{-2}$, $x_{12} = (\lambda-a)^{-1}$, $x_{44} = -(\lambda-b)^{-2}$, $x_{45} = (\lambda-b)^{-1}$.

7.4 Maximum likelihood degrees

Let $\mathbb{S}^n_{>0}$ denote the open convex cone of positive definite real symmetric $n \times n$ matrices. For any fixed $S \in \mathbb{S}^n$, we consider the following *log-likelihood function*:

$$
\ell_S : \mathbb{S}^n_{>0} \to \mathbb{R}, \; M \mapsto \log(\det(M)) - \text{trace}(SM).
\tag{7.10}
$$

We seek to compute the critical points of ℓ_S restricted to a smooth subvariety of $\mathbb{S}^n$. Here, by a *critical point* we mean a nonsingular matrix M in the subvariety whose normal space contains the gradient vector of ℓ_S at M. This is an algebraic problem because the $\binom{n+1}{2}$ partial derivatives of ℓ_S are rational functions.

The determinant and the trace of a square matrix are invariant under conjugation. This implies the following identity for all invertible $n \times n$ matrices g:

$$
\ell_{g^{-1}S(g^{-1})^T}(g^TMg) = \log(\det(g^TMg)) - \text{trace}(g^{-1}SMg) = \ell_S(M) + \text{const.}
\tag{7.11}
$$

Let $\mathcal{L}$ be a linear subspace of $\mathbb{S}^n$, and fix a generic matrix $S \in \mathbb{S}^n$. The *ML degree* $\text{mld}(\mathcal{L})$ is the number of complex critical points of ℓ_S on $\mathcal{L}$. The *reciprocal ML degree* $\text{rmld}(\mathcal{L})$ of $\mathcal{L}$

is the number of complex critical points of ℓ_S on $\mathcal{L}^{-1}$. Both ML degrees do not depend on the choice of S, as long as S is generic. The ML degrees are invariant under the action of GL_n by congruence on $\mathbb{S}^n$:

Lemma 7.4.1. *The ML degree and the reciprocal ML degree of a subspace $\mathcal{L} \subset \mathbb{S}^n$ are determined by its congruence class. In particular, this holds for pencils $\mathcal{L}$.*

Proof. Fix g and $\mathcal{L}$. If the matrix S is generic in $\mathbb{S}^n$ then so is $g^{-1}S(g^{-1})^T$. The image of $\mathcal{L}$ under congruence by g^T consists of all matrices $g^T M g$ where $M \in \mathcal{L}$. By (7.11), the likelihood function of S on $\mathcal{L}$ agrees with that of $g^{-1}S(g^{-1})^T$ on $g^T \mathcal{L} g$, up to an additive constant. The two functions have the same number of critical points, so the subspaces $\mathcal{L}$ and $g^T \mathcal{L} g$ have the same ML degree. The same argument works if $\mathcal{L}$ is replaced by any nonlinear variety, such as $\mathcal{L}^{-1}$. $\qquad\square$

We now focus on pencils ($m = 2$), and we state our main result in Section 7.4.

Theorem 7.4.2. *Let $\mathcal{L}$ be a pencil with Segre symbol $\sigma = [\sigma_1, \ldots, \sigma_r]$. Then*

$$\mathrm{mld}(\mathcal{L}) = r - 1 \quad \text{and} \quad \mathrm{rmld}(\mathcal{L}) = \sum_{i=1}^{r} \sigma_{i1} + r - 3 = \deg(\mathcal{L}^{-1}) + \mathrm{mld}(\mathcal{L}) - 1. \qquad (7.12)$$

For generic subspaces $\mathcal{L}$, with Segre symbol $\sigma = [1, \ldots, 1]$, this implies

$$\mathrm{mld}(\mathcal{L}) = \deg(\mathcal{L}^{-1}) = n - 1 \quad \text{and} \quad \mathrm{rmld}(\mathcal{L}) = 2n - 3. \qquad (7.13)$$

The left formula in (7.13) appears in [107, Section 2.2]. The right formula in (7.13) is due to Coons, Marigliano and Ruddy [31]. We here generalize these results to arbitrary pencils $\mathcal{L}$. The proof of Theorem 7.4.2 appears at the end of this section.

The log-likelihood function (7.10) is important in statistics. The sample covariance matrix S encodes data points in $\mathbb{R}^n$. The matrix M is the concentration matrix. Its inverse M^{-1} is the covariance matrix. These represent Gaussian distributions on $\mathbb{R}^n$. The subspace $\mathcal{L}$ encodes linear constraints, either on M or on M^{-1}. For the former, we get the ML degree. For the latter, we get the reciprocal ML degree. These degrees measure the algebraic complexity of maximum likelihood estimation. In the language in [31, 106], $\mathrm{mld}(\mathcal{L})$ refers to the *linear concentration model*, while $\mathrm{rmld}(\mathcal{L})$ refers to the *linear covariance model*.

If $\mathcal{L}$ is a statistical model, then it contains a positive definite matrix. In symbols, $\mathcal{L} \cap \mathbb{S}^n_{>0} \neq \varnothing$. If this holds and $\dim(\mathcal{L}) = 2$ then $\mathcal{L}$ is called a *d-pencil* [112]. Thus, our numbers $\mathrm{mld}(\mathcal{L})$ and $\mathrm{rmld}(\mathcal{L})$ are interesting for statistics when $\mathcal{L}$ is a *d*-pencil. Here, we can take advantage of the following linear algebra fact.

Lemma 7.4.3. *Every d-pencil $\mathcal{L}$ can be simultaneously diagonalized over $\mathbb{R}$. After a change of coordinates, $\mathcal{L}$ is spanned by the quadrics $\sum_{i=1}^{n} a_i x_i^2$ and $\sum_{i=1}^{n} x_i^2$.*

Proof. We assume $n \geq 3$. A pencil is a d-pencil if and only if it has no zeros in the real projective space $\mathbb{P}^{n-1}$. This is the Main Theorem in [112]. It was also proved by Calabi in [22]. The fact that pencils without real zeros in $\mathbb{P}^{n-1}$ can be diagonalized is [112, page 221, (PM)]. It is also Remark 2 in [22, page 846]. $\qquad\square$

Suppose there are r distinct elements in $\{a_1, \ldots, a_n\}$. Theorem 7.4.2 implies:

Corollary 7.4.4. *If $\mathcal{L}$ is a d-pencil then $\mathrm{mld}(\mathcal{L}) = \deg(\mathcal{L}^{-1}) = r - 1$ and $\mathrm{rmld}(\mathcal{L}) = 2r - 3$, where $\mathcal{L}$ has r distinct eigenvalues. This holds for all statistical models.*

The log-likelihood function for our d-pencil $\mathcal{L}$ can be written as follows:

$$\ell_S(x, y) \;=\; \sum_{i=1}^{n} \Big(\log(a_i x + y) - s_i(a_i x + y) \Big).$$

Here $s_1, \ldots, s_n \in \mathbb{R}$ represent data. The MLE is the maximizer of $\ell_S(x, y)$ over the cone $\{(x, y) \in \mathbb{R}^2 : a_i x + y > 0 \text{ for } i = 1, \ldots, n\}$. Corollary 7.4.4 says that $\ell_S(x, y)$ has $r - 1$ critical points. One of them is the MLE. The reciprocal log-likelihood is

$$\tilde{\ell}_S(x, y) \;=\; \sum_{i=1}^{n} \Big(-\log(a_i x + y) - \frac{s_i}{a_i x + y} \Big). \tag{7.14}$$

The invariant $\mathrm{rmld}(\mathcal{L})$ is the number of critical points (x^*, y^*) of this function with $\prod_{i=1}^{n}(a_i x^* + y^*) \neq 0$, provided $s = (s_1, \ldots, s_n)$ is generic in $\mathbb{R}^n$. Corollary 7.4.4 states that $\tilde{\ell}_S(x, y)$ has $2r - 3$ complex critical points. One of them is the MLE.

The following is an extension of a conjecture stated by Coons et al. [31, §6].

Conjecture 7.4.5. *Let $\mathcal{L}$ be a d-pencil with r distinct eigenvalues. There exists $s = (s_1, \ldots, s_n) \in \mathbb{R}^n$ such that the function (7.14) has $2r - 3$ distinct real critical points.*

We can prove this conjecture for small values of n by explicit computation.

Example 7.4.6. Fix the pencil $\mathcal{L}$ with $n = r$ and $(a_1, \ldots, a_n) = (1, \ldots, n)$. For $n \leq 7$ we found $s \in \mathbb{R}^n$ such that the reciprocal log-likelihood function $\tilde{\ell}_s$ has $2n-3$ distinct real critical points. For $n = 7$ we can take $s = \left(-\frac{74}{39}, \frac{13}{47}, \frac{61}{40}, \frac{1}{7}, \frac{23}{18}, -73, -\frac{27}{43} \right)$.

We now return to arbitrary Segre symbols σ. While non-diagonalizable pencils $\mathcal{L}$ do not arise in applied statistics, their likelihood geometry is interesting.

Proof of Theorem 7.4.2. By Lemma 7.4.1, we may assume that $\mathcal{L}$ is parametrized by $(x, y) \mapsto xP - yQ$ with P and Q as in (7.4). For generic $S \in \mathbb{S}^n$, we seek the number $\mathrm{mld}(\mathcal{L})$ of critical points in $\mathbb{C}^2$ of the following function in two variables:

$$\ell_S(x, y) \;=\; \log(\det(xP - yQ)) - \mathrm{trace}(S(xP - yQ)). \tag{7.15}$$

After multiplying by $d = \prod_{i=1}^{r}(\alpha_i x - y)$, the two partial derivatives of $\ell_S(x, y)$ have the form $f(x, y) = \lambda_S d + C$ and $g(x, y) = \mu_S d + D$. Here $\lambda_S = -\text{trace}(SP)$ and $\mu_S = \text{trace}(SQ)$ are constants, and the following are binary forms of degree $r - 1$:

$$C = \sum_{i=1}^{r}\sum_{j=1}^{n}\sigma_{ij}\,\alpha_i \prod_{k=1,k\neq i}^{r}(\alpha_k x - y) \quad \text{and} \quad D = -\sum_{i=1}^{r}\sum_{j=1}^{n}\sigma_{ij} \prod_{k=1,k\neq i}^{r}(\alpha_k x - y). \tag{7.16}$$

The variety of critical points of ℓ_S in $\mathbb{C}^2$ is $V(f, g) \backslash V(d)$. We adapt the method introduced in [31] to enumerate this set. Let $F(x, y, z)$ and $G(x, y, z)$ denote the homogenizations of f and g with respect to z. Both F and G define curves of degree r in $\mathbb{P}^2$. Since F and G do not share a common component, we can apply Bézout's Theorem to count their intersection points. This tells us that

$$\text{mld}(\mathcal{L}) = r^2 - I_{[0:0:1]}(F, G) - \sum_{q \in V(F,G,z)} I_q(F, G). \tag{7.17}$$

The negated expressions are the intersection multiplicities of F and G at the origin and on the line at infinity. By computing these two quantities, we obtain

$$\text{mld}(\mathcal{L}) = r^2 - (r-1)^2 - r = r - 1.$$

The proof of the second formula in (7.12) is analogous but the details are more delicate. We present an outline. The log-likelihood function for $\mathcal{L}^{-1}$ equals

$$\tilde{\ell}_S(x, y) = -\log\Big(\prod_{i=1}^{r}(\alpha_i x - y)^{\sigma_{i1}+\dots+\sigma_{in}}\Big) - \sum_{i=1}^{r}\sum_{j=1}^{\sigma_{i1}}\tilde{s}_{ij}\frac{x^{j-1}}{(\alpha_i x - y)^j},$$

where the $\tilde{s}_{ij}$ are linear combinations of the entries in the matrix S. This is obtained by replacing the matrix $xP - yQ$ in (7.15) with its inverse. We find

$$\begin{aligned}
\tilde{\ell}_{S_x} &= -\sum_{i=1}^{r}\sum_{j=1}^{n}\frac{\sigma_{ij}\alpha_i}{\alpha_i x - y} + \sum_{i=1}^{r}\sum_{j=1}^{\sigma_{i1}}\tilde{s}_{ij}\frac{(j-1)x^{j-2}(\alpha_i x - y) - j\,x^{j-1}\alpha_i}{(\alpha_i x - y)^{j+1}}, \\
\tilde{\ell}_{S_y} &= \sum_{i=1}^{r}\sum_{j=1}^{n}\frac{\sigma_{ij}}{\alpha_i x - y} + \sum_{i=1}^{r}\sum_{j=1}^{\sigma_{i1}}\tilde{s}_{ij}\frac{j\,x^{j-1}}{(\alpha_i x - y)^{j+1}}.
\end{aligned} \tag{7.18}$$

We claim that the number of common zeros of the two partial derivatives $\tilde{\ell}_{S_x}$ and $\tilde{\ell}_{S_y}$ in $\mathbb{C}^2 \backslash V(d)$ is equal to $\varphi + r - 3$ where $\varphi = \sum_{i=1}^{r}\sigma_{i1} = \deg(\mathcal{L}^{-1}) + 1$,

Clearing denominators in (7.18) yields polynomials $-d'C + U$ and $-d'D + V$, where $d' = \prod_{i=1}^{r}(\alpha_i x - y)^{\sigma_{i1}}$, the binary forms U, V have degree $\varphi + r - 2$, and C, D are precisely as in (7.16). Hence $\deg(d') = \varphi$ and $\deg(C) = \deg(D) = r - 1$. As before, these are sums of binary forms in consecutive degrees. We use (7.17) to count their zeros in $\mathbb{P}^2$. We find $(\varphi + r - 1)^2 - (\varphi + r - 2)^2 - (\varphi + r) = \varphi + r - 3$ $\qquad\square$

Example 7.4.7 ($n = 5$). Let $\sigma = [(2,1),2]$ as in Example 7.2.2. The ML degrees are $\mathrm{mld}(\mathcal{L}) = 1$ and $\mathrm{rmld}(\mathcal{L}) = 3$. Restricting the log-likelihood function to $\mathcal{L}$ gives

$$\ell_S = \log\big((ax-y)^3(bx-y)^2\big) + 2s_{12}(ax-y) + s_{22}x + s_{33}(ax-y) + 2s_{45}(bx-y) + s_{55}x.$$

Its two partial derivatives are rational functions in x and y. Equating these to zero, we find that ℓ_S has a unique critical point (x^*, y^*) in $\mathcal{L}$. Its coordinates are

$$
\begin{aligned}
x^* &= \big(4(a-b)s_{12} + 5s_{22} + 2(a-b)s_{33} - 6(b-a)s_{45} + 5s_{55}\big)/\Delta, \\
y^* &= \big(4a(a-b)s_{12} + (2a+3b)s_{22} + 2a(a-b)s_{33} + 6b(b-a)s_{45} + (2a+3b)s_{55}\big)/\Delta, \\
\Delta &= \big(-s_{22} + 2(a-b)s_{45} - s_{55}\big) \cdot \big(2(a-b)s_{12} + s_{22} + (a-b)s_{33} + s_{55}\big).
\end{aligned}
$$

The restriction of the log-likelihood function to the reciprocal variety $\mathcal{L}^{-1}$ is

$$\tilde{\ell}_S(x,y) = -\log\big((ax-y)^3(bx-y)^2\big) - \frac{s_{11}\,x}{(ax-y)^2} + \frac{2\,s_{12}}{ax-y} + \frac{s_{33}}{ax-y} - \frac{s_{44}\,x}{(bx-y)^2} + \frac{2\,s_{45}}{bx-y}.$$

The two partial derivatives have 3 zeros, expressible in radicals in $a, b, s_{11}, \ldots, s_{45}$.

7.5 Strata in the Grassmannian

We now define a partial order on the set Segre_n of all Segre symbols for fixed n. If σ and τ are in Segre_n then we say that σ *is above* τ if $|\sigma| > |\tau|$ and τ is obtained from σ by replacing two partitions σ_i, σ_j by their sum, or if $|\sigma| = |\tau|$ and σ and τ differ in precisely one partition, with index i, and $\tau_i \lhd \sigma_i$ in the dominance order on partitions. The partial order on Segre_n is the transitive closure of the relation "is above". The top element of our poset is $[1, 1, \ldots, 1]$, and the bottom element is $[(2, 1, \ldots, 1)]$. The Hasse diagrams for $n = 3, 4$ are shown in Figure 7.1.

We wish to study the strata Gr_σ in (7.1). Recall that Gr_σ is the constructible subset of $\mathrm{Gr}(2, \mathbb{S}^n)$ whose points are the pencils $\mathcal{L}$ with $\sigma(\mathcal{L}) = \sigma$. Its closure $\overline{\mathrm{Gr}}_\sigma$ is a subvariety of the Grassmannian $\mathrm{Gr}(2, \mathbb{S}^n)$. Its defining equations can be written either in the $\frac{1}{8}(n+2)(n+1)n(n-1)$ Plücker coordinates, or in the $(n+1)n$ Stiefel coordinates which are the matrix entries in a basis $\{A, B\}$ of $\mathcal{L}$.

Consider the related *Jordan stratification*. For each $\sigma \in \mathrm{Segre}_n$, the Jordan stratum Jo_σ is the set of $n \times n$ matrices whose Jordan canonical form has pattern σ. Its closure $\overline{\mathrm{Jo}}_\sigma$ is an affine variety in $\mathbb{C}^{n \times n}$. Its defining prime ideal consists of homogeneous polynomials in the entries of an $n \times n$ matrix $X = (x_{ij})$.

Theorem 7.5.1. *Our poset models inclusions of both Grassmann strata and Jordan strata. That is, $\sigma \geq \tau$ in Segre_n if and only if $\overline{\mathrm{Gr}}_\sigma \supseteq \overline{\mathrm{Gr}}_\tau$ if and only if $\overline{\mathrm{Jo}}_\sigma \supseteq \overline{\mathrm{Jo}}_\tau$.*

The codimensions of the Jordan strata generally differ from those of the Grassmann strata. While the $\overline{\mathrm{Jo}}_\sigma$ are familiar from linear algebra [34], the $\overline{\mathrm{Gr}}_\sigma$ capture the geometry of the varieties listed on the right in Examples 7.1.3 and 7.3.1. The codimensions are ≥ 1, unless $\sigma = [1, \ldots, 1]$ where both strata are dense.

$$[1,1,1,1]$$
$$|$$
$$[2,1,1]$$

$$[1,1,1] \quad\quad [(1,1),1,1] \quad [3,1] \quad\quad [2,2]$$
$$| \quad\quad\quad\quad\quad\quad | \quad\quad\quad\quad\quad\quad |$$
$$[2,1] \quad\quad\quad [(2,1),1] \quad\quad [4] \quad\quad [2,(1,1)]$$
$$[3] \quad [(1,1),1]$$
$$\quad\quad\quad\quad\quad\quad\quad [(3,1)] \quad [(1,1),(1,1)]$$
$$[(2,1)]$$

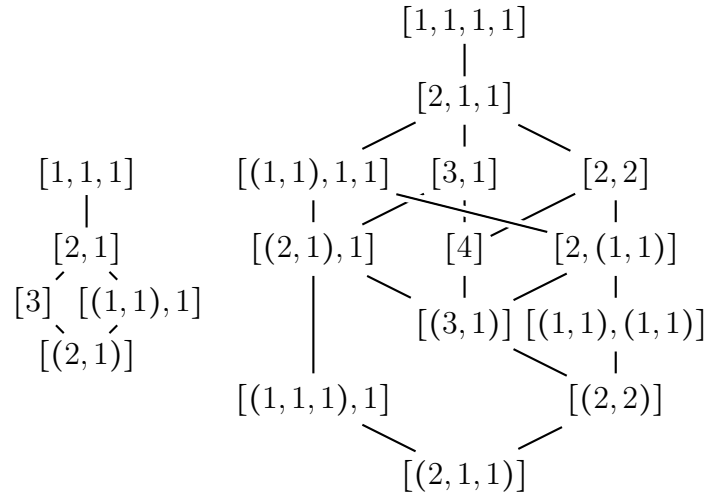$$[(1,1,1),1] \quad\quad\quad\quad [(2,2)]$$

$$[(2,1,1)]$$

Figure 7.1: The posets of all Segre symbols for $n = 3$ (left) and $n = 4$ (right).

Example 7.5.2 ($n = 3$). We computed the prime ideals for the Jordan strata in $\mathbb{C}^{3\times3}$, for the Plücker strata in $\mathrm{Gr}(2, \mathbb{S}^3) \subset \mathbb{P}^{14}$, and for the Stiefel strata in $\mathbb{P}^5 \times \mathbb{P}^5$:

symbol	Jordan	Plücker	Stiefel	codims	degrees
$[2,1]$	6_1	6_1	$(6,6)_1$	$1,1,1$	$6,6,[6,6]$
$[3]$	$2_1, 3_1$	4_{21}	$(2,4)_1, (3,3)_1, (4,2)_1$	$2,2,2$	$6,99,[6,15,6]$
$[(1,1),1]$	3_{20}	3_{20}	$(3,3)_{20}$	$3,2,2$	$6,36,[4,4,4]$
$[(2,1)]$	2_9	2_6	$(2,2)_6$	$4,3,3$	$6,56,[4,12,12,4]$

The sextic in the first row is the discriminant of the characteristic polynomial of X. We shall explain the last row, indexed by $\sigma = [(2,1)]$. The Jordan stratum Jo_σ has codimension 4 and degree 6. Its ideal is generated by nine quadrics, like $x_{11}x_{31} - 2x_{22}x_{31} + 3x_{21}x_{32} + x_{31}x_{33}$. Under the substitution $X = AB^{-1}$, these transform into six quadrics in Plücker coordinates, like $p_{04}p_{14} + p_{12}p_{14} - p_{03}p_{15} - p_{12}p_{23} - 3p_{02}p_{34} + 2p_{01}p_{35}$. Here $p_{01}, p_{02}, \ldots, p_{45}$ denote the 2×2 minors of

$$\begin{pmatrix} a_{11} & a_{12} & a_{13} & a_{22} & a_{23} & a_{33} \\ b_{11} & b_{12} & b_{13} & b_{22} & b_{23} & b_{33} \end{pmatrix}.$$

The stratum Gr_σ has codimension 3 in $\mathrm{Gr}(2, \mathbb{S}^3)$ and degree 56 in the ambient $\mathbb{P}^{14}$. The six Plücker quadrics give six polynomials of bidegree $(2, 2)$ in (A, B). These define a variety of multidegree $4a^3 + 12a^2b + 12ab^2 + 4b^3 \in H^*(\mathbb{P}^5 \times \mathbb{P}^5)$.

Example 7.5.3 ($n = 4$). The column "codims" in Example 7.3.1 gives the codimensions of Jordan strata, Plücker strata and Stiefel strata. The last two agree; they quantify the moduli of quartic curves in $\mathbb{P}^3$ listed on the right. We found equations of low degree for the 13 strata. For instance, $\mathrm{Jo}_{[4]}$ lies on a unique quadric:

$$3x_{11}^2 - 2x_{11}x_{22} - 2x_{11}x_{33} - 2x_{11}x_{44} + 8x_{12}x_{21} + 8x_{13}x_{31} + 8x_{14}x_{41} + 3x_{22}^2$$
$$-2x_{22}x_{33} - 2x_{22}x_{44} + 8x_{23}x_{32} + 8x_{24}x_{42} + 3x_{33}^2 - 2x_{33}x_{44} + 8x_{34}x_{43} + 3x_{44}^2.$$

Proof of Theorem 7.5.1. For Segre symbols σ with one partition σ_1, the Jordan strata Jo_σ are the *nilpotent orbits* of Lie type A_{n-1}. Gerstenhaber's Theorem [58] states that inclusion of nilpotent orbit closures corresponds to the dominance order $\triangleleft$ among the partitions σ_1. This explains the second condition in our definition of "is above" for the poset Segre_n. The other condition captures the degeneration that occurs when two eigenvalues come together. Generally, this leads to a fusion of Jordan blocks, made manifest by adding partitions σ_i and σ_j. For a precise algebraic version of this argument we refer to [58, Theorem 4].

The inclusions of orbit closures are preserved under the map $X \mapsto AB^{-1}$ that links Stiefel strata to Jordan strata. Furthermore, the Plücker stratification is obtained from the Stiefel stratification by taking the quotient modulo GL_2. This operation also preserves the combinatorics of orbit closure inclusions. $\square$

We close with formulas for the dimensions of our strata. For each partition σ_i occurring in a Segre symbol $\sigma = [\sigma_1, \ldots, \sigma_r]$, we write $\sigma_i^* = (\sigma_{i1}^*, \ldots, \sigma_{in}^*)$ for the conjugate partition. For instance, if $n = 5$ and $\sigma_i = (4, 1)$ then $\sigma_i^* = (2, 1, 1, 1)$.

Proposition 7.5.4. *The codimension of the Jordan strata and Grassmann strata are:*

$$\mathrm{codim}(\mathrm{Jo}_\sigma) \;=\; \sum_{i=1}^{r}\sum_{j=1}^{n}(\sigma_{ij}^*)^2 \;-\; r \quad \text{and} \quad \mathrm{codim}(\mathrm{Gr}_\sigma) \;=\; \sum_{i=1}^{r}\sum_{j=1}^{n}\binom{\sigma_{ij}^* + 1}{2} \;-\; r.$$

Proof. The dimension is the number r of distinct eigenvalues plus the dimension of the GL_n-orbit of the general matrix or pencil in the stratum of interest. Thus, the codimension is the dimension of its stabilizer subgroup minus r. The codimension for Grassmann strata agrees with the codimension for Stiefel strata, so we may consider pairs of matrices (A, B) when determining $\mathrm{codim}(\mathrm{Gr}_\sigma)$.

The stabilizer on the left is found in [34, Theorem 2.1] or [58, Proposition 8], using the identity $\sum_{k=1}^{s}(2k-1) = s^2$. The stabilizer dimension on the right is calculated in [35, Corollary 2.2] for general symmetric matrix pencils. For regular pencils, the case studied here, the Kronecker canonical form in [35, eqn. (2.4)] only has H-components. Thus the dimension formula in [35] becomes $d_{A,B} = d_H + d_{HH}$, where $d_H = 0$ and $d_{HH} = \sum_{i \le i', \lambda_i = \lambda_{i'}} \min(h_i, h_{i'})$. In our notation, this is

$$\sum_{i \le k, \alpha_i = \alpha_k} \min(e_i, e_k) \;=\; \sum_{i=1}^{r}\sum_{k=1}^{n} k\sigma_{ik} \;=\; \sum_{i=1}^{r}\sum_{k=1}^{n}\sum_{j=1}^{\sigma_{ik}} k \;=\; \sum_{i=1}^{r}\sum_{j=1}^{n}\sum_{k=1}^{\sigma_{ij}^*} k \;=\; \sum_{i=1}^{r}\sum_{j=1}^{n}\binom{\sigma_{ij}^* + 1}{2}.$$

In conclusion, our proof consists of specific pointers to the articles [37, 35, 58]. $\square$

Concluding remarks

Revisiting classical concepts with a fresh lens can lead to unexpectedly interesting new ideas. In this chapter, we showed how pencils of quadrics, originating in the 19th century, can serve as linear Gaussian or concentration models in the realm of the relatively new field of algebraic statistics. More generally, old ideas can take on new lives when repositioned in the context of newer fields.

Bibliography

[1] Simonetta Abenda and Petr G Grinevich. "Rational Degenerations of M -Curves, Totally Positive Grassmannians and KP2-Solitons". *Communications in Mathematical Physics* 361.3 (2018), pp. 1029–1081.

[2] Daniele Agostini, Türkü Özlüm Çelik, and Demir Eken. "Numerical Reconstruction of Curves from their Jacobians". *Arithmetic, Geometry, Cryptography and Coding Theory, AMS Contemporary Mathematics*. 2021.

[3] Daniele Agostini, Türkü Özlüm Çelik, and John B Little. "On Algebraic Theta Divisors and Rational Solutions of the KP Equation". *arXiv:2112.03147* (2021).

[4] Daniele Agostini, Türkü Özlüm Çelik, Julia Struwe, and Bernd Sturmfels. "Theta Surfaces". *Vietnam Journal of Mathematics* (2020).

[5] Daniele Agostini, Türkü Özlüm Çelik, and Bernd Sturmfels. "The Dubrovin threefold of an algebraic curve". *Nonlinearity* 34.6 (2021), pp. 3783–3812.

[6] Daniele Agostini and Lynn Chua. "Computing theta functions with Julia". *Journal of Software for Algebra and Geometry* 11.1 (2022), pp. 41–51.

[7] Daniele Agostini, Claudia Fevola, Yelena Mandelshtam, and Bernd Sturmfels. "KP solitons from tropical limits". *Journal of Symbolic Computation* 114 (2023), pp. 282–301.

[8] Enrico Arbarello. *Geometry of Algebraic Curves-Volume I*. 1994.

[9] Enrico Arbarello and Corrado De Concini. "On a set of equations characterizing Riemann matrices". *Annals of Mathematics* (1984), pp. 119–140.

[10] Nima Arkani-Hamed, Yuntao Bai, and Thomas Lam. "Positive geometries and canonical forms". *Journal of High Energy Physics* 2017.11 (2017), pp. 1–124.

[11] Nima Arkani-Hamed and Jaroslav Trnka. "The Amplituhedron". *Journal of High Energy Physics* 10 (2014), p. 33.

[12] Anders Björner, Michel Las Vergnas, Bernd Sturmfels, Neil White, and Gunter M Ziegler. *Oriented Matroids*. 2nd ed. Encyclopedia of Mathematics and its Applications. Cambridge University Press, 1999.

[13] Grigoriy Blekherman, Pablo A Parrilo, and Rekha R Thomas. *Semidefinite Optimization and Convex Alegbraic Geometry*. Vol. 13. MOS-SIAM Series on Optimization. SIAM, 2012.

[14] Alexander Bobenko and Ulrike Bücking. "Convergence of Discrete Period Matrices and Discrete Holomorphic Integrals for Ramified Coverings of the Riemann Sphere". *Mathematical Physics, Analysis and Geometry* 24.23 (2021).

[15] Alexander Bobenko and Mikhail Skopenkov. "Discrete Riemann surfaces: linear discretization and its convergence". *Journal für die reine und angewandte Mathematik (Crelles Journal)* 2016.720 (2016), pp. 217–250.

[16] Alexander I Bobenko and Felix Günther. "Discrete complex analysis on planar quad-graphs". *Advances in Discrete Differential Geometry*. Springer Berlin Heidelberg, 2016, pp. 57–132.

[17] Alexander I Bobenko and Felix Günther. "Discrete Riemann surfaces based on quadrilateral cellular decompositions". *Advances in Mathematics* 311 (2017), pp. 885–932. ISSN: 0001-8708.

[18] Alexander I Bobenko, Christian Mercat, and Markus Schmies. "Period matrices of polyhedral surfaces". *Computational Approach to Riemann Surfaces*. Berlin, Heidelberg: Springer Berlin Heidelberg, 2011, pp. 213–226.

[19] Barbara Bolognese, Madeline Brandt, and Lynn Chua. "From curves to tropical Jacobians and back". *Combinatorial Algebraic Geometry: Selected Papers From the 2016 Apprenticeship Program* (2017), pp. 21–45.

[20] Jean-Benoît Bost. "Introduction to compact Riemann surfaces, Jacobians, and Abelian varieties". *From Number Theory to Physics*. Springer Berlin, 1992, pp. 64–211.

[21] Madeline Brandt. "Tropical Geometry of Curves". *PhD dissertation, UC Berkeley* (2020).

[22] Eugenio Calabi. "Linear systems of real quadratic forms". *Proceedings of the American Mathematical Society* 15.5 (1964), pp. 844–846.

[23] Lucia Caporaso and Edoardo Sernesi. "Characterizing curves by their odd theta-characteristics". *Journal für die reine und angewandte Mathematik* 2003.562 (2003), pp. 101–135.

[24] Arthur Cayley. "Recherches sur les Matrices dont les termes sont des fonctions linéares d'une seule indéterminée." (1855).

[25] Türkü Özlüm Çelik. "Thomae-Weber Formula: Algebraic Computations of Theta Constants". *International Mathematics Research Notices* 2021.23 (Dec. 2019), pp. 17798–17822.

[26] Türkü Özlüm Çelik, Samantha Fairchild, and Yelena Mandelshtam. "Crossing the transcendental divide: from translation surfaces to algebraic curves". *Experimental Mathematics* (2023), pp. 1–19.

[27] Türkü Özlüm Çelik, Avinash Kulkarni, Yue Ren, and Mahsa Sayyary Namin. "Tritangents and their space sextics". *Journal of Algebra* 538 (2019), pp. 290–311.

[28] Türkü Özlüm Çelik and David Lehavi. "Reconstruction of curves from their theta hyperplanes in genera 6 and 7". *arXiv:2401.02235* (2024).

[29] Melody Chan. "Combinatorics of the tropical Torelli map". *Algebra & Number Theory* 6.6 (2012), pp. 1133–1169.

[30] Lynn Chua, Mario Kummer, and Bernd Sturmfels. "Schottky algorithms: Classical meets tropical". *Mathematics of Computation* 88.319 (2018), pp. 2541–2558.

[31] Jane Ivy Coons, Orlando Marigliano, and Michael Ruddy. "Maximum likelihood degree of the two-dimensional linear Gaussian covariance model". *Algebraic Statistics* 11.2 (2020), pp. 107–123.

[32] Bernard Deconinck, Matthias Heil, Alexander Bobenko, Mark van Hoeij, and Marcus Schmies. "Computing Riemann theta functions". *Mathematics of Computation* 73 (2004), pp. 1417–1442.

[33] Bernard Deconinck and Mark van Hoeij. "Computing Riemann matrices of algebraic curves". *Physica D: Nonlinear Phenomena* 152-153 (2001). Advances in Nonlinear Mathematics and Science: A Special Issue to Honor Vladimir Zakharov, pp. 28–46.

[34] James W Demmel and Alan Edelman. "The dimension of matrices (matrix pencils) with given Jordan (Kronecker) canonical forms". *Linear algebra and its applications* 230 (1995), pp. 61–87.

[35] Andrii Dmytryshyn, Bo Kagstrom, and Vladimir Sergeichuk. "Symmetric matrix pencils: Codimension counts and the solution of a pair of matrix equations". *The Electronic Journal of Linear Algebra* 27 (2014), pp. 1–18.

[36] Igor V Dolgachev. *Classical algebraic geometry: a modern view.* Cambridge University Press, 2012.

[37] Jan Draisma and Rob H Eggermont. "Plücker varieties and higher secants of Sato's Grassmannian". *Journal für die reine und angewandte Mathematik (Crelles Journal)* 2018.737 (2018), pp. 189–215.

[38] Boris A Dubrovin. "Theta functions and non-linear equations". *Russian Mathematical Surveys* 36.2 (1981), pp. 11–92.

[39] Eduard Duryev and Leonid Monin. "Eigenforms of hyperelliptic curves with many automorphisms". *arXiv:2104.08920* (2021).

[40] Mathieu Dutour. "The six-dimensional Delaunay polytopes". *European Journal of Combinatorics* 25.4 (2004), pp. 535–548.

[41] R. M. Erdahl and S. S. Ryshkov. "The Empty Sphere". *Canadian Journal of Mathematics* 39.4 (1987), pp. 794–824.

[42] Chaim Even-Zohar, Tsviqa Lakrec, and Ran J Tessler. "The BCFW tiling of the amplituhedron". *Sém. Lothar. Combin. B* 89 (2023).

[43] Hershel M Farkas, Samuel Grushevsky, and Riccardo Salvati Manni. "An explicit solution to the weak Schottky problem". *Physica D: Nonlinear Phenomena* 8.3 (2021), pp. 358–373.

[44] Claudia Fevola and Christiane Görgen. "The mathematical research-data repository MathRepo". *arXiv:2202.04022* (2022).

[45] Claudia Fevola and Yelena Mandelshtam. "Hirota varieties and rational nodal curves". *Journal of Symbolic Computation* 120 (2024), p. 102239.

[46] Claudia Fevola, Yelena Mandelshtam, and Bernd Sturmfels. "Pencils of quadrics: old and new". *Le Matematiche* 76.2 (2021), pp. 319–335.

[47] Lukas Finschi. "A Graph Theoretical Approach for Reconstruction and Generation of Oriented Matroids". PhD thesis. Swiss Federal Institute of Technology Zürich, 2001.

[48] Lukas Finschi. *Homepage of Oriented Matroids.* https://finschi.com/math/om/?p=home.

[49] Jon Folkman and Jim Lawrence. "Oriented matroids". *Journal of Combinatorial Theory, Series B* 25.2 (1978), pp. 199–236.

[50] Jörg Frauendiener, Carine Jaber, and Christian Klein. "Efficient computation of multidimensional theta functions". *Journal of Geometry and Physics* 141 (2019), pp. 147–158.

[51] Komei Fukuda, Hiroyuki Miyata, and Sonoko Moriyama. "Complete enumeration of small realizable oriented matroids". *Discrete & Computational Geometry* 49 (2013), pp. 359–381.

[52] Pavel Galashin and Thomas Lam. "Parity duality for the amplituhedron". *Compositio Mathematica* 156.11 (2020), pp. 2207–2262.

[53] Pavel Galashin and Pavlo Pylyavskyy. "Ising model and the positive orthogonal grassmannian". *Duke Mathematical Journal* 169.10 (2020), pp. 1877–1942.

[54] Sohrab Ganjian and Nils Bruin. *RiemannTheta: A SageMath package for evaluating Riemann theta functions.* 2021. URL: https://github.com/nbruin/RiemannTheta.

[55] Felix R Gantmacher and Mark G Krein. "Oscillyacionye matricy i yadra i malye kolebaniya mehaniceskih sistem". *Gosudarstv. Isdat. Tehn.-Teor. Lit.* (1950).

[56] Bert van Geemen. "Some equations for the universal Kummer variety". *Transactions of the American Mathematical Society* 368.1 (2016), pp. 209–225.

[57] Bert van Geemen. "The Schottky problem and second order theta functions". *Workshop on Abelian Varieties and Theta Functions (Spanish)(Morelia, 1996)*. Citeseer. 1998, pp. 41–84.

[58] Murray Gerstenhaber. "On dominance and varieties of commuting matrices". *Annals of mathematics* (1961), pp. 324–348.

[59] D. Grayson and M. Stillman. "Macaulay2, a software system for research in algebraic geometry". *available at http://www.math.uiuc.edu/Macaulay2/* ().

[60] Phillip Griffiths and Joseph Harris. *Principles of algebraic geometry.* Pure and Applied Mathematics. Wiley-Interscience [John Wiley & Sons], New York, 1978, pp. xii+813. ISBN: 0-471-32792-1.

[61] Samuel Grushevsky. "The Schottky problem". *Current Developments in Algebraic Geometry.* MSRI Publications 59. Cambridge University Press, 2012, pp. 129–164.

[62] Jordi Guàrdia. "Jacobian Nullwerte and algebraic equations". *Journal of Algebra* 253 (2002), pp. 112–132.

[63] Jordi Guàrdia. "On the Torelli problem and Jacobian Nullwerte in genus three". *Michigan Mathematical Journal* 60.1 (2011), pp. 51–65.

[64] F. Hess. "Computing Riemann–Roch Spaces in Algebraic Function Fields and Related Topics". *Journal of Symbolic Computation* 33.4 (2002), pp. 425–445.

[65] William Vallance Douglas Hodge and Daniel Pedoe. *Methods of Algebraic Geometry.* Vol. 2. Cambridge University Press, 1994.

[66] Yu-tin Huang and CongKao Wen. "ABJM amplitudes and the positive orthogonal grassmannian". *Journal of High Energy Physics* 2014.2 (2014), pp. 1–51.

[67] Yu-Tin Huang, CongKao Wen, and Dan Xie. "The positive orthogonal Grassmannian and loop amplitudes of ABJM". *Journal of Physics A: Mathematical and Theoretical* 47.47 (2014), p. 474008.

[68] Jun-ichi Igusa. "On the irreducibility of Schottky's divisor". *Journal of the Faculty of Science, the University of Tokyo. Sect. 1 A, Mathematics* 28 (1982), pp. 531–545.

[69] Philipp Jell. "Constructing smooth and fully faithful tropicalizations for Mumford curves". *Selecta Mathematica* 26.4 (2020).

[70] Steven N Karp. "Sign variation, the Grassmannian, and total positivity". *Journal of Combinatorial Theory, Series A* 145 (2017), pp. 308–339.

[71] Steven N Karp and John Machacek. "Shelling the $m = 1$ amplituhedron". *arXiv:2104.02786* (2021).

[72] Steven N Karp and Lauren K Williams. "The $m = 1$ Amplituhedron and Cyclic Hyperplane Arrangements". *International Mathematics Research Notices* 2019.5 (2019), pp. 1401–1462.

[73] Kiumars Kaveh and Christopher Manon. "Khovanskii Bases, Higher Rank Valuations, and Tropical Geometry". *SIAM Journal on Applied Algebra and Geometry* 3.2 (2019), pp. 292–336.

[74] Yuji Kodama. "KP Solitons and the Grassmannians. Combinatorics and Geometry and Two-dimensional Wave Patterns". *SpringerBriefs in Mathematical Physics* 22 (2017).

[75] Yuji Kodama. "Young diagrams and N-soliton solutions of the KP equation". *Journal of Physics A: Mathematical and General* 37.46 (2004), p. 11169.

[76] Yuji Kodama and Yuancheng Xie. "Space Curves and Solitons of the KP Hierarchy. I. The l-th Generalized KdV Hierarchy". *Symmetry, Integrability and Geometry: Methods and Applications* (2021).

[77] Maxim Kontsevich and Anton Zorich. "Connected components of the moduli spaces of Abelian differentials with prescribed singularities". *Invent. Math.* 153.3 (2003), pp. 631–678. ISSN: 0020-9910.

[78] Igor Krichever. "Methods of Algebraic Geometry in the Theory of Non-linear Equations". *Russian Mathematical Surveys* 32.6 (Oct. 1977), pp. 185–213.

[79] Igor Krichever and Takahiro Shiota. "Soliton Equations and the Riemann–Schottky Problem. Handbook of Moduli, Vol. II, 205–258, Adv. Lect. Math.(ALM), 25". *Int. Press, Somerville* (2013).

[80] Thomas Lam. Personal communication. 2023.

[81] Thomas Lam. "Totally nonnegative Grassmannian and Grassmann polytopes". *Current developments in mathematics 2014*. Int. Press, Somerville, MA, 2016, pp. 51–152.

[82] David Lehavi. "Effective Reconstruction of Generic Genus 4 Curves from Their Theta Hyperplanes". *International Mathematics Research Notices* 2015.19 (2015), pp. 9472–9485.

[83] David Lehavi. "Effective Reconstruction of Generic Genus 5 Curves from their Theta Hyperplanes". *Experimental Mathematics* 0.0 (2022), pp. 1–15.

[84] Tomasz Lukowski, Matteo Parisi, and Lauren K Williams. "The Positive Tropical Grassmannian, the Hypersimplex, and the $m = 2$ Amplituhedron". *International Mathematics Research Notices* (Mar. 2023).

[85] Yelena Mandelshtam, Dmitrii Pavlov, and Elizabeth Pratt. "Combinatorics of $m = 1$ Grasstopes". *arXiv:2307.09603* (2023).

[86] Daniel Massart. "A short introduction to translation surfaces, Veech surfaces, and Teichmüller dynamics". *Surveys in geometry I*. Springer, Cham, 2022, pp. 343–388.

[87] Christian Mercat. "Discrete Riemann Surfaces and the Ising model". *Communications in Mathematical Physics* 218.1 (Apr. 2001), pp. 177–216.

[88] Mateusz Michalek and Bernd Sturmfels. *Invitation to Nonlinear Algebra*. Vol. 211. Graduate Studies in Mathematics. American Mathematical Society, 2021.

[89] David Mumford. *Tata Lectures on Theta I*. Boston: Birkhäuser, 2007.

[90] Atsushi Nakayashiki. "Degeneration of trigonal curves and solutions of the KP-hierarchy". *Nonlinearity* 31.8 (2018), pp. 3567–3590.

[91] Atsushi Nakayashiki. "On Reducible Degeneration of Hyperelliptic Curves and Soliton Solutions". *Symmetry, Integrability and Geometry: Methods and Applications* (2019).

[92] Matteo Parisi, Melissa Sherman-Bennett, and Lauren K Williams. "The $m = 2$ amplituhedron and the hypersimplex: signs, clusters, triangulations, Eulerian numbers". *arXiv:2104.08254* (2021).

[93] Alexander Postnikov. "Total Positivity, Grassmannians, and Networks". *arXiv:0609764* (2006).

[94] Bernard Riemann. *Zur Theorie der Abelschen Funktionen für den Fall p = 3*. Leipzig: Gesammelte mathematische Werke und wissenschaftlicher Nachlass, Teubner, 1876.

[95] Oliver Rodriguez. "On the Teichmüller geodesic generated by the L-shaped translation surface tiled by three squares". *Revista de la Real Academia de Ciencias Exactas, Fisicas y Naturales. Serie A. Matematicas* 107 (2013), pp. 391–417.

[96] Jean-Pierre Roudneff and Bernd Sturmfels. "Simplicial cells in arrangements and mutations of oriented matroids". *Geometriae Dedicata* 27.2 (Aug. 1988).

[97] Simon Rubinstein-Salzedo. "Period computations for covers of elliptic curves". *Mathematics of Computation* 83.289 (2014), pp. 2455–2470.

[98] SageMath developers. *SageMath class: "Hyperelliptic curves of genus 2 over a general ring"*. URL: https://www.sagemath.org.

[99] Mikio Sato. "Soliton Equations as Dynamical Systems on Infinite Dimensional Grassmann Manifold". *Nonlinear Partial Differential Equations in Applied Science; Proceedings of The U.S.-Japan Seminar, Tokyo, 1982 North-Holland Mathematics Studies* (1982), pp. 259–271.

[100] Takahiro Shiota. "Characterization of Jacobian varieties in terms of soliton equations". *Inventiones mathematicae* 83.2 (1986), pp. 333–382.

[101] Robert Silhol. "Genus 2 translation surfaces with an order 4 automorphism". *The Geometry of Riemann Surfaces and Abelian Varieties: III Iberoamerican Congress on Geometry in Honor of Professor Sevin Recillas-Pishmish's 60th Birthday, June 8-12, 2004, Salamanca, Spain*. Vol. 397. American Mathematical Soc. 2006, p. 207.

[102] Stanislav Smirnov. "Discrete complex analysis and probability". *Proceedings of the International Congress of Mathematicians 2010 (ICM 2010)*. New Delhi, India, 2010, pp. 595–621.

[103] Richard P. Stanley. *Enumerative combinatorics. Volume 2*. Cambridge University Press, 2001.

[104] Bernd Sturmfels. "Gröbner Bases and Convex Polytopes". *American Mathematical Society, University Lecture Series, No 8* (1996).

[105]   Bernd Sturmfels. "Totally positive matrices and cyclic polytopes". *Linear Algebra and its Applications* 107 (1988), pp. 275–281.

[106]   Bernd Sturmfels, Sascha Timme, and Piotr Zwiernik. "Estimating linear covariance models with numerical nonlinear algebra". *Algebraic Statistics* 11.1 (2020), pp. 31–52.

[107]   Bernd Sturmfels and Caroline Uhler. "Multivariate Gaussians, semidefinite matrix completion, and convex algebraic geometry". *Annals of the Institute of Statistical Mathematics* 62.4 (2010), pp. 603–638.

[108]   James Joseph Sylvester. "XVII. An enumeration of the contacts of lines and surfaces of the second order". *The London, Edinburgh, and Dublin Philosophical Magazine and Journal of Science* 1.2 (1851), pp. 119–140.

[109]   Johannes Thomae. "Beitrag zur Bestimmung von $\theta(0,0,\dots,0)$ durch die Klassenmoduln algebraischer Funktionen". *J. Reine Angew. Math.* 71 (1870), pp. 201–222.

[110]   Robert C Thompson. "Pencils of complex and real symmetric and skew matrices". *Linear Algebra and its Applications* 147 (1991), pp. 323–371.

[111]   Frank Uhlig. "A canonical form for a pair of real symmetric matrices that generate a nonsingular pencil". *Linear Algebra and Its Applications* 14.3 (1976), pp. 189–209.

[112]   Frank Uhlig. "A recurring theorem about pairs of quadratic forms and extensions: A survey". *Linear algebra and its applications* 25 (1979), pp. 219–237.

[113]   Heinrich Weber. *Theorie der Abelschen Funktionen vom Geschlecht 3.* Berlin: Druck und Verlag von Georg Reimer, 1876.

[114]   Lauren K Williams. "The positive Grassmannian, the amplituhedron, and cluster algebras". *International Congress of Mathematicians.* Oct. 2021. arXiv: 2110.10856 [math.CO].

[115]   Alex Wright. "Translation surfaces and their orbit closures: an introduction for a broad audience". *EMS Surv. Math. Sci.* 2.1 (2015), pp. 63–108.

[116]   Thomas Zaslavsky. *Facing up to Arrangements: Face-Count Formulas for Partitions of Space by Hyperplanes.* Vol. 154. Memoirs of the American Mathematical Society. 1975.

[117]   Anton Zorich. "Explicit Jenkins–Strebel representatives of all strata of Abelian and quadratic differentials". *Journal of Modern Dynamics* 2.1 (2008), pp. 139–185.